

REMOTE SENSING-BASED MAPPING AND MODELLING OF  
COASTAL SALT MARSH HABITATS BASED ON OPTICAL,  
LIDAR AND SAR DATA

Thesis submitted for the degree of  
Doctor of Philosophy  
at the University of Leicester

by

Sybrand Jucke van Beijma MSc  
Department of Geography  
University of Leicester

2015

REMOTE SENSING-BASED MAPPING AND MODELLING OF SALT MARSH HABITATS  
BASED ON OPTICAL, LIDAR AND SAR DATA

by

Sybrand van Beijma

**Abstract**

There is much interest in the ability of Remote Sensing (RS) technologies for mapping natural environments. Meanwhile, coastal zones need monitoring in order to find a balance between human use and sustainable functioning of coastal zone ecosystems. This research explores methods for characterising coastal salt marsh zone habitats using multi-source RS data, focussing on under-exploited Synthetic Aperture Radar (SAR) remote sensing data, thereby providing additional information in support of the mapping of natural habitats in coastal zones.

This research examined the use of quad-polarimetric airborne S-band and X-band SAR data, in conjunction with optical and LiDAR RS data variables, for assessment of environmental parameters, mapping and modelling of salt marsh habitats in a research area set in the Llanrhidian salt marshes in Wales. In the first analysis it was researched how SAR descriptors (backscatter intensity and polarimetric decomposition variables) were affected by salt marsh environmental and botanical factors. It was found that SAR backscatter from the most seaward pioneer zone of the salt marsh was most affected by soil moisture variations. Differences in botanical structure caused variations in SAR backscatter mechanisms active in different habitats. In the second analysis habitat mapping was carried out with optical, LiDAR and SAR variables, with the supervised classifiers Support Vector Machine (SVM) and Random Forest (RF). With these classifiers accurate salt marsh habitat maps were produced, the most accurate classification achieved was 78.20% with RF based on all available RS variables. The last research experiment involved multivariate regression analysis of correlations between RS variables and biophysical parameters vegetation cover, height and volume and showed that multivariate SVM regression was the most accurate technique for all three biophysical parameters. This research indicated that SAR is complementary to optical and LiDAR data for ecological mapping and therefore recommended to be included in similar ecological studies.

## **Acknowledgements**

Doing a PhD is not for the faint-hearted, it involves prolonged periods of self-doubt and feelings of loneliness. Coming out on the other end with a finished PhD thesis is never the work of one single individual, therefore I would like to express sincere gratitude to a number of people.

I would like to thank my supervisor at Airbus Defence and Space in Farnborough Alistair Lamb for hiring me in the first place and by always being available with expert advice whenever needed. Greatest gratitude also goes to my academic supervisor at the University of Leicester Professor Lex Comber for being honest about what a PhD involves and by keeping me focussed and productive on moments I had no clue whatsoever.

My thanks also go to Paul Robinson (JNCC), Andy Richman, Kyle Brown (both Environment Agency) and Geoff Smith (Specto Natura) for their expert advice on Remote Sensing and coastal management. An introduction into the ecology of the wonderful Llanrhidian Marshes was provided by Lily Pauls (NRW), which was an enjoyable experience for which I thank her a lot.

As one of the GIONET ESRs I have been very fortunate to be working among a group of talented and smart fellow researchers. James, Pedro, Martyna, Maxim, Stephanie, Dimitris, Matthew, Shailesh, Linda, Christoff, Jessica, Penelope and especially Bernard: thank you guys for the good company, food for thought and cultural enrichment during the four Summer Schools, many workshops and a lovely holiday in South Africa. My gratitude also goes to Virginia Nicolas-Perea, Rhiannon Harte-Chance and Professor Heiko Balzter for their excellent coordination of the GIONET project.

The last three years were not all about work. I have often been happily distracted from the research work by friends old and new in both Holland and England for which many thanks. Finally, I would like to thank my family with special mention of my parents Barbara and Rik for their endless support, by helping me out whenever I had to move stuff to yet another new place and for their knowledgeable and pleasant company during the fieldwork in Wales.

## List of Contents

Abstract.....	i
Acknowledgements .....	ii
List of Contents .....	1
List of Figures .....	ix
List of Tables .....	xii
List of Acronyms and Abbreviations .....	xiv
1. Introduction .....	1
2. Literature review.....	7
2.1. Coastal zone issues.....	7
2.1.1 Coastal zone management .....	7
2.1.2 Ecosystem services .....	9
2.2. Salt marshes .....	9
2.2.1 Geographical setting.....	10
2.2.2 Environmental setting.....	12
2.2.3 Ecological characteristics .....	12
2.2.4 Salt marsh management.....	15
2.3. Remote sensing technologies .....	15
2.4. Research of RS for coastal mapping and monitoring.....	17
2.4.1 Operational projects .....	17
2.4.2 Use of RS for mapping of coastal dynamics.....	18
2.4.3 Use of RS for salt marsh vegetation mapping .....	20
2.4.4 Use of RS for estimation of vegetation biophysical parameters .....	23
2.5. Literature review summary.....	24
2.5.1 Research gaps .....	25
2.5.2 Research questions .....	26

## List of Contents

3.	SAR remote sensing .....	27
3.1.	SAR introduction .....	27
3.1.1	Radar platforms .....	27
3.1.2	Airborne SAR systems .....	30
3.1.3	SAR speckle .....	30
3.2.	SAR polarimetry .....	31
3.2.1	Scattering matrix.....	32
3.2.2	Scatter mechanisms.....	33
3.2.3	Polarimetric decomposition .....	35
3.2.3.1	Cloude-Pottier decomposition .....	35
3.2.3.2	Freeman-Durden decomposition .....	36
3.2.3.3	Van Zyl decomposition.....	37
4.	Research area and data processing .....	38
4.1.	Research area.....	38
4.1.1	Geomorphological setting .....	39
4.1.2	Ecological setting .....	40
4.1.3	Management practices .....	42
4.2.	Data description and processing.....	43
4.2.1	Optical data sets .....	43
4.2.1.1	Pre-processing optical aerial imagery .....	44
4.2.1.2	Pre-processing optical satellite imagery .....	45
4.2.2	LiDAR data sets .....	45
4.2.3	Airborne SAR data.....	46
4.2.3.1	SAR data import .....	47
4.2.3.2	SAR radiometric correction.....	48
4.2.3.3	SAR geometric correction .....	48
4.2.3.4	SAR polarimetric descriptors.....	49
4.2.3.5	SAR geo-registration .....	50

## List of Contents

4.3.	Reference data .....	54
4.3.1	CCW survey (1998).....	54
4.3.2	Field survey (2013).....	55
4.3.3	Salt marsh habitat classes.....	58
5.	SAR backscatter signatures in salt marshes.....	59
5.1.	Introduction .....	59
5.2.	Methods .....	59
5.3.	Results .....	60
5.3.1	Polarimetric backscatter intensity variables .....	61
5.3.2	CP polarimetric decomposition variables.....	65
5.3.3	VZ polarimetric decomposition variables.....	71
5.3.4	Integration of results .....	74
5.4.	Discussion.....	75
5.4.1	SAR signatures of salt marsh habitats .....	75
5.4.2	S-band and X-band backscatter variations .....	76
5.4.3	Backscatter intensity and polarimetric decomposition variables .....	77
5.5.	Summary .....	79
6.	Mapping of salt marsh habitats.....	80
6.1.	Introduction .....	80
6.2.	Methods .....	81
6.2.1	Unsupervised habitat classification with SAR data .....	81
6.2.2	Supervised habitat classification .....	82
6.2.2.1	Variable combinations .....	82
6.2.2.2	Supervised classification variable importance.....	84
6.2.2.3	Supervised classification accuracy.....	86
6.2.2.4	Vegetation extent change.....	86
6.3.	Results.....	89

## List of Contents

6.3.1	Unsupervised habitat classification with CP variables .....	89
6.3.2	Supervised habitat classification .....	93
6.3.2.1	SVM habitat classification .....	93
6.3.2.2	RF habitat classification.....	99
6.3.3	Supervised vegetation extent classification .....	105
6.3.4	Integration of results .....	109
6.3.4.1	Classifier analysis.....	109
6.3.4.2	Vegetation extent change analysis .....	110
6.3.4.3	Habitat change analysis.....	112
6.4.	Discussion.....	113
6.4.1	Unsupervised habitat classification with CP variables .....	113
6.4.2	Supervised habitat classification .....	115
6.4.2.1	SVM habitat classification .....	115
6.4.2.2	RF habitat classification.....	116
6.4.2.3	Habitat maps .....	117
6.4.3	Habitat change analysis .....	118
6.4.4	Supervised vegetation extent classification .....	118
6.4.5	Vegetation extent change analysis .....	119
6.5.	Summary .....	119
7.	Regression modelling of biophysical parameters.....	121
7.1.	Introduction .....	121
7.2.	Methods .....	122
7.2.1	Biophysical parameters regression analysis .....	122
7.2.2	Biophysical parameter mapping.....	123
7.3.	Results .....	124
7.3.1	Biophysical parameter regression analysis.....	124
7.3.1.1	Univariate linear regression .....	124
7.3.1.2	Multivariate linear regression .....	128

## List of Contents

7.3.2	Biophysical parameter regression mapping .....	131
7.3.2.1	MLS regression .....	132
7.3.2.2	SVM regression .....	132
7.3.2.3	RF regression .....	134
7.3.2.4	Biophysical parameter maps .....	136
7.3.3	Integration of results .....	138
7.4.	Discussion .....	139
7.4.1	Regression variable analysis .....	139
7.4.2	Biophysical parameter mapping variable analysis .....	140
7.4.3	Biophysical parameter mapping accuracy .....	141
7.5.	Summary .....	142
8.	Considerations and recommendations .....	143
8.1.	Methodological considerations .....	143
8.1.1	Pre-processing .....	143
8.1.2	Data analysis .....	144
8.1.2.1	Vegetation classes .....	144
8.1.2.2	Variable importance .....	144
8.1.2.3	Data consistency .....	145
8.1.3	Environmental and seasonal factors .....	146
8.1.3.1	Tidal level .....	146
8.1.3.2	Soil moisture .....	147
8.1.3.3	Phenology .....	147
8.2.	Research feasibility and recommendations .....	148
8.2.1	Feasibility and repeatability of the research .....	148
8.2.2	Research contributions .....	149
8.2.3	Future research .....	150
9.	Conclusions .....	154
	Appendices .....	159



## List of Contents

Appendix A – Ecological field survey (July 2013) data sheets .....	160
Appendix B – Pictures from selected sample locations.....	166
Appendix C – Flowchart of analysis steps.....	168
Appendix D – Flowchart of SAR data pre-processing steps.....	169
Appendix E – Publications.....	170
Bibliography .....	171

## List of Figures

Figure 1 – Location of salt marshes along the UK coastline indicated in bold lines,.....	11
Figure 2 – Impression of a salt marsh, displaying different vegetation habitats and drainage network.....	12
Figure 3 – Idealised cross profile through a Northwest European salt marsh. ....	14
Figure 4 – Geometry of SAR acquisition platform, oblique view. ....	28
Figure 5 – Geometry SAR acquisition platform, frontal view. ....	29
Figure 6 – The shape of basic scatterers,.....	34
Figure 7 – The most common scatter mechanisms. ....	35
Figure 8 – Overview map of research area location in Wales. ....	39
Figure 9 – Photographic overview of major salt marsh vegetation habitats in the Llanrhidian Marsh. ....	41
Figure 10 – RGB composite of the aerial photography data set used in this research. .	44
Figure 11 – LiDAR DSM data set used in this research. ....	46
Figure 12 – Antenna pattern correction curves for S-band SAR image from pre-processing in RAT.....	49
Figure 13 – Location of GCPs used to geo-register airborne SAR data. ....	50
Figure 14 – Visual check of geo-registration of RS data sets used in this research. ....	52
Figure 15 – RGB composite of S-band polarimetric intensity channels. ....	53
Figure 16 – RGB composite of X-band polarimetric intensity channels. ....	53
Figure 17 – Habitat classification map based on the CCW ecological field survey (1998). .....	55
Figure 18 – Overview map of sample locations of field survey in July 2013.....	56
Figure 19 – Annotated picture of ecological field survey quadrat. ....	57
Figure 20 – Scatterplots SAR polarimetric intensity channels X-band against S-band...	62
Figure 21 – Boxplots SAR backscatter intensity channels against land cover classes...	63
Figure 22 – Scatterplots SAR Cloude-Pottier decomposition variables X-band against S-band. ....	67
Figure 23 – Scatter plots and density plots of $\alpha$ against H for S-band SAR data.....	68
Figure 24 – Scatter plots and density plots of $\alpha$ against H for X-band SAR data.....	69
Figure 25 – Boxplots SAR CP decomposition variables against land cover classes. ....	70
Figure 26 – Scatterplots SAR Van Zyl decomposition variables X-band against S-band.	72

## List of Figures

Figure 27 – Boxplots SAR VZ decomposition variables against land cover classes. ....	73
Figure 28 – Observed SAR backscatter mechanisms in different salt marsh habitats. ..	75
Figure 29 – Vegetation extent map based on EA salt marsh survey data (2007). ....	88
Figure 30 – Vegetation extent map based on CCW ecological survey data (1998).....	88
Figure 31 – Habitat map of unsupervised CP Wishart K-means S-band SAR classification.....	91
Figure 32 – Habitat map of unsupervised CP Wishart K-means X-band SAR classification.....	92
Figure 33 – SVM feature selection analysis of variable model based on all available RS variables.....	97
Figure 34 – Habitat map of supervised SVM classification, based on subset of the 21 most important variables of all available RS variables. ....	98
Figure 35 – RF variable importance analysis of variable model based on all available RS variables.....	102
Figure 36 – Habitat map of supervised RF classification, based on all available RS variables.....	104
Figure 37 – Variable importance plot RF vegetation extent classification model 17...	108
Figure 38 – Salt marsh vegetation extent map of supervised RF classification, based on all available RS variables. ....	109
Figure 39 – Vegetation cover extent change map for the period 1998-2010.....	111
Figure 40 – Salt marsh habitat change map .....	113
Figure 41 – Scatterplots of the best-fitting RS variables for biophysical parameters, based on the full sample data set (n=110). ....	125
Figure 42 – Scatterplots of the best-fitting RS variables for biophysical parameters, based on a subset of the sample data set, GVV < 20% (n=91). ....	127
Figure 43 – SVM feature analysis of biophysical parameter regressions with all available RS variables.....	133
Figure 44 – RF variable importance analysis of biophysical parameter regressions with all available RS variables.....	134
Figure 45 – Vegetation cover map, based on SVM regression with all available RS variables.....	136

List of Figures

Figure 46 – Vegetation height map, based on SVM regression with all available RS variables..... 137

Figure 47 – Vegetation volume map, based on SVM regression with all available RS variables..... 137

## List of Tables

Table 1 – SMP policies in relationship with coastal processes and population and economic pressures, .....	9
Table 2 – Salt marsh vegetation habitat zonations. ....	14
Table 3– Overview of the three most common remote sensing sensor types .....	16
Table 4 – Microwave bands used in remote sensing.....	27
Table 5 – Overview of RS data used in this research.....	43
Table 6 – Airborne SAR geo-registration GCP statistics.....	51
Table 7 – Relationships between NVC and Habitat Directive Annex 1 habitat classes..	58
Table 8 – Mean and standard deviations of backscatter intensity variables per habitat. ....	64
Table 9 – Mean and standard deviations of CP polarimetric decomposition variables per habitat. ....	70
Table 10 – Mean and standard deviations of VZ polarimetric decomposition variables per habitat. ....	73
Table 11 – Variable combinations used for supervised classifications .....	83
Table 12 – Confusion table of unsupervised CP Wishart K-means with S-band SAR classification.....	91
Table 13 – Confusion table of unsupervised CP Wishart K-means with X-band SAR classification.....	92
Table 14 – Overall classification accuracy and Kappa coefficient for the SVM classification models.....	94
Table 15 – SVM feature selection analysis. ....	96
Table 16 – Confusion table of supervised SVM classification based on 21 input variables.....	98
Table 17 – Overall classification accuracy and Kappa coefficient for the RF classification models.....	101
Table 18 – Accuracy assessment of supervised RF classifications with subsets of the model based on all available RS variables. ....	103
Table 19 – Confusion table of supervised RF habitat classification based on all available RS variables. ....	104

## List of Tables

Table 20 – Overall accuracy and Kappa coefficients for vegetation extent mapping variable models.....	106
Table 21 – Confusion table of supervised RF vegetation extent classification based on all available RS variables. ....	108
Table 22 – Highest classification accuracies of variable combination category for supervised classifications.....	110
Table 23 – Salt marsh vegetation extent change. ....	110
Table 24 –Habitat area change between CCW survey and RF habitat classification. ..	113
Table 25 – Pearson correlation coefficients (R-value) of biophysical parameters for all RS variables for entire sample location set (n=100).....	125
Table 26 – Pearson correlation coefficients (R-value) of biophysical parameters for all RS variables for subset of sample locations with GVV < 20%. (n=81). ....	126
Table 27 – Adjusted coefficients of determination (adjusted R <sup>2</sup> ) of MLR models of biophysical parameters, based on the full sample data set (n=110). ....	128
Table 28 – Adjusted coefficients of determination (adjusted R <sup>2</sup> ) of MLR subset models of biophysical parameters, based on the full sample data set (n=110). ....	128
Table 29 – Significance analysis of MLR coefficients of the subset model for vegetation cover. ....	129
Table 30 – Significance analysis of MLR coefficients of the subset model for vegetation height. ....	130
Table 31 – Significance analysis of MLR coefficients of the subset model for vegetation volume (GVV).....	130
Table 32 – Accuracy assessment of MLS regression of biophysical parameters.....	132
Table 33 – Accuracy assessment of SVM regression of biophysical parameters. ....	132
Table 34 – Accuracy assessment of RF regression of biophysical parameters.....	134

## List of Acronyms and Abbreviations

ACD	Admiralty Chart Datum
ALOS	Advanced Land Observing Satellite
C-band	Microwave band domain with wavelength between 3.75-7.5 cm
CCW	Countryside Council for Wales
Chl-a	Chlorophyll-a
CIR	Colour Infrared
CP	Cloude-Pottier polarimetric decomposition
DEFRA	Department of Environment, Food and Rural Affairs
DEM	Digital Elevation Model
DLR	Deutsches Zentrum für Luft- und Raumfahrt (German Aerospace Centre)
DSM	Digital Surface Model
DTM	Digital Terrain Model
EA	Environmental Agency
EC	European Commission
EEA	European Environmental Agency
EO	Earth Observation
ERS	ESA Remote Sensing Satellite
ESA	European Space Agency
ETM+	Enhanced Thematic Mapper Plus
EU	European Union
FAO	Food and Agricultural Organisation
FD	Freeman-Durden polarimetric decomposition
GCP	Ground Control Point
GMES	Global Monitoring for Environment and Security (renamed to Copernicus)
GMT	Greenwich Mean Time
GPS	Global Positioning System
GSE	GMES Service Element
GVV	Gross Vegetation Volume

## List of Acronyms and Abbreviations

H, A, $\alpha$	CP Entropy, Anisotropy and alpha angle
HH	Horizontal transmitted and Horizontal received
HR	High Resolution
HV	Horizontal transmitted and Vertical received
ICZM	Integrated Coastal Zone Management
IEEE	Institute of Electrical and Electronics Engineers
IGARSS	IEEE Geosciences and Remote Sensing Symposium
InSAR	Interferometric Synthetic Aperture Radar
IQR	Interquartile Range
ISPRS	International Society for Photogrammetry and Remote Sensing
JNCC	Joint Nature Conservation Committee
L-band	Microwave band domain with wavelength between 15-30 cm
LAE	Leaf Area Index
LiDAR	Light Detection and Ranging
ML	Maximum Likelihood
MLR	Multiple Linear Regression
MLS	Multivariate Least-Squares
MSP	Maritime Spatial Planning
NASA	National Aeronautics and Space Administration
NDVI	Normalised Difference Vegetation Index
NERC	Natural Environment Research Council
NTSLF	National Tidal and Sea Level Facility
NRW	Natural Resources Wales
NVC	National Vegetation Classification
OBIA	Object-Based Image Analysis
OD	Ordnance Datum
OOB	Out-Of-Bag
OS	Ordnance Survey
P-band	Microwave band domain with wavelength between 30-100 cm
Pol-InSAR	Polarimetric Interferometric Synthetic Aperture Radar
$P_v, P_d, P_s$	FD or VZ Volume Scatter, Double-bounce Scatter and Surface Scatter



## List of Acronyms and Abbreviations

$R^2$ -value	Coefficient of determination
RAT	Radar Tools
RF	Random Forest
RGB	Red, Green, Blue
RMSE	Root Mean Squared Error
RS	Remote Sensing
SAC	Special Area of Conservation
SAR	Synthetic Aperture Radar
S-band	Microwave band domain with wavelength between 7.5-15 cm
SEPA	Scottish Environmental Protection Agency
$S_{HH}$ , $S_{HV}$ , $S_{VH}$ , $S_{VV}$	Element of the scattering matrix in HH, HV, VH and VV polarisations
SLC	Single Look Complex
SM##	NVC Salt Marsh class (class number on ##)
SMP	Shoreline Management Plan
SPA	Special Protected Area
SPOT	Système Pour l'Observation de la Terre (System for Observation of Earth)
SSSI	Site of Specific Scientific Interest
SVM	Support Vector Machine
TM	Thematic Mapper
TSX	TerraSAR-X
UK	United Kingdom
ULR	Univariate Linear Regression
US	United States
USGS	United States Geological Survey
VH	Vertical transmitted and Horizontal received
VHR	Very High Resolution
VI	Variable Importance
VV	Vertical transmitted and Vertical received
VZ	Van Zyl polarimetric decomposition
X-band	Microwave band domain with wavelength between 2.4-3.75 cm

## **1. Introduction**

Coastal zones are areas where, put simply, land meets sea. Their morphology varies from cliffs, beaches and mangrove forests to low-lying coastal salt marshes (Bird 2008). Due to the impact of wave activity, tidal currents and sediment supply, form and morphology of coastal zones are subject to constant change (Haslett 2003). The resulting environment is highly dynamic with frequently changing morphology and ecology, creating a major challenge for development of long-term and sustainable coastal management plans. Other challenges to the management of coastal zones are the expected effects of climatic change. It is expected that coastal areas will take the brunt of the effects of climate change due to sea level rise. Additionally, environmental pressures on coastal zones increase as a result of expanding population and economic developments in coastal areas (McGranahan et al. 2007).

The need for a more integrated approach to coastal management has resulted in the adoption of the Integrated Coastal Zone Management (ICZM) policy in the European Union (EC 2011). The ways of implementation of ICZM has been discussed progressively (EEA 2006), in recent years focus has been given to eco-system based management of coastal areas (Katsanevakis et al. 2011).

Low-lying intertidal coastal marshes are some of the main areas of concern when it comes to coastal monitoring and management. Coastal marshes are expressed as mangrove forests in tropical zones and salt marshes in temperate climates (Zisenis 2010). These areas are particularly sensitive to climatic change, as they are directly exposed to sea-level rise and have limited space to shift landwards as they are often bounded by sea walls (Boorman 2003). Many of the world's low-lying coastal habitats are in adverse ecological condition, degrading or eroding (FAO 2007). Nonetheless, coastal marshes provide valuable ecosystem services like flood and storm wave protection, as well as food provision (Adam 2002).

Along the diverse coastline of the United Kingdom extensive areas are lined with salt marsh habitats. These habitats are characterised by specific halophytic grassy and shrubby vegetation types that are subject to varying levels of inundation by tidal activity (Adam 1990). Over time, many salt marshes have been converted to grazing or agricultural land, with an often detrimental effect on the natural vegetation habitats (Bakker 1985; Alber et al. 2008). Accordingly, some salt marsh regeneration projects

have been carried out to improve ecosystem services provided by salt marsh habitats (Garbutt and Wolters 2008).

Mapping and monitoring of salt marsh areas poses some specific challenges. These areas are situated between high and low tidal level marks and therefore regularly flooded. Even at low tide salt marshes are difficult areas to access, the sub-strata are often very muddy and numerous creeks and channels make navigation difficult. Therefore, regular mapping of salt marshes along the UK's coast is done based on interpretation of aerial imagery by the Environment Agency (Environment Agency 2011). Primary goal of these surveys is to monitor decadal changes of salt marsh vegetation extent. The use of remote sensing (RS) technologies has shown to be a useful alternative to ground based surveys. Over the past two decades numerous publications have focussed on the use of RS of mapping and monitoring of salt marshes. Reviewing the literature reveals that research results have shown that RS can be used successful to map specific intertidal vegetation species with hyperspectral RS imagery (Stevens 2009) and LiDAR (Environment Agency and Natural England 2011). More fundamental research into the use of satellite-based RS sensors has shown that RS derived variables can successfully be used for salt marsh mapping (Hladik and Alber 2014), and that combination of RS data from different sensors can improve mapping of salt marsh habitats (Dehouck et al. 2012). In recent years, the use of Synthetic Aperture Radar (SAR) data for mapping of intertidal and salt marsh areas has been gaining attention. SAR has specific advantages over optical RS sensors. Due to their relatively long wavelength, most electromagnetic pulses in the microwave domain pass through clouds unhindered. Additionally, they interact with targets on the Earth's surface in a physical way, thereby providing information about the physical appearance of these targets. SAR remote sensing has been used for forestry and vegetation mapping studies (Woodhouse 2006; Lucas 2008). Research of the use of SAR in intertidal and salt marsh areas has shown that the interaction of radar pulses with the surface can provide useful information about the surface composition (van der Wal et al. 2005), presence of oyster beds (Choe et al. 2012) or vegetation habitat classification (Lee et al. 2012).

From the literature the following research aim was postulated:

**Research to which extent multi-frequency polarimetric SAR can contribute to the mapping and modelling of coastal salt marsh habitats.**

In order to support the research aim, a number of research experiments were designed, consisting of quantitative and qualitative approaches to investigate the contribution of SAR data for mapping of salt marsh habitats. It has to be acknowledged that this research has been data-driven due to the coincidence that an appropriate SAR data set was available for a well-suited salt marsh research area. It is aimed to use this data set starting from a traditional RS study: usually operational use of RS data sets focusses on optical and LiDAR data as these data sets are more readily available and easier to interpret. In this study the SAR data set is added to the optical and LiDAR data sets a complementary data source. With this combined data source it has been attempted to explain the outcomes of the research experiments in terms of environmental and ecological processes taking place in a salt marsh setting.

This research starts with a report on the specific properties of SAR and the pre-processing steps taken with the SAR data set used in this research. The airborne SAR data set used in this research was acquired as test data for the upcoming NovaSAR-S SAR satellite mission, set to launch in 2016. The data set was acquired in the S-band and X-band frequencies and is quad-polarimetric. The airborne quad-polarimetric SAR data has been pre-processed and polarimetric decomposition was performed. Polarimetric decomposition variables were extracted by decomposing the scatter matrix of the polarimetric backscatter channels according to model representations of the different scatter mechanisms.

Subsequently, three research experiments were carried out, each focussing on specific processes or characteristics of salt marsh areas. In the first research experiment the response of SAR data to different environmental and physical characteristics throughout a salt marsh area were analysed, with focus on respective backscatter responses of SAR frequencies to salt marsh vegetation habitats, in this research S-band and X-band. Due to the physical interaction of microwave pulses with specific objects on the Earth's surface, response of different microwave frequencies can differ

significantly (Schmullius and Evans 1997). For each SAR frequency band, specific optimal application domains exist. For example, longer wavelengths are better suited to map forest biomass, whereas shorter wavelengths are better suited to map grasslands. S-band SAR has rarely been used on SAR RS platforms; analysis of S-band interaction with salt marsh vegetation will provide excellent insight how this frequency band can be used to map this or other grassy and shrubby habitats.

Polarimetric decomposition variables provide information about backscatter mechanisms and are more intuitively interpretable than variables based on polarimetric backscatter intensity channels (Li et al. 2012). However, polarimetric decomposition variables can only be extracted from quad-polarimetric SAR systems. Quad-polarimetric SAR systems are not commonly installed on satellite platforms as they consume relatively much power, are expensive and technologically complex. In this part of the research the added value of polarimetric decomposition variables over backscatter intensity channels has been researched. This was achieved by comparing accuracy assessment of habitat classifications based on the respective variables. Additionally, an initial habitat classification was carried out with the K-means Wishart classifier (Ferro-Famil et al. 2001). This classification is based on SAR polarimetric decomposition variables alone, the CP polarimetric decomposition variables are used for unsupervised classification that takes into account the specific statistical distribution of SAR data.

The second research experiment focussed on the potential of SAR data to complement salt marsh vegetation habitats. In order to research to what extent SAR variables can complement with variables from other RS sensors, supervised image classification was carried out with an aggregate RS data set consisting of S-band and X-band SAR data (backscatter intensity channels and polarimetric decomposition parameters), optical data based on aerial photography and satellite-imagery derived vegetation indices and a LiDAR Digital Surface Model (DSM). The classifiers used in this research were Support Vector Machine (SVM) and Random Forest (RF). The versatility of the SVM and RF classifiers, especially their potential to use multi-source data, has made them popular for ecological studies (Cutler et al. 2007; Mountrakis et al. 2011). These classifiers provide additional information about variable performance or importance, which was

analysed in detail. The classifications resulted in maps of different salt marsh vegetation habitats, as well as a general vegetation extent cover map.

Subsequently, a vegetation extent map was made to assess change in salt marsh vegetation cover, compared to earlier salt marsh mapping efforts. The resulting vegetation cover change analysis provided a model of vegetation cover dynamics in the research area in the last 12 years.

The final research experiment involved the modelling of biophysical parameters with regression analysis with the multi-source RS data set used for the image classification. The term biophysical parameter is used for three biophysical parameters: vegetation cover percentage, average vegetation height and volume of vegetation within a specified area. The regression methods under consideration were: univariate linear, multivariate linear, SVM and RF regression. Of the latter two regression methods analysis of variable importance for the regression model has been carried out.

The outcomes of the different research experiments resulted in a comprehensive study into complementary application of polarimetric SAR for ecological mapping and vegetation modelling. In this way different observations made of the SAR data and its application in conjunction with other data sets were highlighted.

The outline of this thesis is as follows:

- **Chapter 2** provides a **Literature Review** related to the field of coastal management and ecological characteristics of salt marshes. Subsequently, recent advances in RS research for coastal mapping are reviewed, with focus on SAR technologies and applications. At the end of this chapter, research gaps are identified and the research questions formally stated.
- In **Chapter 3** an introduction into **SAR remote sensing** technologies is provided, with focus on extracting and use of polarimetric descriptors
- In **Chapter 4** the **Research area and data processing** are described. First focus is given to the research area; after which the RS data set and the processing steps are described in detail. Appendix C and Appendix D provide a graphic overview of the processing and analysis steps of the research.
- In **Chapter 5** the analysis of **SAR backscatter signatures in salt marshes** is presented. The chapter starts with a description of the methodology, followed

by research results. At the end of the results section, a paragraph is dedicated to the integration of the results in the environmental setting. Subsequently, a discussion of the results is provided and the chapter is finished with a summary.

- In **Chapter 6** the results of the **Mapping of salt marsh habitats** are presented and analysed. This chapter has a similar structure to Chapter 5.
- In **Chapter 7** the results of the **Regression modelling of biophysical parameters** are presented and analysed. This chapter has a similar structure to Chapter 5.
- The significance and implications of the results are discussed in **Chapter 8**, the **Considerations and recommendations**. This chapter puts the research methodologies in a wider context and discusses the most important considerations in terms of validity and repeatability. This is followed by a discussion of recommendations for future research.
- In the final **Chapter 9, Conclusions** are drawn. The key findings are presented and answers to the research questions in Chapter 2 are provided.

## **2. Literature review**

This chapter presents a literature study of recent research in the field of coastal zone management, current coastal management policies and research of ecology and management of salt marsh habitats. Subsequently, research into use of remote sensing technologies for monitoring of coastal zones with a specific focus on application development and analysis techniques are discussed. In the last section a summary of the most important findings from the literature review is provided, the most important research gaps are identified and the research questions of this thesis are re-stated.

### **2.1. Coastal zone issues**

Coastal zones with elevation of less than 10 meters cover only 2% of the global land mass, but they host 10% of the world's population (McGranahan et al. 2007). It is predicted that low-lying coastal areas will experience the majority of human population growth and economic development (Adam 2002; Foresight 2011). For example, an increase of 7.5% of artificial surfaces between 1990 and 2000 was recorded along Europe's coastlines (Zisenis 2010). Coastal zones provide an important mixture of economic, environmental and ecological services, but many of these habitats are degrading at alarming rates (Boorman 2003; FAO 2003; FAO 2007; Giri et al. 2011). In tropical climates, the total area of intertidal mangrove communities are declining in high rates (Kuenzer et al. 2014), globally they declined by 20% between 1980 and 2005 (FAO 2007). Even though it is uncertain what effect sea level rise will have in the near future, coastal areas are expected to experience the adverse effects of it (Nicholls et al. 2007). It is likely that climate change increases frequency of flooding and extreme storms, which have a profound effect on the degradation of coastal zones (Doody et al. 2004).

#### **2.1.1 Coastal zone management**

Coastal zone management has been on the political agenda since the 1990s. In 2002, the European Union (EU) drafted the Integrated Coastal Zone Management (ICZM) Recommendation, which aims to develop a legal ICZM framework that defines ecological sustainable management practices for coastal European member states (EC 2011). To define what ICZM might exactly imply, a number of pilot studies have been carried out to research robust integrated coastal management practices (EC 2011;



OURCOAST 2011). The European Environmental Agency (EEA) has published a comprehensive report that addresses the urgent need for a more integrated long-term approach with regard to ICZM (EEA 2006). Two major recommendations stressed in the EEA report are:

- 1) the need to research the expected impact of climate change on the coastal zone,
- 2) move towards more ecosystem-based coastal management policy (Zisenis 2010).

The concept of ecosystem-based marine management involves integrated ecosystem-driven coastal management, supported by improved marine spatial planning (Katsanevakis et al. 2011). A recent example of this approach is the 'Building with Nature' project in the Netherlands (Ecoshape 2011), promoting ecosystem-driven coastal management principles to show how ecosystem-driven coastal management practices can work. In the United Kingdom (UK), further definition of ICZM policies is performed by the Ministerial Department of Environment, Food and Rural Affairs (DEFRA) and its advisory conservation body, the Joint Nature Conservation Committee (JNCC). They propose a holistic approach to coastal management, enhanced by the recent improvements in the field of Marine Spatial Planning (Collins 2012).

The Environmental Agency (EA) is responsible for the development of Shoreline Management Plans (SMP) in the UK (Environment Agency 2011). SMPs outline the management principles along a specific stretch of the UK coastline. The strategic options are: 1) no active intervention, 2) maintaining the current limit ('hold the line'), 3) managed retreat and 4) advancement. The first and fourth strategies are in place along stable or accreting stretches of the coast, where human pressure and economic activity is low. The second and third strategies are followed in coastal zones where erosion takes place (Table 1).

*Table 1 – SMP policies in relationship with coastal processes and population and economic pressures, from Environment Agency (2011).*

<b>Dominant coastal process</b>	<b>Low population pressure or economic activity</b>	<b>High population pressure or economic activity</b>
Erosion	Managed retreat	Hold the line
Stable	No active intervention	
Accretion	Advancement	

### **2.1.2 Ecosystem services**

Ecosystem services are goods and services derived from ecosystem functions that benefit human populations, directly or indirectly (Costanza et al. 1997; Katsanevakis et al. 2011). Coastal ecosystems provide a number of ecosystem services in the form of 1) biodiversity support, 2) water quality improvement, 3) flood mitigation and 4) carbon management (Zedler and Kercher 2005). Research has been carried out into the flood mitigation capability of healthy coastal ecosystems, by dissipation of wave energy during storms and extreme events like tsunamis (Möller 2006; Kamthonkiat et al. 2011). It was found that healthy coastal ecosystems like salt marshes and mangrove forests are effective buffers against storms, extreme events and sea level rise, provided that these ecosystems have space to migrate inland.

Other research focussed on the ability of vegetated coastal ecosystems to uptake carbon (Pendleton et al. 2012). Even though there is much uncertainty about their relative role in the carbon cycle, it is estimated that degradation of coastal ecosystems contributes significantly to the release of carbon into the atmosphere.

A further ecosystem service highlighted is food provision. For example, salt marsh areas are often used for grazing cattle. This pastoral activity can have a beneficial impact on plant diversity as it functions as a plant debris litter clean-up, provided the density of animals is limited (Bakker 1985). On the other hand, if overgrazing occurs the salt marsh ecosystem can degrade to bare areas, which makes them vulnerable to erosion (Alber et al. 2008).

## **2.2. Salt marshes**

Salt marshes are coastal wetlands in temperate climates that are situated in the upper intertidal zone and are therefore regularly flooded. They are dominated by halophytic (salt-tolerant) plants such as herbs, grasses and shrubs (Adam 1990). They are important habitats in terms of ecosystem services, but are often converted to

agricultural land or suffer from pollution (Adam 2002). In this section the general geographical, environmental and ecological characteristics of salt marshes are described. Eventually, attention is given to salt marsh management practices.

### 2.2.1 Geographical setting

Salt marshes fringe many of the world's soft sedimentary coasts exposed to low-energy wave action (Adam 2002). Many salt marshes are located along estuarine shores, sheltered by barrier islands, spits, embayments, lagoons and along open shores exposed to low wave energy (Adam 1990). Three general types of salt marsh morphology can be distinguished (Boorman 2003):

1. **Open coast barrier-connected salt marshes.** In the UK, such as are found in North Norfolk and on the Dutch Wadden Sea. These salt marshes form behind a spit or island as a protective barrier. These marshes are often rich in plant species.
2. **Foreland salt marsh.** These can be found in The Wash and Morecambe Bay in the UK. They form in front of sheltered alluvial coastal areas.
3. **Estuarine salt marshes fringing larger estuaries.** Examples of this type of salt marsh can be found in the UK in the Essex and Severn estuaries. In these salt marshes a transition from halophytic to fresh water plant species is visible, reflecting the salinity transition gradient of the estuarine water.

Salt marsh communities in the United Kingdom (UK) are most abundant in the south, where most of the UK's soft sedimentary coastlines are located (Figure 1). Along the English and Welsh coastline the UK's largest salt marsh communities can be found, of which the largest are (Boorman 2003): The Wash (Lincolnshire), Burry Inlet (Llanelli), River Ribble (Lancashire), Morecambe Bay (Cumbria), Blackwater (Essex) and Wells to Blakeney (Norfolk). In Scotland no large salt marsh complexes exist due to the rocky nature of the coast, their presence is often confined to estuaries and firths (JNCC 2004). In Europe, the largest salt marshes can be found along the shores of the Wadden Sea (Netherlands, Germany and Denmark) and other smaller complexes can be found in Portugal, France, Italy, Albania and Bulgaria. Outside Europe, salt marshes are commonly found along the east coast of North America and in Arctic zones.

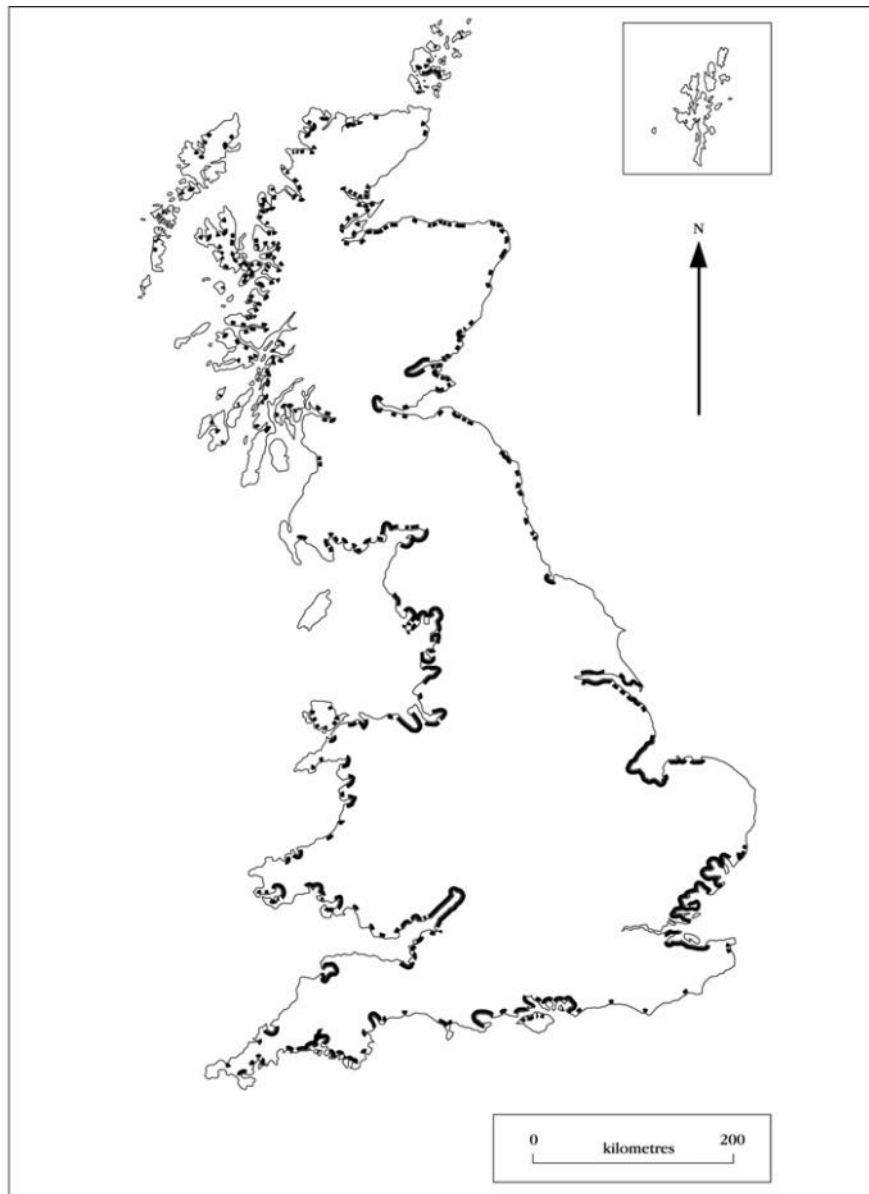


Figure 1 – Location of salt marshes along the UK coastline indicated in bold lines, after (Boorman 2003).

Salt marsh areas are characterised by complex network of drainage channels, creeks and ponds (Figure 2). The channels and creeks are capable of draining most of the salt marshes during low tides. These networks are best developed in the seaward facing, lower parts of salt marshes, as these are most often flooded. In areas further away from drainage channels (usually the higher, less-frequently flooded parts of salt marshes) water often collects in ponds (Adam 1990). According to (Moffett et al. 2010), salt marshes are relatively stable once drainage is established. The salt marsh surface is usually very flat, with a topographic gradient between the land and seaward sides of less than five metres (Adam 1990).



Figure 2 – Impression of a salt marsh, displaying different vegetation habitats and drainage network.  
Photo taken by the author in the Llanrhidian Marshes, Wales.

### 2.2.2 Environmental setting

Salt marshes are influenced by fluxes from the sea, namely tides, waves and sediment, as well as climatic variations. Due to the influence of tidal flooding, edaphic conditions in salt marsh areas are changing constantly (Moffett et al. 2010). This results in changes in soil saturation between areas that are well-drained and areas where water remains longer. Due to evapotranspiration, soil salinity increases in areas where water remains longer. As a result of this, soil salinity is usually higher in the landward part of salt marshes than in the, seaward side of the salt marshes (Silvestri and Marani 2004; Moffett et al. 2010).

### 2.2.3 Ecological characteristics

In temperate regions salt marshes are characterised by a suite of halophytic herbaceous or low woody vascular plants, dominated by grasses, herbs and shrubs. *Salicornia spp.* and *Spartina anglica* are the most abundant and most researched species (Adam 2002).

The spatial distribution of different salt marsh vegetation habitats is not random, but shows a distinctive pattern that can be recognised in many different salt marsh areas around the world (Rodwell 2000; Silvestri and Marani 2004). These patterns or

zonations are highly dependent upon the aforementioned soil salinity and inundation frequency. Topography and the related flooding frequency and duration are therefore important, albeit not the only, factors that drive variations of salt marsh vegetation habitats. Salt marsh vegetation communities also respond to seasonal temperature changes and rainfall. Some of the plant species are perennial. Other species are annual and are senescent in winter. The resumption of annual plant growth occurs in early spring. During summer droughts, growth can be inhibited by increased evapotranspiration which leads to hyper-saline conditions (Boorman 2003).

Vegetation habitats can be classified according to many different classification schemes (Rodwell 2000; JNCC 2006). In the UK, the National Vegetation Classification (NVC) scheme is often used (Rodwell 2000). The European Union adopted the Habitats Directive in 1992 to improve the conservation of habitats (European Commission 1992). With the Habitats Directive, the Annex 1 habitat classification scheme, in which intertidal habitats are subdivided in a number of zonation, based on geographical and environmental parameters like inundation frequency and topography (Boorman 2003). In Table 2 the classification of general salt marsh vegetation habitats according to Boorman (2003) is summarised. A graphical overview of the most common salt marsh zonation with their environmental characteristics is provided in Figure 3.

Table 2 – Salt marsh vegetation habitat zonations.

Zonation	Dominant species	Vegetation life cycle	Vegetation structure	Inundation frequency	Drainage network characteristics
Pioneer zone	<i>Spartina</i> spp., <i>Salicornia</i> spp., <i>Aster tripolium</i>	Annual	Incomplete ground coverage, vegetation height 0.1-1 metre	Every high tide	Shallow creeks, tidal flat
Lower-Mid Marsh	<i>Festuca rubra</i> , <i>Puccinellia maritima</i> , Previously named species	Perennial	Complete ground coverage, Vegetation height 0.05-0.2 m	Most high tides	Complex network of channels and creeks, ponds
Middle-Upper Marsh	<i>Juncus maritimus</i> , previously named species	Perennial	Complete coverage, Vegetation height 0.5-1m	Spring high tide	Ponds, large deep channels
Upper Marsh	<i>Armeria maritima</i> , <i>Elytrigia</i> spp. Previously named species	Perennial	Complete ground coverage Vegetation height 0.5-1m	Highest spring tides	Ponds, some channels

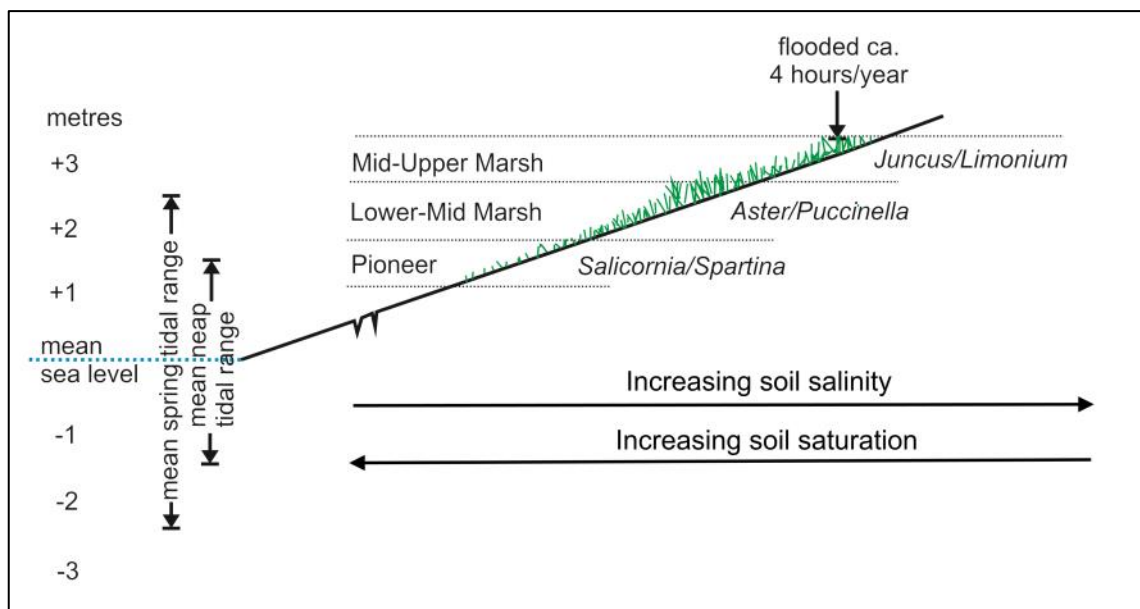


Figure 3 – Idealised cross profile through a Northwest European salt marsh. From seaward side (left) to landward side (right).

Salt marshes are dynamic environments and salt marsh vegetation communities can be subject to rapid changes in vegetation cover if vegetation habitat space accretes or

erodes (Boorman 2003). Accordingly, there is an urgent need for high-resolution mapping and monitoring of salt marsh habitats (DEFRA 2006).

#### **2.2.4 Salt marsh management**

Specific management of salt marshes in the UK is not carried out to a formal protocol yet. It is recognised that salt marshes do provide very useful ecosystem services (Boorman 2003) and they provide excellent buffers against storms and other extreme events (Möller 2006). In the Essex estuaries experiments have been carried out in managed realignment of the coastline, due to erosion of fringing salt marsh areas (Garbutt et al. 2006). The program is successful in terms of providing more space for coastal ecosystems, but it was found out that the biodiversity of recreated salt marsh areas is lower than untouched salt marshes considerably, even 50 years after recreation (Garbutt and Wolters 2008). Salt marsh species richness can be enhanced by allowing grazing in salt marshes (Bakker 1985; Adam 1990; Bos et al. 2002), although overgrazing can lead to destruction of the top soil in lower parts of the marsh, thereby decreasing species richness (Bakker 1989).

The development of novel methods for mapping of salt marshes is needed to improve monitoring of their environmental, anthropogenic and ecological dynamics. This thesis contributes to these issues by researching novel methods for mapping vegetation habitats in salt marsh areas using remote sensing technologies.

### **2.3. Remote sensing technologies**

Remote sensing (RS) sensors, either deployed on airborne or spaceborne platforms, have proven to be invaluable tools for the mapping and monitoring of the natural environment (Barrett 2013). Natural habitats are often difficult to access from the ground, making ground-based surveys difficult, more subjective and less cost-effective than remote sensing studies (Mumby et al. 1999).

Most of the common remote sensing sensors are operational in the electromagnetic spectrum (Vincent 1997). Table 3 describes three of the most widely used remote sensing sensors: optical, Light Detection and Ranging (LiDAR) and Synthetic Aperture Radar (SAR), with their respective advantages and disadvantages.



Table 3– Overview of the three most common remote sensing sensor types (Lillesand et al. 2004; Wooster 2007).

Sensor	Advantages	Disadvantages
Optical	<ul style="list-style-type: none"> <li>• Passive sensors; limited power consumption,</li> <li>• Intuitive imagery, operating in similar way to human eye or camera,</li> <li>• High spatial resolution, up to 0.2-0.5 meter resolution from spaceborne systems,</li> <li>• Large data archives available,</li> <li>• Well-established data processing and classification routines.</li> </ul>	<ul style="list-style-type: none"> <li>• Cloud and atmosphere sensitive, resulting in unwanted variations of emissivity and data gaps,</li> <li>• Reflected sunlight needed for operation; no data acquisition at night.</li> </ul>
LiDAR	<ul style="list-style-type: none"> <li>• Precise topography acquisition,</li> <li>• Active sensor, operation independent of daylight conditions.</li> </ul>	<ul style="list-style-type: none"> <li>• Active system, large power consumption.</li> <li>• Limited deployment on spaceborne platforms so far, commonly deployed on airborne platforms.</li> </ul>
SAR	<ul style="list-style-type: none"> <li>• Active sensors, data acquisition possible day and night,</li> <li>• Little sensitivity to atmospheric condition, solid data acquisition and repeatability,</li> <li>• Information about structural/geometric features and dielectric properties of subsurface,</li> <li>• Different wavelengths and polarisations available,</li> <li>• Interferometric capabilities; displacement and topographic modelling.</li> </ul>	<ul style="list-style-type: none"> <li>• Lower spatial resolution,</li> <li>• Higher energy consumption; expensive deployment on spaceborne platforms,</li> <li>• Signal difficult to interpret.</li> <li>• Few established processing and classification routines available.</li> </ul>

Research into SAR sensors has led to successful applications (Schmullius and Evans 1997; Koch 2010; Hensley et al. 2012), but it lags behind the application development with optical sensors. SAR systems are more complex to deploy and the generated data is less intuitive than optical data and requires specialist knowledge to understand. However, obvious advantages of SAR sensors are more reliable and repeatable data acquisition and information about structural characteristics of surface targets, which justifies research of new applications of these sensors. Therefore, in the following

review of literature on the research and use of RS technologies for coastal mapping and management, special attention is given to research incorporating SAR.

## **2.4. Research of RS for coastal mapping and monitoring**

This section describes recent and on-going research into the use of remote sensing techniques for mapping of salt marsh habitats. Research gaps will be identified that can support the formulated research questions. These are indicated in *italic*.

### **2.4.1 Operational projects**

Several RS projects have been initiated to research and develop operational tools for ICZM. The European Commission and the European Space Agency support a number of RS research projects that research and apply Earth Observation (EO) techniques to support the marine side of ICZM. Coastwatch, which was part of the European Space Agency (ESA) GMES Service Element (GSE) programme has finished in 2007 (Coastwatch 2010; GMES 2011). This project provided water quality products (Chl-a, Secchi depth, suspended sediment). The oceanographic part of the Copernicus program is now incorporated in myOcean (myOcean 2011). Projects with a terrestrial focus comprise EUROSION, a project focussed on mapping of erosional processes along the shorelines of Europe (Doody et al. 2004). A project involving InSAR applications is the Copernicus-funded FP7 project *subCoast* (subCoast 2011), a successor to the ESA GSE TerraFirma project. This project involves monitoring of vertical movements (subsidence or uplift) of low-lying coastal areas by interferometric SAR. The BIO\_SOS project researches monitoring of ecological habitats using different EO technologies (Nagendra 2011). It has been acknowledged use of SAR in addition with optical data could improve habitat mapping (Nagendra et al. 2013). In this report it was mentioned that SAR is able to distinguish land cover types that are spectrally similar, but structurally different.

In the UK, the Environmental Agency (EA) carries out a regular salt marsh mapping project around the UK (Environment Agency 2011). This mapping effort has focussed on salt marsh extent change, based on aerial photography solely. It is the first nationwide salt marsh mapping effort since the 1980s and part of the UK's obligation to map coastal habitats within the Water Framework Directive. Another project in Scotland is carried out by the Scottish Environmental Protection Agency (SEPA) (Stevens 2009).

This project was based on the use of airborne hyperspectral RS data to map intertidal habitats.

In a report for DEFRA in 2007 it was stated that RS is essential for the monitoring of climate change impacts on coastal areas, and that the biggest opportunity of RS in coastal zone management lies in habitat mapping of intertidal areas, especially with regard to the new and upcoming satellite sensors becoming available over the next few years (Pradhan 2007). JNCC has acknowledged the potential usefulness of new EO sensors with regard to habitat mapping (Medcalf et al. 2011). Accordingly, the Crick Framework was recently drafted to define how RS technologies can contribute to habitat mapping (JNCC 2011). According to this framework, more investigation is needed to test the applicability of Very High Resolution (VHR) EO imagery for the identification of different salt marsh habitats.

*A number of (semi-)operational RS projects have been initiated over the last decade to aid ICZM. However, there has been no project that has included operational use of SAR for mapping and monitoring of coastal habitats.*

#### **2.4.2 Use of RS for mapping of coastal dynamics**

Coastline dynamics (erosion and accretion) can have profound effects on economic activity, coastal security and coastal habitats. Therefore, it is essential to research and monitor geomorphological processes to shape coastal areas. Research into the use of RS for mapping and monitoring of coastal dynamics has been carried out frequently.

The repetitive nature of data acquisition of spaceborne platforms provides an excellent opportunity to monitor the changes of coastline position on a regular basis. A recent overview of the remote sensing of coastlines is provided by (Gens 2010), which summarises different RS technologies and approaches for monitoring of coastal areas. Several EO methodologies have been developed to delineate coastlines, including SAR tools, during the last twenty years. A major advantage of SAR for morphological mapping is strong backscatter contrast between land and sea, which can be less clear in optical imagery. Lack of temporal resolution of spaceborne SAR systems (only operational since 1991) has led to multi-sensor studies combining optical, airborne and spaceborne SAR data to construct multiple decade-spanning, time series (Souza-Filho

and Paradella 2003). A number of methodologies have been proposed to identify coastline location from SAR imagery (Yu and Acton 2004; Shu et al. 2010). Automated systems to delineate flood extent have been developed at DLR, which have been successfully applied to delineate the position of the coastline (Hahmann et al. 2008).

In macro-tidal areas, coastline position extracted from RS imagery is merely a representation of the tidal level at the moment of overpass (Lee et al. 2011). This is used to develop a Digital Terrain Model (DTM) with the waterline method (Mason et al. 2010). This method is based on extraction of waterlines from a number of different RS images, acquired at different tidal levels. It is possible to construct a DTM by assigning a vertical height to the extracted water-land boundaries corresponding to tidal levels at time of acquisition. The main assumption of this method is unchanging morphology of the intertidal flats over the imagery acquisition period.

Hong et al. (2010) researched wetland water level fluctuations in Florida, using repeat pass interferometric SAR (InSAR) data. It was found that SAR data can be used successfully for monitoring of water level changes, because flooded vegetation creates stable double bounce scatterers (more on this in Chapter 3). Although this double bounce effect benefits water level modelling, it complicates the delineation of flood extent under flooded vegetated areas. A number of studies have been done to investigate how this problem can be overcome (Kasischke and Bourgeau-Chavez 1997; Henderson and Lewis 2008), focussing on mapping of flooding regimes in wetland coasts of Florida. With increasing availability of multi-polarimetric SAR platforms new possibilities for flood monitoring are being researched. It has been shown that polarimetric decomposition (which analyses the SAR response according to different types of surface scattering mechanism, more in Chapter 3) can be applied successfully in detecting change in wetland environments (Schmitt et al. 2010; Brisco et al. 2011).

Fluctuations of soil moisture and soil salinity can impact the ecology of intertidal habitats. Soil moisture and salinity of salt marshes change along the slope from sea to land. Intertidal habitats are adapted to specific ranges of soil moisture and salinity. Soil moisture values correlate with SAR backscatter signatures (Kasischke and Bourgeau-Chavez 1997); thus a combination of optical data and SAR can be used to monitor of vegetation and soil moisture dynamics in wetlands (Dabrowska-Zielinska et al. 2009).

Intertidal sand and mudflats are located below the pioneer zone of lowest salt marsh vegetation habitats. Intertidal sand and mudflats are flooded during every high tide. Research of SAR for mapping of intertidal mudflats and their geological composition with SAR has shown that variations in SAR backscatter from intertidal mudflats are related to surface roughness, which in turn correlates with sedimentary structures (ripple structures at the surface of intertidal flats) and inherent grain size (van der Wal et al. 2005). Mapping of intertidal sediment mapping is improved by using multi-frequency SAR data (Gade et al. 2008).

A thin layer of remaining water during low tide can affect radar backscatter by creating a specular scatterer (Gade et al. 2008). Effect of this phenomenon is low backscatter and low signal-to-noise ratio. Soil moisture variability of intertidal flats in different stages of the tidal cycle has been modelled by using multi-temporal SAR data images (Lee et al. 2011). Soil moisture on intertidal mudflats changes during the tidal cycle due to drainage, evaporation and tidal inundation, and has a significant effect on SAR backscatter.

*Research into the use of RS for mapping and monitoring of coastal dynamics has shown that these technologies provide useful tools. The integration of SAR data in mapping coastal dynamics has been researched with changeable success. The impact of environmental factors can have a significant impact on SAR backscatter signatures. Further research into the impact of environmental factors on SAR backscatter for the mapping of salt marsh habitats is needed.*

### **2.4.3 Use of RS for salt marsh vegetation mapping**

The applicability of RS tools for mapping of natural habitats is actively researched (JNCC 2011; Nagendra 2011; Corbane et al. 2015). As an example, a habitat classification of the natural habitats of Wales has been compiled, the first of its kind on a national scale (Lucas et al. 2011). Very High Resolution (VHR) optical RS data (SPOT, aerial photography) was used to create rule-based classification schemes for identification of vegetation habitats of Wales and the research suggested that the use of SAR would improve habitat classification initiatives. The EA carries out surveys of salt marsh vegetation extent approximately every ten years, based on high-resolution

aerial photography. Due to the use of different methodologies, there are significant differences in estimated salt marsh extent (Environment Agency 2011). The most recent survey was carried out in 2010, using aerial photography datasets acquired between 2006 and 2009. Airborne photography and LiDAR are commonly used to map salt marshes habitats and other low-lying coastlines. As Hladik and Alber (2014) have shown, GIS variables extracted from a single LiDAR Digital Elevation Model (DEM) input layer in a salt marsh setting can be used successfully for classification of salt marsh habitats. Most of the variables they used were derived from one DEM input layer, the combination of these variables provided different contributions to the classification model. Their RS model was more accurate than the model based on non-RS GIS variables.

According to Corbane et al. (2015), the use of active microwave sensors (e.g. SAR) is generally unsuitable for mapping of wetlands, although it has been acknowledged that SAR does provide complementary information about vegetation structure to multispectral optical imagery. Maghsoudi et al. (2013) found that vegetation classification (in their case a boreal forest) based on SAR generally results in moderate classification accuracies.

A number of studies into the use of satellite imagery for mapping coastal habitats have been carried out, review articles are provided by Adam et al. (2010) and Klemas (2011). Recent examples of coastal wetland mapping are the discrimination of different plant species communities in small coastal wetland research areas with VHR multispectral optical imagery (Lu et al. 2004; Tuxen et al. 2011), as well as coastal habitat mapping studies based on hyperspectral imagery (Belluco et al. 2006; Gilmore et al. 2008; Stevens 2009). Tuxen et al. (2011) have shown that vegetation indices like the Normalised Difference Vegetation Index (NDVI) have shown to be very useful for distinction between vegetation, bare soil and waterbodies. It has also been found that multi-temporal RS imagery analysis can improve wetland classification by using seasonal variations of different habitats (Davranche et al. 2010). Use of LiDAR for monitoring of intertidal has shown to provide information about vegetation structure as well as geomorphological features (Mason et al. 2006; Gilmore et al. 2008).

Early research into the use of SAR to discriminate different vegetation habitats by Kasischke et al. (2003) showed that different wetland vegetation habitats can be

discriminated with SAR, but that backscatter signature is significantly affected by flood level and soil moisture variations. More recent research into use of SAR for classification of salt marsh habitats has been researched (Choe et al. 2011; Dehouck et al. 2011; Gade et al. 2011; Lee et al. 2012). All the above studies found that combining SAR, optical and elevation data generated better results than the use of either alone optical or SAR data. Clint Slatton et al. (2008) showed that a combination of multi-frequency SAR data (quad-polarimetric C-band and L-band airborne SAR) with LiDAR can be used to identify seasonal variations in an intertidal coastal marsh. Furthermore it was found that L-band data generated better classification results than C-band data. The differences in behaviour between SAR frequency bands will be discussed in Chapter 3.

Analysis of multi-temporal data sets showed that polarimetric SAR is capable of detecting phenological changes of salt marsh vegetation throughout the year (Lee et al. 2012). Annual salt marsh vegetation species show distinctive seasonal growth and senescence, whereas perennial species do not change much in size or shape throughout the seasons. The optimal moment to distinguish between these two types of vegetation is winter, when the annual species are senescent.

Lee et al. (2012) also researched the effect of salt marsh creeks and channels on SAR backscatter. Some of the creek and channel walls faced the radar platform, which resulted in very strong radar backscatter returns. This led to misclassifications and it was advised to include high-resolution DTM data to correct for this. One of the main recommendations of this research was to investigate how the use of quad-polarimetric and polarimetric decomposition routines can improve habitat mapping. They argued that: 'when the microwave scattering mechanisms associated with herbaceous halophytes and the surrounding areas are fully understood via a polarimetric scattering decomposition approach, it will greatly contribute to tidal flat studies.' Polarimetric decomposition of SAR data has been developed to model scatter mechanisms of surface features, improving extraction of information from SAR data (Cloude and Pottier 1997; Freeman and Durden 1998), its potential advantages are reviewed in Chapter 3.2.3.

Intertidal sand and mudflat habitats have been mapped with multi-frequency SAR by Gade et al. (2011). They argued that different sediment types (gravel, sand and mud),

macrophytes and mussel beds could be distinguished with SAR data, primarily due to different surface roughness of the different land cover types. Oyster and mussel beds were detected because of differences in surface roughness (Adam et al. 2010), findings that were confirmed in a Korean intertidal flat and salt marsh (Choe et al. 2011). Here it was found that oyster beds can be detected by analysing the polarimetric SAR signatures. Oyster beds primarily created volumetric backscattering; the main scatter mechanism observed on sand and mudflats was surface scattering.

*Mapping of salt marsh vegetation habitats has usually been carried out with multispectral optical and/or LiDAR data, usually focussing on vegetation extent, without considering mapping different salt marsh vegetation habitats. Limited research has included SAR to complement mapping of salt marsh habitats, due to limited availability and complex processing and interpretation. Increased availability of polarimetric SAR and development of polarimetric decomposition routines have potential to expand the applicability of SAR in salt marsh mapping. Combination of optical, LiDAR and SAR RS data to map salt marsh habitats has never been done before.*

#### **2.4.4 Use of RS for estimation of vegetation biophysical parameters**

Research into correlation between RS variables and vegetation biophysical parameters have been carried out intensively (Le Toan et al. 1992; Beaudoin et al. 1994; Schmullius and Evans 1997; Woodhouse 2006). SAR data has shown to have a significant correlation with vegetation biomass (Le Toan et al. 1992). Englhart et al. (2011) have researched the use of two different SAR frequency bands to estimate biomass in a tropical peat swamp. It was found that combining the two frequency bands in one regression model yielded more accurate results over the whole biomass range than a model based on one single SAR frequency band. It has been shown that SAR is capable to estimate height of objects (Guida et al. 2010), which can be used to model the height of vegetation. Additionally, LiDAR data is used for estimation of vegetation height and correlation with biomass in peat swamps (Englhart et al. 2011) or mangrove forests (Fatoyinbo and Simard 2012). Wang et al. (2009) have used LiDAR data for modelling vegetation height in salt marshes. They found that grassy and shrubby



vegetation associated with salt marsh habitats limited the potential to use LiDAR data to construct a reliable vegetation height model.

*Using multiple RS data sources to model biophysical parameters in salt marsh vegetation habitats is not commonly done, although previous studies in different natural habitats have shown that correlations of biophysical parameters with aggregate RS data sets are usually stronger than with RS data sets based on a single RS sensor.*

## **2.5. Literature review summary**

The management of coastal zones is a complex task. Coastal areas provide ecosystem services, as well as principal location for economic and social development. However, they have a very dynamic nature and are vulnerable to environmental and climatic changes. This suggests the need for reliable and timely mapping and monitoring in order to support their management.

Salt marsh habitats provide valuable ecosystem services like natural storm buffers and food provision. The ecosystem service value of salt marshes is being acknowledged, and in the UK current salt marsh management practices focus on preservation and restoration of these habitats. Within salt marsh habitats distinct vegetation zonations can be identified, ranging from non-vegetated sand and mudflats on the seaward side, via pioneer vegetation and grass meadows to shrubby areas in the land-ward sections. Remote sensing technologies have been shown to be capable tools for mapping and monitoring of salt marsh areas. The synoptic capabilities of earth observation technologies facilitate information acquisition in inaccessible areas and provide an objective and consistent platform for mapping and monitoring purposes. Remote sensing research into mapping and monitoring of salt marsh habitats has been carried out to a limited extent. Most effort has been put into the mapping of changes in extent of salt marshes; the mapping of different vegetation habitats has only been tested in pilot studies.

New remote sensing technologies provide new opportunities for mapping and monitoring of habitats. For example, data acquired from SAR sensors can provide new tools that can complement existing coastal habitat mapping. It has been shown that

SAR is capable of mapping and monitoring vegetation. SAR is virtually weather-independent and provides information about the earth's surface that complements optical and LiDAR RS data. The application of SAR technologies for salt marsh habitats mapping and monitoring has rarely been studied, even though these habitats and their environmental setting provide a unique area of research.

### **2.5.1 Research gaps**

The Literature Review identified a number of critical research gaps in relation to RS of ICZM. These are re-stated below:

- A number of (semi-)operational RS projects have been initiated over the last decade to aid ICZM. However, there has been no project that has included operational use of SAR for mapping and monitoring of coastal habitats.
- Research into the use of RS for mapping and monitoring of coastal dynamics has shown that these technologies provide useful tools. The integration of SAR data in mapping coastal dynamics has been researched with changeable success. The impact of environmental factors can have a significant impact on SAR backscatter signatures. Further research into the impact of environmental factors on SAR backscatter for the mapping of salt marsh habitats is needed.
- Mapping of salt marsh vegetation habitats has usually been carried out with multispectral optical and/or LiDAR data, usually focussing on vegetation extent, without considering mapping different salt marsh vegetation habitats. Limited research has included SAR to complement mapping of salt marsh habitats, due to limited availability and complex processing and interpretation. Increased availability of multi-frequency and quad-polarimetric SAR and development of polarimetric decomposition routines have potential to expand the applicability of SAR in salt marsh mapping. Combination of optical, LiDAR and SAR RS data to map individual salt marsh habitats has never been done before.
- Using multiple RS data sources to model biophysical parameters in salt marsh vegetation habitats is not commonly done, although previous studies in different natural habitats have shown that correlations of biophysical parameters with aggregate RS data sets are usually stronger than with RS data sets based on a single sensor.

### **2.5.2 Research questions**

From the research gaps the following over-arching Research Question has been deducted:

**To what extent can multi-frequency polarimetric SAR contribute to the mapping and monitoring of coastal salt marsh habitats?**

This over-arching Research Question can be split in three specific Research Questions, which are guidance for the research experiments carried out in this thesis:

- 1. How are polarimetric SAR backscatter signatures affected by salt marsh characteristics, like specific environmental parameters (sea level, soil moisture or soil salinity) or botanical structure?*
- 2. Does the inclusion of SAR in a RS data set based on optical and LiDAR data improve mapping of both salt marsh extent and individual salt marsh habitats?*
- 3. Is a combined RS data set from optical, LiDAR and SAR sensors better suited for regression modelling of biophysical parameters (vegetation cover, height and volume) than regression models based on a data set based on a single RS sensor?*

### 3. SAR remote sensing

The research presented in this thesis has been data-driven, focussing on a particular SAR data set (further described in Chapter 4.2.3). Therefore, most attention is given to the pre-processing and extraction of parameters from this SAR data set. This chapter provides a summary of the most important principles of SAR remote sensing, explaining the underlying physical principles of scatter, as well as presenting the polarimetric decomposition models used in this thesis.

#### 3.1. SAR introduction

SAR remote sensing can be dated back to the 1950's, when the principles of Doppler beam-sharpening concepts were developed (Richards 2009). This section will explain some of the basic principles of radar and more specifically SAR remote sensing, as well as give an overview of the current status of technological development.

The microwave domain used in remote sensing ranges from 0.3 GHz (wavelength 100 cm) to about 20 GHz (wavelength 1.5 cm) (Richards 2009). This range is subdivided into bands with specific names (Table 4):

*Table 4 – Microwave bands used in remote sensing.*

<b>Band name</b>	<b>Frequency (GHz)</b>	<b>Wavelength (cm)</b>
P-band	0.3-1.0	30-100
L-band	1.0-2.0	15-30
S-band	2.0-4.0	7.5-15
C-band	4.0-8.0	3.75-7.5
X-band	8.0-12.5	2.4-3.75
Ku-band	12.5-18.0	1.7-2.4

A number of publications have been dedicated to explain the principles of SAR RS to great detail (Woodhouse 2006; Lee and Pottier 2009; Richards 2009). The following paragraphs provide a short summary, with special focus on SAR principles most appropriate for this research.

##### 3.1.1 Radar platforms

Radar platforms have a common observational configuration (Figure 4) in which the antenna on the platform emits radar pulses laterally, 90 degrees to the direction of

platform travel, with a certain angle from the vertical (nadir), the incidence angle. The direction of flight is the 'azimuth' direction; the area perpendicular to the flight direction is the 'range' direction. The radar pulse has a specific opening angle in slant range direction, nearest to the sensor is called the near slant range, furthest away the far slant range. The area covered between this is the swath width.

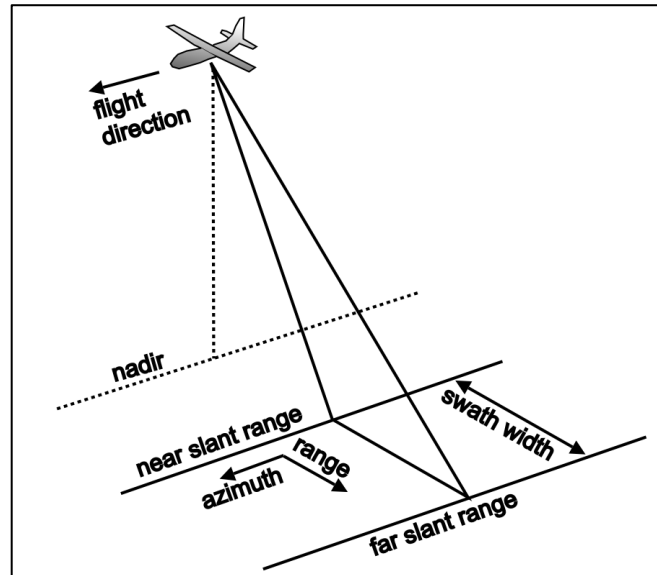


Figure 4 – Geometry of SAR acquisition platform, oblique view.

The angle of incidence (see Figure 5) has influence on the amount of energy and the geometric distortion of the returned signal. The backscattered signal from near slant range will be higher in intensity than the signal backscattered from far slant range, due to the shorter pathway the signal travels and the lower incidence angle and therefore with less signal attenuation. During data processing, a normalisation correction has to be applied to overcome these geometric differences. In areas with strong topography, geometric distortion phenomena occur due to differences in signal travel times. Foreshortening is observed when the backscatter from the base of a tall feature (like a mountain) tilted towards the SAR sensor is received before backscattered signal from the top is received. Because the SAR system measures distance in slant range, the slope of the object will appear compressed and the length of the slope will be represented incorrectly. When signal backscattered from the top is received earlier at the antenna than signal backscattered its base geometric layover is observed. Signal shadowing is observed from areas that are placed behind objects, with regard to the SAR sensor. However, in low-lying and flat coastal regions, these geometric distortions

are very small, although strong backscatter can be observed from slopes tilted towards the sensor, like channel walls.

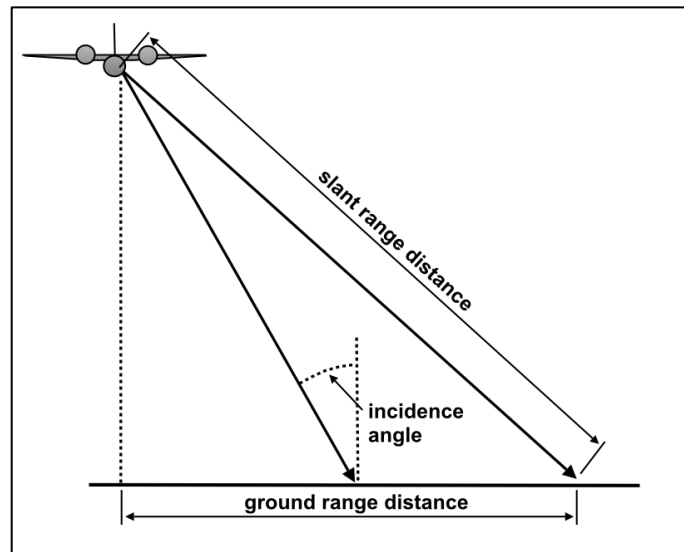


Figure 5 – Geometry SAR acquisition platform, frontal view.

The radar transmitter emits radar pulses with a certain beamwidth in the azimuth direction. If pulses are backscattered to the antenna, the received signal will consist of a combination of backscatter from a range of targets that fall within this beamwidth (Richards 2009). The quality of the backscattered signal rapidly deteriorates with increasing distance between the radar sensor and the target on the ground. To receive the backscattered signal from a specific target at a large distance with fine resolution, the receiving antenna should be of sufficient physical length, which cannot be achieved for sensors in space or with difficulty on airborne platforms. To overcome this problem, SAR systems have been developed. SAR uses the forward motion of the platform to create a 'synthetic aperture' by using signal returns from a position the platform is laterally still ahead of a certain target until it has passed it, using the respectively first, intermediate and last returns from a wide beam. By recording a sequence of signal returns from the same ground feature, as it is passed by the leading, central and trailing sections of the wide beam, correcting each return using the Doppler shift (a higher microwave frequency is received back when the platform is ahead of a target and a lower frequency when the platform has passed a target, just like the siren sound of a passing ambulance) a synthetic (long) aperture (i.e. a pseudo long antenna) can be created. This can be used to sharpen and improve the quality of the resulting SAR image in azimuth direction.

### **3.1.2 Airborne SAR systems**

Airborne SAR systems have fewer technological limitations than spaceborne SAR systems in terms of power supply, weight and resolution. Therefore airborne systems can consist of multiple frequency bands and full polarimetric capabilities (Reigber et al. 2013). Added to this, a major advantage of airborne SAR surveying over spaceborne systems is higher spatial resolution (Hensley et al. 2012), often sub-metre pixel size in azimuth and range directions. Systems can be operational in multiple microwave frequency bands simultaneously, and new systems are tested to provide scientific input for proposed satellite missions (Natale et al. 2011).

### **3.1.3 SAR speckle**

Radar images have a distinctive speckled, or 'salt and pepper noise' appearance. The resulting grainy appearance is commonly referred to as speckle noise. It is observed in all coherent imaging systems and can be attributed to interference among the coherent backscatter echoes of individual scatterers within a resolution cell (Woodhouse 2006). The interference pattern that exists in the scattered wave is effectively chaotic and unpredictable; it is effectively a random pattern. This randomness is visible in the radar image as speckle. The interference of the different scatterers within one resolution cell can be constructive (amplification of the backscatter intensity) or destructive (suppression of the backscatter intensity). An important aspect of speckle is that causes differentiation in areas with homogeneous cover, i.e. the backscatter signal from one cell can differ substantially from the signal from an adjacent cell of similar composition (Richards 2009).

One way to correct for speckle is the multilook method, in which the azimuth beam of the radar system is split in a number of sub-beams (Oliver and Quegan 2004). In this way each resolution cell is 'looked at' by every sub-beam during the passing of the SAR antenna from different directions (from forward looking to backward looking). The result is that speckle variation for each cell can be estimated and be averaged. The resulting images have improved radiometric resolution. Disadvantage is the degradation of geometrical resolution, depending on the number of looks defined. Therefore in general a balance is sought between these two resolutions (Woodhouse 2006).

Additionally, specific spatial filters have been developed that use statistical estimations to suppress speckle noise while keeping intact the geometric resolution. Some of the most commonly used are the Enhanced Lee (Lee et al. 2009) and Frost filters (Frost et al. 1982). These filters aim to filter strongly in homogeneous areas, like waterbodies while preserving radiometric variance in heterogeneous zones like built-up areas.

### **3.2. SAR polarimetry**

Even though the concept of radar polarimetry is relatively understandable, the acquisition, description and interpretation of polarimetric radar data pose some of the most challenging aspects of remote sensing as a whole (Woodhouse 2006). This section aims to describe the most important fundamentals, without delving too deeply into the underlying mathematical and physical complexities.

Research and development of applications of polarimetric SAR has been successful in a number of domains (Schmullius and Evans 1997; Zhang et al. 2008; Reigber et al. 2013). In comparison to conventional single channel SAR, the inclusion of SAR polarimetry consequently leads to a significant improvement in the quality of classification and segmentation results (Cloude and Pottier 1997; Lee et al. 1999). Polarimetric SAR is applied in land-use classification, forestry monitoring, ground surface roughness and soil moisture estimation (Lee and Ainsworth 2010). More advanced technologies such as polarimetric interferometric SAR (Pol-InSAR) data are used for SAR tomography, for example the three dimensional modelling of vegetation structures (Lee et al. 2004). An increasing number of operational polarimetric SAR systems on either airborne or spaceborne platforms require further research and development of applications (Reigber et al. 2013).

The polarimetric signature of microwaves is defined as the direction in which the electric field oscillates. Electromagnetic waves oscillate transversely (i.e. perpendicular to the direction of the wave), which adds another parameter to describe the wave: the direction in which this oscillation takes place, the polarisation (Woodhouse 2006). If the propagating electric field oscillates in a vertical direction with regard to a plane parallel to the earth's surface, it is named vertical polarisation. A field that oscillates in the horizontal direction is polarised horizontally. SAR antennae are capable of emitting and receiving radar pulses in specific polarimetric directions, most commonly in



horizontal (H) and vertical (V) directions. Different sensors operate with different polarimetric capabilities. SAR sensors that transmit in one polarimetric direction (which can be H or V) and receive in the same polarimetric direction are named single polarimetric systems. Systems that transmit in either H or V, but receive in both H and V are dual-polarimetric systems. Systems that transmit in both H and V and also receive in H and V are called quad or fully polarimetric systems. Fully polarimetric SAR systems with advanced polarimetric capabilities are very sophisticated and therefore expensive. This means that the installation of a fully polarimetric system on a spaceborne platform is risky in terms of technical failures and financial losses. Therefore single or dual polarimetric systems are often preferred over fully polarimetric systems.

Backscatter intensity of HH, VH, HV and VV polarimetric channels can be expressed in intensity decibel units (dB). Usually, SAR intensity channels are expressed in sigma-nought ( $\sigma^0$ ), which is a normalised coefficient of backscatter intensity that takes into account the size of the footprint or a pixel (Woodhouse 2006).

### 3.2.1 Scattering matrix

Polarimetric data incorporates a wealth of information about the ground surface that the radar pulses interact with. Even though the underlying physical description is very complex, a brief overview of the principles is provided here. For a more comprehensive explanation of polarimetric principles, (Richards 2009) and (Woodhouse 2006) are recommended reads.

The most common way to describe polarimetric SAR data is by means of a scattering matrix S:

$$\begin{bmatrix} E_h^s \\ E_v^s \end{bmatrix} = \begin{bmatrix} S_{hh} & S_{hv} \\ S_{vh} & S_{vv} \end{bmatrix} \begin{bmatrix} E_h^i \\ E_v^i \end{bmatrix} \quad (1)$$

It describes the transformation of the electromagnetic field ( $E$ ) of the incident wave (with superscript  $i$ ) to the electromagnetic field of the scattered wave (with superscript  $s$ ) for all polarizations ( $S_{HH}$ ,  $S_{HV}$ ,  $S_{VH}$  and  $S_{VV}$ ). The four elements of the scattering matrix can be obtained from the magnitudes and phases measured from the four channels of a polarimetric radar system. In monostatic radar systems (i.e. the emitting and receiving antennae on the same platform) the  $S_{HV}$  and  $S_{VH}$  factors are assumed to

perform in the same way. This assumption means that the SAR system is reciprocal ( $S_{HV} = S_{VH}$ ), the scatter matrix consists of only three independent elements:  $S_{HH}$ ,  $S_{VV}$  and either  $S_{HV}$  or  $S_{VH}$ . The scattering vector or covariance vector  $k_c$  is a vectorised version of the scattering matrix. Assuming reciprocity this vector is:

$$k_c = \begin{pmatrix} S_{hh} \\ \sqrt{2}S_{hv} \\ S_{vv} \end{pmatrix} \quad (2)$$

This vector can be expressed in a power-domain representation of the scattering properties, which is done by forming the product of this vector with itself.

$$C = k_c \times k_c^+ = \begin{pmatrix} |S_{hh}|^2 & \sqrt{2}S_{hh}S_{hv}^* & S_{hh}S_{vv}^* \\ \sqrt{2}S_{hv}S_{hh}^* & 2|S_{hv}|^2 & \sqrt{2}S_{hv}S_{vv}^* \\ S_{vv}S_{hh}^* & \sqrt{2}S_{vv}S_{hv}^* & |S_{vv}|^2 \end{pmatrix} \quad (3)$$

In this matrix the + denotes the conjugate transpose and \* the conjugate. The advantage of the covariance matrix is that it represents the power of the electromagnetic field; it relates the power of the scattered wave to the power of the incident wave (CCRS 2008).

The scattering matrix can also be expressed in a coherency vector. This is closely related to the covariance vector and is preferred by some analysts, because each of its elements has a physical interpretation. It takes the following shape:

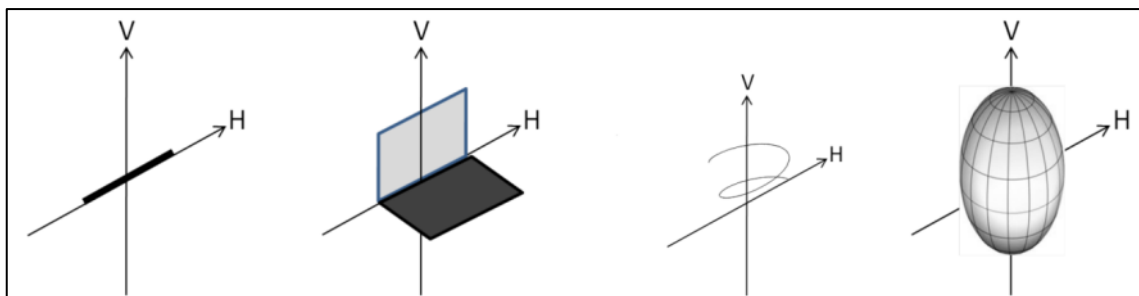
$$k_T = \frac{1}{\sqrt{2}} \begin{pmatrix} S_{hh} + S_{vv} \\ S_{hh} - S_{vv} \\ 2S_{hv} \end{pmatrix} \quad (4)$$

The three elements of the vectors are often used in SAR image analysis, as the elements closely relate to the odd-bounce, even-bounce and diffuse bounce scatter mechanisms (Richards 2009).

### 3.2.2 Scatter mechanisms

A next level of complexity in the interpretation of polarimetric microwave data involves an understanding of the scattering mechanisms present. Polarimetric decomposition methods have been developed over the last two decades to extract specific scatter mechanisms from the scatter matrix. Scatter mechanisms are pathways

that the radar signal takes when it interacts with features (targets) on the Earth's surface (Freeman and Durden 1998). A natural target always shows a complex scattering response due to complexities in its reflectivity properties and geometrical structure. Therefore some elementary targets can be defined to describe the basic scattering mechanisms in order to provide a basis for describing more complex structures. Some of these elementary scatterers are dipole, dihedral, helix, and prolate spheroid scatterers (Figure 6). For further detailed information about basic scatterers and their properties, a good overview is provided by (Lee and Pottier 2009).



*Figure 6 – The shape of basic scatterers,  
From left to right dipole, dihedral, helix and prolate spheroid.*

Basic scatterers can be used to model the scatter mechanism, which is a description of the dominant scatter process of a certain surface material or target. Modelling these processes is done in the concept of polarimetric decomposition. Polarimetric decomposition theories are used to model the abstract scatter matrix into intuitively understandable scatter mechanisms. Three scatter mechanisms that are generally used for polarimetric decomposition modelling are (Touzi et al. 2004), (Figure 7):

1. Rough surface, single or odd-bounce scatter. This occurs over surfaces that have a certain roughness, like grasslands, bare soils or sea surfaces with a certain wave height. Surfaces that are smooth, like paved areas or calm sea cause specular reflection of the incident wave, reflecting the signal away from the sensor.
2. Double or even-bounce scatter. This occurs when the radar wave bounces on both the horizontal surface and a vertical structure, like tree stems or walls of buildings. As expected this scatter mechanism is dominant in built-up and forested areas.
3. Canopy, volume or diffuse scatter. This occurs most frequently on surfaces where the wavelength of the incident wave is able to penetrate the surface in

some way, and is often backscattered following a complex pathway. This scatter mechanism occurs often in shrubby vegetation, tree canopies or snow-covered terrain.

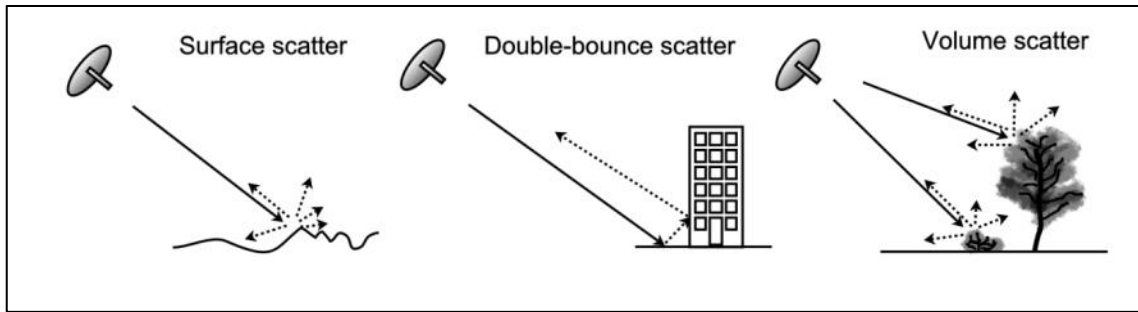


Figure 7 – The most common scatter mechanisms.

### 3.2.3 Polarimetric decomposition

Target decomposition is developed to express the average scatter mechanisms as the sum of independent elements in order to associate a physical mechanism with each scatter matrix element (Touzi et al. 2004). Many target decomposition routines have been developed (Touzi et al. 2004; Zhang et al. 2008; Lee and Ainsworth 2010). As polarimetric SAR signal behaves differently on different surfaces, a number of different polarimetric decomposition routines are developed for specific target domains (Zhang et al. 2008). A few of the polarimetric decomposition routines and associated specific classification algorithms which are most commonly used and relevant for this research are described in the following paragraphs.

#### 3.2.3.1 Cloude-Pottier decomposition

The Cloude-Pottier (CP) or H/A/ $\alpha$  polarimetric decomposition is proposed in Cloude and Pottier (1997). This decomposition theory is based on the coherency matrix, by extracting matrix eigenvalues and eigenvectors entropy ( $H$ ), anisotropy ( $A$ ) and an eigenvector value alpha ( $\alpha$ ). The coherency matrix is built from the complex scattering vector in Pauli basis (Cloude and Pottier 1997):

$$K_P = \frac{1}{\sqrt{2}} [S_{HH} + S_{VV} \quad S_{HH} - S_{VV} \quad 2S_{HV}]^T \quad (5)$$

This can be re-written into the coherency matrix:

$$[T] = \langle K_P K_P^T \rangle = \frac{1}{2} \begin{bmatrix} \langle |S_{HH} + S_{VV}|^2 \rangle & \langle (S_{HH} + S_{VV})(S_{HH} - S_{VV}) \rangle & 2\langle (S_{HH} + S_{VV})S_{HV} \rangle \\ \langle (S_{HH} - S_{VV})(S_{HH} + S_{VV}) \rangle & \langle |S_{HH} - S_{VV}|^2 \rangle & 2\langle (S_{HH} - S_{VV})S_{HV} \rangle \\ 2\langle S_{HV}(S_{HH} + S_{VV}) \rangle & 2\langle S_{HV}(S_{HH} - S_{VV}) \rangle & 4\langle |S_{HV}|^2 \rangle \end{bmatrix} \quad (6)$$

The eigenvalues and the eigenvectors of this matrix are the foundation for the CP decomposition parameters, which are representative for three independent scattering mechanisms (surface scattering, double bounce scattering and volume scattering). The importance of each mechanism is found by analysis of the eigenvalues and eigenvectors entropy, anisotropy and alpha angle.

Entropy ( $H$ ) represents the predominance of a certain scatter mechanism.  $H$  is a dimensionless feature that varies between zero and one, where zero is the effect of simple mechanism and  $H$ -values of one represent pure noise. In real-life scenarios,  $H$  is low on surfaces that are relatively smooth, like ocean surfaces or sand flats.  $H$  tends to be higher in vegetated areas, because of multiple scatter mechanisms.

Alpha angle ( $\alpha$ ) gives an estimate of the dominant scatter type and ranges between  $0^\circ$  and  $90^\circ$ . An  $\alpha$ -angle of  $0^\circ$  is related to single bounce or surface scatter, values near  $45^\circ$  are associated with even bounce or double-bounce scatter. Values near  $90^\circ$  are associated with multiple bounce or volume scattering.

Anisotropy ( $A$ ) is the third eigenvalue used in the CP decomposition. It is, like  $H$ , a dimensionless feature which ranges in value between zero and one. It describes the relation between the second and third scattering contribution. High values of  $A$  denote the presence of only two scatter mechanisms, whereas low  $A$ -values denote equal measures of a second and third scatter mechanism. In classification applications it is not very commonly used, but it can serve as an additional distinguishing feature (Schmitt et al. 2010).

### ***3.2.3.2 Freeman-Durden decomposition***

The Freeman-Durden (FD) decomposition is a target model-based decomposition theorem proposed by Freeman and Durden (1998). This decomposition routine is based on extraction of three different scatter mechanisms: surface or Bragg scatter from a moderately rough surface, double bounce scatter from a pair of orthogonal surfaces and volume or canopy scatter from a cloud of randomly oriented dipoles. A detailed description of the calculation of the different scatter mechanisms is beyond the scope of this thesis, more details can be found in Freeman and Durden (1998). It uses geometric surface target shapes to model microwave behaviour, resulting in the three different scatter mechanism models: volume scatter ( $P_v$ ), double-bounce scatter

( $P_d$ ) and surface scatter ( $P_s$ ). The advantages of this decomposition is that it is straightforward to interpret and well suited for classification of natural targets (Zhang et al. 2008). The disadvantages are that the decomposition theorem tends to overestimate volume scatter and produces erroneous negative eigenvalues for surface and double-bounce scatter (Van Zyl et al. 2011).

### ***3.2.3.3 Van Zyl decomposition***

The Van Zyl (VZ) polarimetric decomposition theorem is proposed by Van Zyl et al. (2011) as a modification to the three-component FD decomposition. It is a similar model-based decomposition and decomposes the scatter matrix in the same components: volume scatter ( $P_v$ ), double-bounce scatter ( $P_d$ ) and surface scatter ( $P_s$ ). However, it corrects for the over-estimation of  $P_v$  and the possible negative values of  $P_d$  and  $P_s$ , that can occur with the FD decomposition.

## **4. Research area and data processing**

This chapter describes the research methodologies used during the research. It has to be acknowledged that this research has been a data-driven research, focussing on the utilisation of a polarimetric SAR data set for habitat mapping in a salt marsh. One of the main aims of the research is to interpret the remote sensing analysis results of the in terms of the ecological and environmental processes taking place in the research area.

This chapter starts with a detailed description of the research area, focussing on the geomorphological setting, the ecology, current management practices and a justification why this particular area has been selected as research area. Subsequently, the remote sensing data used during this research will be described and the final part of the chapter presents the processing and analysis steps.

### **4.1. Research area**

The area of investigation was the Llanrhidian salt marsh complex, which is located along the southern coast of Wales, on the southern shore of the Burry Inlet. This inlet separates the Gower Peninsula from the mainland of Wales and forms the estuary of the River Loughor and is connected to the Bristol Channel (Prosser and Wallace 1999). The Burry Inlet and the wider area of the Camarthen Bay are designated Sites of Specific Scientific Interest (SSSI), one of the main reasons for this designation is the presence of the largest continuous salt marsh area in Wales (Countryside Council for Wales 2011). A number of environmental and ecological surveys have been carried out over the past two decades (Countryside Council for Wales 2005), including salt marsh habitat mapping (Farleigh 2010). Special mention is made to Prosser and Wallace (1999) have carried out detailed salt marsh vegetation habitat mapping based on the NVC classification. In general the area is regarded as one of the UK's most biodiverse salt marsh areas (Countryside Council for Wales 2015). The field surveys have been carried out in conjunction with the Countryside Council for Wales (now re-named to Natural Resources Wales), to ensure the quality of the recorded ecological field data. An overview map of the research area is shown in Figure 8.

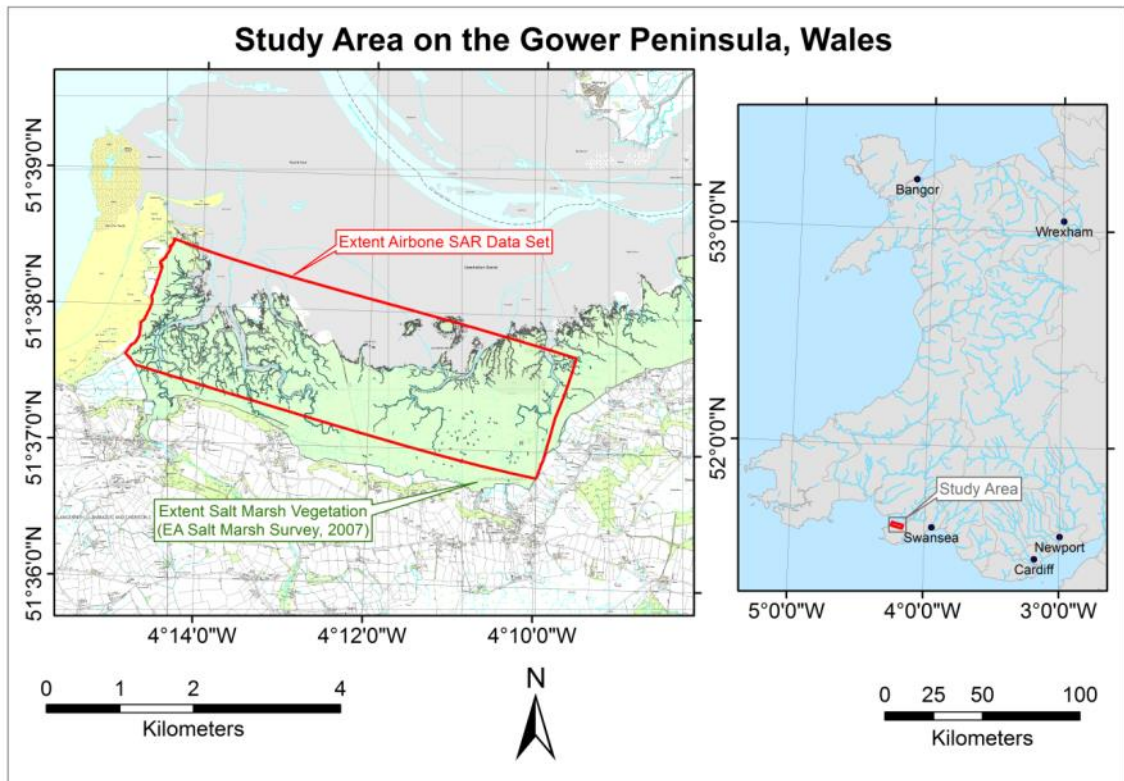


Figure 8 – Overview map of research area location in Wales.

#### 4.1.1 Geomorphological setting

The Llanrhidian salt marshes measure over 2000 ha in extent and represent almost 5% of the total area of salt marsh in the UK (May 2007; Environment Agency 2011). From a geomorphological point of view the marshes are of interest for the range of features they display: saltmarsh creeks, salt pans, erosion cliffs and a range of sediment types. The marshes have developed in a sequence from east to west: more mature marshes in the east display well-developed terraces and a marsh cliff undergoing erosion, whereas at Llanrhidian in the centre of the marshes pans and creeks are present and display much dissection. At Landimore in the west, an intricate and deep creek network can be found. The sequence of marshes makes this specific salt marsh area a key area for an understanding of saltmarsh dynamics, sediment transport and sea-level changes.

The marshes extend for about 15 km along the northern shore of the Gower Peninsula and are up to 1.5 km wide. In the western part near Landimore the marsh is sheltered by the Whiteford Burrows dune system and is the youngest part of the marshes. The central Llanrhidian Marsh is more exposed to waves entering the Burry Inlet from the west, but the eastern marshes near Crofty are in the more sheltered upper part of the



estuary. The spring tidal range is 6.6 metres and 3.7 metres at neap (Pye and French 1993). Fine-grained sediment deposition is restricted to the more sheltered upper intertidal zone and upper reaches of the estuaries. Finer sediment grain size can be found on higher topographical elevation (Carling 1981). Generally, the mean sediment grain size on the upper tidal flat are sands, on the marsh edge sandy silts, and on the upper marsh clayey silts (Pye and French 1993). The marsh-edge is widely marked by a low cliff formed during periodic storm activity. Gently sloping ramped margins occur in areas of pioneer marsh progradation. There are some weakly developed terraces, the transition being marked by low cliff, ramp or residual mud-mound topography. Many creeks on the upper marshes show infilling in response to a reduction in tidal capacity while the marshes grow both vertically and laterally (Pye and French 1993). Small-scale mass-movements in rills and creeks in the muddy intertidal zone play an important role in the changes in creek morphology, the supply of sediment into the creeks, and in intertidal drainage patterns (Allen 1989).

#### **4.1.2 Ecological setting**

Figure 9 provides a photographic overview of the major salt marsh vegetation habitats of the Llanrhidian Marsh; the photos were taken during a reconnaissance fieldwork in November 2012. Over the decades, some ecological field studies have been carried out in the Llanrhidian Marshes (Prosser and Wallace 1999). The Llanrhidian Marshes are notable for a number of transitional sequences of vegetation communities from pioneer through middle to upper marsh vegetation. These transitions are particularly well developed in the western reaches of the salt marsh near Landimore and in the central part near Llanrhidian. In the latter location *Juncus maritimus* cover an uninterrupted extensive area in excess of 150 ha. In Landimore, the Burry and Great Pill bisect the marsh and provide habitat for extensive areas of pioneer *Spartina anglica*. This species was introduced to Loughor in 1931 and colonised rapidly in the 1950s and 1960s, but appears to have declined since (Hubbard and Stebbings 1967). On the seaward end of the salt marsh, near the end of the Whiteford Burrows dunes, large areas of pioneer *Salicornia* have developed, and these are found along most of the lower reaches of the salt marsh.



Figure 9 – Photographic overview of major salt marsh vegetation habitats in the Llanrhidian Marsh.

The majority of the marsh is covered with *Festuca rubra* and *Puccinellia maritime* meadows. These areas are intensely grazed by cattle, the central part around the causeway from Weobly Castle resembles a bowling green (Prosser and Wallace 1999). There are some erosional edges in the central and eastern parts, near Llanrhidian. Here, a sudden transition from *Festuca rubra* meadows on higher terrain to and areas with dominantly *Spartina anglica* habitat on lower reaches is visible. The nett area of salt marsh vegetation is increasing (Environment Agency 2011).

### **4.1.3 Management practices**

The Llanrhidian Marshes are owned by the National Trust (Pembrokeshire Council 2011) and in use as common land, i.e. free for all to use within certain management limits. It is intensely used for grazing cattle, sheep and horses. Ungar and Woodell (1996) have carried out research on the marsh to assess the differences in botanical composition between grazed and un-grazed marshes. They found that grazing reduces plant species diversity. The Countryside Council for Wales (CCW), now re-named Natural Resources Wales (NRW), has advised to limit grazing to avoid the loss of plant diversity (Countryside Council for Wales 2005). The SMP for the Llanrhidian Marsh (Pembrokeshire Council 2011) mentions the marsh is in healthy condition and no intervention is needed to increase resilience to floods.

The EA is the UK's governmental organisation in charge of coastal protection and carries out a national salt marsh extent survey approximately every decade. The most recent survey was published in 2011 and is based upon aerial photography acquired in the years from 2006 and 2009 (Environment Agency 2011). The aerial photography for the Llanrhidian Marsh was acquired in 2007.

In 1998 CCW carried out a comprehensive ecological field survey to map the vegetation habitats according to the NVC classification was carried out (Prosser and Wallace 1999). The NVC classification scheme provides detailed habitat descriptions of salt marsh communities. NVC classifications can be converted to other habitat classification schemes, for this research the NVC classes were converted to the EU Habitat Directive Annex 1 classes for salt marsh habitats (JNCC 2006).

## 4.2. Data description and processing

This paragraph describes the remotely sensed data used in this research and the consecutive processing steps. Table 5 provides an overview of the different RS data sets used for this research.

*Table 5 – Overview of RS data used in this research.*

Mission	Sensor	Acquisition Date	Acquisition time (UTC)	Spatial resolution (m)	Tidal level The Mumbles (m CD)	Remarks
Airborne campaign	ADS40	02/06/2006	Not known	0.25 x 0.25	Not known	Visible light variables used, referred to as R, G and B
Airborne campaign	LiDAR	2007	Not known	2.0 x 2.0	+6.89, based on lowest DSM elevation	Digital Surface Model, referred to as DSM
Landsat-7	ETM	04/06/2010	11:03:04	30 x 30	+7.37	Used for NDVI calculation, variable referred to as NDVI_1
AirSAR campaign	Astrium SAR Demonstrator	28/07/2010	16:49:43	0.75 x 0.75	+5.20	Polarimetric channels HH, VV, HV, acquired in S-band and X-band
Landsat-5	TM	28/04/2011	11:00:34	30 x 30	+3.86	Used for NDVI calculation, variable referred to as NDVI_2

### 4.2.1 Optical data sets

Aerial photographic imagery was added to the data selection: a Red, Green and Blue (RGB) colour aerial imagery collected by a Leica ADS40 scanner with 0.25x0.25 metres spatial resolution. This data set was extracted from the Astrium Geostore data dissemination platform (Airbus DS 2015). The RGB aerial photography data set is shown in Figure 10.

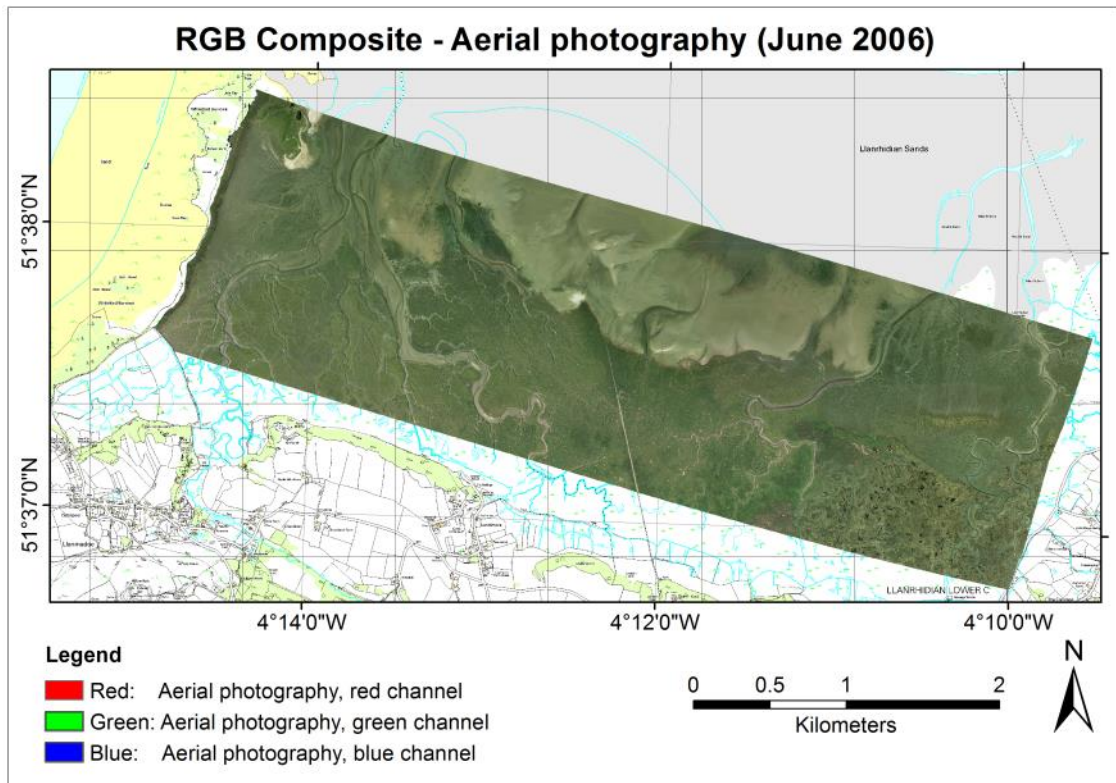


Figure 10 – RGB composite of the aerial photography data set used in this research.

Two Landsat satellite images added to the selection of optical images. These Landsat images were downloaded from the United States Geological Survey (USGS) EarthExplorer repository. The main reason to include the satellite imagery was to be able to use the information of the near-infrared and vegetation indices based on this channel, which were not available VHR resolution from aerial imagery. A relatively cloud-free image was found with an acquisition date closely coinciding with the SAR data used in this research, described in Chapter 4.2.3. This image was a Landsat-7 ETM+ scene acquired on 04/06/2010. Additionally another Landsat-5 TM scene acquired on 28/04/2011 was added to the selection of optical imagery. This image was added in order to be able to research seasonal variation of salt marsh habitats, with one image from the early growing season and one during the maximum growing season.

#### 4.2.1.1 Pre-processing optical aerial imagery

The pre-processing of the optical images was carried out with Envi 4.8. Initially, the aerial imagery was checked for inconsistencies in illumination and reflectance throughout the research areas. The RGB aerial imagery was acquired on one single day

on 02/06/2006 which meant there were no differences in illumination conditions, which can occur when imagery from different dates are stitched together in a mosaic. Subsequently, the RGB imagery was checked for geo-registration errors. In order to achieve this, the Ordnance Survey Mastermap, with scale of 1:10,000 was downloaded from the EDINA repository. Even though the area posed some problems in terms of finding stable Ground Control Points (GCP), there were some features in the area that could be used very well. Example imagery of the geo-registration check of all different data sets is provided in Figure 14. Finally, the spatial resolution of the RGB imagery was re-sampled from 0.25x0.25 metres to 2x2 metres, in order to coincide with the resolution of the other data sets.

#### ***4.2.1.2 Pre-processing optical satellite imagery***

Initially, the geo-registration of the two Landsat images was checked in the same way as the aerial photography was checked, see Figure 13. It was found that the images were very well geo-registered and no further modifications were needed. Subsequently, NDVI was calculated from both Landsat images with the NDVI calculation module in Envi 4.8. Subsequently, the NDVI images were re-sampled from the native Landsat spatial resolution of 30x30 metres to 2x2 metres, in order to coincide with the other data sets.

#### **4.2.2 LiDAR data sets**

A LiDAR Digital Surface Model (DSM) data set was obtained from the Landmap repository (Millin-Chalabi et al. 2011). A DSM data set is a model of the Earth's surface including the objects placed on it, like buildings and vegetation (Axelsson 1999). The data set had a native spatial resolution of 2x2 metres in the X and Y directions and a vertical resolution of 1-2 cm. The metadata delivered with the LiDAR data set was sufficiently vague that it only the year of acquisition could be identified as 2007.

The geo-registration was checked with the Ordnance Survey Mastermap images, in which a number of GCPs were checked. In Figure 13 the positioning of the DSM data set with regard to the Mastermap is shown.



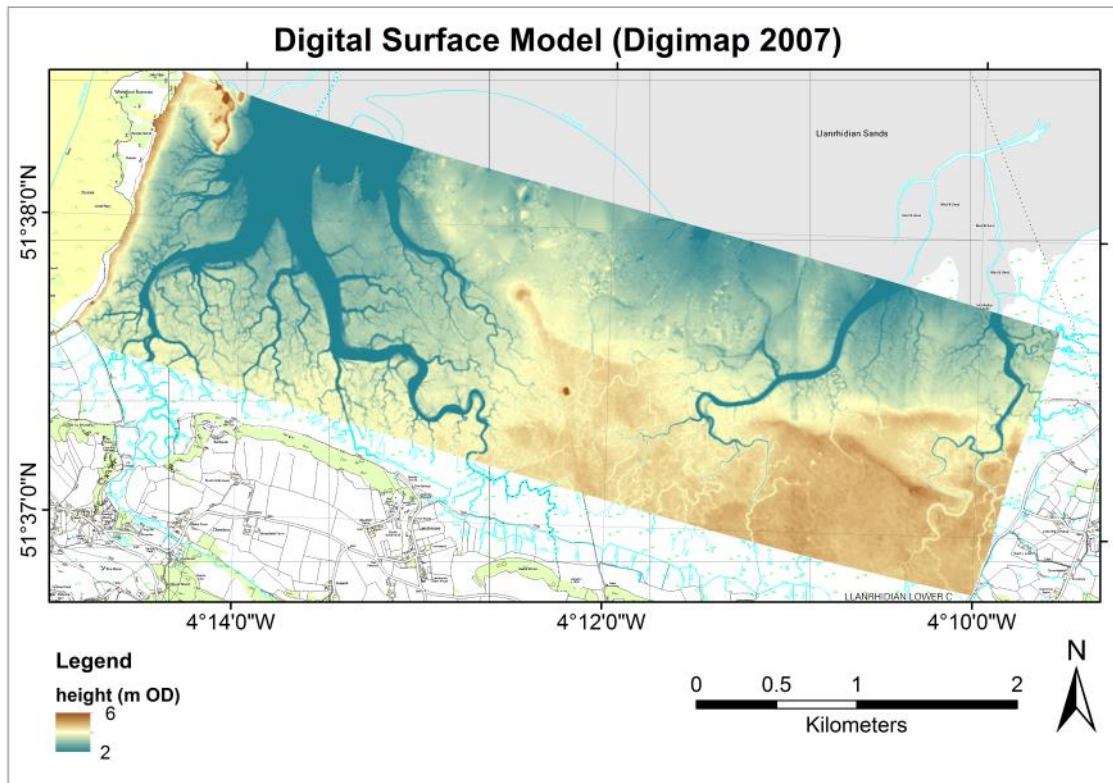


Figure 11 – LiDAR DSM data set used in this research.

#### 4.2.3 Airborne SAR data

The airborne SAR data set used in this thesis was acquired by the Astrium SAR Demonstrator (Natale et al. 2011). This system operates in both S- and X-band and is quad polarimetric. In July 2010, a survey campaign was carried out to acquire SAR data as preparation for the upcoming NovaSAR-S satellite mission, which will be equipped with an S-band SAR instrument. A number of other research experiments have been carried out to test the suitability of S-band SAR for land cover mapping (Guida et al. 2012; Iervolino et al. 2013). The S-band frequency domain has been used on the ill-fated Soviet Union's Almaz-1 satellite, which was operational for a very short period and endured numerous technical problems. Recently, it has also been installed on the operational Chinese HJ-1C EO satellite.

The SAR image was acquired over the Llanrhidian Marsh on the 28<sup>th</sup> of July 2010 at 16:49 GMT. The airborne SAR data was acquired using three polarimetric channels, HH, HV and VV. Although the data was not a full quad-polarimetric mode image, the data could still be analysed as if it was fully quad-polarimetric. For monostatic radars (i.e. transmitting and receiving antennas on the same location), both cross-polarimetric

channels are assumed to behave similarly (HV=VH). This is the reciprocity principle (Touzi et al. 2004; CCRS 2008) and it simplifies the coherency matrix considerably.

The tidal level during acquisition of the airborne SAR data was  $\pm 5.20$  m Admiralty Chart Datum (ACD) and the water level was rising during image acquisition. The tidal information is extracted from the tidal recordings of the UK Hydrographic Office and accessed through the National Tidal and Sea Level Facility (NTSLF 2012). The nearest tidal station is located at The Mumbles, on the southern shore of the Gower Peninsula. This tidal level is halfway between spring low and high tide that ranges between 0.1 and 10.3 meters ACD respectively. For reference, ACD chart level is placed -5.00 meters with regard to Ordnance Datum (OD) at the tidal station of the Mumbles. This means that the tidal level during SAR acquisition was +0.20 m OD. This relates directly to the elevation values of the LiDAR DSM variable, described in Chapter 4.2.2.

#### ***4.2.3.1 SAR data import***

The airborne SAR data pre-processing steps taken are summarised in Appendix D.

The data set was delivered in a native generic FPI format, which included header information and the SAR data for the different polarimetric channels and both frequency bands. The SAR data was presented in Single Look Complex (SLC) format; in which amplitude and phase information are stored as the real and imaginary part of the data, respectively. The spatial resolution of the raw data set was 0.75 metres in both azimuth and slant range directions. The polarimetric channels were calibrated during the initial tests (Natale et al. 2011) using the procedure described by van Zyl (1990), using the returns from natural targets assumed to present azimuthal symmetry and at least one trihedral reflector. This technique allowed correction for cross-talk between polarimetric channels, and provides robust inter-channel calibration (Natale et al. 2011).

A dedicated IDL script was used to extract the header information and prepare the SLC SAR data for import in Envi. In Envi the SAR data format was changed from complex format into two-layer float format files, after which it was ready to be imported in PolSARpro.



#### **4.2.3.2 SAR radiometric correction**

For processing of the airborne SAR data set, the PolSARpro toolbox was used. This package is developed for ESA as a learning and processing tool for polarimetric SAR data and has a number of in-built processing and classification routines (ESA 2013).

During the initial import into PolSARpro, a multilook correction was applied. Multilooking is a way to reduce the inherent speckle noise in SAR images, as described in Chapter 3.1.3. It was chosen to apply a multilook of 3x3 in the azimuth and slant range, respectively. This was chosen to preserve as much of the spatial resolution, while still reducing SAR speckle considerably. After the multilook, the SAR image spatial resolution was resampled from 0.75x0.75 metres to 2.25x2.25 metres.

After multilook correction the data was imported in the RAT Radar Tools. This is a standalone SAR processing tool developed by Technical University of Berlin (Reigber and Hellwich 2010). The reason to use this tool is because it incorporates some SAR processing functions that are not available in PolSARpro. In this research it was primarily used to correct for antenna pattern. Returned microwave signal in the near slant range attenuates less than the signal retrieved from the far slant range (see also Chapter 3.1.1). This results in an image whose intensity is too high in the near slant range and too low in the far slant range. This artefact was corrected by applying an antenna pattern correction. In Figure 12, a plot of the antenna pattern correction curves are shown. The average backscatter of the three polarimetric channels is shown over the slant range, near slant on the left and far slant on the right of the plot. Consequently, a curve is fitted through the backscatter profile. This curve is used to correct for backscatter attenuation differences, it suppresses backscatter intensity in the near slant range and amplifies backscatter intensity in the far slant range.

#### **4.2.3.3 SAR geometric correction**

Geometric correction was carried out by performing a conversion from slant to ground range with RAT Radar Tools. Header information about near slant range and instrument (airplane) height was used to calculate incidence angles during acquisition. From this, the actual footprints of the image resolution cells were calculated. This information was used to project the slant range image on the ground. The image dimensions were changed to fit this footprint (Richards 2009).

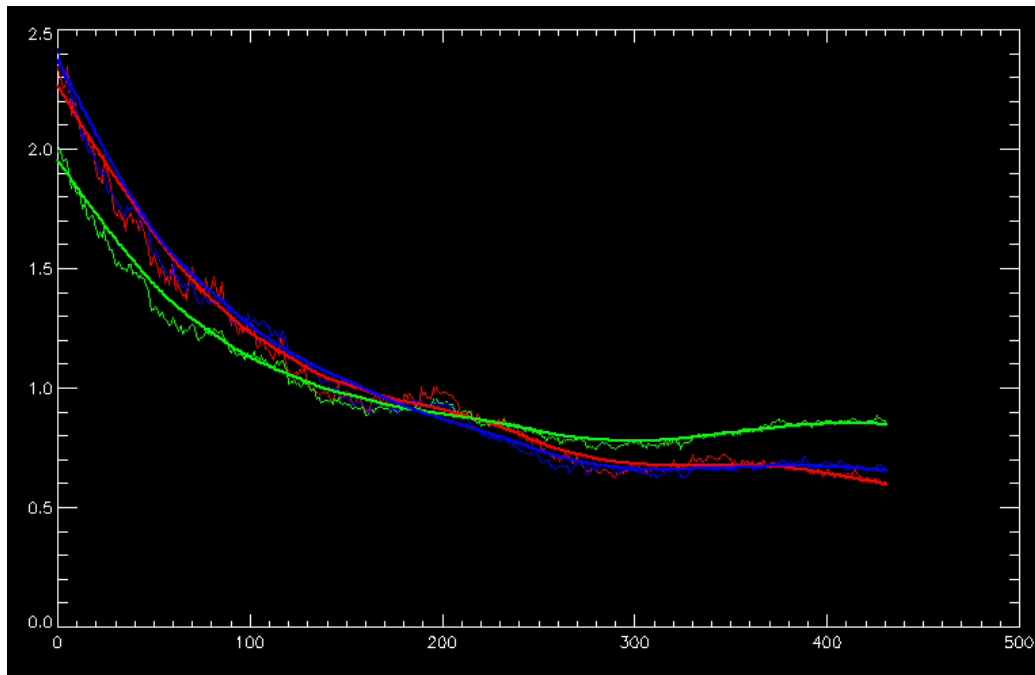


Figure 12 – Antenna pattern correction curves for S-band SAR image from pre-processing in RAT. R: HH backscatter intensity, G: HV backscatter intensity, B: VV backscatter intensity.

#### 4.2.3.4 SAR polarimetric descriptors

After radiometric and geometric correction, polarimetric decomposition parameters were extracted. PolSARpro offers a large suite of polarimetric decomposition tools and specific classification algorithms to extract additional information from polarimetric SAR data. An introduction into polarimetric decomposition methods was provided in the Chapter 3.2.3. The following four types of polarimetric descriptors were extracted:

1. HH, HV and VV backscatter intensity channels. For the airborne SAR data set no  $\sigma^0$  calibration coefficients were available. Therefore backscatter intensity dB values could not be quantified per square ground unit. However, the data was corrected for signal attenuation by the antenna pattern correction. Considering the flat topography of the research area, it was assumed that intra-scene backscatter intensity variation was sufficiently corrected.
2. Cloude-Pottier (CP) decomposition  $H$ ,  $A$  and  $\alpha$ -values. See Chapter 3.2.3.1 for more information.
3. Freeman-Durden (FD) decomposition, volume scatter ( $P_v$ ), double-bounce scatter ( $P_d$ ) and surface scatter ( $P_s$ ). See Chapter 3.2.3.2 for more information.

4. Van Zyl (VZ) decomposition volume scatter ( $P_v$ ), double-bounce scatter ( $P_d$ ) and surface scatter ( $P_s$ ). See Chapter 3.2.3.3 for more information.

#### 4.2.3.5 SAR geo-registration

After extraction of the polarimetric descriptors, the image was projected in a geographical format. It was assumed that small topographical relief in the imagery (height difference 4-5 metres over the entire research area, see Figure 11) did not cause significant geometric distortions normally associated with SAR data. Assuming this, implementation of a height model to enhance the geometric correction could be avoided. The metadata of the raw airborne SAR data only provided two geographic coordinates, one of the first pixel and one of the last pixel of the first scan line, accompanied with an average aircraft flight heading. This proved to be too little information for a confident and accurate geo-registration. Therefore, it was decided to perform the geo-registration by selecting twenty Ground Control Points (GCPs) in both the SAR data set and the reference OS Mastermap topographical map. The geo-registration was performed with Envi 4.8. Special attention was given to an even spreading of the GCPs in the image, as well as finding GCPs as close to each four corners of the SAR image as possible. The image posed a specific challenge as there were very few man-made (i.e. stable) objects in the SAR data set. Therefore it had to be assumed that some of the features in the salt marsh are more or less stable over time, like major creeks and ponds. In Figure 13 the locations of the GCPs are shown.

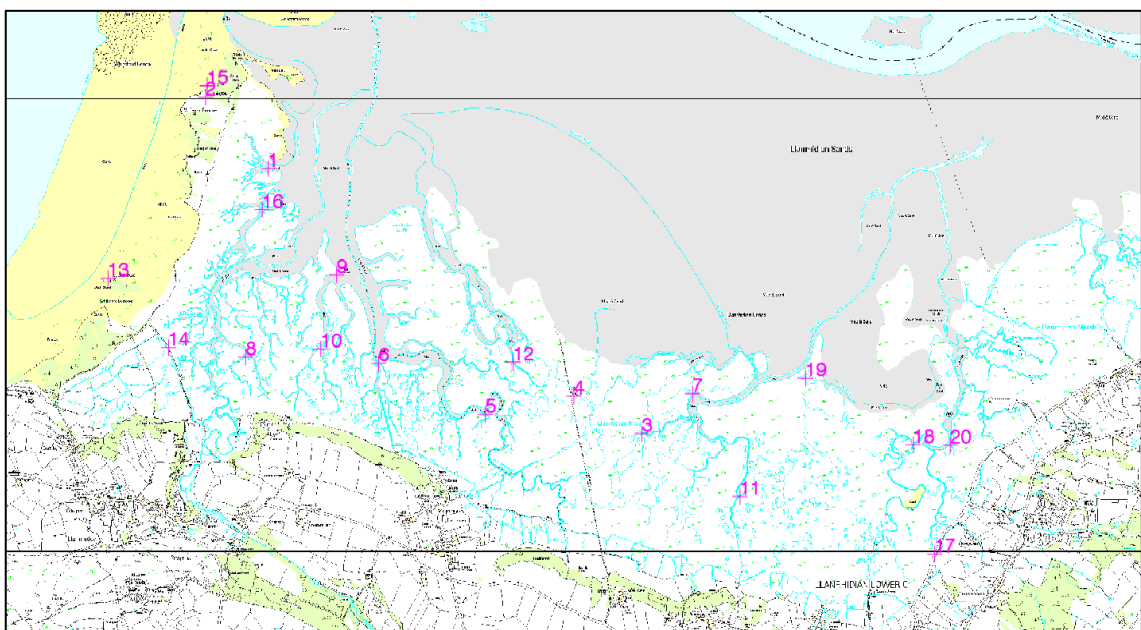


Figure 13 – Location of GCPs used to geo-register airborne SAR data.

Even though the raw SAR imagery was delivered with correction for roll, pitch and yaw errors of the survey airplane, a second degree polynomial correction was needed to warp the image to obtain the best geographic fit. In Table 6 the statistics of the geo-registration are shown, with the predicted and observed locations of the warped image, as well as the Root Mean Square (RMS) error of each GCP. The total RMS error was 5.20 metres.

*Table 6 – Airborne SAR geo-registration GCP statistics.*

GCP	Base image		Warp image		Predicted location		Location error		RMS error
	x	y	x	y	x	y	x	y	
1	5133.50	4731.00	721.00	621.00	714.25	622.43	-6.75	1.43	6.90
2	4907.75	4494.00	875.00	369.00	875.60	369.30	0.60	0.30	0.67
3	6480.75	5609.25	242.50	1994.00	240.64	1995.10	-1.86	1.10	2.16
4	6235.50	5485.00	292.25	1755.75	295.56	1754.44	3.31	-1.31	3.56
5	5916.50	5546.00	134.75	1498.00	134.65	1497.52	-0.10	-0.48	0.49
6	5531.50	5376.00	188.75	1129.50	190.06	1125.86	1.31	-3.64	3.87
7	6663.75	5477.25	432.00	2113.00	435.38	2118.08	3.38	5.08	6.10
8	5051.75	5356.00	60.00	712.00	60.91	711.16	0.91	-0.84	1.24
9	5380.00	5083.50	436.00	925.00	439.15	922.40	3.15	-2.60	4.09
10	5323.00	5329.50	175.00	941.00	172.22	936.05	-2.78	-4.95	5.68
11	6834.75	5818.25	133.25	2346.50	126.40	2349.80	-6.85	3.30	7.60
12	6017.00	5373.00	346.25	1541.50	344.14	1539.63	-2.11	-1.87	2.82
13	4555.75	5095.00	160.00	221.50	163.59	221.25	3.59	-0.25	3.59
14	4774.25	5324.25	4.00	459.75	5.95	466.15	1.95	6.40	6.69
15	4913.25	4456.75	909.50	364.75	914.62	364.55	5.12	-0.20	5.13
16	5111.75	4867.75	578.00	638.00	569.74	638.53	-8.26	0.53	8.27
17	7537.00	6009.00	124.00	2998.00	127.95	2996.77	3.95	-1.23	4.14
18	7460.00	5647.00	504.25	2838.50	496.88	2840.37	-7.37	1.87	7.61
19	7071.50	5425.75	609.00	2451.00	615.84	2453.24	6.84	2.24	7.19
20	7593.00	5648.00	534.00	2959.00	535.97	2954.13	1.97	-4.87	5.25

Subsequently, the geo-registration quality of the projected images was visually checked using the OS Mastermap. Figure 13 shows the geographical fit of the different RS data sets with regard to the only truly stable point in the research area, a foundation along the causeway through the centre of the area. The projected S-band and X-band SAR backscatter intensity images are presented as RGB composites in Figure 15 and Figure 16, respectively.

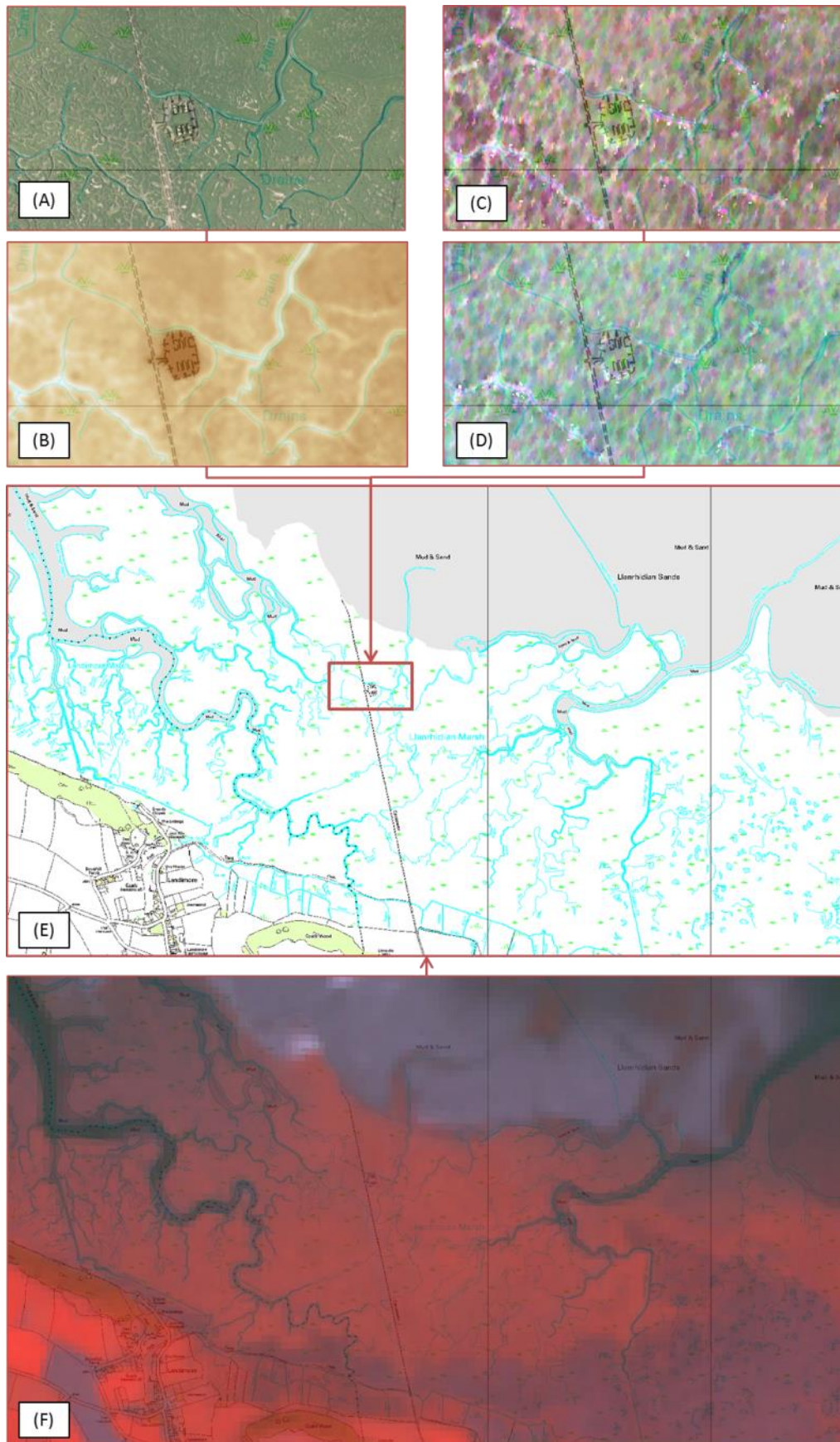


Figure 14 – Visual check of geo-registration of RS data sets used in this research.

(A) RGB imagery, (B) DSM data, (C) S-Band SAR, (D) X-band SAR,  
(E) Ordnance Survey Mastermap, used as reference, (F) False colour Landsat-7 imagery.



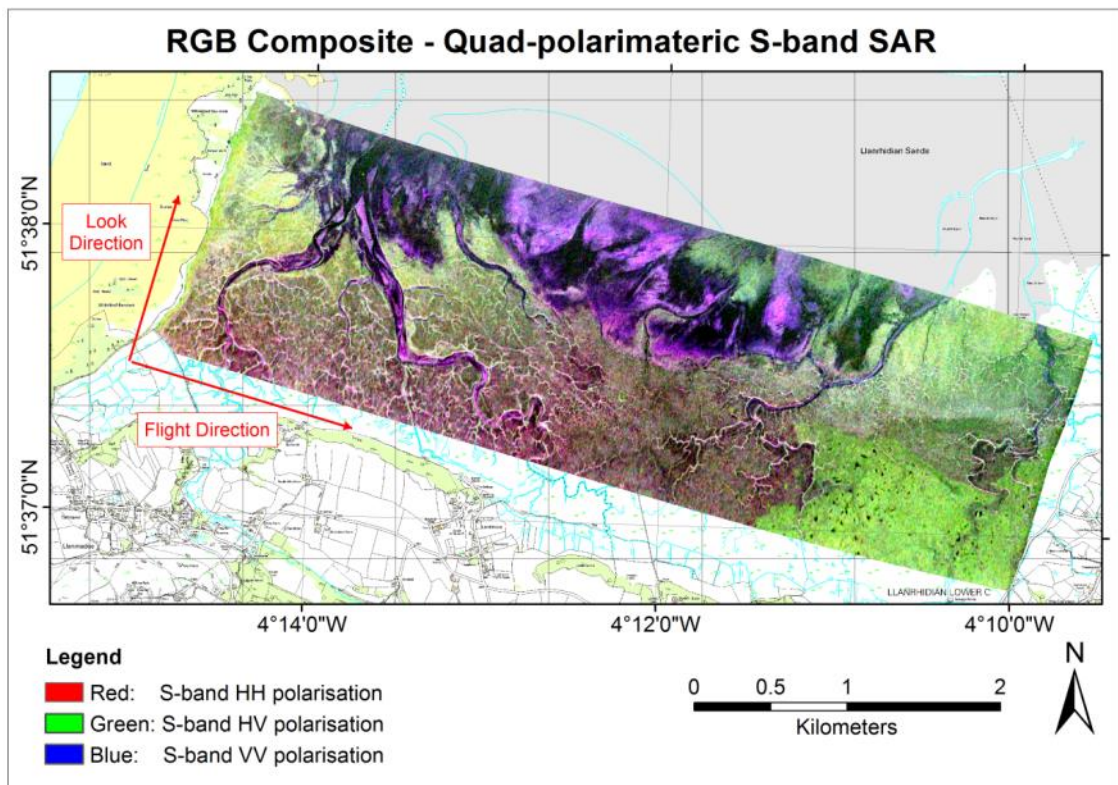


Figure 15 – RGB composite of S-band polarimetric intensity channels.

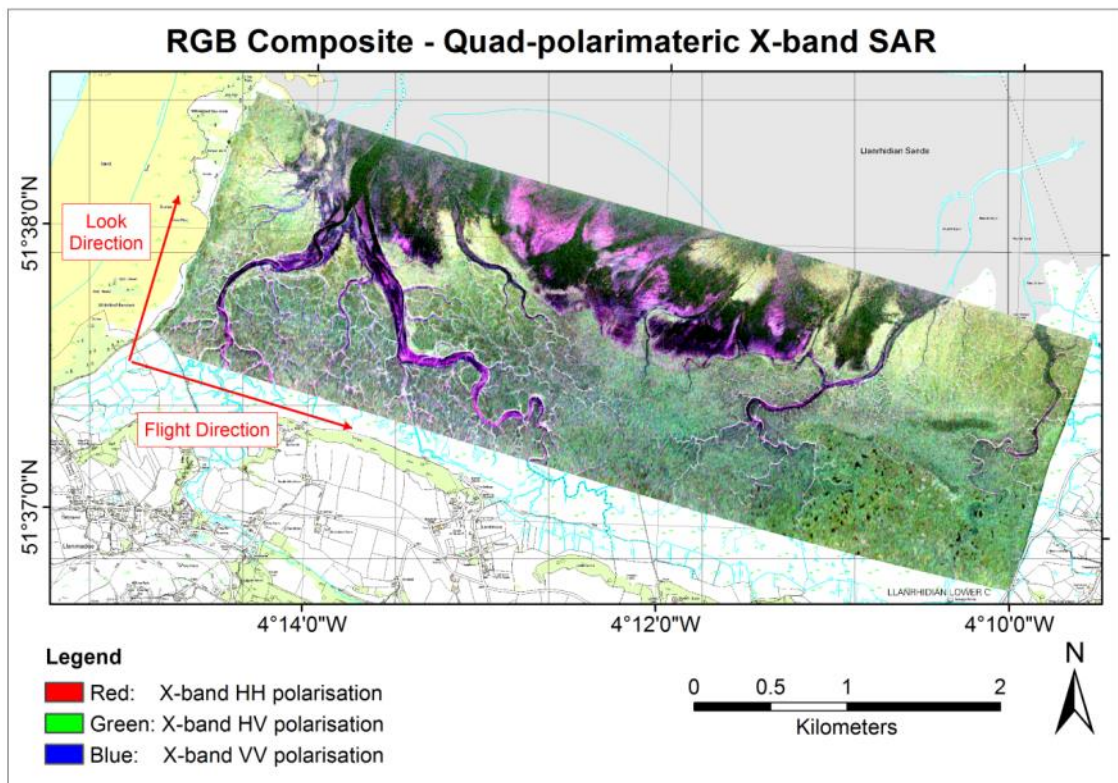


Figure 16 – RGB composite of X-band polarimetric intensity channels.

### **4.3. Reference data**

In this section the reference data is described, which has been used to correlate the RS data sets with the actual presence of different salt marsh vegetation habitats and biophysical parameters in the research area.

#### **4.3.1 CCW survey (1998)**

In 1998 an ecological field survey in the Burry Inlet and the Loughor Estuary was carried out (Prosser and Wallace 1999). The survey was initiated by the CCW. At the time, the survey was carried out to provide more detailed information on the distribution of key habitats for designation of a Special Area of Conservation (SAC). One of the key findings of this field survey was that *Juncus maritimus* was particularly well represented in the Llanrhidian Marsh (Prosser and Wallace 1999). A decline of *Salicornia* pioneer marsh vegetation was also observed. The vegetation habitats were mapped according to the NVC vegetation habitat classification, which is the most commonly used habitat classification scheme in the United Kingdom, which has detailed description of salt marsh vegetation habitats (Rodwell 2000). The NVC classes were re-grouped into the more broad classification of the Annex 1 habitats listed under the EC Habitat Directive (European Commission 1992). In Table 7 an overview of the relationships between the NVC and Annex 1 classes is provided, further explained in Chapter 4.3.3. The CCW data was made available as reports and GIS data, and is plotted in Figure 17.

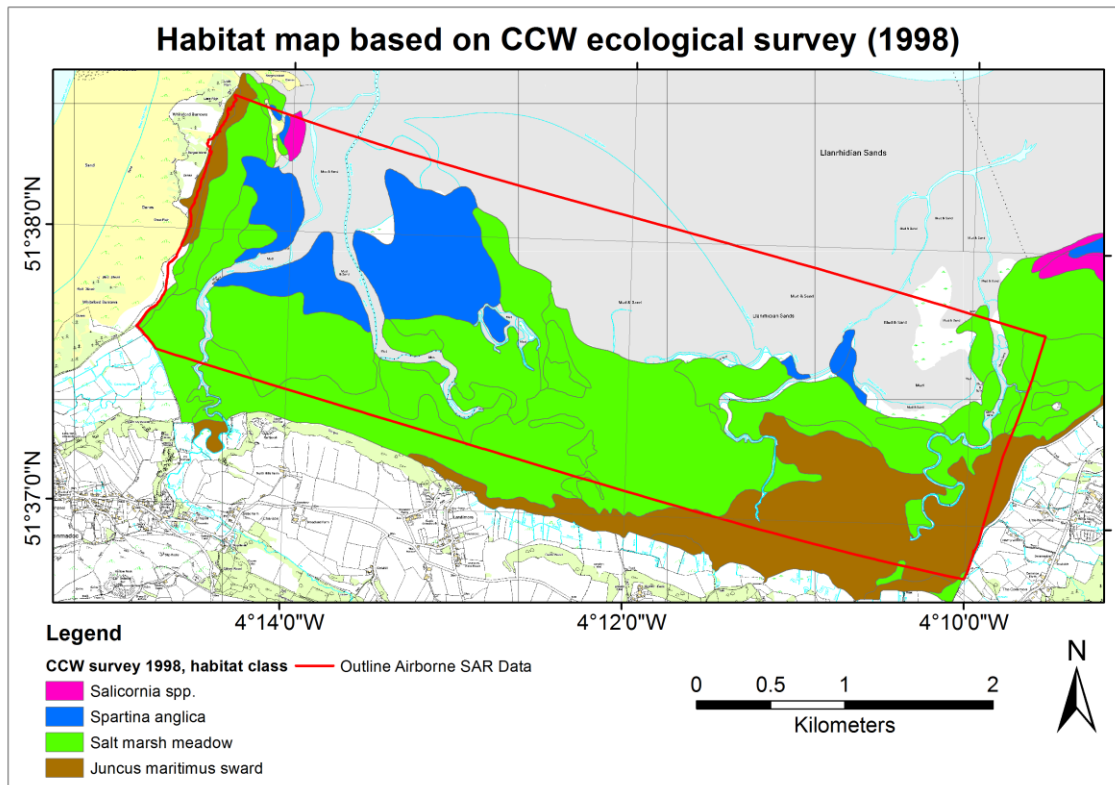


Figure 17 – Habitat classification map based on the CCW ecological field survey (1998).

#### 4.3.2 Field survey (2013)

Between 23<sup>rd</sup> and 25<sup>th</sup> July 2013, an ecological fieldwork specifically dedicated to collect ecological data for this PhD research was carried out in the Llanrhidian Marsh. It was carried out in this period to coincide as much seasonally with the SAR data acquisition, which was on the 26<sup>th</sup> of July 2010. Specific focus was given to the recording of habitat type and biophysical parameters of the vegetation for correlation with the RS data set. On a total of 100 locations samples were taken. The location and appearance of each sample site was recorded with Global Positioning System (GPS) and geo-registered photos. Figure 18 is an overview map of all sample locations. On each survey day another transect through the salt marsh was sampled. On July 23<sup>rd</sup>, 2013 the western part of the salt marsh near Landimore was recorded. This part of the salt marsh can be characterised by a quick succession of upper salt marsh habitats to pioneer *Spartina* vegetation. This area was bisected by a number of major gullies and creeks and was very muddy in the *Spartina* swards. On the second day on July 24<sup>th</sup>, 2013 the central part around the causeway crossing the salt marsh from Weobly Castle was investigated. In this *Festuca rubra* and *Puccinellia maritima* salt marsh meadows were dominant and it was the primary cattle grazing area. Further towards the pioneer



zone there are extensive sandflats with swaths of pioneer *Salicornia spp.* On the last day on July 25<sup>th</sup>, 2013 the eastern part of the marshes were visited, near the village of Llanrhidian itself. This area is dominated by dense *Juncus maritimus* fields in the upper part of the salt marsh. This gave way to salt marsh meadows in direction of the sea until a former erosive cliff was reached. Beyond this cliff a transition from salt marsh meadows to *Spartina anglica* was observed. The soil became progressively muddy and difficult to access. In Figure 18 the sample sites are plotted, with reference to the CCW habitat survey and the EA salt marsh extent survey maps. What can be seen from the map is that the vegetation cover in the pioneer zone has extended along the central and eastern transects, in each of the habitats samples have been collected.

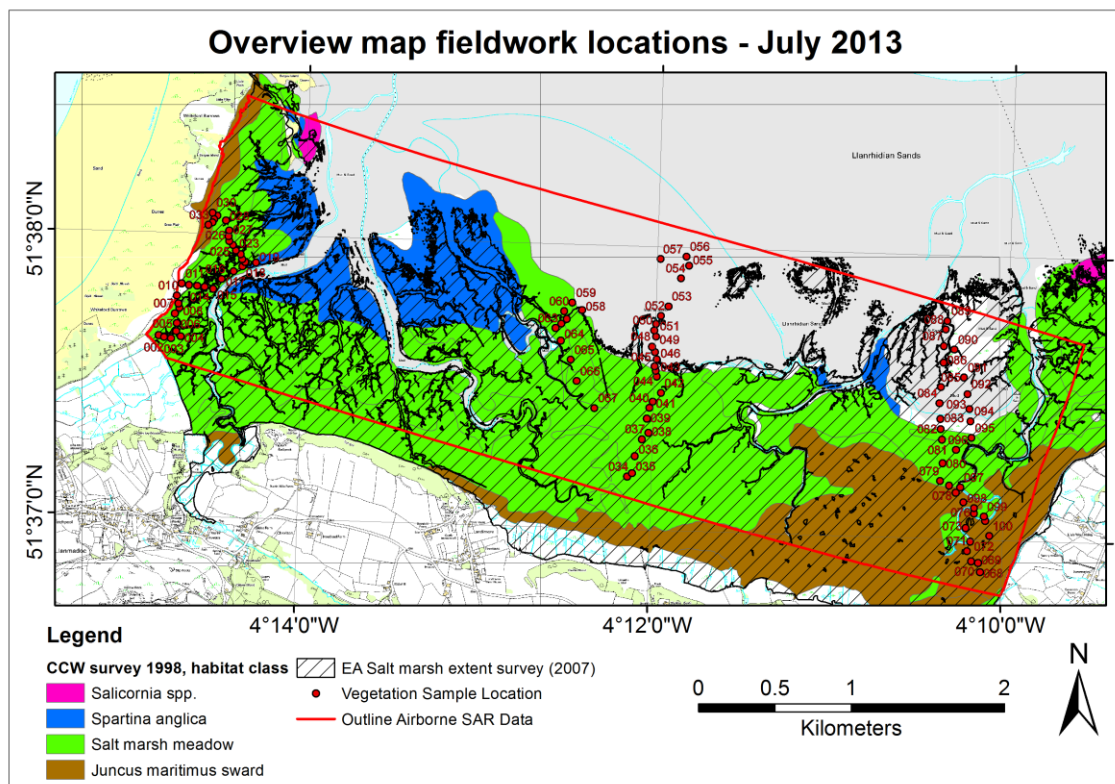


Figure 18 – Overview map of sample locations of field survey in July 2013. CCW and EA surveys are plotted in background for reference.

In order to make sure that positioning errors in either the RS data set or during the field survey would least affect correlations it was made sure that each sample site was ‘representative’ of the wider surroundings, also considering the average RMS error of the RS data geo-registration of 5.20 metres (Table 6). With representative it is meant that there were no sharp boundaries or transitions within a radius of 10 meters around the sample site. Also it was made sure that the vegetation type and cover found at the

sample site was similar with the vegetation type and cover within this 10 meters buffer zone.

At each site information was acquired by placing a 1x1 metre quadrat as a bounding box (Figure 19). Even though the spatial resolution of the combined RS data set was 2x2 metre the quadrat size was chosen for practical purposes, it would have been very difficult to carry a quadrat of 2x2 metre around in a salt marsh.

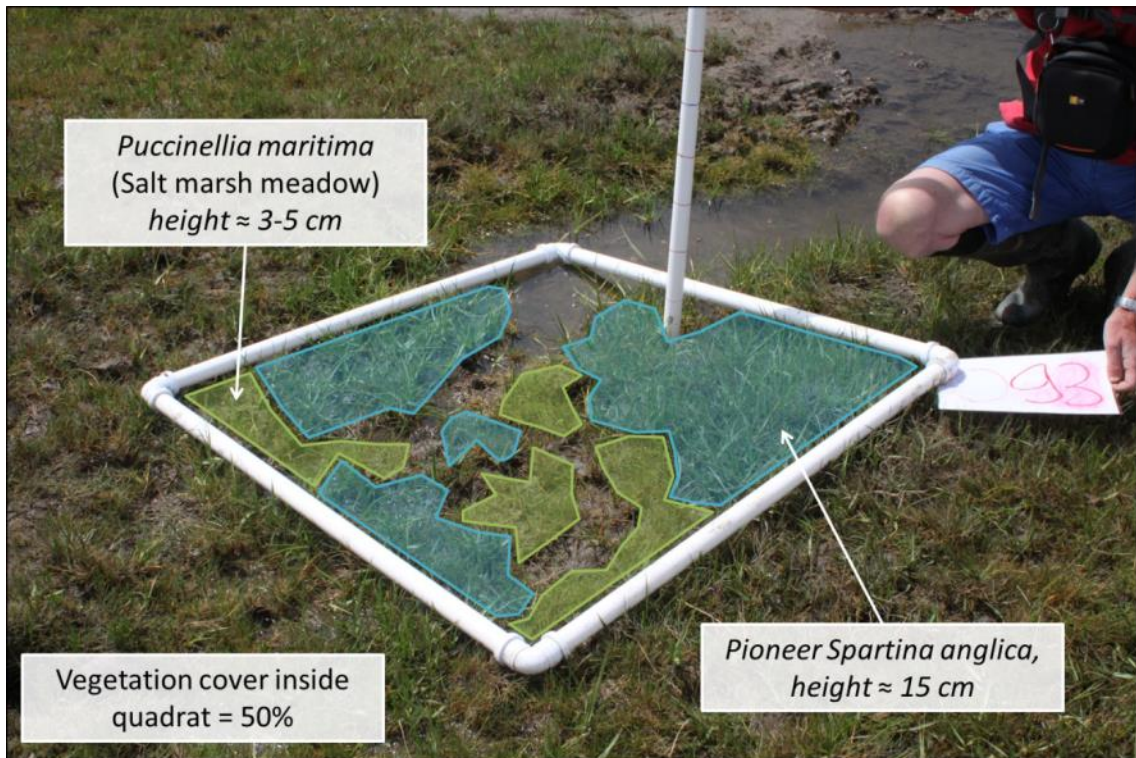


Figure 19 – Annotated picture of ecological field survey quadrat.

At each sample site the following parameters were recorded (shown in Figure 19):

1. NVC habitat, according to the NVC habitat classification scheme, later re-grouped in Annex 1 habitats
2. Vegetation species present within the quadrat ( $i_n$ ),
3. Percent cover of each species ( $C_i$ ) in  $\text{dm}^2$  per  $\text{m}^2$ ,
4. Vegetation height of each species ( $h_i$ ) in centimetre.

From these parameters the Gross Vegetation Volume ( $GVV$ ) which is defined as vegetation volume in  $\text{dm}^3$  inside the quadrat area of  $1 \text{ m}^2$  was calculated:

$$GVV = \sum_{i=1}^n h_i * C_i \quad (7)$$

As equation 7 shows, *G<sub>VV</sub>* is a summation of the respective volumes of the species present in the quadrat. The volume was calculated by multiplying percentage cover with the height of each present species, similarly to the methodologies described in Suchar and Crookston (2010) and Axmanová et al. (2012). The recorded field data is presented in tabulated form in Appendix A, a number example pictures from a selection of sample site locations are presented in Appendix B.

### 4.3.3 Salt marsh habitat classes

The habitats were recorded during the field survey according to the NVC classification (Rodwell 2000). To convert these to other classification schemes, JNCC has drawn a conversion table (JNCC 2015). This table was used to convert the habitat classes to the Annex 1 classification. Table 7 is an overview of the relationships between the classes used in this research and the NVC and Habitat Directive.

The EU Habitat Directive Annex 1 classification (Habitats Directive 1992) was designed as a comprehensive scheme to classify all of Europe's natural habitats. Even though most member states still have their existing national classification schemes, wider implementation of Annex 1 scheme is considered (Lee 2001).

It was acknowledged that the habitats 'mid-upper salt marsh meadows' and 'upper *Juncus maritimus*' are normally grouped in one habitat in the Annex 1 classification. These habitats were separated for this research as they show considerable differences in spectral reflectance and vegetation structure. In this way, the different RS responses of these two habitats can be distinguished. Additionally, a separation between wet and dry sand and mudflats was used for the mapping of salt marsh habitats.

Table 7 – Relationships between NVC and Habitat Directive Annex 1 habitat classes.  
Common NVC classes are indicated in bold.

Classes used in this research	NVC class	Annex 1 class
Sand or mudflats	None, not vegetated	H1140
Pioneer <i>Salicornia spp.</i>	<b>SM8</b> , SM9	H1310
Pioneer <i>Spartina anglica</i>	SM4, SM5, <b>SM6</b>	H1320
Mid-upper salt marsh meadows	SM10, SM11, SM12, <b>SM13</b> , SM14, SM15, <b>SM16</b> , SM17, SM19, SM20	H1330
Upper marsh <i>Juncus maritimus</i>	SM18	H1330

## **5. SAR backscatter signatures in salt marshes**

### **5.1. Introduction**

This chapter presents the methods, results and discussion of the research experiment that was designed to provide answers to the first research question:

*'How are polarimetric SAR backscatter signatures affected by salt marsh characteristics, like specific environmental parameters (sea level, soil moisture or soil salinity) or botanical structure?'*

One of the main aims of this research experiment was to investigate the performance of S-band SAR in general. S-band SAR operates with wavelengths in the frequency band of 7.5 to 15 cm and X-band in the wavelength domain of 2.4 to 3.75 cm. These two frequencies interact with targets on the earth's surface differently. As has been shown in previous studies, longer microwave wavelengths are better capable to penetrate through vegetation canopy or the upper part of soils (Schmullius and Evans 1997; Gade et al. 2011). With this in mind, behaviour of polarimetric S-band against polarimetric X-band was expected to differ in salt marsh habitats.

The second aim of this research experiment was to research the influence of salt marsh environmental and botanical parameters on SAR backscatter signatures. It has been known that soil moisture varies largely in a salt marsh throughout the tidal cycle (Silvestri and Marani 2004) and that these variations can have profound effect on SAR backscatter signatures (Dabrowska-Zielinska et al. 2009). The SAR data set was acquired when the tidal level was approximately half-way between low and high tide. From visual interpretation it is interpreted that there are moisture differences within the area of sand and mudflats, while the vegetation habitats are all dry. Therefore, the soil moisture analysis will focus on the sand and mudflats. The influence of botanical parameters on SAR backscatter is analysed focussing on the four vegetation habitats.

### **5.2. Methods**

This section describes the different data analyses carried out with the RS and reference data sets, focussing on the analysis of SAR backscatter signatures in salt marshes. A

flowchart overview summarising the different analyses and their inter-relations are shown in Appendix C.

The two frequency bands of the airborne polarimetric SAR data sets (S-band and X-band) and its derived polarimetric descriptors are used to quantify the impact of environmental parameters as well as botanical differences in salt marshes. In order to achieve this, the analysis is split in two parts. The first part concerns statistical analysis of the polarimetric descriptors.

In the initial analysis the response of S-band and X-band polarimetric intensity channels in different locations throughout the research area that represented different habitats and environmental settings was investigated. One of the main research topics of this research was to analyse backscatter signatures of S-band SAR. Additionally, attention was given to comparative analysis of CP, FD and VZ decomposition variables and understanding the added value of these variables for salt marsh vegetation characterisation.

For the analysis of influence of environmental parameters on SAR variables, samples were taken from the SAR variables that corresponded with ecological field survey sample locations. For each of the sample locations, a buffer zone of 10 meters was defined and random samples were selected of each of the pixels within these buffer zone. Of each of the vegetation classes, 500 pixels were randomly selected and the corresponding SAR variable values were extracted. Qualitative analysis of backscatter behaviour in different salt marsh habitats was done by plotting the sampled S-band and X-band values in scatterplots. Subsequently, scatterplots of CP and VZ decomposition SAR variables were drawn to analyse differences between the behaviour of backscatter intensity channels and polarimetric decomposition parameters for S-band and X-band SAR. Besides analysing scatterplots, a number of boxplots of SAR variables were plotted for quantitative analysis of statistical distributions of habitats with different vegetation characteristics in a number of environmental settings.

### **5.3. Results**

Analysis of polarimetric SAR variables provides insight into the interaction of microwave pulses with surface targets and materials. The performance of S-band with

relation to X-band and the performance of polarimetric decomposition data variables with relation to polarimetric intensity channels are analysed.

In this section the results from the polarimetric SAR descriptor analysis are presented. The section consists of four parts: in the first the polarimetric backscatter intensity variables are analysed, followed by two parts about CP and VZ polarimetric decomposition variables. In the last part all the results are combined and integrated in a model of backscatter behaviour in all considered salt marsh habitats.

### **5.3.1 Polarimetric backscatter intensity variables**

In the following paragraph the results are briefly described, subsequently an interpretation per habitat with consideration to environmental and botanical factors is made.

Scatterplots were drafted showing relationships of the three polarimetric intensity channels (HH, HV and VV, normalised to dB) between X-band and S-band (Figure 20). These plots reveal a consistent difference between S-band and X-band behaviour of all three separate polarimetric channels. A best-fit linear regression line is drawn in all three scatter plots. This gradient can be interpreted as the relative sensitivity, or dynamic range, of the X-band SAR system relative to the S-band SAR system. In case the sensitivity of S-band and X-band SAR to different surface targets were the same, the best-fit line would have a gradient of 1 (parallel to the dashed line in the scatterplots, which is the line  $y=x$ ). The three linear regression lines calculated for the three intensity channels have slopes of 0.7376 for HH polarisation, 0.5961 for HV polarisation and 0.6929 for VV polarisations channels, respectively. This indicates that the degree in which X-band changes with respect to S-band is lower, with a lower variance between the points. This implies that variance, or separation of X-band data points between different habitat classes is lower. From this it appears that X-band is less sensitive to differences in surface roughness or vegetation cover than S-band.

The scatterplots give some indication of backscatter behaviour differences between salt marsh habitat classes, but this is shown clearer in Figure 21. This figure displays a series of boxplots of all SAR backscatter intensities channels against different land cover classes. In these boxplots the data is split into quartiles. The box of the boxplots goes from the first quartile (Q1) to the third quartile (Q3). Within the box, a vertical

line is drawn at the Q2, the median of the data set. Two horizontal lines, called whiskers, extend from the front and back of the box. The front whisker goes from Q1 to the smallest non-outlier in the data set, and the back whisker goes from Q3 to the largest non-outlier. Outliers are plotted separately as points on the chart.

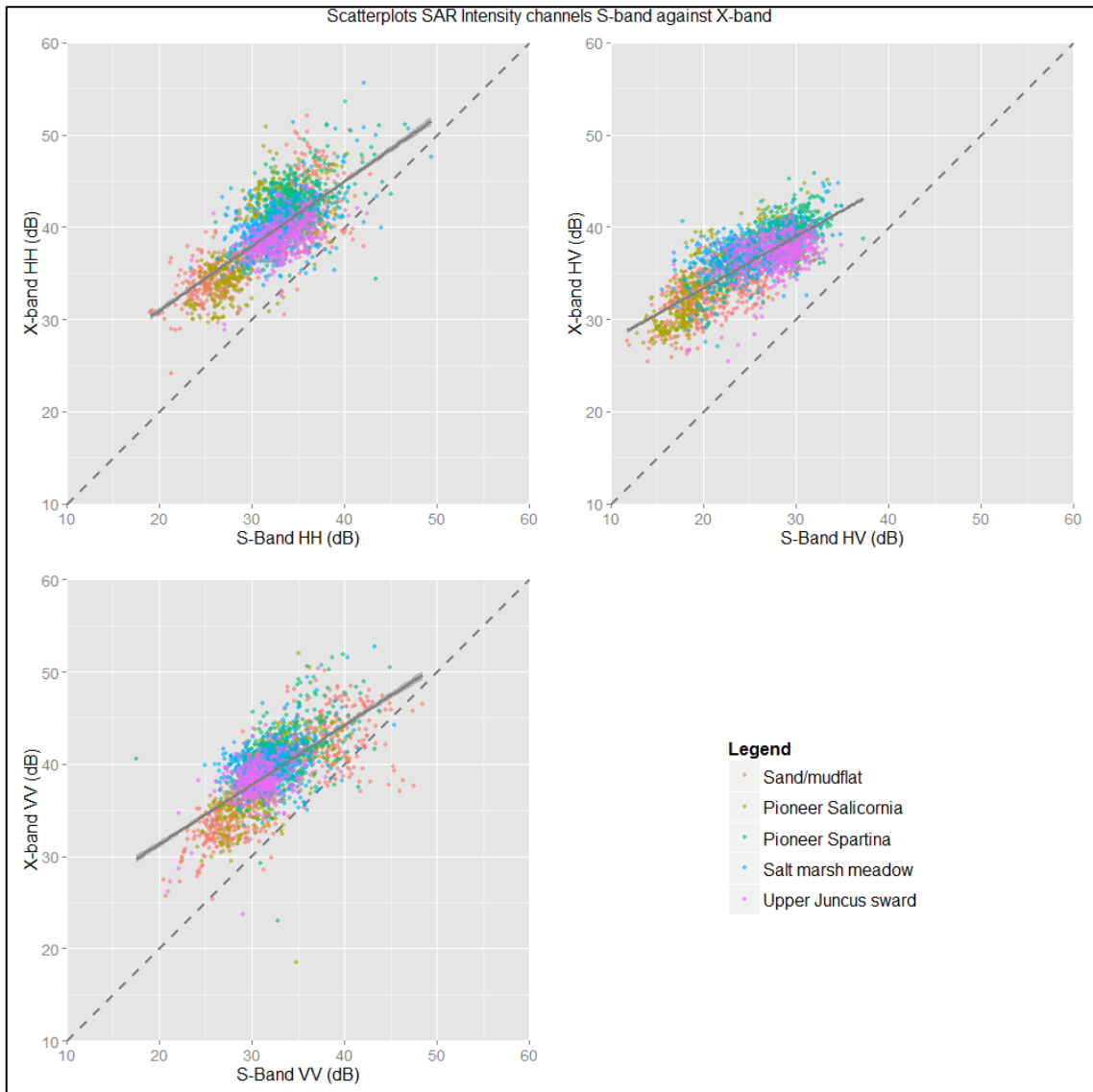


Figure 20 – Scatterplots SAR polarimetric intensity channels X-band against S-band.

The boxplots show that backscatter intensities from different land cover classes have different mean values and variability. The most notifiable difference in pattern between S-band and X-band data is visible in the HV backscatter intensity channels. S-band HV backscatter intensity displays a wider dynamic range than X-band HV backscatter intensity. What is also noticeable is that there is a wider variety between vegetation classes for S-band HV intensity than can be observed with X-band HV

intensity. Generally it appears that S-band intensity channels display a wider dynamic range than X-band intensity channels and are better for discrimination between different vegetation habitats.

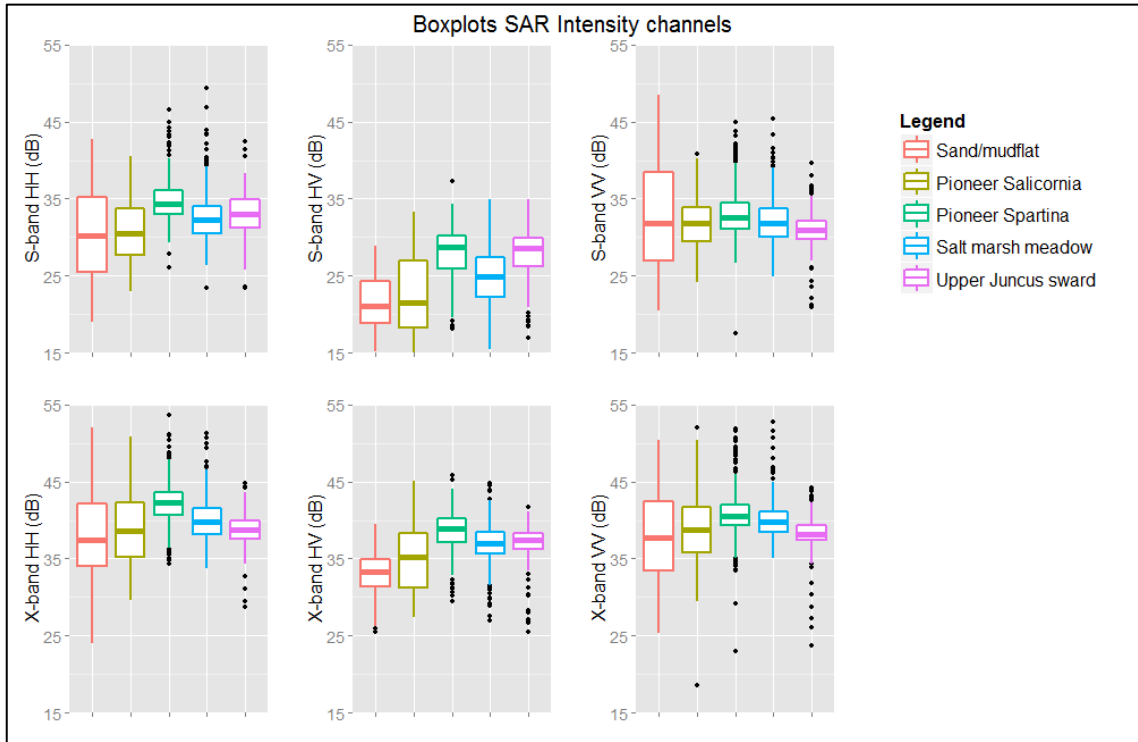


Figure 21 – Boxplots SAR backscatter intensity channels against land cover classes.

The mean and standard deviation values of the backscatter intensity variables are tabulated in Table 8.



Table 8 – Mean and standard deviations of backscatter intensity variables per habitat.

Habitat	Mean S HH	SD S HH	Mean S HV	SD S HV	Mean S VV	SD H VV
Sand/mudflats	30.48	5.82	21.13	3.52	32.91	6.43
Pioneer <i>Salicornia</i>	30.85	3.92	22.25	4.95	31.75	3.18
Pioneer <i>Spartina</i>	34.67	2.47	28.09	3.21	33.05	2.94
Salt marsh meadow	32.52	3.81	24.84	4.00	31.95	3.48
Upper <i>Juncus</i> sward	33.07	2.46	27.94	2.85	30.98	2.11
Habitat	Mean X HH	SD X HH	Mean X HV	SD X HV	Mean X VV	SD X VV
Sand/mudflats	38.06	5.14	32.93	2.68	37.99	5.50
Pioneer <i>Salicornia</i>	38.64	4.49	34.90	4.05	38.58	3.77
Pioneer <i>Spartina</i>	42.16	3.28	38.51	2.40	40.57	4.27
Salt marsh meadow	39.87	3.73	36.88	3.41	39.72	3.87
Upper <i>Juncus</i> sward	38.84	1.95	37.13	1.95	38.31	2.04

Interpretation of the backscatter intensity variable analysis results per habitat can provide more information about influence of environmental and botanical parameters:

- Sand and mudflats are characterised by the highest standard deviation for HH and VV polarisation in both frequencies. This might be caused by the variations of water cover or soil moisture in this habitat. Parts of the habitat are often covered by a thin layer of water, even at low tide. This results in large backscatter variations between dry areas and wet areas where the layer of water can act as a specular reflector to the radar pulses (Woodhouse 2006). Example pictures from the research area in Appendix B show the differences in appearance. Further worth noting are the relatively low mean values of HV for both S-band and X-band. This might be attributed to the relative smooth surface of the sand and mudflats, which does not cause re-polarisation often observed in vegetated areas (Le Toan et al. 1992).
- The pioneer *Salicornia* salt marsh habitat displays backscatter signatures with comparable values as the sand and mudflat habitat. However, the standard deviations are lower for HH and VV backscatter, but higher for HV backscatter. This indicates that there is more variability in re-polarisation, which is likely related to increased variability of surface roughness and features. Meanwhile, ,

*Salicornia* shows distinctly lower backscatter intensity compared to other vegetation habitats. These two observations show that there is more vegetation backscatter compared to the sand and mudflats, but with low intensity. This can be well explained if we realise the habitat is partially covering bare soil with low (up to 10-15 cm) *Salicornia* vegetation.

- The *Spartina* habitat has the highest backscatter intensity for all backscatter intensity channels in both S-band and X-band frequencies, with a relatively low standard deviation. Especially the HV backscatter from both frequency bands is distinctly higher than other habitats. This indicates that the habitat has a well-developed botanical structure which shows relatively little variability and appears little influenced by environmental factors
- The salt marsh meadow habitats cause lower SAR backscatter intensity than the *Spartina* habitat, which might be attributed to the lesser volume of vegetation. Additionally, the standard deviations of the backscatter intensity channels in S-band are higher, indicating there is more variability in backscatter returns in this frequency domain. On average, the average backscatter intensity is coinciding with the *Salicornia* habitat, which is botanically characterised by vegetation of similar height.
- The *Juncus* vegetation habitat shows the lowest standard deviation of all habitats, indicating a relatively homogeneous environmental and botanical setting. The backscatter intensity in S-band HV polarisation is relatively high, indicating that the structural composition of this habitat causes a considerable re-polarisation of polarimetric SAR. On the whole, the backscatter signature of this habitat is largely coinciding with the *Spartina* habitat, albeit with lower standard deviations.

### 5.3.2 CP polarimetric decomposition variables

Similar to the presentation of the SAR variable analysis results in the previous section, variables from the Cloude-Pottier decomposition (Entropy ( $H$ ), Anisotropy ( $A$ ) and alpha angle ( $\alpha$ )), are presented as scatterplots of S-band against X-band values in Figure 22 and as boxplots in Figure 25. A tabulated overview of the mean values and the standard deviations is provided in Table 9. In the following paragraph the results

are briefly described, subsequently an interpretation with regard to environmental and botanical factors is made.

The alpha angle is indicative of the scatter mechanism dominant within a resolution cell, alpha angles between  $0^\circ$  and  $40-42.5^\circ$  indicate predominant surface scattering, angles between  $40-42.5^\circ$  and  $47.5-50^\circ$  to volume scattering and from  $47.5-50^\circ$  to  $90^\circ$  at double-bounce or multiple scattering. The entropy values are measure of the predominance of a single scatter mechanism. Entropy values between 0 and 0.5 indicate one scatter mechanism is predominant, between 0.5 and 0.9 there is clear presence of more than one scatter mechanism and beyond 0.9 the data is almost random noise. Anisotropy describes the relation between the second and third scattering contribution. High values of  $A$  denote the presence of only two scatter mechanisms, whereas low  $A$ -values denote equal measures of a second and third scatter mechanism.

The scatterplots of X-band against S-band CP decomposition variables show little correlation for the  $H$  and  $A$  variables and negative correlation for  $\alpha$ . The latter observation is especially worth noting: low  $\alpha$ -values for S-band data correspond with relatively high  $\alpha$ -values for X-band. In areas where S-band surface scatter (low  $\alpha$ -values) is the dominant scatter mechanism, double bounce (high  $\alpha$ -values) scatter is dominant for X-band SAR data. In locations with dominant S-band volume scatter ( $\alpha$ -values around  $45^\circ$ ), the  $\alpha$ -values for X-band are approaching  $50^\circ$ , also indicating volume scatter.

Another common way of presenting CP variables is in an  $H/\alpha$ -plot. In this plot entropy values are plotted on the horizontal axis, expressed in values between 0 and 1. The associated entropy value density plot is displayed above the scatterplot. The alpha values are expressed in values between 0 and 90 degrees and plotted on the vertical axis, with the associated density plot to the right of the scatterplot. In the scatterplot two curves are drawn that represent boundaries of maximum and minimum observable  $H/\alpha$ -values, in practice no values are observed that fall outside the feasible region. The straight dotted lines demarcate nine classification zones, as proposed by (Cloude and Pottier 1997). The  $H/\alpha$ -plots for S-band and X-band variables are presented in Figure 23 and Figure 24, respectively. The two  $H/\alpha$ -plots show a distinct different pattern,  $H/\alpha$ -values follow a gradual increasing trend for S-band SAR and

seem to be more clustered in an area with relatively  $H$  and  $\alpha$ -values for X-band SAR. The significance of this will be discussed in the end of this section, when behaviour of CP variables per habitat is discussed.

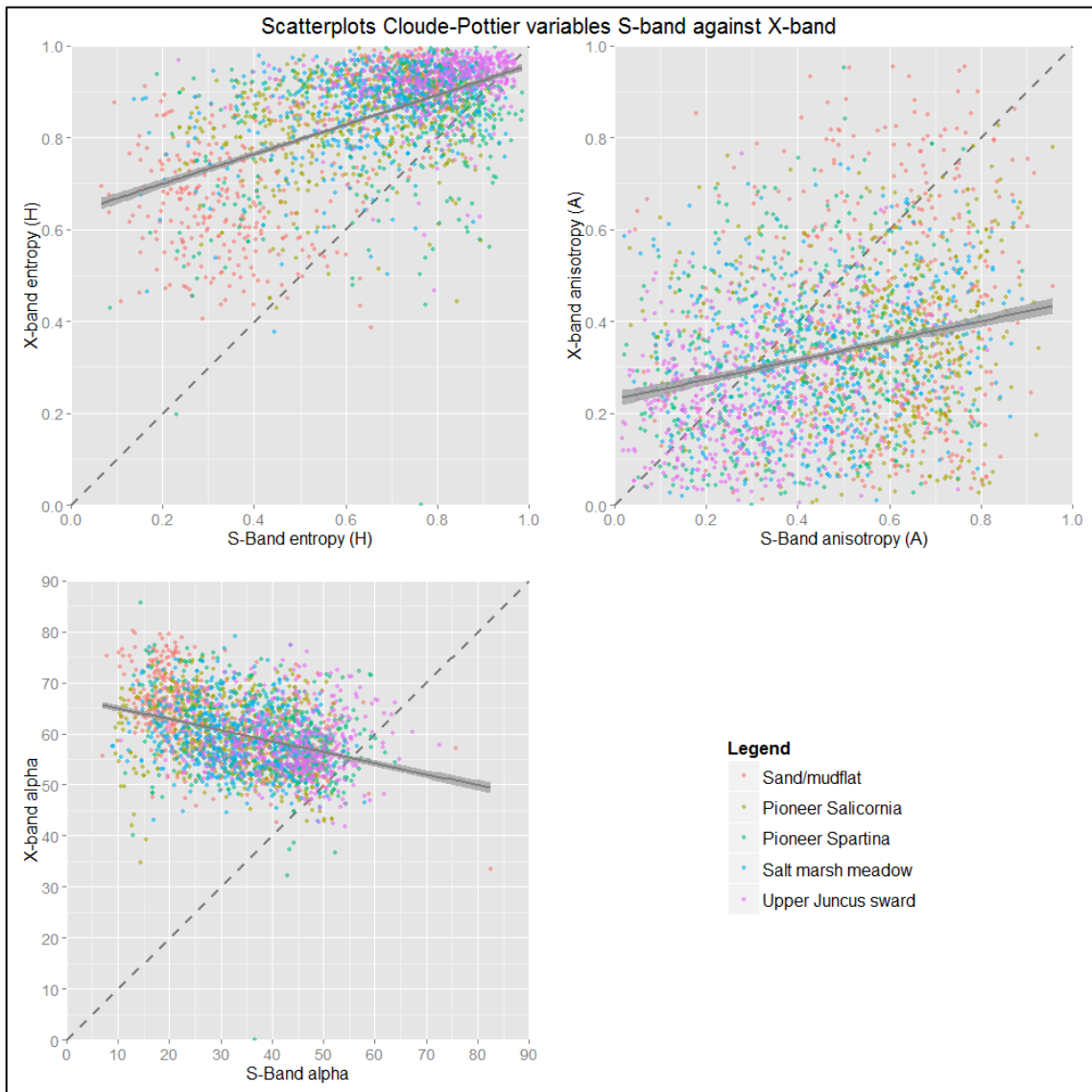


Figure 22 – Scatterplots SAR Cloude-Pottier decomposition variables X-band against S-band.



Figure 23 – Scatter plots and density plots of  $\alpha$  against  $H$  for S-band SAR data.

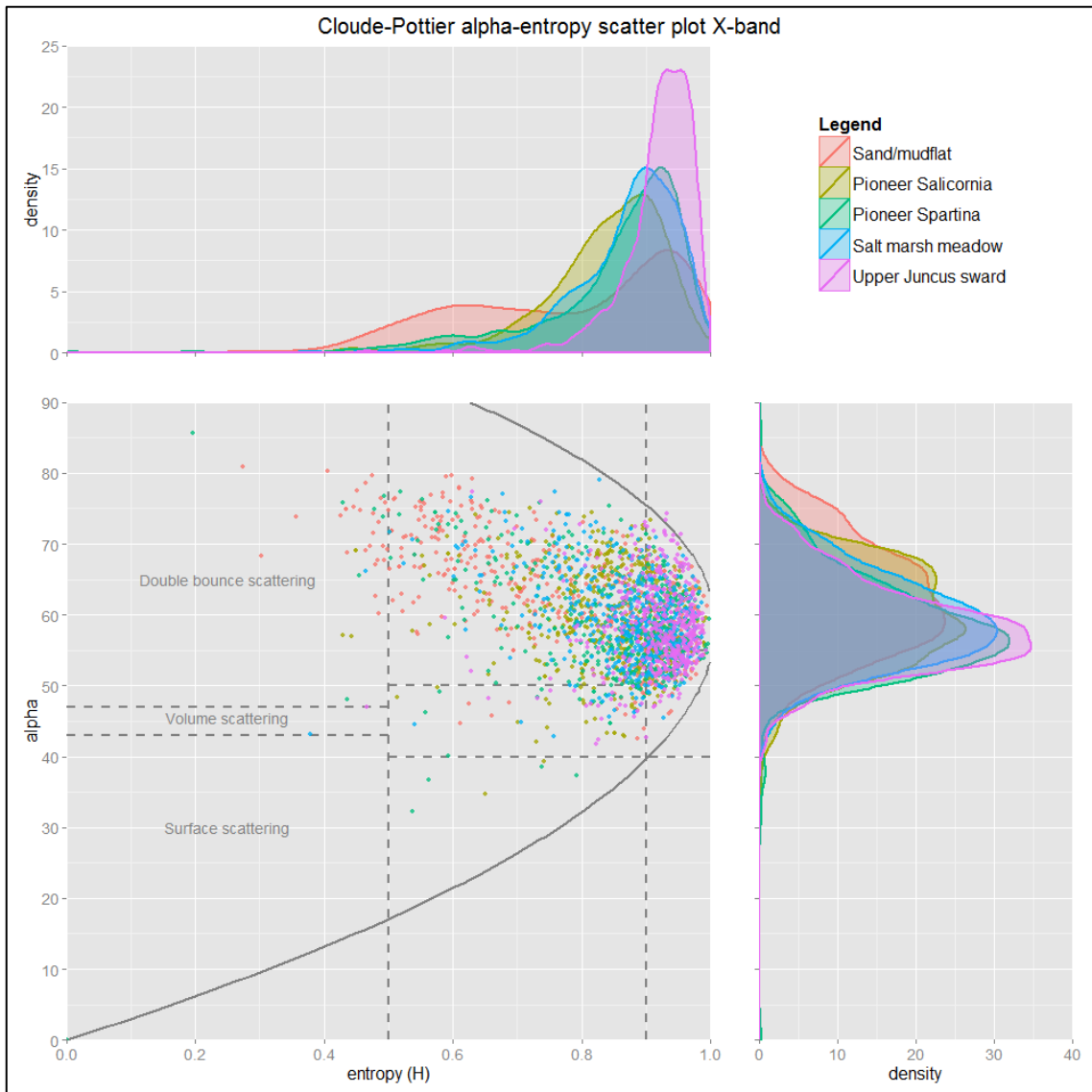


Figure 24 – Scatter plots and density plots of  $\alpha$  against  $H$  for X-band SAR data.

Boxplots (Figure 25) and the tabulated values (Table 9) of the CP variables for both frequency bands show a large variability in the different salt marsh habitats. The entropy and anisotropy values of the different habitats show high standard deviations for most habitats. The alpha angle values are more consistent, although there seems little variation between the different habitats, especially for X-band.

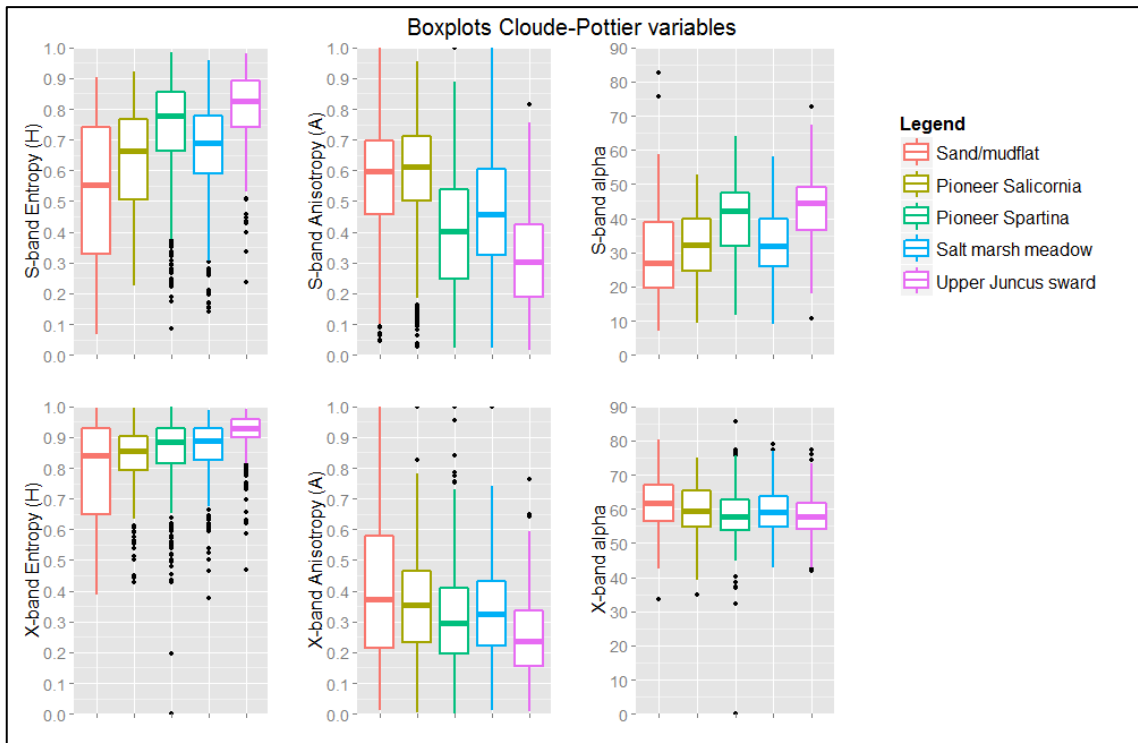


Figure 25 – Boxplots SAR CP decomposition variables against land cover classes.

Table 9 – Mean and standard deviations of CP polarimetric decomposition variables per habitat.

Habitat	Mean S H	SD S H	Mean S A	SD S A	Mean S alpha	SD S alpha
Sand/mudflats	0.53	0.22	0.57	0.18	29.53	11.80
Pioneer <i>Salicornia</i>	0.63	0.17	0.58	0.18	31.91	10.28
Pioneer <i>Spartina</i>	0.73	0.18	0.40	0.19	39.51	10.94
Salt marsh meadow	0.67	0.16	0.46	0.19	32.32	9.33
Upper <i>Juncus</i> sward	0.80	0.12	0.31	0.16	42.59	9.66
Habitat	Mean X H	SD X H	Mean X A	SD X A	Mean X alpha	SD X alpha
Sand/mudflats	0.79	0.16	0.40	0.23	62.04	7.64
Pioneer <i>Salicornia</i>	0.84	0.09	0.36	0.17	59.86	6.86
Pioneer <i>Spartina</i>	0.85	0.12	0.32	0.18	58.51	7.39
Salt marsh meadow	0.87	0.09	0.33	0.15	59.50	6.41
Upper <i>Juncus</i> sward	0.92	0.06	0.25	0.13	58.23	5.98

Interpretation of CP variable results per habitat tells us that:

- Sand and mudflats show the highest variability for all CP variables. This is exemplified in the highest standard deviations. This can be attributed to the environmental variation within this habitat, from dry sand flats to areas

covered with a thin layer of water. However, the entropy values are on average lower than the values of other habitats, especially for S-band. This indicates there is a more predominant scatter mechanism in this habitat compared to other habitats. Worth noting is the difference in alpha angle between S-band and X-band for this habitat, it indicates surface scatter for S-band and double-bounce scatter for X-band. This will be further discussed at the end of this section.

- The pioneer *Salicornia* habitat has entropy values between the sand and mudflats and the other vegetation habitats, indicating a gradual transition from bare surface to fully vegetated soil. The alpha angle indicates that surface scatter is the primary scatter mechanism for S-band, while double-bounce scatter is more dominant for X-band.
- The pioneer *Spartina* vegetation habitat has relatively high entropy values for both S-band and X-band, indicating there no clear pre-dominant scatter mechanism. The alpha angle ranges within the area of surface scatter for S-band and double bounce for X-band.
- Analysis of the CP variables for salt marsh meadow show a pattern largely coinciding with the *Salicornia* values, especially for  $H$  and  $\alpha$ . However, the values for  $A$  are considerably lower for the salt marsh meadows compared to the *Salicornia* habitat in S-band, indicating that in this frequency domain in salt marsh meadows a second and third scatter mechanism are more present than in *Salicornia* habitats.
- The *Juncus* habitat has the highest entropy for both frequencies, indicating that in this habitat there the main scatter mechanism is least dominant. The main scatter mechanism is volume scatter for S-band and double-bounce scatter for X-band.

### 5.3.3 VZ polarimetric decomposition variables

Variables from van Zyl decomposition variables (Surface (*Odd*), Volume (*Vol*) and Double Bounce (*DbI*) Scatter) are presented as scatterplots of S-band against X-band values in Figure 26. The scatterplots of S-band VZ variables against X-Band VZ variables show that the only decomposition variable of which the regression line approaches a



slope of 1 is VZ Double Bounce with slope of 0.9293, indicating that X-band VZ Double Bounce scatter approaches the sensitivity of S-band VZ Double Bounce scatter for this decomposition.

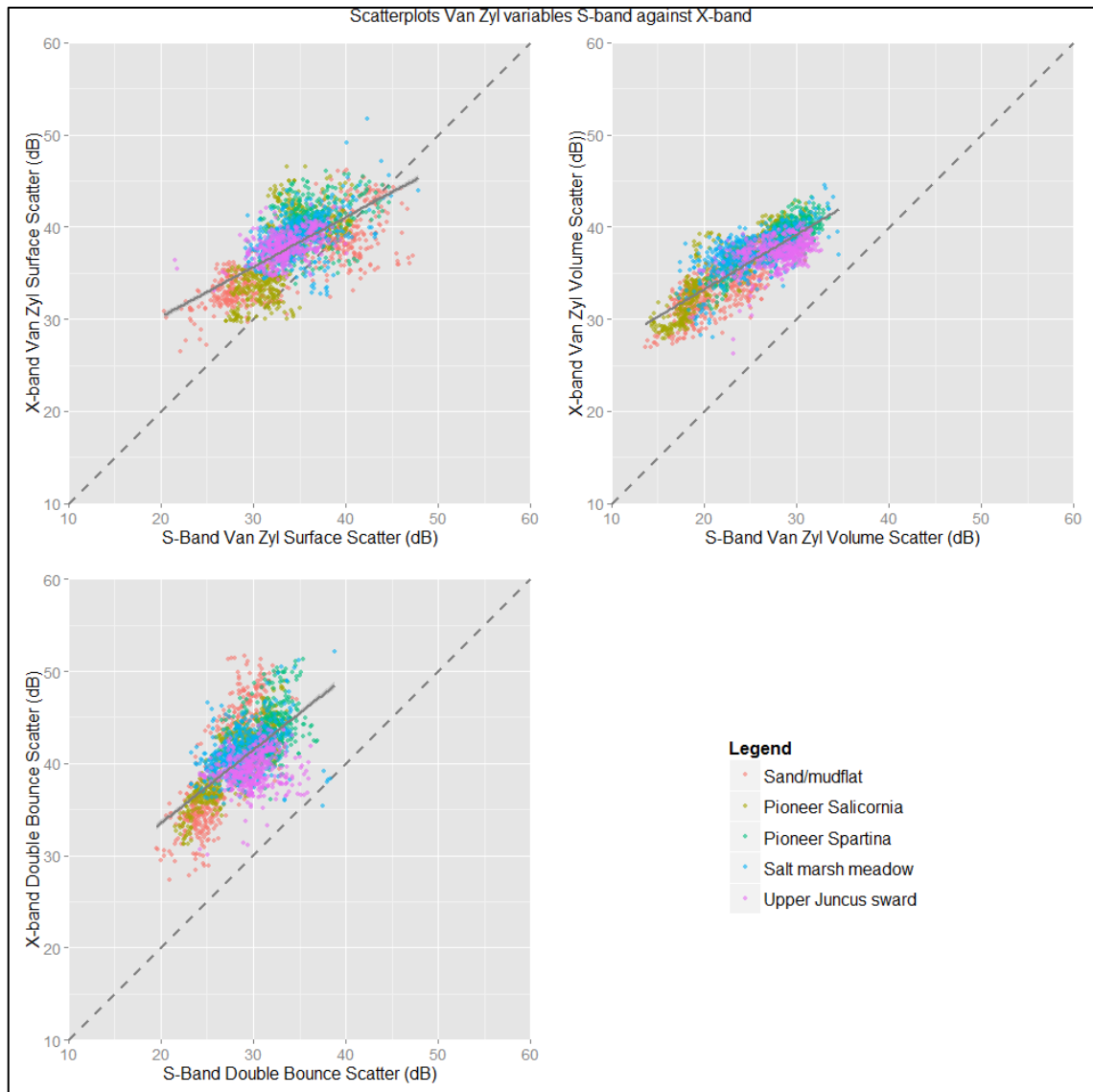


Figure 26 – Scatterplots SAR Van Zyl decomposition variables X-band against S-band.

The boxplots of the VZ variables for the different habitats are shown in Figure 27, the tabulated results in Table 10. From the boxplots it appears that the variability within the habitats is less than observed for the backscatter intensity polarimetric channels (Figure 21) and the CP variables (Figure 25). The highest values observed for the S-band variables are for surface scatter for all habitats, for X-band these are for double bounce scatter.

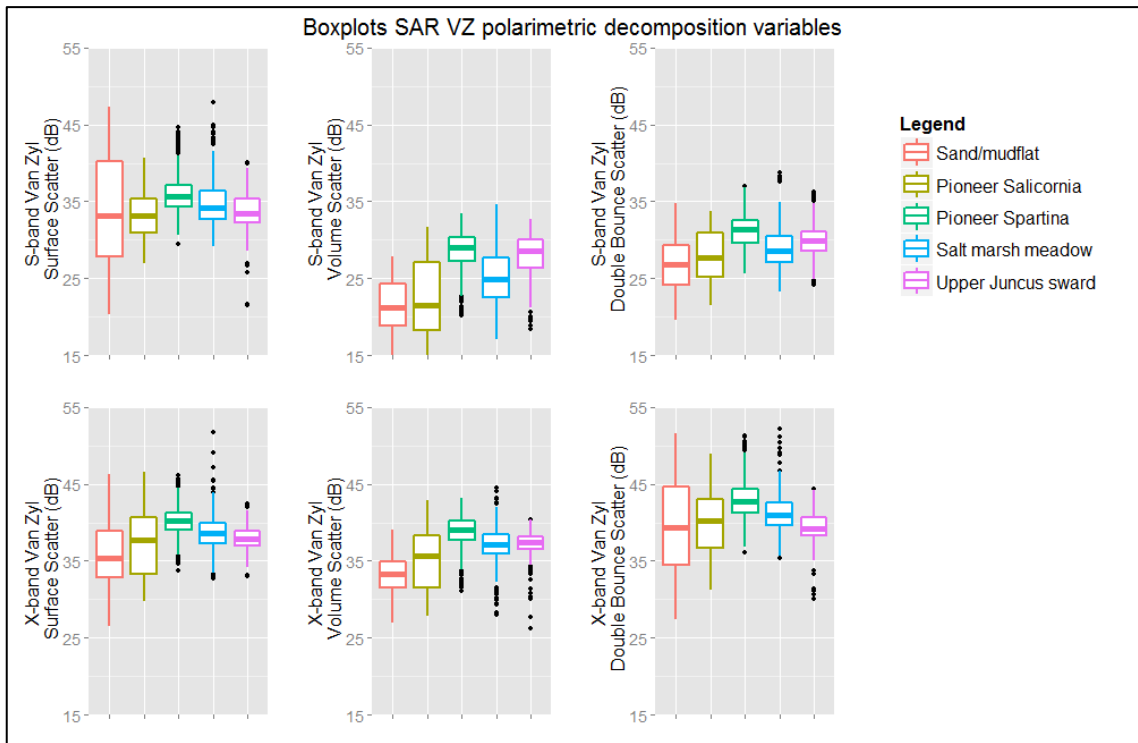


Figure 27 – Boxplots SAR VZ decomposition variables against land cover classes.

Table 10 – Mean and standard deviations of VZ polarimetric decomposition variables per habitat.

Habitat	Mean S Odd	SD S Odd	Mean S Vol	SD S Vol	Mean S Dbl	SD S Dbl
Sand/mudflats	34.09	6.65	21.43	3.13	26.79	3.01
Pioneer <i>Salicornia</i>	33.40	3.42	22.37	4.82	27.92	3.28
Pioneer <i>Spartina</i>	35.91	2.49	28.31	3.01	31.07	2.19
Salt marsh meadow	34.48	3.60	25.07	3.85	28.81	3.20
Upper <i>Juncus</i> sward	33.65	2.36	28.04	2.63	29.89	2.16
Habitat	Mean X Odd	SD X Odd	Mean X Vol	SD X Vol	Mean X Dbl	SD X Dbl
Sand/mudflats	36.19	3.94	33.15	2.46	39.61	5.81
Pioneer <i>Salicornia</i>	37.10	4.30	35.06	3.96	39.98	3.79
Pioneer <i>Spartina</i>	40.13	2.73	38.59	2.73	42.93	3.23
Salt marsh meadow	38.54	3.32	37.00	3.28	41.03	3.55
Upper <i>Juncus</i> sward	37.84	1.48	37.24	1.59	39.38	1.90

Interpreting the results for the VZ variables per habitat, the following things are worth mentioning:

- The values for sand and mudflats show the highest standard deviations for S-band surface scatter and for X-band double bounce scatter. This has been

similarly observed for the HH and VV backscatter intensity channels, with which surface and double bounce scatter is calculated in the VZ decomposition. The large variability indicates that there is relatively large impact of environmental factors.

- The VZ variables in the *Salicornia* habitat shows relatively high standard deviations for volume scatter in both frequency domains. This corresponds with relatively high standard deviations for the HV backscatter intensity channels, with which volume scatter is calculated in the VZ decomposition. Generally, values for any of the backscatter mechanisms are higher than backscatter from the sand and mudflats and lower than backscatter from the other vegetation habitats. This is consistent with findings for the CP variables, in which it appeared that *Salicornia* is a gradual transition from bare surface to fully vegetated terrain.
- The VZ variables in the *Spartina* habitat are consistently the highest for all backscatter mechanisms, which has been observed with the backscatter intensity channels as well. The standard deviations are relatively small.
- The salt marsh meadows show backscatter values that coincide with the values observed in the *Salicornia* habitat, albeit with smaller standard deviations. This coincides with the interpretation of the results of the backscatter intensity channels for the salt marsh meadow habitat.
- The *Juncus* habitat results for the VZ variables shows that this habitat has relatively high volume and double bounce backscatter for S-band. For X-band variables the habitat appears not to have a dominant scatter mechanism, which coincides with the high X-band CP entropy values observed. The standard deviations are the smallest for all VZ variables, which indicates that the habitat is relatively homogeneous in terms of environmental and botanical factors.

#### **5.3.4 Integration of results**

The three data sets extracted from the SAR data allows to model average SAR backscatter responses of each habitat. A graphic interpretation of the SAR mechanisms active in each habitat is provided in Figure 28. It was observed that backscatter from all polarimetric channels from the sand and mudflat is lower than the backscatter

intensity of other habitats. It was interpreted that this is to a certain extent due to specular reflection of SAR signal, caused by thin cover of water on the sand and mudflats. The influence of environmental factors in the vegetation habitats was less, with lower standard deviations of the backscatter intensity returns.

In the S-band domain the dominant backscatter mechanism was surface scatter, in the X-band domain double-bounce scatter. This is likely to be attributed to different interactions of the radar pulses due to their different wavelengths.

The last main observation is that CP entropy is lower in areas with less voluminous vegetation cover, or even bare areas. This indicates that in these areas less re-polarisation occurs and therefore less variation in scatter mechanism is observed. Contrary, in the habitats characterised by voluminous shrubby vegetation (*Spartina* and *Juncus*) all three scatter mechanisms are present, especially volume scatter differentiates these habitats from others.

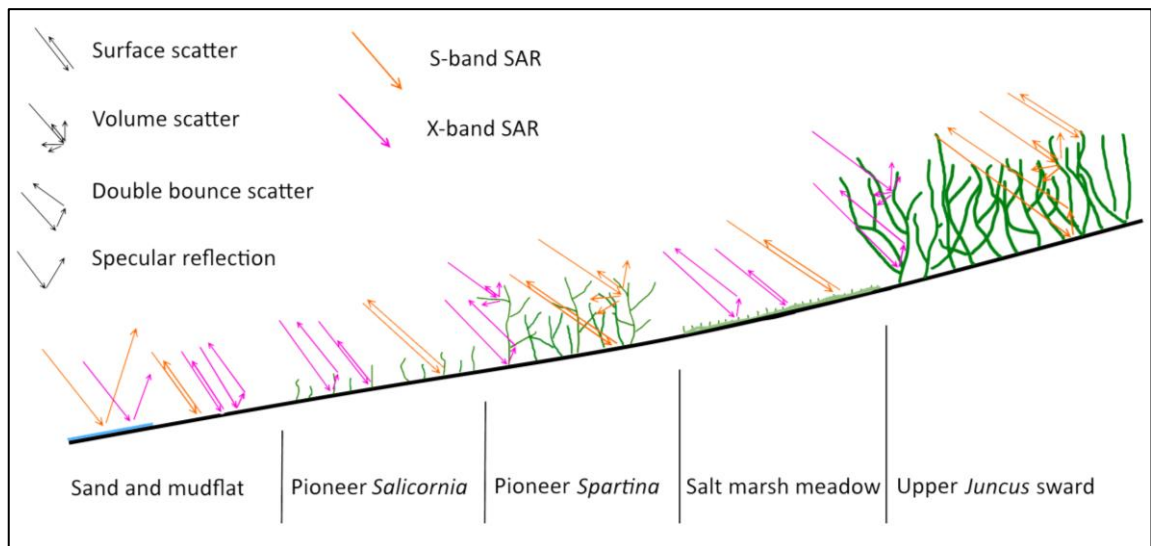


Figure 28 – Observed SAR backscatter mechanisms in different salt marsh habitats.

## 5.4. Discussion

### 5.4.1 SAR signatures of salt marsh habitats

Comparison of SAR backscatter response of different land cover classes was carried out by sampling SAR variables at specific field locations. Values of SAR variables were found to differ considerably between the land cover classes considered in this research. This is shown in the boxplots of backscatter intensity (Figure 21) and VZ polarimetric decomposition variables (Figure 27). The most distinctive habitat was

sand/mudflats, with higher standard deviation values for all backscatter intensity and polarimetric decomposition variables than the other habitats. This might be ascribed on a large extent to environmental factors, in this case predominantly variations in soil moisture. On sand and mudflats areas are often covered with a thin layer of water on the surface, causing specular reflections of the radar pulses. This phenomenon was also observed by Gade et al. (2011) and Lee et al. (2011). The implications of this specular backscatter effect are further discussed in the discussion of the methods (Chapter 5.4.1), as it is closely related to the repeatability of this research. The four vegetation classes showed less clear differentiation, although S-band HV backscatter intensity and VZ volume scatter showed clearly different values among these classes. The differences between these variables are discussed in more detail in the chapter about supervised classifications based on SAR variables (Chapter 6.4).

#### **5.4.2 S-band and X-band backscatter variations**

The CP variables showed that in the vegetation habitats surface scatter is the dominant scatter mechanism with S-band while the dominant scatter mechanism in X-band is double bounce scatter. This was confirmed by the VZ variables. This can be ascribed to the penetration of SAR signal into the vegetation. It has been observed by (Schmullius and Evans 1997) that higher frequency SAR bands do interact with the branches and leaves of trees, where longer wavelength bands can penetrate up to the trunks of trees or the soil. Salt marsh vegetation is quite a different habitat from a forest, so other relationships are valid. X-band SAR interacts mostly as double-bounce and volume scatter for the salt marsh habitats, while S-band tends to interact more as surface and volume scatter.

The analysis of SAR frequency bands showed that S-band displays a larger variability between the different land cover classes than X-band data. From the scatterplots of S-band and X-band data for both backscatter intensity (Figure 20) and VZ polarimetric decomposition variables (Figure 26) it was observed that more distinction between habitats was possible with S-band variables due to larger variability of backscatter intensity or backscatter mechanism. The average variance of backscatter intensity for the five habitats for S-band is 3.68 and for X-band it is 2.27. This indicated that there is more distinction between habitats possible with S-band than with X-band. However, it

appeared that X-band SAR was able to detect more subtle differences in surface roughness, suggesting X-band is more suited to detect subtle differences in vegetation composition such as are found in the pioneer zone of the salt marsh. This was in line with the results from Clint Slatton et al. (2008), who argued that C-band SAR was too sensitive to structural differences in salt marsh vegetation to be able to identify distinctions among the major vegetation habitats. In contrast, S-band SAR wavelength distinguished the main salt marsh vegetation habitats.

Other research into application of different SAR frequencies in coastal environments confirmed that different SAR frequency bands respond in different ways to different land cover types and each frequency band had its optimal application domain (Clint Slatton et al. 2008; Choe et al. 2012; Gade et al. 2014). The research carried out by Gade et al. (2014) was based on L-band, C-band and X-band SAR data acquired by the ALOS-PALSAR, Envisat ASAR and Terrasar-X satellites, respectively. It focused primarily on the characterisation of sediment type and surface roughness of sand and mudflats in the German Wadden Sea. They argued that multi-frequency SAR data, when used as in an integrated model, is capable of characterising different sandflat morphologies to a large extent, although they did not discuss the specific contribution of each SAR frequency band in detail. In the research carried out by Choe et al. (2012) more attention was given to different behaviour of the used SAR frequency bands (C-band and L-band) and they found that differences in surface roughness between mudflats and oyster banks are well identified with C-band data due to significant depolarisation of SAR channels. Contrary, this phenomenon was not observed in the L-band SAR data set, which led to the conclusion that longer wavelengths are not sensitive to differences in surface roughness between mudflat and oyster bed. Focussing more on salt marsh vegetation Clint Slatton et al. (2008) found L-band SAR to be preferable to C-band for vegetation characterisation, as it was less disturbed by small changes in vegetation structure and provided more homogeneous data.

### **5.4.3 Backscatter intensity and polarimetric decomposition variables**

The boxplots of the S-band and X-band backscatter intensity values (Figure 21) and the S-band and X-band VZ polarimetric decomposition values (Figure 27) showed that statistical distribution of values for the different salt marsh habitats showed smaller

variance for VZ polarimetric decomposition than for backscatter intensity variables. This was confirmed by calculating the variance of all mean values of the backscatter intensity variables of all habitats (Table 8) and the variance of the VZ polarimetric decomposition variables (Table 10). The total variance for backscatter intensity variables was 27.99, compared to 31.36 for the VZ polarimetric decomposition variables. This indicates that the mean VZ polarimetric decomposition values for different habitats than are more different from each other than the backscatter intensity values for the different habitats. Additionally, the mean standard deviation of all backscatter intensity variables is calculated as 3.59, the mean standard deviation from VZ polarimetric decomposition variables is 3.26, indicating that the statistical distribution of values of each habitat for VZ polarimetric decomposition variables is slightly less dispersed.

This shows that polarimetric decomposition variables differentiate more between salt marsh habitats than polarimetric backscatter intensity variables. This has been confirmed by previous research in other environments. Freeman and Durden (1998) argued that their three-component scattering mechanism (the FD decomposition as used in this thesis) was useful for distinguishing between different land cover types. The popularity of the FD decomposition algorithms in polarimetric SAR studies (Ballester-Berman and Lopez-Sanchez 2010; Taghvakish 2012) has demonstrated the utility of this model. However, few studies that directly compared polarimetric decomposition variables and SAR backscatter intensity variables have been carried out. Huang et al. (2011) compared backscatter intensity variables with Pauli and CP decomposition in order to map glacial land cover types. They found that image classification based on  $H$ ,  $A$  and  $\alpha$ -variables of the CP decomposition provide higher accuracies than classification based on the Pauli decomposition, which in turn provided higher levels of accuracy than classification based on backscatter intensity variables alone. In the research described by Choe et al. (2012) FD decomposition variables were analysed to distinguish backscatter mechanism differences in an intertidal mudflats. They found that these variables were sensitive to differences in surface roughness and provide useful additional information for mapping of coastal habitats. Lönnqvist et al. (2010) described a number of different classification routines based on both backscatter intensity variables and CP decomposition variables. They found CP

decomposition variables were preferable over backscatter intensity variables, as they provided better classification accuracies and were better suited to be used for unsupervised classification. However, the availability of quad-polarimetric SAR data is limited and the processing of quad-polarimetric SAR to polarimetric decomposition variables complex.

### **5.5. Summary**

The results from the research experiment presented in this chapter indicate that quad-polarimetric SAR data provides a lot of information about environmental and botanical parameters in a salt marsh setting. Analysis of backscatter signatures from S-band and X-band SAR data sets indicate that each of these SAR frequencies show different response to salt marsh habitats, with a larger dynamic range observed for S-band variables. The extraction of polarimetric decomposition variables showed that these variables are slightly better for discrimination different salt marsh habitats than backscatter intensity variables alone.



## 6. Mapping of salt marsh habitats

### 6.1. Introduction

In this chapter it is aimed to provide an answer to the second research question:

*Does the inclusion of SAR in a RS data set based on optical and LiDAR data improve mapping of both salt marsh extent and individual salt marsh habitats?*

Initially, unsupervised classification of salt marsh habitats based on CP polarimetric variables is done. This habitat map is based upon the unsupervised Wishart K-means classifier, which has been developed to deal specifically with SAR data (Cloude and Pottier 1997). This is carried out to check the performance of polarimetric SAR for habitat mapping on its own.

Subsequently, habitat mapping is carried out with supervised classifiers, using a combined RS data set consisting of optical, LiDAR and SAR data. In order to answer the RQ in the most logical way first a number of supervised classification results based on a combination of optical and LiDAR variables are presented. After this a number of supervised habitat mapping based on SAR variables are presented. The last stage involves combinations of optical, LiDAR and SAR variables.

The supervised habitat mapping is carried out with the Support Vector Machine (SVM) and Random Forest (RF) classifiers, which have been used for ecological mapping previously (Gislason et al. 2006; Mountrakis et al. 2011) and have shown to provide accurate results (Lardeux et al. 2009; Rodriguez-Galiano et al. 2012). These classifiers allow analysis of variable importance for classification, which has been carried out for the different variable combinations. The habitat classes under consideration for this research experiment were:

1. Wet sand or mudflat
2. Dry sand or mudflat
3. Pioneer *Salicornia spp.*
4. Pioneer *Spartina anglica*
5. Salt marsh meadow
6. Upper *Juncus maritimus* sward

The only difference from the classes used in the SAR variable analysis chapter (Chapter 5) is that the sand and mudflats are differentiated in wet and dry areas, as interpreted from the SAR imagery. This is done to analyse classification accuracy difference for these classes. In this way additional information can be extracted from the impact of soil moisture differences on SAR signal and classification potential.

In the last part of the analysis a salt marsh vegetation extent map based on the combined RS data set is compared with salt marsh vegetation extent maps from previous mapping efforts. The change of salt marsh vegetation cover is analysed over a period of 12 years.

## **6.2. Methods**

This section describes the methods used for the analysis of salt marsh vegetation mapping with the combined RS data set. A flowchart overview summarising the different analyses and their inter-relations are shown in Appendix B.

### **6.2.1 Unsupervised habitat classification with SAR data**

The CP polarimetric decomposition creates entropy ( $H$ ), anisotropy ( $A$ ) and alpha angle ( $\alpha$ ) variables that can be used for unsupervised image classification based on the Wishart K-means classifier (Lee et al. 1999). The relationships between CP decomposition  $H$ ,  $A$  and  $\alpha$  parameters provide information about the dominant scatter mechanisms in different habitats, as highlighted in Chapter 5. Analysis of the relationships between these parameters for the different vegetation habitats provides information about how SAR pulses interact (Cloude and Pottier 1997).

It has been found that covariance matrices of SAR data follow the complex Wishart distribution (Lee et al. 1999). The unsupervised K-means Wishart classifier implemented in PolSARpro classifies SAR data according to this distribution. This algorithm has been applied successfully in other studies (Lee et al. 1999; Reigber et al. 2010). The classifier works by assigning an arbitrary set of initial class centres and classification of the pixels by using Wishart distance. A set of updated class centres is derived from all pixels in each class, and a new class assignment is carried out. This iterative process is repeated until class membership converges.

By default, the K-Means Wishart classifier creates eight classes roughly corresponding to the eight common regions in the  $H/\alpha$ -plane defined by Cloude and Pottier (1997). In

the research area some of the eight classes were re-grouped according to the most likely land cover class they represented.

Two unsupervised habitat classification maps were created, one based on S-band CP variables, the other on X-band CP variables. Around each field survey sample locations a buffer zone with diameter of 10 meter was defined and from these areas 5597 pixels were randomly selected from the salt marsh vegetation habitats as well and dry and wet sand/mudflats for classification accuracy. The accuracy of the unsupervised classification was analysed with confusion matrices (Congalton 1991), for further explanation see Chapter 6.2.2.3.

## **6.2.2 Supervised habitat classification**

Mapping of salt marsh habitats in the research area has been carried out with supervised classifiers. Supervised classification models are based on known input values from locations within the research area. These models are generally more accurate than unsupervised classification models, and their accuracy can be assessed better (Lillesand et al. 2004). In this thesis two supervised classification methods were considered: Support Vector Machine (SVM) and Random Forest (RF) with the free-ware tool EnMAP-Box was used (Earth Observation Center (EOC) DLR 2014). This toolbox is developed by DLR and Humboldt University in Berlin and incorporates a number of advanced classification and regression algorithms.

### **6.2.2.1 Variable combinations**

For the salt marsh habitat mapping, a number of different variable combination scenarios have been used, summarised in Table 11. The underlying reason for the specific order of variable combination scenarios are that the habitat mapping effort starts off from the aerial imagery most commonly used for coastal mapping and adds more variables until all variables are included in the final variable model.

Table 11 – Variable combinations used for supervised classifications

Input variables		Classification model																			
		1	2	3	4	5	6	7	8	9	10	11	12	13	14	15	16	17	18	19	20
Optical	RGB	X					X													X	
	NDVI_1		X	X		X	X												X	X	
	NDVI_2		X		X	X	X													X	
LiDAR	DSM	X		X	X	X	X												X	X	
S-band SAR	Intensity							X				X						X	X	X	X
	CP								X										X		X
	FD									X									X		X
	VZ										X	X						X	X	X	X
X-band SAR	Intensity												X				X	X	X	X	X
	CP													X					X		X
	FD														X				X		X
	VZ															X	X	X	X	X	X

The first model incorporates three variables from the RGB optical imagery (R, G and B channels) and the LiDAR DSM variable, which are commonly used in coastal mapping projects (Environment Agency 2011; Environment Agency and Natural England 2011). This variable combination is analysed in variable model 1. Subsequently, the use of NDVI variables (extracted from easily obtainable medium-resolution Landsat satellite imagery) for salt marsh habitat mapping is analysed. Initially an assessment is made of most useful NDVI variable from different seasons for salt marsh vegetation mapping. This is analysed in variable model 2 to 5. Subsequently, in variable model 6, all optical and LiDAR variables are combined.

The use of SAR variable combinations for salt marsh habitat mapping are analysed in variable models 7 to 18. In total 12 polarimetric descriptors were used from each SAR frequency channel, which meant there were 24 SAR variables in total. The following S- and X-band SAR variables were used for habitat mapping:

1. HH, HV and VV channel backscatter intensity,
2.  $H$ ,  $A$  and  $\alpha$  variables from CP polarimetric decomposition,
3.  $P_v$ ,  $P_s$  and  $P_d$  variables from FD polarimetric decomposition,
4.  $P_v$ ,  $P_s$  and  $P_d$  variables from VZ polarimetric decomposition.

Each of these polarimetric descriptor types are tested singly in variable combination models 7 to 10 for S-band SAR and variable combination models 12 to 15 for X-band SAR. The SAR variables that create the most accurate salt marsh habitat maps are

combined in variable models 11, 16 and 17 for S-band alone, X-band alone and both frequencies combined, respectively. All available SAR variables are combined in Model 18. Finally, the optical, LiDAR and SAR variables are combined in models 19 and 20. The former model uses the most accurate variables of the three different sensors only, the latter uses all available variables. It consists of 30 variables in total.

Classification training samples were randomly selected from the field survey data. At each of the 100 field survey vegetation sample locations and 23 un-vegetated locations a circular buffer zone of with a radius of 5 meters was defined. On average in each buffer location contained 60 pixels, a grand total of 7376 pixels in 123 locations. Of each of the six land cover classes 300 pixels were selected randomly for training of the classification models, a total training data set of 1800 pixels.

#### ***6.2.2.2 Supervised classification variable importance***

Analysis of variable importance was carried out on the SVM and the RF classifiers. In the next two paragraphs a brief introduction into these two supervised classifiers is provided, explaining the specific steps needed to perform a variable importance analysis for both classifiers.

SVM classification is based upon an algorithm that fits hyperplanes (the support vectors) in hyper-dimensional feature spaces for the calculation of maximum separability between classes (Melgani and Bruzzone 2004). A good explanation of the working of the SVM classifier for land cover mapping is provided by Huang et al. (2002). Unlike ML classification, it is a nonparametric classifier that is trained on and for the data set under analysis. As such, SVM classifiers have been found to provide higher classification accuracies than other widely used classifiers and can cope well with multi-dimensional data and need little training data for good results (Melgani and Bruzzone 2004). The SVM classification algorithm implemented in EnMap-Box searches the optimal combination of parameters for the  $g$  and  $C$  variables, and trains the model with these parameters. The  $g$  parameter defines the width of the Gaussian kernel function. The Gaussian kernel is a so-called universal kernel, thus an SVC with this kernel can separate any class distribution at any precision. The regularisation parameter  $C$  controls the trade-off between the maximization of the margin between the training data vectors and the decision boundary plus the penalisation of training

errors (more precisely margin errors). Therefore  $C$  directly limits the influence of individual training data vectors. The use of a smaller number of input variables can result in a non-inferior accuracy compared to classifications based on all available variables. It has been observed by Chi et al. (2008) that SVM classification accuracy increases slightly if more variables are added, until it reaches an optimum number of variables after which the accuracy begins to decrease. Besides the accuracy decrease, image classification with fewer input variables provides some additional advantages in terms of data storage and computational processing costs (Pal and Foody 2010). Therefore the optimal number of variables was analysed after the initial SVM classification and the model was re-trained using a subset of the most important variables.

Random Forest (RF) classifiers have been applied successfully in ecological research (Cutler et al. 2007) and land cover mapping (Gislason et al. 2006). They are especially well suited for classification of multi-source remote sensing and geographical data. The RF algorithm is based on decision tree classification; it fits many classification trees to a multivariate data set and combines predictions from all the trees (Breiman 2001). The RF algorithm has been found to be relatively robust and superior to standard classification approaches (Rodriguez-Galiano et al. 2012). The output of the classifier is determined by a majority vote of the trees. The number of input variables is user-defined and can be any combination of remotely-sensed and other geographical data. At the onset of classification, the maximum number of decision trees is set sufficiently large and the random forest is grown using the input variables. A bootstrapped sample of the original training data is used to train the model. Test set accuracy is determined by cross-validation of the remaining training set samples (out-of-bag samples) with the RF model. The importance of variables can be estimated by randomly permuting the value of out-of-bag samples for a certain variable. The error increase that this out-of-bag sample permutation produces is a measure of the importance of this specific variable, indicating the influence of an input layer on the overall accuracy (Genuer et al. 2010). RF variable importance ( $VI$ ) of variable  $X^j$  is calculated by considering the associated out-of-bag sample ( $OOB_t$ , data not included in the samples used to construct the decision trees ( $t$ )), of which the error ( $err_{OOB_t}$ ) is calculated. Consequently, the values of  $X_j$  are randomly permuted ( $OOB_t^j$ ) and error calculated

( $errOOB_t^j$ ), the error of predictor  $t$  on the perturbed sample. Variable importance of  $X^j$  is then equal to:

$$VI(X^j) = \frac{1}{ntree} \sum_t errOOB_t^j - errOOB_t \quad (8)$$

which sums the error of a variable of all trees  $t$  of the RF.  $ntree$  denotes the total number of trees of the RF. The variable importance can be normalised by dividing the variable importance of each variable by its standard deviation. In this research analysis of variable importance was performed to rank all input variables according to their contribution to RF classification.

### **6.2.2.3 Supervised classification accuracy**

Validation samples were created by using remaining sample pixels that were not selected during random sampling of the training data. In total 5593 validation pixels were used. These validation samples were used to assess the accuracy of the supervised classifications by calculating overall classification accuracy and Kappa coefficients of each classification model (Congalton 1991). The overall classification accuracy is a measure of the number of pixels classified correctly and its predicting capabilities, the Kappa coefficient is a measure of to what extent these capabilities are due to chance. As a rule of thumb  $K < 0.4$  is regarded as poor agreement, between  $K > 0.4$  and  $K < 0.7$  as a good agreement and  $K > 0.7$  as excellent agreement. More information was provided by a confusion or error matrix, in which correctly and incorrectly classified pixels were tabulated, and producer and user accuracies were calculated (Congalton and Green 2008). In order to keep the size of this thesis manageable only the confusion matrix and classification map of the variable input model that generated the most accurate result for each classifier are presented in the results.

### **6.2.2.4 Vegetation extent change**

In order to analyse temporal change of vegetation cover, classification of vegetation extent was done with the same data set that was used for the habitat mapping. For this analysis two classes were distinguished:

1. Salt marsh habitat vegetation cover

## 2. No salt marsh habitat vegetation cover

For the extent mapping, 1000 training pixels were randomly selected from the sample locations for each land cover class. Accuracy was assessed by means of analysing classification accuracy assessment and Kappa coefficients, as discussed in the previous paragraph. In order to keep the number of reported maps and confusion matrices limited only the classification results of the most accurate classifier are presented in the results.

The vegetation extent map was based on RS data sets acquired in different years, spanning a period between 2006 and 2011. For comparison with other salt marsh vegetation extent maps it was needed to define the year in which the most important variables were acquired. From , the variable importance plot of the vegetation extent map it is clear that the most important variable is the NDVI\_1, from June 2010. Additionally, the SAR variables were also acquired in 2010. The importance of these to RS data sets amounted for 72.6% of total variable importance. Therefore it was decided to set the acquisition year of the RS data set on 2010.

Other time steps were provided by the following data sets:

1. The salt marsh vegetation extent map compiled by the EA (Environment Agency 2011). This vegetation mask is based on aerial photography acquired in June 2007. The EA salt marsh vegetation extent map is shown in Figure 29.
2. The CCW salt marsh survey of 1998 (Prosser and Wallace 1999), based on ecological field survey data and manual mapping with aerial photography. The reference vegetation extent map is derived from the CCW ecological survey salt marsh habitat map (Figure 17), dated 1998. NVC classes with prefix 'SM' correspond to salt marsh vegetation habitats; these were clustered into one class: 'Vegetation cover'. The rest of the pixels within the boundaries of the research area are classified as 'No vegetation cover'. The resulting vegetation extent map is shown in Figure 30.

Three time steps were used for the temporal analysis: from 1998 to 2007, from 2007 to 2010 and from 1998 to 2010. The last change analysis was done mainly to check if the total change of the former two change analyses were adding up to the same amount. The change in vegetation extent was presented in a vegetation change map, as well as a table with respective change values.



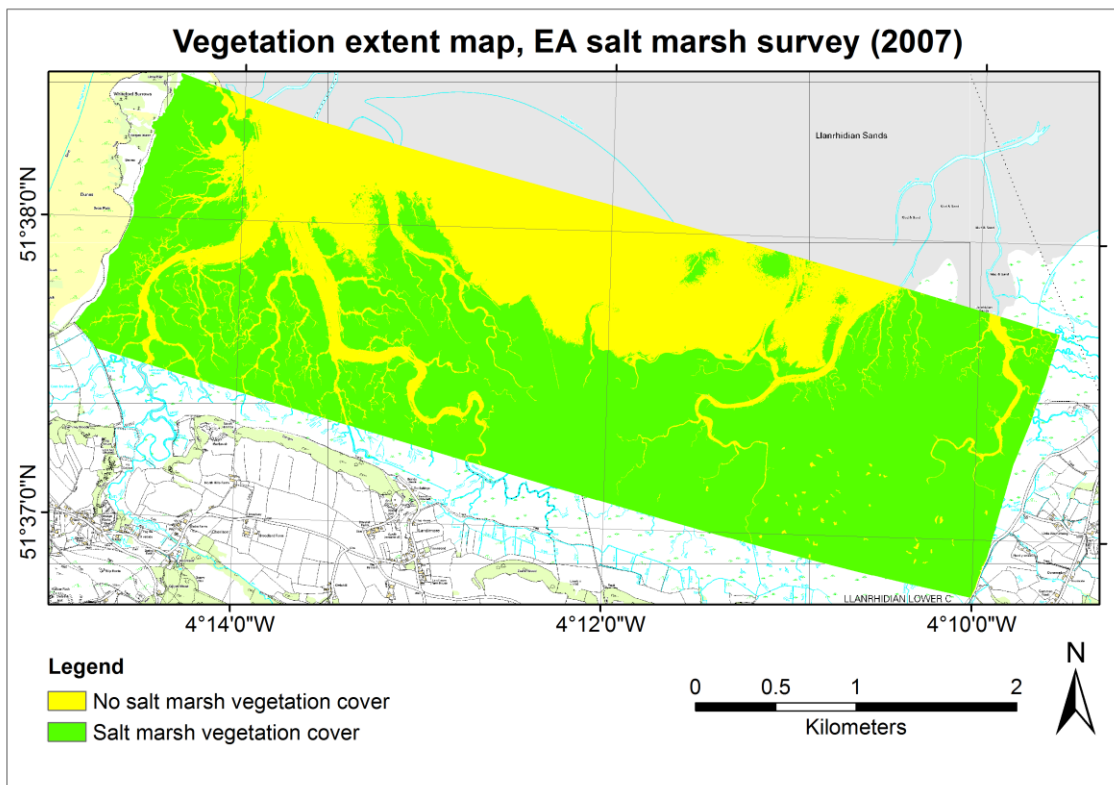


Figure 29 – Vegetation extent map based on EA salt marsh survey data (2007).

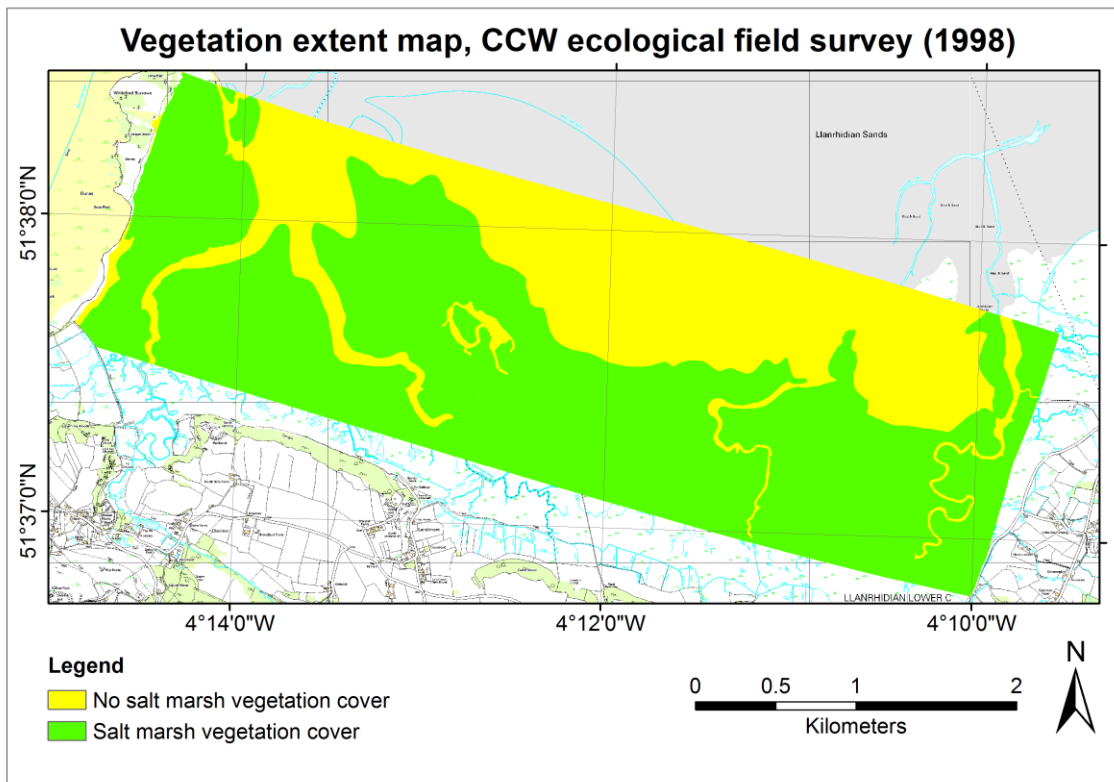


Figure 30 – Vegetation extent map based on CCW ecological survey data (1998).

## 6.3. Results

### 6.3.1 Unsupervised habitat classification with CP variables

In this section the results of unsupervised image classification with CP polarimetric decomposition parameters are presented, based on the unsupervised Wishart K-means classification. The classification map based on S-band is shown in Figure 31, the one based on X-band variables in Figure 32.

Confusion matrices of classification accuracy proposed by Congalton (1991) are calculated with validation data of the ecological field survey and are displayed in Table 12 and Table 13 for S-band and X-band classifications, respectively.

From the classification maps and accuracy assessments a number of observations can be made:

- The overall accuracy of unsupervised classification based on S-band is higher than the classification based on X-band, with values of 52.33% and 43.24% respectively. The kappa coefficients for the unsupervised classifications are 0.4191 and 0.2967 for S-band and X-band respectively. It can be stated that S-band classification is within statistically acceptable limits, although neither of the two classifications are satisfactory.
- Visual interpretation of the classification map based on S-band CP variables shows there is over-classification of *Salicornia spp.* This is particularly visible in the southeast of the research area where it is found surrounding the *Juncus maritimus* sward. It is likely that in this transitional zone from dense *Juncus maritimus* vegetation to salt marsh meadow the surface roughness corresponds most with *Salicornia*-covered areas. Furthermore the S-band classification map shows some confusion between wet sand and mudflats on one hand and salt marsh meadows, two land cover classes that have similar surface roughness. Accuracy assessment (Table 12) of this map shows that user and producer accuracies for *Salicornia* are lowest of all land cover classes with 7.71% and 19.81%, respectively.
- Distinction between vegetation habitats differing considerably in terms of vegetation height and volume is poorly achieved with unsupervised classification based on X-band CP variables. There is a large amount of mis-

classification between salt marsh meadows and *Juncus maritimus* swards on one hand and between *Spartina anglica* and *Salicornia* on the other hand. Nonetheless, distinction of subsidiary creeks and ponds is better achieved than in the S-band classification. Analysis of accuracy of X-band classification (Table 13) shows that the *Salicornia* land cover class is similar to the S-band classification, least accurately mapped with user and producer accuracies of 2.46% and 3.72%, respectively.

- In the far slant range part of the SAR images (the northern rim of the research area) extensive mis-classification occurs. The original SAR data is corrected for antenna pattern to compensate for signal attenuation differences over the slant range of the SAR image. Therefore, the signal-to-noise ratio of the far slant range part of the image is relatively low, which might have caused these mis-classifications.

Unsupervised classification algorithms group pixels without a-priori knowledge of land cover or reference data. Due to speckle noise, unsupervised classification of SAR data poses a unique challenge. The custom Wishart K-means classifier is capable of dealing with speckle to a large extent. On one hand the classification is far from perfect, overall accuracy and Kappa coefficients are quite low. On the other hand the classification results provide highly-detailed, quickly produced maps that distinguish well between different vegetation habitats and non-vegetated areas.

Table 12 – Confusion table of unsupervised CP Wishart K-means with S-band SAR classification.

		Reference data							User accuracy (%)
		Bare sand / mud wet	Bare sand / mud dry	Pioneer <i>Salicornia</i>	Pioneer <i>Spartina</i>	Salt Marsh Meadow	<i>Juncus maritimus</i>	Row total	
Classified data	Bare sand / mud wet	804	126	191	30	200	34	1385	58.05
	Bare sand / mud dry	1	742	10	79	147	2	981	75.64
	Pioneer <i>Salicornia</i>	1	0	64	22	520	223	830	7.71
	Pioneer <i>Spartina</i>	0	22	54	191	560	153	980	19.49
	Salt Marsh Meadow	3	16	4	19	972	73	1087	89.42
	<i>Juncus maritimus</i>	0	1	0	74	103	156	334	46.71
	Column total	809	907	323	415	2502	641	5597	
	Producer accuracy (%)	99.38	81.81	19.81	46.02	38.85	24.34		<b>Overall accuracy 52.33 %</b>

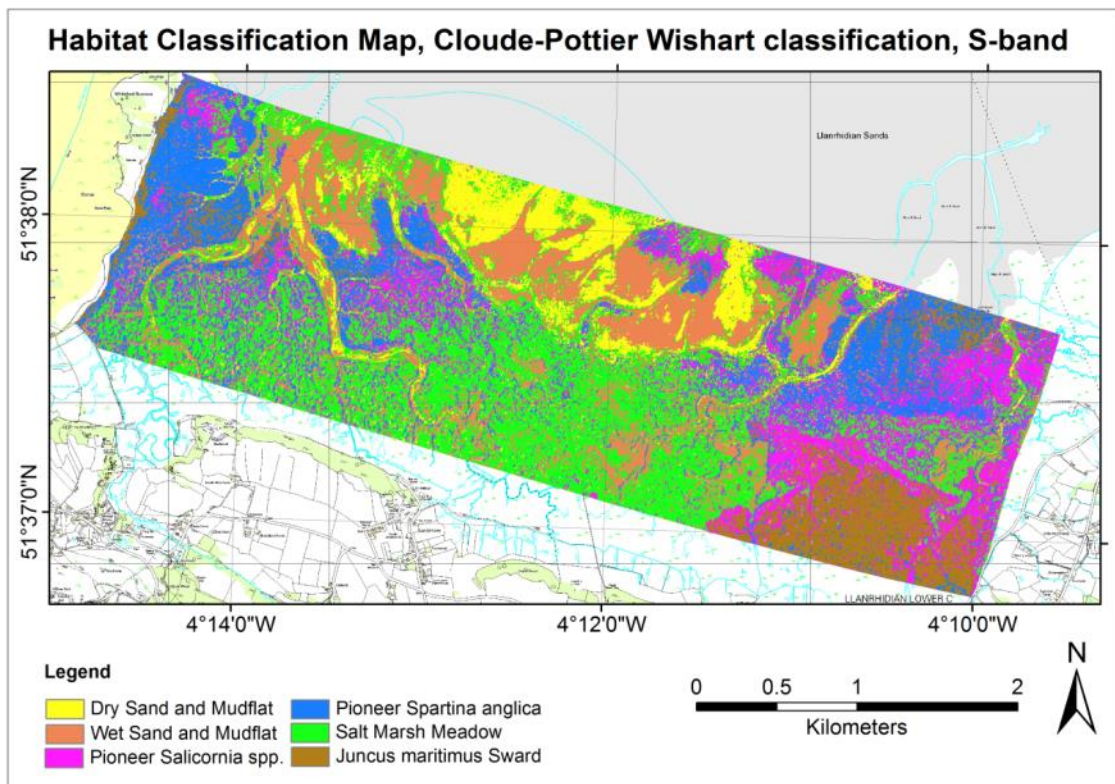


Figure 31 – Habitat map of unsupervised CP Wishart K-means S-band SAR classification.

Table 13 – Confusion table of unsupervised CP Wishart K-means with X-band SAR classification.

		Reference data						Row total	User accuracy (%)
		Bare sand / mud wet	Bare sand / mud dry	Pioneer <i>Salicornia</i>	Pioneer <i>Spartina</i>	Salt Marsh Meadow	<i>Juncus maritimus</i>		
Classified data	Bare sand / mud wet	775	6	153	0	68	23	1025	75.61
	Bare sand / mud dry	2	213	10	45	74	1	345	61.74
	Pioneer <i>Salicornia</i>	0	296	12	56	123	0	487	2.46
	Pioneer <i>Spartina</i>	3	12	115	218	648	148	1144	19.06
	Salt Marsh Meadow	2	300	29	63	870	137	1401	62.10
	<i>Juncus maritimus</i>	26	80	4	33	716	332	1191	27.88
	Column total	808	907	323	415	2499	641	5593	
	Producer accuracy (%)	95.92	23.48	3.72	52.53	34.81	51.79		<b>Overall accuracy 43.24 %</b>

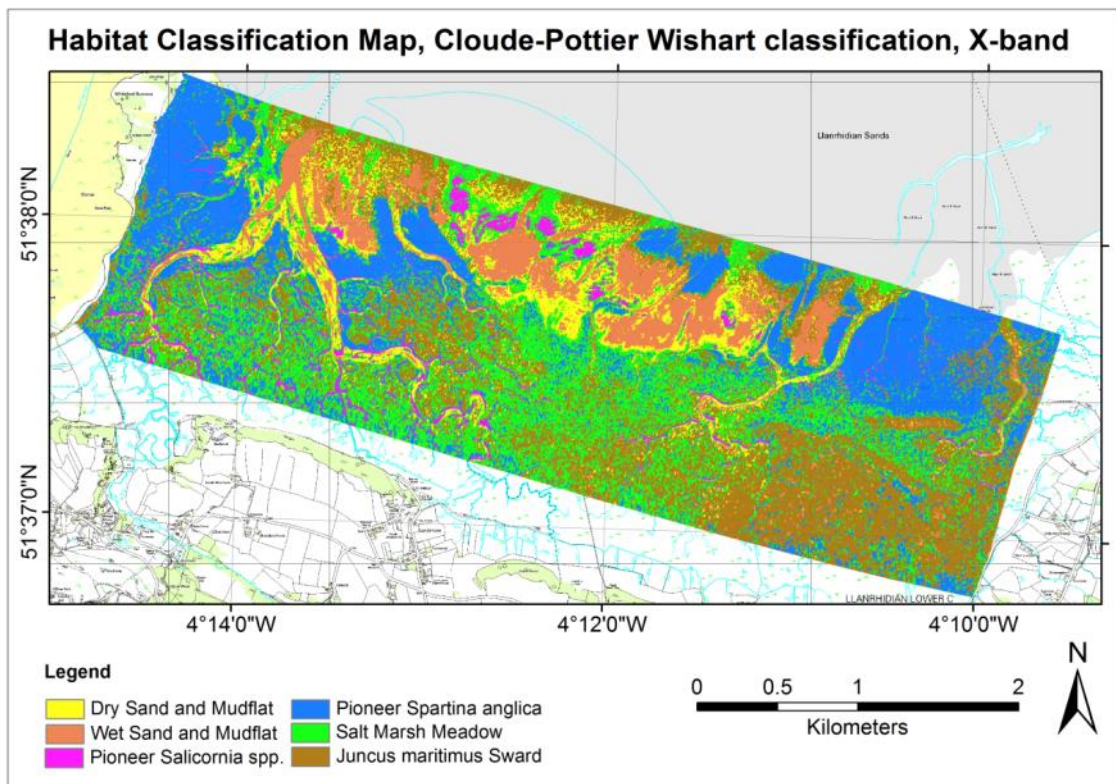


Figure 32 – Habitat map of unsupervised CP Wishart K-means X-band SAR classification.

### **6.3.2 Supervised habitat classification**

This section presents results of supervised habitat classification mapping for the SVM and RF classifiers. To test the classification performance of different RS data types a number of different data variable combinations are used. The different variable combinations are discussed in Chapter 6.2.2.1.

#### ***6.3.2.1 SVM habitat classification***

The SVM supervised classification algorithm allows extra tuning of classification by variable analysis after initial classification, selection of the most significant variables and re-classification with this subset of variables. Accuracy assessments of SVM supervised classification with the different variable combination models are shown in Table 14. This table is subdivided in five sections, the first section provides accuracy assessment values of variable models based on optical and LiDAR data, the second on S-band SAR, followed by a section on X-band SAR and one combining S-band and X-band SAR. The last section shows accuracy assessments of two models combining the optical, LiDAR and SAR variables.

Table 14 – Overall classification accuracy and Kappa coefficient for the SVM classification models.  
The model with highest accuracy is indicated in bold.

Variable Model	Overall accuracy (%)	Kappa coefficient
DSM, RGB	50.22	0.38
NDVI (1,2)	51.44	0.35
DSM, NDVI (1)	57.82	0.45
DSM, NDVI (2)	51.60	0.36
DSM, NDVI (1,2)	54.03	0.38
DSM, RGB, NDVI (1,2)	58.25	0.44
S-band (Int)	57.01	0.45
S-band (CP)	37.13	0.24
S-band (FD)	58.33	0.48
S-band (VZ)	56.73	0.46
S-band (Int,VZ)	59.64	0.47
X-band (Int)	44.22	0.31
X-band (CP)	25.89	0.15
X-band (FD)	46.56	0.35
X-band (VZ)	44.49	0.34
X-band (Int,VZ)	45.35	0.33
S-band (Int,VZ), X-band (Int,VZ)	61.87	0.50
S-band (Int,CP,FD,VZ), X-band (Int,CP,FD,VZ)	60.43	0.50
DSM, NDVI (1), S-band (Int,VZ), X-band (Int,VZ)	70.18	0.59
<b>DSM, RGB, NDVI (1,2), S-band (Int,CP,FD,VZ), X-band (Int,CP,FD,VZ)</b>	<b>72.09</b>	<b>0.64</b>

Per variable input section, the most interesting observations can be made about the classification accuracies:

- The optical and LiDAR variable models have accuracies between 50 and 58%, with the most accurate model the model based on all optical and LiDAR variables with 58.25%. The model based on the DSM and NDVI\_1 variables is more accurate than the model based on DSM and NDVI\_2 variables, with 57.82% and 51.60% accuracy, respectively. This indicates that the NDVI variable derived from a Landsat image acquired in June provides more distinction between different salt marsh habitats than an NDVI variable derived from a



Landsat image acquired in April. Combining multiple NDVI variables in one classification model does not necessary improve classification.

- The classification models based on S-band SAR variables are between 37 and 60% accurate, with the most accurate model based on backscatter intensity and VZ polarimetric decomposition variables with 59.64%. It appears that CP polarimetric decomposition variables are not well suited for SVM classification with accuracy of 37.13%. The accuracies are in general very similar to or slightly higher than the variable models based on optical and LiDAR data.
- X-band SAR variable models are less accurate than S-band SAR variable models, ranging between 25% and 47% overall accuracy. The most accurate model is based on X-band FD variables, with 46.56%. Again, the model based on X-band CP polarimetric decomposition variables is the least accurate (25.89%).
- The models based on a combination of S-band and X-band SAR variables are slightly more accurate than the models based on S-band SAR variables alone, with accuracies between 60% and 62%. Interestingly, the model based on backscatter intensity and VZ polarimetric decomposition variables from both frequency bands is slightly more accurate than the model based on all available SAR variables.
- The models based on a combination of optical, LiDAR and SAR variables have an accuracy of 70.13% and 72.09% for the model based on a selection of the most important (selection based on interpretation of the previously mentioned accuracy assessments) and the model based on all available RS variables, respectively. It appears that these combination models have a significant higher accuracy than the models based on either optical, LiDAR or SAR variables alone.

After initial classification a variable analysis has been carried out with the model incorporating all available RS variables. Results of this analysis are shown in tabulated form Table 15 and graphically in Figure 33.



Table 15 – SVM feature selection analysis.

Optical variables are highlighted in red, LiDAR variable in grey, S-band variables in green, X-band variables in blue. The 21 most important variables are bounded by a white line.

Variable name	Rank	Accuracy assessment (%)	
		Internal validation	Independent validation
NDVI_1	1	52.36	39.32
X_Int_VV	2	69.96	52.83
S_Int_HV	3	74.85	62.14
DSM	4	77.01	62.50
NDVI_2	5	79.96	72.18
S_VZ_Odd	6	82.34	76.65
RGB_R	7	83.06	74.75
RGB_G	8	85.34	75.59
S_Int_VV	9	86.45	76.70
S_CP_alpha	10	87.28	77.72
S_FD_Dbl	11	87.73	75.04
RGB_B	12	88.56	74.54
X_FD_Dbl	13	88.62	74.47
X_CP_H	14	89.06	73.63
S_VZ_Vol	15	89.56	73.66
X_Int_HH	16	89.39	73.95
S_Int_HH	17	89.56	73.74
X_CP_alpha	18	90.51	74.02
X_VZ_Dbl	19	90.39	74.49
S_CP_H	20	90.73	73.97
X_FD_Vol	21	90.95	74.04
S_FD_Vol	22	90.23	73.88
X_VZ_Odd	23	90.34	73.74
S_FD_Odd	24	90.06	73.72
X_Int_HV	25	90.56	73.88
X_VZ_Vol	26	89.95	73.91
S_CP_A	27	90.45	73.79
S_VZ_Dbl	28	90.12	73.61
X_CP_A	29	90.39	73.24
X_FD_Odd	30	88.62	72.34

The variables were ordered according to their contribution to the SVM classification model. Two validations have been done, an internal cross-validation with a subset of the training samples and an independent validation using external validation samples. Internal validation samples are part of the sample population on which the SVM classification model is based, therefore overall accuracy of the internal validation is generally higher than the independent validation. Independent validation samples are

not used in improving the SVM model, therefore more attention was given to the internal validation for further classification. The highest ranked variable is NDVI\_1, accounting for 52.36% classification accuracy for internal validation. After the second-ranked variable (X-band VV intensity) was added the overall accuracy increased to 69.96% for the internal validation.

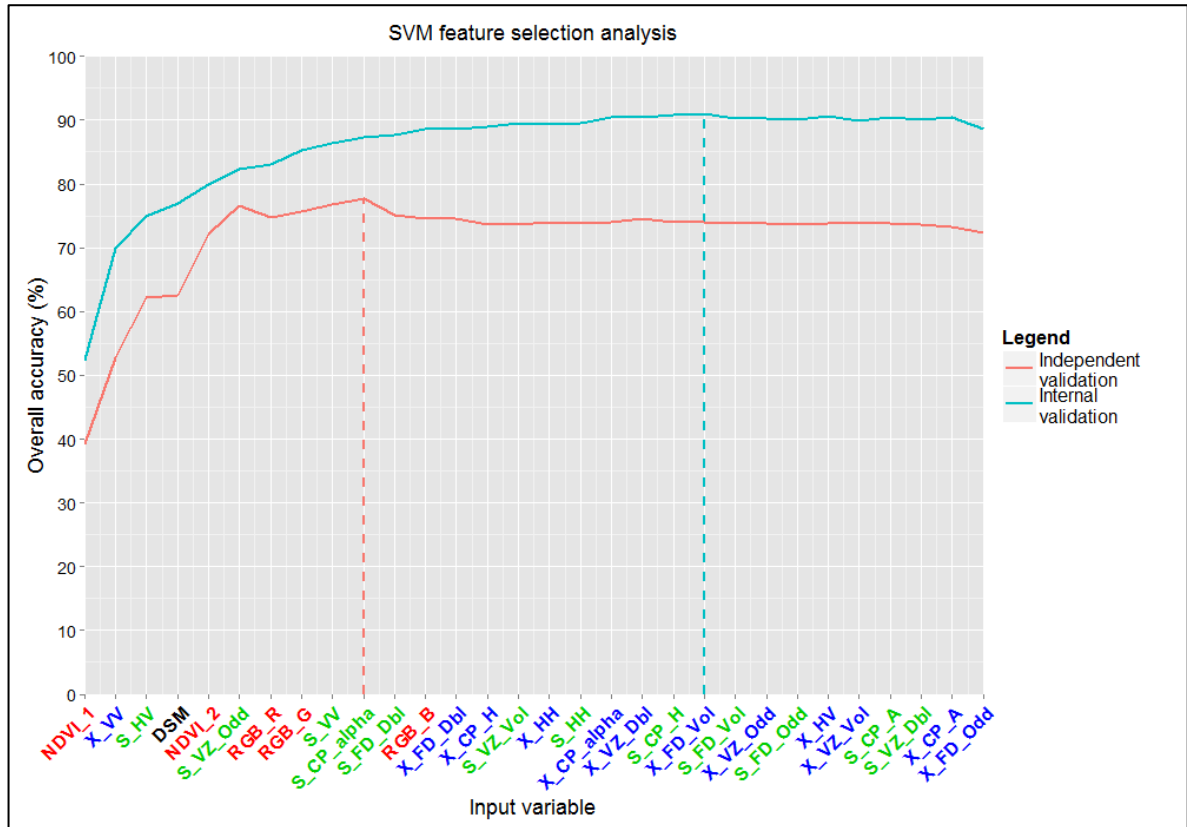


Figure 33 – SVM feature selection analysis of variable model based on all available RS variables. Variable selection numbers with highest accuracies are indicated with dashed lines. Optical variables are annotated in red, LiDAR variable in grey, S-band variables in green, X-band variables in blue.

The top 10 variables consists of four optical variables, one X-band SAR variable, four S-band SAR variables and the LiDAR DSM variable. In Figure 33 it can be seen that overall accuracy increases if more variables are included in the model, until an optimal number of variables was reached after which accuracy decreased again. The first 21 variables provided the highest accuracy according to the internal validation, which is indicated as with a blue dashed line in Figure 33 and is marked with a white space in Table 15. The SVM model is re-run with the 21 most important variables, producing a habitat classification map (Figure 34) and confusion table (Table 16).

Table 16 – Confusion table of supervised SVM classification based on 21 input variables.

		Reference data						Row total	User accuracy (%)
		Bare sand / mud wet	Bare sand / mud dry	Pioneer <i>Salicornia</i>	Pioneer <i>Spartina</i>	Salt Marsh Meadow	<i>Juncus maritimus</i>		
Classified data	Bare sand / mud wet	764	9	25	0	2	0	800	95.50
	Bare sand / mud dry	1	813	24	61	17	0	916	88.76
	Pioneer <i>Salicornia</i>	37	12	168	65	46	0	328	51.22
	Pioneer <i>Spartina</i>	0	3	71	249	320	66	709	35.12
	Salt Marsh Meadow	7	70	35	40	1817	251	2220	81.85
	<i>Juncus maritimus</i>	0	0	0	0	300	324	624	51.92
	Column total	809	907	323	415	2502	641	5576	
	Producer accuracy (%)	94.44	89.64	52.01	60.00	72.62	50.55		<b>Overall accuracy 73.87 %</b>

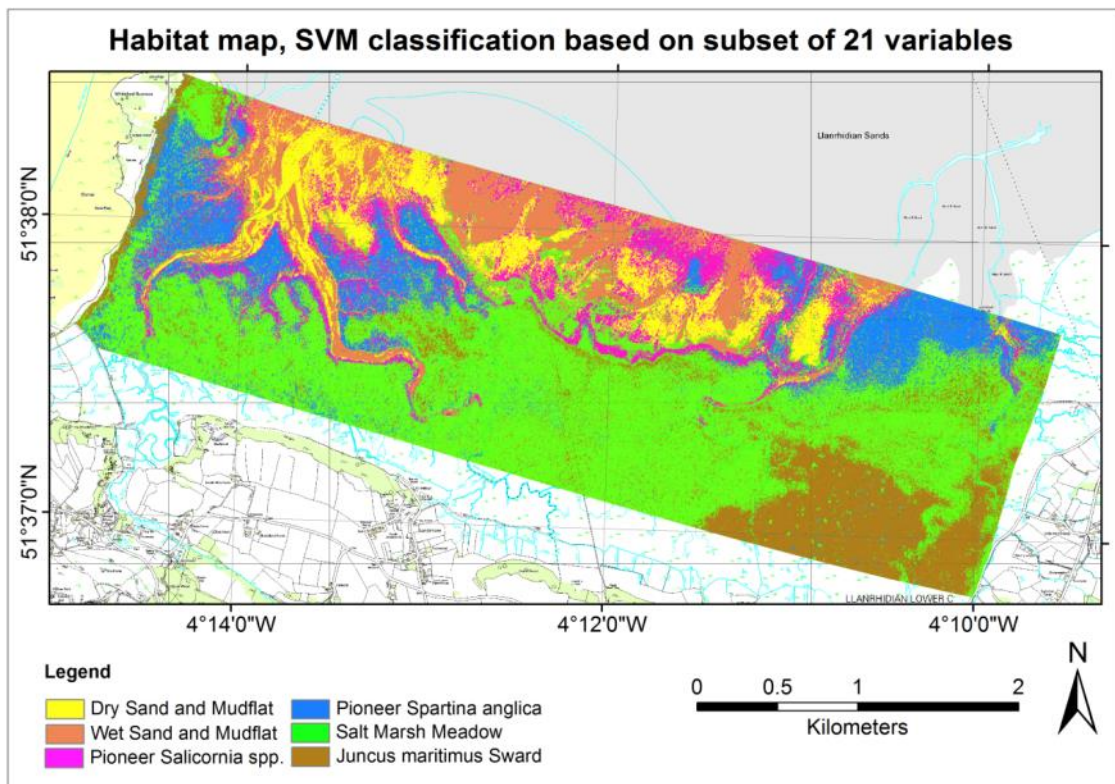


Figure 34 – Habitat map of supervised SVM classification, based on subset of the 21 most important variables of all available RS variables.

From the feature subset analysis and the subsequent SVM habitat mapping based on the subset the following things are worth mentioning:

- The overall accuracy of a SVM classification models can be improved by using a subset. In this example the accuracy improved from 72.09% to 73.87%. This indicates that, besides saving computational power and time, feature selection for SVM classification models can improve accuracy.
- The confusion table shows that both the dry and wet sand and mudflats are characterised very well, with producer and user accuracies of more than 88%. Of the vegetation habitats, pioneer *Spartina* has the lowest user accuracy, which is 35.12%. A considerable amount of salt marsh meadow is mis-classified as pioneer *Spartina*, but also as *Juncus maritimus*.
- The classification map provides reasonable realistic representation of presence of different land cover types. The aforementioned misclassification of salt marsh meadows as pioneer *Spartina* and *Juncus maritimus* is visible in some areas, especially towards the central pioneer zone. A considerable part of this area is classified as *Juncus maritimus*, although during field visits in this area no vegetation of this type has been found. Similarly, in the western part of the salt marsh, a large area has been classified as pioneer *Spartina*, not confirmed by field surveys.

### **6.3.2.2 RF habitat classification**

Similar to the results of the SVM classifiers, for the RF classification a total of 20 different variable combination models are used (Table 11). In order to assess the variable combination generating the most accurate result, as well as qualitative comparison of variable combination models the overall accuracies and Kappa coefficients (Congalton 1991) were calculated. The accuracy assessments of the RF classifications of variable combination models are shown in Table 17. Similar to the interpretation of the results of the SVM classifier, the variable combination models are presented according to RS data type:

- The optical and LiDAR variable combination models have accuracies between 47% and 61%, the highest achieved by the model based on all optical and DSM

variables. The model based on NDVI\_1 showed higher accuracies than the model based on NDVI\_2, similar to the SVM results.

- The S-band SAR models have accuracies between 32% and 68%, with accuracy of the model based on CP variables significantly lower than other variable combinations.
- The X-band SAR models have accuracies between 24% and 51%, with accuracy of the model based on CP variables significantly lower than other variable combinations.
- The S-band and X-band combination models show slight improvement of the classification accuracies based on S-band alone (63.41% and 66.41%). The model based on the backscatter intensity channels and VZ polarimetric decomposition variables is more accurate than the model based on all S-band and X-band SAR variables.
- The classification models based on optical, LiDAR and SAR variables are significantly more accurate than the classifications based on fewer variables. The highest accuracy was achieved with a variable model based on all available optical, LiDAR and SAR variables, with accuracy of 78.20%.

All in all the classification accuracies of the RF models are higher than the SVM models, although the relative performance of each model (its ranking among the 20 variable models) is the same.

Table 17 – Overall classification accuracy and Kappa coefficient for the RF classification models.  
The model with highest accuracy is indicated in bold.

Classification Model	Overall accuracy (%)	Kappa coefficient
DSM, RGB	47.70	0.36
NDVI (1,2)	52.40	0.36
DSM, NDVI (1)	57.69	0.46
DSM, NDVI (2)	54.62	0.40
DSM, NDVI (1,2)	49.92	0.35
DSM, RGB, NDVI (1,2)	60.41	0.48
S-band (Int)	51.08	0.40
S-band (CP)	32.12	0.20
S-band (FD)	53.65	0.42
S-band (VZ)	54.39	0.44
S-band (Int,VZ)	62.86	0.52
X-band (Int)	40.04	0.28
X-band (CP)	24.82	0.12
X-band (FD)	32.62	0.20
X-band (VZ)	42.72	0.31
X-band (Int,VZ)	50.69	0.39
S-band (Int,VZ), X-band (Int,VZ)	66.41	0.56
S-band (Int,CP,FD,VZ), X-band (Int,CP,FD,VZ)	63.41	0.53
DSM, NDVI (1), S-band (Int,VZ), X-band (Int,VZ)	74.88	0.67
<b>DSM, RGB, NDVI (1,2), S-band (Int,CP,FD,VZ), X-band (Int,CP,FD,VZ)</b>	<b>78.20</b>	<b>0.71</b>

The RF classifier analysed the relative importance of RS variables used for training of the classification model. A plot of the variable importance analysis of the variable model based on all available optical, LiDAR and SAR variables is provided in Figure 35. This plot is a graphical display of the importance of the input variables for the classification. The plotted values indicate raw variable importance, coloured according to input variable type. The two optical NDVI and elevation DSM variables are by far the most important for the RF classification model. The rest of the top 10 variables are a mix of S-band and X-band variables, mostly polarimetric decomposition variables. On the other end of the scale, the least important variables are three X-band variables and

the three optical aerial photography variables. Eight variables in total fall under the 1% total variable importance threshold, plotted as a dashed line in the diagram.

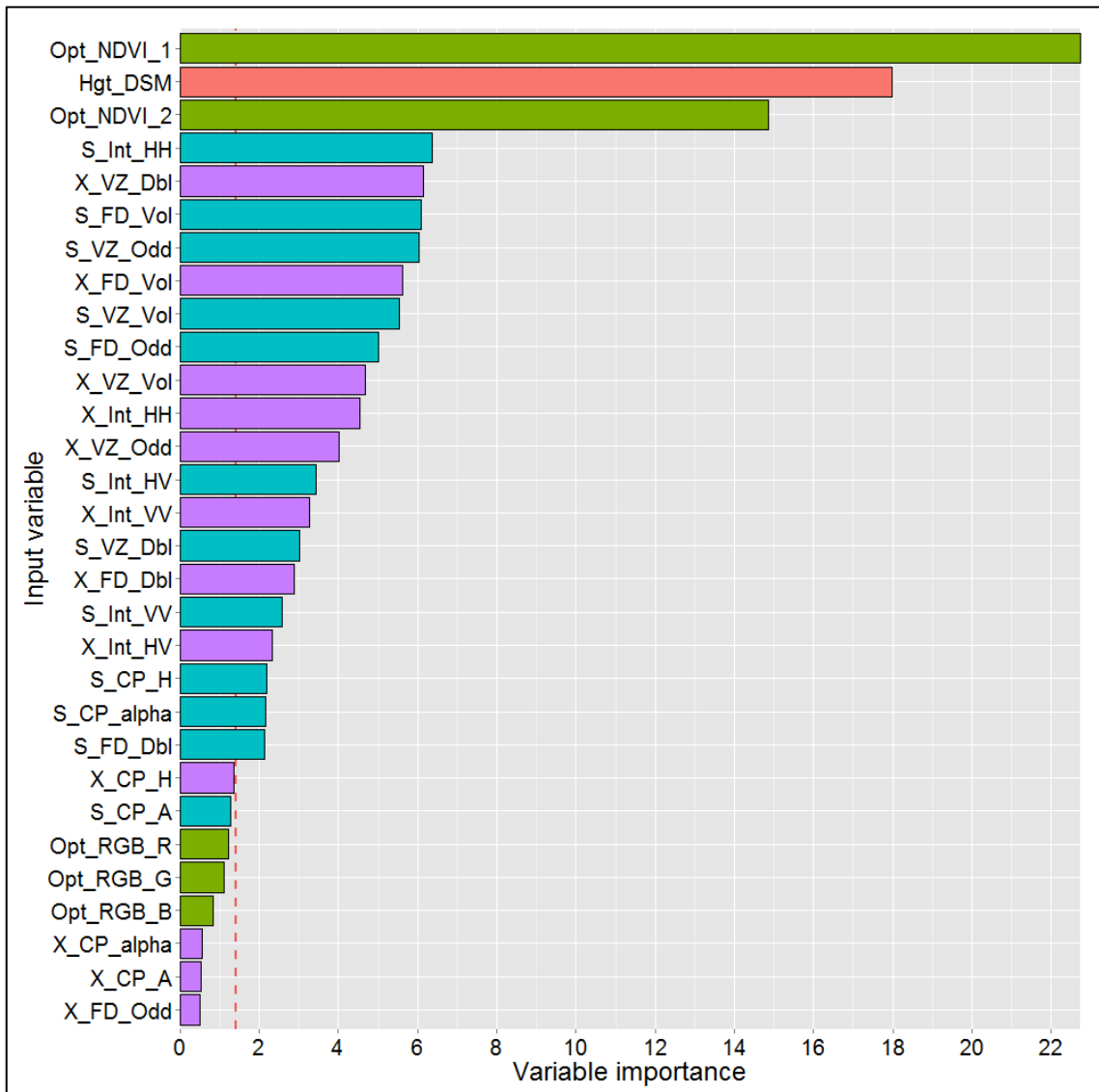


Figure 35 – RF variable importance analysis of variable model based on all available RS variables. Optical variables are highlighted in green, LiDAR variable in pink, S-band variables in blue and X-band variables in purple. The dashed red line indicates 1% of total variable importance.

The classification has been re-run on a number of subsets to test whether leaving less important variables created significant degradation of classification accuracy. These re-runs are summarised in Table 18. The model using the top 22 variables is the model excluding the variables with less than 1% contribution to total variable importance.

When interpreting the results the following observations are most important:

- The ten most important variables are responsible for 74.13% classification accuracy. Inclusion of the remaining 20 variables increases accuracy with only 4.07% to 78.20%.

- Overall accuracy gradually increases when number of input variables grows. This indicates that all variables have a positive effect on the classification (i.e. not decreasing overall accuracy). Unlike the SVM classification, best overall accuracy is achieved using all available input variables.

Table 18 – Accuracy assessment of supervised RF classifications with subsets of the model based on all available RS variables.

Data set	Overall accuracy (%)	Kappa coefficient
Top 3 variables used	49.92	0.35
Top 5 variables used	67.98	0.58
Top 10 variables used	74.13	0.66
Top 15 variables used	76.76	0.69
Top 22 variables used	77.58	0.70
All variables used	78.20	0.71

From the model based on all available RS variables a salt marsh habitat map was created (Figure 36), the confusion matrix of classification accuracy of the among the different habitat classes is shown in Table 19. From the resulting habitat map and confusion table the following observations are worth noting:

- Overall classification accuracy of bare sand and mudflats is high, with user and producer accuracies above 82%. Pioneer *Salicornia* is the least accurately classified, with user and producer accuracies around 50%.
- On the habitat classification map, pioneer *Salicornia* and *Spartina* habitats are restricted to the pioneer part of the salt marsh, without significant appearance in other parts of the salt marsh. This coincides well with the findings of the field survey. Furthermore, little confusion exists between the salt marsh meadow and the two pioneer classes.
- The transition between upper *Juncus maritimus* sward and the surrounding salt marsh meadow in the south-eastern part of the research area is very abrupt in the classification map. This corresponds with sharp boundaries between these two habitats that were observed during field surveys.
- The classification map revealed a realistic image of spreading of salt marsh habitats. Compared to the SVM habitat classification map, the RF classification map seemed more consistent and less noisy.



Table 19 – Confusion table of supervised RF habitat classification based on all available RS variables.

		Reference data						Row total	User accuracy (%)
		Bare sand / mud wet	Bare sand / mud dry	Pioneer <i>Salicornia</i>	Pioneer <i>Spartina</i>	Salt Marsh Meadow	<i>Juncus maritimus</i>		
Classified data	Bare sand / mud wet	719	6	61	0	9	0	795	90.44
	Bare sand / mud dry	4	900	25	76	81	0	1086	82.87
	Pioneer <i>Salicornia</i>	86	0	161	41	31	0	319	50.47
	Pioneer <i>Spartina</i>	0	0	72	289	308	27	696	41.52
	Salt Marsh Meadow	0	1	4	9	1933	239	2186	88.43
	<i>Juncus maritimus</i>	0	0	0	0	140	375	515	72.82
	Column total	809	907	323	415	2502	641	5576	
	Producer accuracy (%)	88.88	99.23	49.85	69.64	77.26	58.50		<b>Overall accuracy 78.20 %</b>

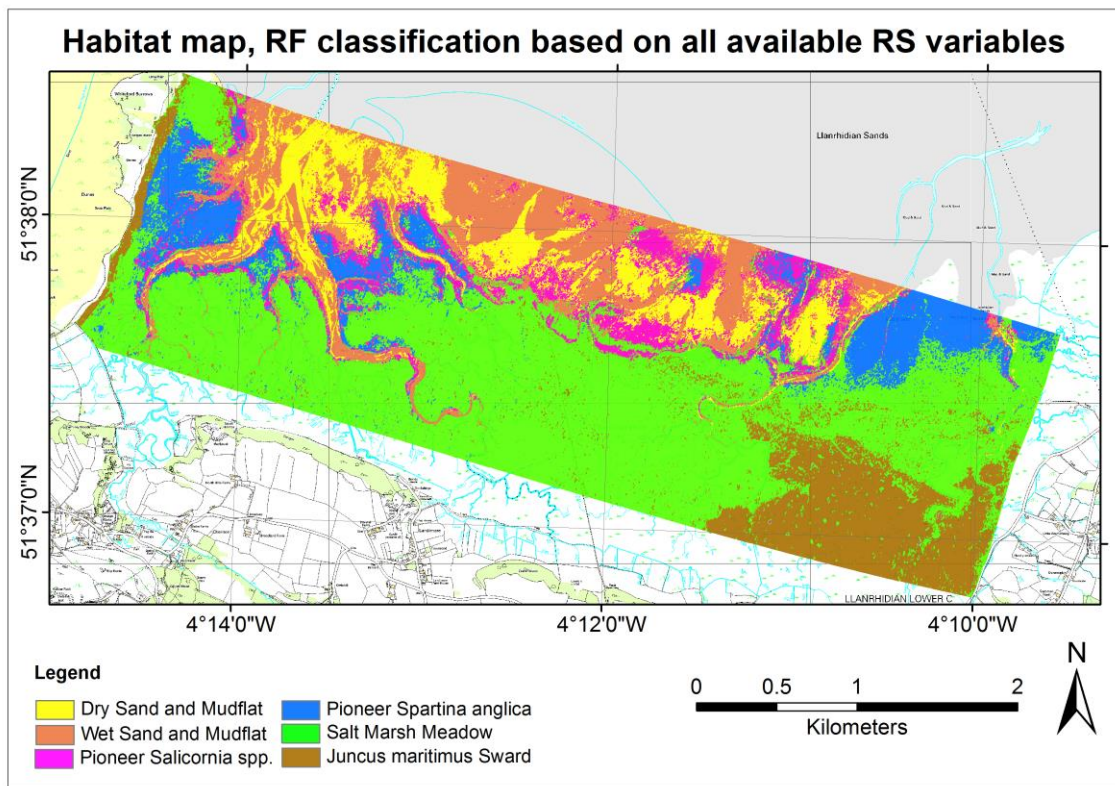


Figure 36 – Habitat map of supervised RF classification, based on all available RS variables.

### 6.3.3 Supervised vegetation extent classification

In the previous section performance of different classifiers was analysed. The RF classifier has shown to be best considering the input variables available for this project. Therefore it was decided to use this classifier for mapping the extent of salt marsh vegetation in the research area.

Similar to the supervised RF habitat classification, different variable combinations were used and their respective performance analysed. The classes considered were 'No vegetation cover' and 'Vegetation cover', irrespective of salt marsh vegetation habitat. In Table 21 the overall accuracy and kappa coefficient of the classification models are shown. Similar to the interpretation of the results in the previous section, the results are presented per RS variable type:

- The variable models based on optical and LiDAR variables all achieve high accuracies, between 88% and 92%. The most accurate model is based on NDVI\_1 and DSM variables with accuracy of 91.80%. This shows that a model based on only two variables can result in a highly accurate vegetation extent map.
- The vegetation extent classification accuracies of the models based on S-band SAR variables range between 66.95% for the model based on CP polarimetric decomposition variables and 90.25% for the model based on FD polarimetric decomposition variables. This shows that models based on S-band SAR achieve similar accuracies as models based on optical and LiDAR variables.
- The classification models based on X-band SAR variables show lower accuracies than the models based on either optical and LiDAR or SAR variables. This is similar to the relative accuracies observed in the previous paragraph.

Table 20 – Overall accuracy and Kappa coefficients for vegetation extent mapping variable models.  
The model with highest accuracy is indicated in bold.

Classification Model	Overall accuracy (%)	Kappa coefficient
DSM, RGB	88.30	0.77
NDVI (1,2)	87.98	0.73
DSM, NDVI (1)	91.80	0.81
DSM, NDVI (2)	89.84	0.77
DSM, NDVI (1,2)	89.05	0.78
DSM, RGB, NDVI (1,2)	90.15	0.80
S-band (Int)	89.60	0.79
S-band (CP)	66.95	0.34
S-band (FD)	90.25	0.81
S-band (VZ)	88.35	0.77
S-band (Int,VZ)	90.21	0.78
X-band (Int)	82.50	0.65
X-band (CP)	64.90	0.30
X-band (FD)	84.05	0.68
X-band (VZ)	84.35	0.69
X-band (Int,VZ)	86.16	0.68
S-band (Int,VZ), X-band (Int,VZ)	91.94	0.81
<b>S-band (Int,CP,FD,VZ), X-band (Int,CP,FD,VZ)</b>	<b>92.43</b>	<b>0.82</b>
DSM, NDVI (1), S-band (Int,VZ), X-band (Int,VZ)	89.91	0.77
DSM, RGB, NDVI (1,2), S-band (Int,CP,FD,VZ), X-band (Int,CP,FD,VZ)	91.59	0.81

- The models based on a combination of S-band and X-band SAR variables are the most accurate classification models in this analysis, with accuracies of 91.94% for the model based on S-band and X-band backscatter intensity and VZ polarimetric decomposition variables and 92.43% for the model based on all available SAR variables. This is different from the results of the habitat mapping, where these models performed rather well, but were not the most accurate ones.

- The models based on combination of optical, LiDAR and SAR variables show high accuracies, with accuracy of 91.59% for the variable model based on all available RS variables.

Variable importance analysis is carried out on the classification model based on all available RS variables. The variable importance plot (Figure 37) shows that NDVI variables are most important for vegetation extent mapping. The DSM variable completes the top 3 important variables. X-band SAR variables constitute the following three variables. On the bottom end of the variable importance plot ten variables fall under the 1% variable importance threshold. As was shown in the previous section, improving classification model efficiency by decreasing variable number by leaving those that have low importance degrades overall classification accuracy only slightly. The overall accuracy of RF extent mapping classification with a subset of the twenty most important variables results in accuracy of 90.69%, a decrease in overall accuracy of 0.86%. This decrease in accuracy is comparable the decrease in accuracy observed for the RF habitat mapping, as described in the previous section.

The resulting vegetation extent map (Figure 38) showed that the RF classifier produced a smooth and realistic picture of the extent of vegetation cover in the research area. The confusion table of the extent map (Table 21) shows that there are good user and producer accuracies for the two classes. The lowest accuracy is the producer accuracy for the class 'Non-vegetated' (82.11%), indicating a slight tendency to over-classification of vegetation on the expense of non-vegetated area.

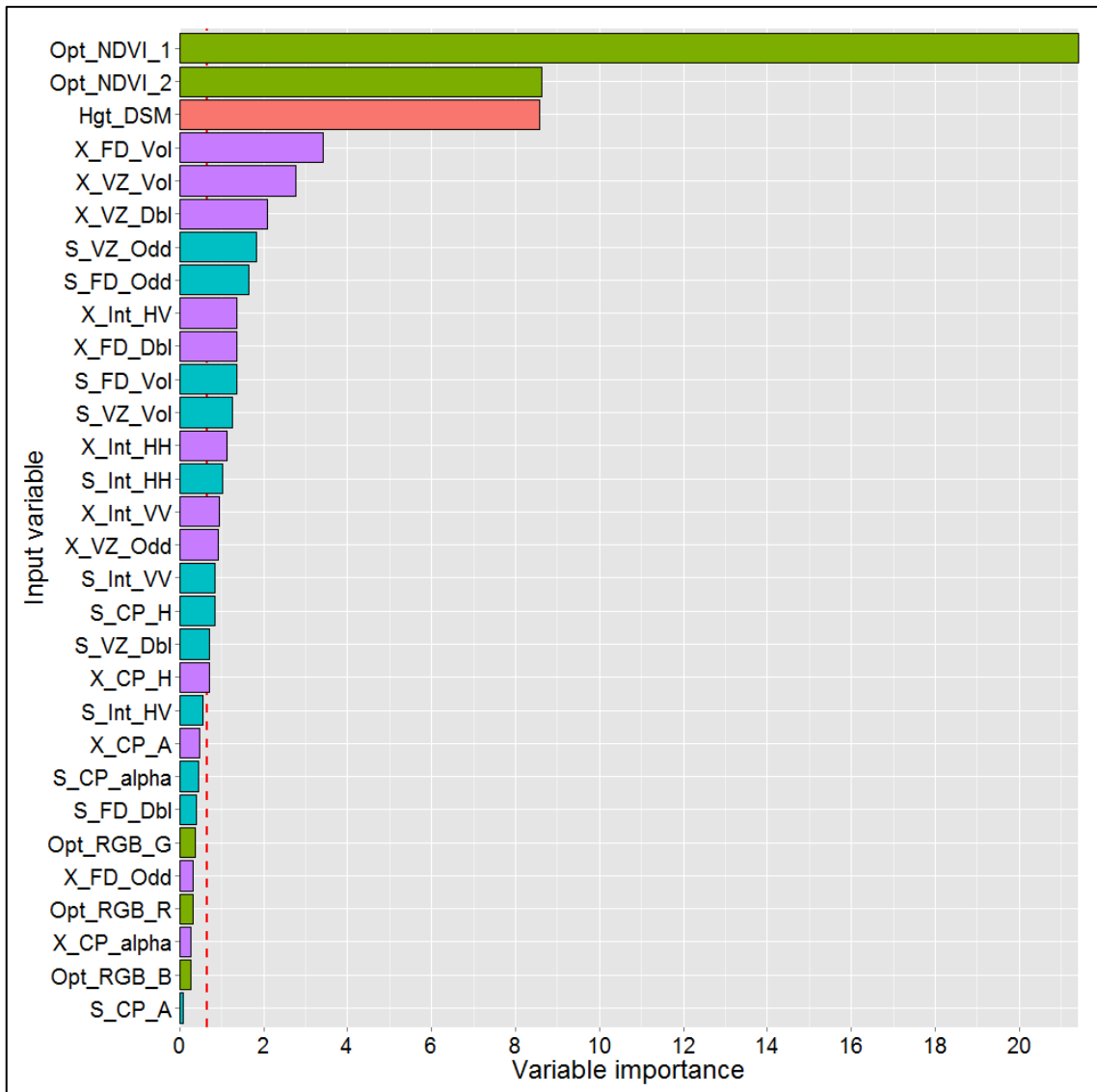


Figure 37 – Variable importance plot RF vegetation extent classification model 17. S-band variables are highlighted in blue, X-band variables in purple, optical variables in green and the elevation variable in pink. The dashed red line indicates 1% of total variable importance

Table 21 – Confusion table of supervised RF vegetation extent classification based on all available RS variables.

		Reference data			
		Non-vegetated	Vegetated	Row total	User accuracy (%)
Classified data	Non-vegetated	1583	126	1709	92.63
	Vegetated	345	3545	3890	91.13
	Column total	1928	3671	5599	
	Producer accuracy (%)	82.11	96.57		<b>Overall accuracy 91.59 %</b>

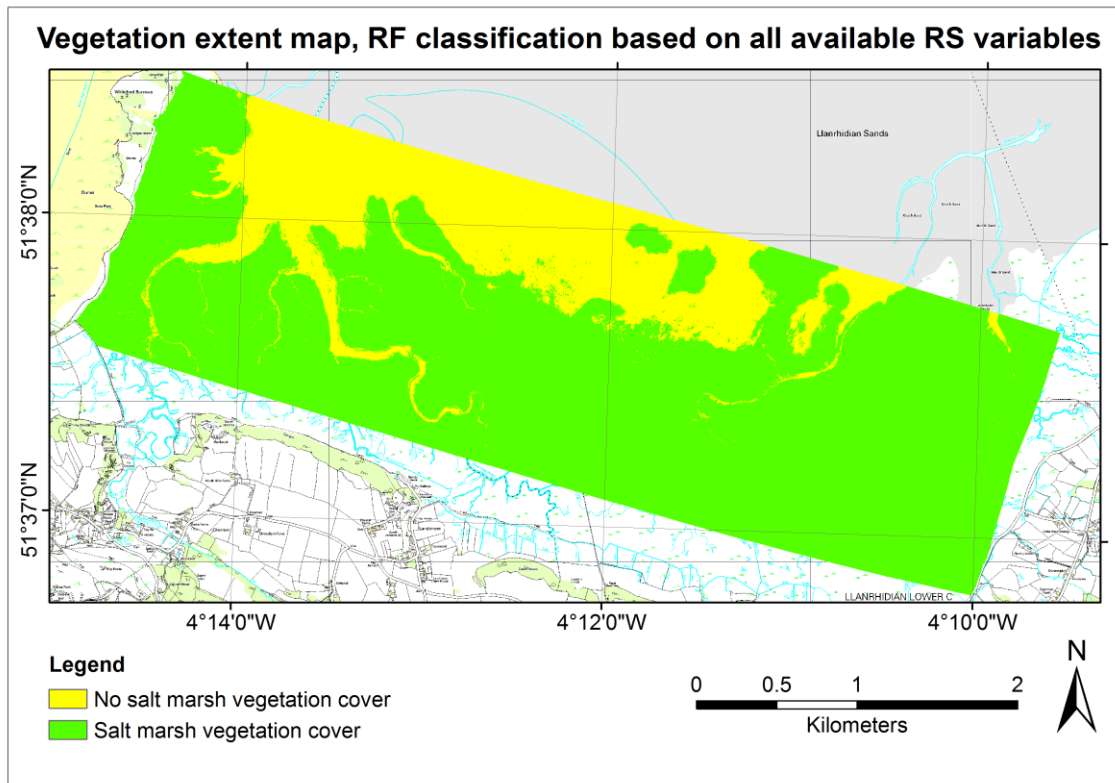


Figure 38 – Salt marsh vegetation extent map of supervised RF classification, based on all available RS variables.

### 6.3.4 Integration of results

#### 6.3.4.1 Classifier analysis

The use of a combined RS data set for salt marsh habitat and salt marsh vegetation extent mapping has been used in this research experiment. The main aim of this experiment was to research whether using SAR data would improve the accuracy of salt marsh habitat maps, starting off from a perspective of more readily available optical and LiDAR data sets. In Table 22 the highest classification accuracies for each variable combination category is shown. From this table it can be deduced that inclusion of SAR in a combined RS variable model does provide an improvement for habitat mapping, but less for vegetation extent mapping. The observed classification accuracy improvement for SVM habitat mapping is 13.84% and 17.79% for RF habitat mapping when SAR variables are included in the variable combination models. However, this improvement is not observed in the vegetation extent map, where the inclusion of SAR variables in the classification variable model results in a decrease of 0.21% in classification accuracy. Moreover, it appears that the most accurate classification model is based on S-band SAR variables alone.

Table 22 – Highest classification accuracies of variable combination category for supervised classifications.

Supervised classification	Optical, LiDAR	S-band SAR	X-band SAR	S-band SAR, X-band SAR	Optical, LiDAR, S-band SAR, X-band SAR
RF vegetation extent	91.80	90.25	86.16	<b>92.43</b>	91.59
SVM habitat	58.25	59.64	46.56	61.87	<b>72.09</b>
RF habitat	60.41	62.86	50.69	66.41	<b>78.20</b>

#### 6.3.4.2 Vegetation extent change analysis

The vegetation extent map presented in Figure 38 is compared with two reference vegetation cover extent maps from the EA salt marsh survey (Figure 29) and the CCW salt marsh habitat survey (Figure 30). From the three extent maps vegetation extent change amounts were calculated (Table 23). The geographical component of salt marsh vegetation extent change is shown in Figure 39. From the change table it can be derived that vegetation cover gain has been larger than vegetation cover loss. The net vegetation cover area gain between 1998 and 2007 is 59.24 ha, between 2007 and 2010 it is 60.90 ha. Considering the second time interval is only one third length of the first one it can be observed the change rate (stated between brackets) has accelerated.

Table 23 – Salt marsh vegetation extent change. Values are hectares. Change rate in hectare per year is between brackets.

Time interval	1998-2007	2007-2010
Vegetation cover gain	103.51 (11.50)	65.29 (21.76)
Vegetation cover loss	44.27(4.92)	4.40 (1.47)
Net vegetation cover change	59.24 (6.58)	60.90 (20.30)
Unchanged	805.06	

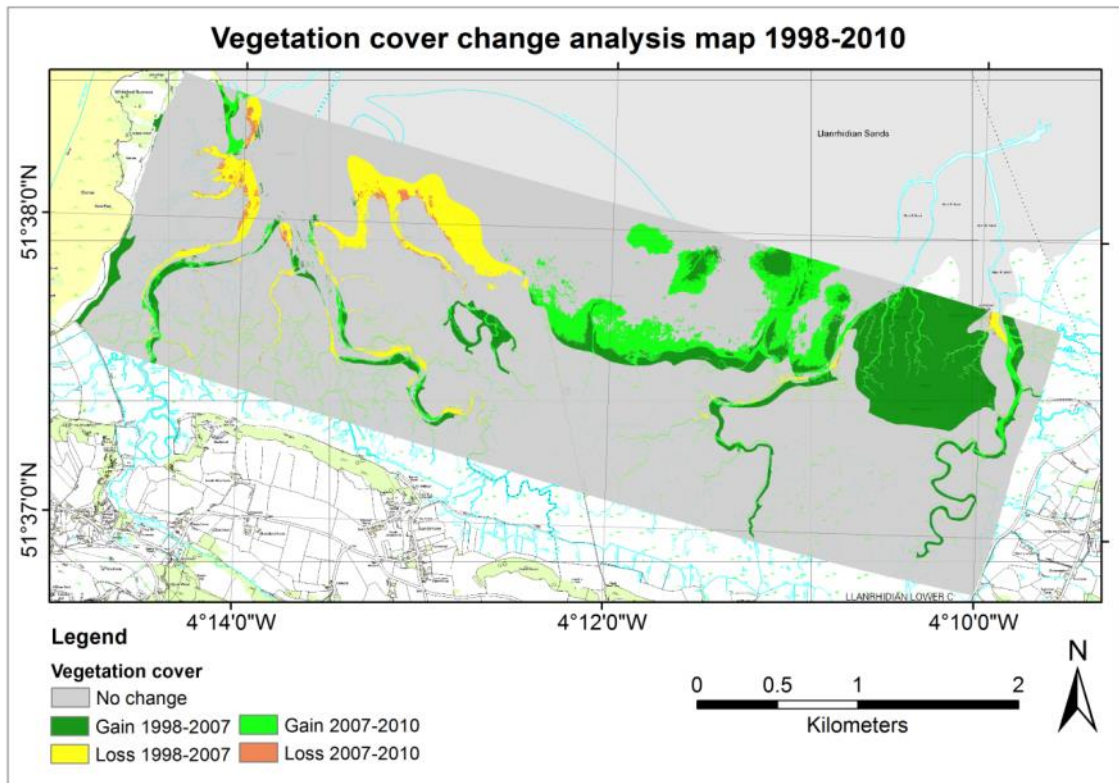


Figure 39 – Vegetation cover extent change map for the period 1998-2010

From the change analysis the following observations can be made:

- Areas of vegetation gain and vegetation loss are located in the eastern and western part of the research area, respectively. This pattern is consistent during both time intervals, with most vegetation gain in the eastern pioneer zone of the research area and most vegetation loss in the western part.
- Most vegetation loss and gain occurs in the pioneer zone of the salt marsh. However, there is considerable vegetation cover change noted along some of the major channels. This can be due to change of channel position, as these are known to migrate slowly. This is particularly visible in the major channel beds in the western part of the research area. However, most of the vegetation cover increase observed along the two major creeks in the eastern part of the research area can be ascribed to mis-classification due to methodological differences between the three mapping efforts.
- The salt marsh seems to be in favourable ecological condition with net expansion of the area covered by salt marsh vegetation.



### **6.3.4.3 Habitat change analysis**

The most accurate salt marsh habitat map, based on RF classification with all available RS variables was compared to the CCW salt marsh survey habitat map. This analysis was carried out by a cross-classification of the two data sets, using aggregated NVC classes for the CCW data set. The resulting change analysis map is shown in Figure 40. In Table 24 the habitat changes are expressed in a confusion table with change in hectares. The colours in the map correspond to the colours used in the corresponding classes in the confusion table. In the confusion table the CCW survey classes are plotted in the rows, the RF classification results in the columns. On the diagonal no colour is used, as this indicates that no transition of habitat has taken place. The total values in the right column indicate the total area each habitat occupied according to the CCW survey in 1998. The total values in the bottom row indicate the total area each habitat occupied according to the RF habitat classification in 2010. Per habitat some important observations can be made:

- The largest habitat change observed is the transition from sand and mudflat to salt marsh vegetation. The total area covered by sand and mudflat decreased from 346.72 hectare to 236.34 hectare. This will be confirmed in the vegetation extent change analysis in Chapter 6.3.4.2.
- The habitat that increased most in area is *Salicornia*, with an area increase from 2.89 hectare to 86.19 hectare. This increase has gone mostly to the expense of sand and mudflats. This habitat also shows it is the least unchanged
- It appears that *Spartina* is the only vegetation habitat that decreased in area, from 116.51 to 100.29 hectare. This is mostly attributed to an increase of *Salicornia*. The area of *Spartina* cover has decreased mostly in the western side of the research area and increased in the eastern side.
- The salt marsh meadows have gradually expanded, especially to the expense of sand and mudflats in the eastern side of the research area. Most of the area decrease is transition to *Spartina* in the western part of the research area.
- The *Juncus* area is relatively stable, with mutual area exchange with salt marsh meadow as the largest dynamic.

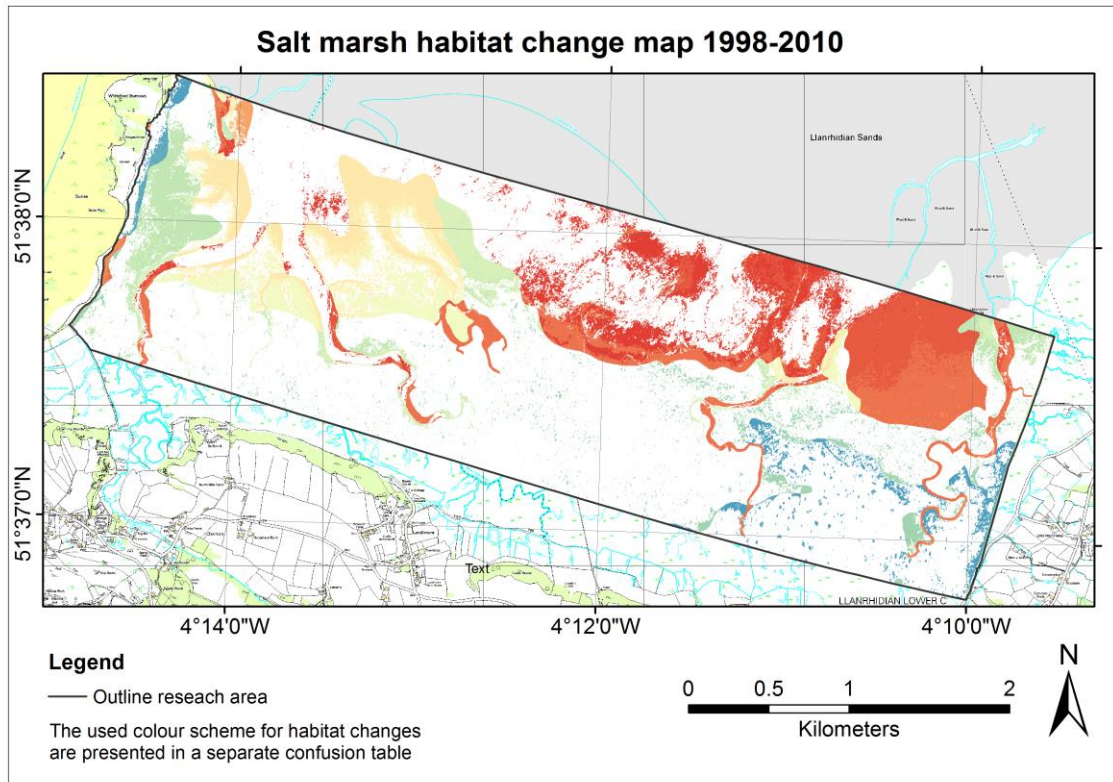


Figure 40 – Salt marsh habitat change map  
Colours used in the map coincide with the colours in Table 24.

Table 24 –Habitat area change between CCW survey and RF habitat classification.  
Area change expressed in hectares.

		RF habitat classification					Total	% not changed
		Sandflat	<i>Salicornia</i>	<i>Spartina</i>	Meadow	<i>Juncus</i>		
CCW survey	Sandflat	184.45	54.18	37.98	65.99	4.12	346.72	53.20
	<i>Salicornia</i>	1.86	0.66	0.30	0.06	0.00	2.89	22.86
	<i>Spartina</i>	34.64	21.74	29.16	30.84	0.13	116.51	25.03
	Meadow	15.39	9.47	30.66	364.12	18.95	438.59	83.02
	<i>Juncus</i>	0.00	0.14	2.19	16.68	92.47	111.47	82.95
	Total	236.34	86.19	100.29	477.69	115.67		
Area gain/loss		-110.4	83.3	-16.2	39.1	4.2		

## 6.4. Discussion

### 6.4.1 Unsupervised habitat classification with CP variables

Plotting CP decomposition variables  $\alpha$  against  $H$  has been common practice for initial analysis of fully polarimetric SAR data (Cloude and Pottier 1997). The CP decomposition alpha angle ( $\alpha$ ) to entropy ( $H$ ) plots of the S-band (Figure 23) and X-

band data (Figure 24) showed very different patterns for both frequency bands. The S-band  $H/\alpha$ -plot revealed that the predominant scatter mechanisms were surface and volume scatter and a large variation of  $H$  for the different land cover classes. In contrast, the X-band  $H/\alpha$ -plot showed much less variation of  $H$  and higher  $\alpha$ -values, indicating predominant volume and double-bounce scatter mechanisms. This was further exemplified in Figure 22, in which scatterplots were displayed for direct comparison of S-band and X-band CP variables. Cloude and Pottier (1997) observed similar differences for L-band and C-band backscatter signatures over a forested area. Focussing on variations of the  $H/\alpha$ -relationships of six land cover classes, it was evident that dry sand/mudflats had lower entropy than the other land cover classes for both S-band and X-band. This indicated that this class is the most deterministic, i.e. more dominated by a single scatter mechanism than the other land cover classes. The dominant scatter mechanism for dry sand/mudflats was surface scatter in S-band and double bounce scatter in X-band. The other land cover classes largely overlap with similar values for  $H$  and  $\alpha$ , especially for the X-band CP variables. The largest variation for the land cover classes within a single variable was S-band entropy.

The  $H/\alpha$ -relationships revealed some differentiation between the land cover classes. However, previous use of these variables with an unsupervised classifier based on normal population distribution was not successful. The K-means Wishart unsupervised classification (Lee et al. 1999) was developed to handle with the specific statistic distribution of SAR data. The unsupervised classification maps based on S-band CP (Figure 31) and X-band CP variables (Figure 32) showed considerable differences. The overall accuracies of the maps were insufficient to be used for land cover mapping: 52.33% for S-band, 43.24% for X-band. However, close examination of the specific feature and differences between the maps based on S-band and X-band showed some interesting features. The habitat map based on S-band CP variables showed a well-defined area of *Juncus maritimus*, which was barely observed on the X-band map. Contrary, the area where pioneer *Salicornia* vegetation occurred was more realistically portrayed in the X-band map, on the S-band map pioneer *Salicornia* was over-classified. The unsupervised Wishart classification result could be improved by integrating the two SAR frequencies into one single Wishart classification model, as proposed by Ferro-Famil et al. (2001). Even though this creates a rather large

classification model, it can take advantage of the different backscatter responses of the different SAR frequencies. Further analysis of CP decomposition variable capabilities for land cover mapping is provided by Dickinson et al. (2013). They found that the Wishart classifier can characterise broad vegetation composition, in research areas with reasonably low entropy values. When entropy reached a certain threshold, backscatter was found to be random and unsuitable for classification.

Analysis of polarimetric SAR variables did provide insight into the behaviour of radar pulses, and unsupervised K-means Wishart classification merely confirms these processes. The production of the K-means Wishart unsupervised SAR classification was relatively straightforward and found to be capable to deal with complex SAR data. However, interpretation of the resulting map was not always straightforward and large mis-classifications occurred as boundaries were drawn based on statistical properties, not necessarily ecological ones. From this analysis it has been shown that S-band and X-band SAR complemented each other for mapping of the entire research area. This implied that the use of both SAR frequencies in a single classification model can improve the overall classification.

#### **6.4.2 Supervised habitat classification**

This section discusses the results of the supervised habitat classification variable importance analysis and the resulting habitat maps.

##### ***6.4.2.1 SVM habitat classification***

The SVM classifier proved to be a more successful method and provides opportunity to analyse the outcomes of the initial classification to optimise the number of input variables. The overall accuracies of the different variable input models for the SVM classification (Table 14) shows a clear improvement over the accuracies obtained with the ML classification (best overall accuracy 72.09%). The use of a variable subset of 21 of the 30 available variables (Table 15) increased the overall accuracy slightly to 73.87% (Table 16) Focussing on the importance of respective variables for the optimal variable subset (Figure 33) the variables that contributed most to classification accuracy were a mix of optical, elevation and SAR. The nine least important variables (which were not used for the re-training of the SVM model) primarily consisted of X-band SAR variables. This indicated again that S-band SAR variables were more

successful than X-band variables in distinguishing between the salt marsh vegetation habitats. However, it was noted that the most important variable was one of the NDVI variables, followed closely by the DSM elevation variable on fourth place and the other NDVI variable on fifth place.

As Melgani and Bruzzone (2004) argued, the SVM classifier is not dependent explicitly upon a certain dimensionality of input spaces, or distributions. It creates a hyper-dimensional feature space in which it defines optimal hyperplanes to separate the classes under consideration. As such, it has been applied successfully in other RS research that includes SAR in the input variables (Lardeux et al. 2009; Huang et al. 2011). As these two studies observed, the SVM classification produced higher accuracies than supervised Wishart and ML classifications, respectively. As indicated by Lardeux et al. (2009), use of a subset of the most significant variables to re-train the SVM model produced non-inferior results to an SVM model based on the complete variable data set. This concept was further researched and described by Pal and Foody (2010). They concluded that the accuracy of SVM classification was actually often reduced when more variables are added, because fitting of hyperplanes can become more troublesome after an optimal number of variables was reached. They advised to use a variable subset to improve classification accuracy.

#### **6.4.2.2 RF habitat classification**

The RF classification algorithm allowed analysis of variable importance. Examination of the variable importance plot for RF classification (Figure 35) revealed that the two NDVI and the DSM elevation variables dominated, followed by a combination of S-band and X-band SAR variables. This was also observed in the variable subset selection of the SVM classification. The use of a variable subset did not improve the accuracy, as was showed in Table 18. According to this table, the 15 least important variables only increase overall accuracy with 1.64%. The small contribution of some variables for RF classification means that a subset could be used to save computational time, although they do not have a detrimental effect like with SVM classification.

The most accurate RF classification result was obtained with the model incorporating all available SAR, optical and elevation variables, with overall accuracy of 78.20% (Table 17). This was almost 15% more than the variable model based on SAR variables

alone (63.41%) and almost 18% better than the variable model based on optical and elevation variables (60.41%). This confirmed that a combination of SAR, optical and elevation data had a complementary effect. This was confirmed in previous research into application of RF classifiers for ecological and land cover mapping (Cutler et al. 2007; Waske and Braun 2009). They concluded that the RF classifier is very robust in handling with noisy data; it performs very well on multi-source RS data sets.

The high importance of optical NDVI variables could be ascribed to the consistency of optical data quality with regard to SAR data. Speckle noise deteriorates the quality of SAR data, resulting in larger variance of the variable values of a certain habitat. A possible explanation for the high importance of elevation in classification is that the occurrence of different salt marsh vegetation habitats is highly dependent on flooding frequency, and therefore altitude.

The habitat classification maps showed that the RF classifier produced the most accurate habitat classification maps, more accurate than maps generated with the SVM classifier. A reason for the better results of the RF classifier compared to the SVM classifier could lie in the different underlying principles of the two classifiers. The SVM classifier aims to find the optimal statistical separability between classes, the RF classifier simply creates a large set of decision trees, with less focus on statistical population distributions. It appears that this approach is more successful when handling multi-source RS data.

### ***6.4.2.3 Habitat maps***

The maps from the SVM classifier (Figure 34) and the RF classifier (Figure 36) showed that both classification methods generated classification maps of good quality, without obvious mis-classifications. However, it was observed that the SVM classification map had a more grainy appearance than the RF classification map. This might attributed to speckle noise from the SAR variables that influenced the SVM classifier. Contrastingly, the RF classifier generated a smoother classification result. It appeared to suppress SAR speckle noise better than the SVM classifier, as was also observed by Pal (2003) and Gislason et al. (2006).

The results of these supervised classifications implied that multi-source RS data sets were capable of producing good quality high-resolution habitat maps. The resulting

classification accuracies in Table 22 indicated that the inclusion of SAR variables in the RS data set helps to dis-aggregate salt marsh maps from merely vegetation extent maps, as produced by Environment Agency (2011) into habitat maps of the major habitats, according to the Annex 1 classification scheme.

#### **6.4.3 Habitat change analysis**

The habitat change analysis was carried out between the two habitat maps available, the habitat map from the CCW survey of 1998 and the habitat map derived from RF supervised classification, dated 2010. The habitat change map (Figure 40) and corresponding confusion table (Table 24) showed that the habitats associated with the higher, more stable parts of the salt marsh corresponded well, with 83.02% and 82.95% similarity between CCW data and RF classification data for salt marsh meadows and *Juncus maritimus* swards, respectively. This was an indication that the resulting habitat map is a valid representation of the habitats when the RS data set was acquired. The pioneer salt marsh habitats showed less coherence between 1998 and 2010, but this was largely attributed to natural dynamics.

#### **6.4.4 Supervised vegetation extent classification**

The same RS data set as was used for salt marsh habitat mapping, a salt marsh vegetation extent map was created. This was done with the RF classifier, as it produced the best results for the habitat mapping and the goal of this analysis was to analyse vegetation changes, not to analyse respective performance of different classifiers. Table 20 shows that most variable input combinations produced excellent results for the extent mapping, with the highest accuracy of 92.43% achieved by the model based on all SAR variables combined. This contrasted with results from RF habitat mapping (Table 17) where highest classification accuracy was reached with the model based on all available RS variables. However, overall accuracy of vegetation extent based on all variables was only slightly lower. Analysis of variable importance (Figure 37) indicated that the optical NDVI and elevation variables are most important, followed by X-band SAR variables. The high importance of optical NDVI and LiDAR variables is also observed in SVM and RF salt marsh habitat mapping. The preference of X-band SAR over S-band SAR variables for vegetation extent mapping could be attributed to higher sensitivity of X-band SAR to subtle changes in surface roughness

than S-band, detecting the sparse pioneer zone vegetation more easily. This coincided with the findings of Chapter 5.4.2. and was also found by Lee et al. (2012), who argued that X-band SAR provides an excellent tool to monitor pioneer salt marsh vegetation.

#### **6.4.5 Vegetation extent change analysis**

Change analysis was based on vegetation extent differences between the CCW survey vegetation extent map, compiled based on data recorded in 1998 (Figure 30), the EA salt marsh survey map, based on data from 2007 (Figure 29) and the RF classification extent map, based primarily on data from 2010 (Figure 38). The extent of vegetation cover change (Figure 39) showed that in both time intervals a continuous trend of vegetation extent increase was observed. Most vegetation cover loss was located in the western part of the research area, most vegetation extent gain in the eastern part. The net area of salt marsh vegetation cover has increased. This process was confirmed by Farleigh (2010), who observed that the seaward boundaries of the entire Burry Inlet (the western side of the research area) was subject to erosion due to development along the northern shore of the estuary. Vegetation cover in the research area has shown to be dynamic, with rapid changes in the 12 years this change analysis spanned. However, the validity of the temporal analysis results needed to be discussed, considering there was a three-year time gap between RS data acquisition and recording of training and reference field data. This issue is further addressed in the methodological considerations (Chapter 8).

#### **6.5. Summary**

A combination of optical, LiDAR, S-band SAR and X-band SAR variables was used to test a number of classifiers for habitat classification. Unsupervised classification was varied out with the K-means Wishart classifier, using CP polarimetric decomposition variables. This classifier did not yield satisfactory results in terms of habitat discrimination, although the results were worth analysing. Analysis of the variable importance for the SVM and RF supervised classifiers indicated that optical NDVI and LiDAR DSM variables were in general most important for habitat classification, followed by S-band SAR variables.

The resulting habitat classification maps showed that the RF classifier produced the most accurate habitat classification maps, closely followed by the SVM classifier. It appeared that the RF classification technique was able to suppress inherent SAR speckle noise to a



large extent. Analysis of the habitat change between two habitat maps dated 1998 and 2010 showed that extensive change has occurred in the pioneer area of the salt marsh, whereas the upper parts appeared more stable.

Mapping of general vegetation extent was carried out with the RF classifier. The most important variables were optical NDVI and LiDAR DSM variables, followed by X-band SAR variables. The high importance of X-band SAR instead of S-band SAR variables was ascribed to higher sensitivity of X-band SAR to subtle changes in surface, detecting sparse pioneer zone vegetation better. Change analysis of the resulting vegetation cover mask (dated 2010) with vegetation cover maps from previous studies (dated 2007 and 1998) indicated that vegetation cover has remained stable in the upper part of the salt marsh. However, in the lower, more seaward part of the salt marsh significant change in vegetation cover has been observed, with vegetation cover retreat in the western half and accretion in the eastern half. The net area of salt marsh vegetation cover increased.

## **7. Regression modelling of biophysical parameters**

### **7.1. Introduction**

In this chapter it is aimed to find answers to the third research question:

*Is a combined RS data set from optical, LiDAR and SAR sensors better suited for regression modelling of biophysical parameters (vegetation cover, height and volume) than regression models based on a data set based on a single RS sensor?*

It has been known that SAR backscatter can provide an estimation of vegetation biomass, this link has been researched extensively (Le Toan et al. 1992; Englhart et al. 2011). Combining SAR and optical data has shown to be useful to delineate different land cover types (Englhart et al. 2012), it has been shown that LiDAR is strongly related to above-ground biomass (Englhart et al. 2013). Relationships between measurements from RS platforms and biophysical parameters in coastal marshes have been researched to some extent (Heumann 2011; Fatoyinbo and Simard 2012), although no previous record of modelling of biophysical parameters of salt marsh habitats with RS variables has been found.

In this chapter the methods, results and discussion of results of modelling of biophysical parameters with a combined RS data set consisting of optical, LiDAR and SAR variables is presented. The same RS data variables used for mapping of salt marsh extent and habitats (Chapter 6) were used for this research experiment. The biophysical parameters considered were vegetation cover, vegetation height and gross vegetation volume, calculated from vegetation cover and height. For more information about the biophysical parameters, see Chapter 4.3.2. Initially, the correlations of each available RS variable with the three biophysical variables is analysed in univariate linear modelling. Subsequently, all available RS variables are used to construct and analyse multivariate linear regression models. In the second part of the analysis, three different regression modelling techniques are used to map and analyse biophysical parameters in the salt marsh research area. The regression models of choice are Multivariate Least Squares regression, SVM regression and RF regression.

## 7.2. Methods

This section describes the different data analyses carried out with the RS and reference data sets, focussing on the regression modelling of biophysical parameters with the combined RS data set. A flowchart overview summarising the different analyses and their inter-relations are shown in Appendix B.

During the field survey vegetation cover and height were recorded. From these parameters *G<sub>VV</sub>* was derived (see Chapter 4.3.2), as a measure of vegetation volume. These three biophysical parameters offer valuable information about the three-dimensional composition of vegetation in the research area. The RS input data was provided by calculating mean values from pixels from all available RS variables within a buffer zone of 10 meters around each of the 100 fieldwork locations, with an added 10 extra sample locations on the bare sand and mudflats.

### 7.2.1 Biophysical parameters regression analysis

Several regression models were used to research the relationships between the recorded biophysical parameters and the RS data variables, resulting in tables of correlation coefficients for each relationship. Two regression models were used:

1. Univariate Linear Regression (ULR)
2. Multivariate Linear Regression (MLR)

The ULR regression is used to test each RS variable's specific correlation with the biophysical parameters. Linear correlation coefficients (*R*-values) were calculated of all relations between the RS variables and the three biophysical parameters. For the strongest correlation coefficients for each biophysical parameter a scatterplot was constructed to visualise the relationship. Subsequently, correlation coefficients were re-calculated using a subset of the sample population with *G<sub>VV</sub>* under 20%, leaving samples from the *Juncus maritimus* areas out. This was done to focus on subtle changes between non-vegetated sand flats, scarcely vegetation pioneer salt marsh habitats and densely vegetated salt marsh meadows.

For the MLR models four different variable models were used:

1. All optical and LiDAR variables
2. All S-band SAR variables
3. All X-band SAR variables

4. All optical and LiDAR, S-band SAR, X-band SAR variables

The main aim of this approach was to test whether multivariate regression models improved when SAR variables were added to the optical and LiDAR variables. The initial MLR models were calculated with all variables for each variable combination model. Subsequently, variable subset models were designed by stepwise regression methods to improve the initial regression models. The stepwise regression technique has been applied in other RS studies successfully (Huang and Townshend 2003), although it has also been regarded controversial (Rencher and Pun 1980). It was used to research which RS variable combinations showed the strongest linear relationship with biophysical parameters.

### 7.2.2 Biophysical parameter mapping

The last analysis of this thesis was assessment of accuracy of biophysical parameter maps based on multivariate regression methods. Training and validation data was provided by sampling pixels in a buffer zone of 10 meters around each of the 100 field survey sample locations and 10 additional non-vegetated locations. From the pixels within these buffer zones, 500 were randomly selected to training data for the regression models. The rest of the pixels within the buffer zones ( $n=5797$ ) were used for validation purposes. Accuracy assessments are expressed in tables of the adjusted  $R^2$ -values ( $R^2$ -values adjusted for number of input variables and training samples). Of each of the three biophysical parameters the map of most accurate regression result was displayed.

Three regression models are tested to research their capabilities for the mapping of biophysical parameters:

1. Multivariate Least Squares (MLS) regression
2. Multivariate SVM regression
3. Multivariate RF regression

The MLS regression is the general multivariate linear regression model which is generally used for linear regression.

SVM regression is based on the same principles as the SVM classification (see Chapter 6.2.2.2 for more information about SVM). In general, SVM for regression estimate a linear dependency by fitting an optimal approximating hyperplane to the training data

in the multi-dimensional feature space. Initially, for all four variable input combinations, the coefficients of determination were calculated. Consequently, the best fitting models were re-run with a feature subset. Similar to SVM classification, feature analysis was carried out to identify the most important variables.

RF regression is based on the same principle as RF classification (see Chapter 6.2.2.2 for more information about RF). Similarly, analysis of variable importance was done to rank the input variables according to their contribution to the regression models. Even though these models do not necessarily produce the best-fitting regression results, variable importance of the regression models based on all variables was analysed.

### **7.3. Results**

#### **7.3.1 Biophysical parameter regression analysis**

In this section results from regression analysis of relationships between RS variables and recorded biophysical parameters are presented. Main focus will lie on correlation and regression methods. In the first paragraphs of this section relationships between three biophysical parameters and each of the 30 available RS variables will be tested initially using univariate analysis, followed by variable combinations for multivariate regressions. In the second section analysis of regression model for biophysical parameter mapping with the MLS, SVM and RF regression techniques are described. In the final section, the results are integrated and their meaning is highlighted.

##### ***7.3.1.1 Univariate linear regression***

The calculated Pearson correlation coefficients ( $R$ -value) for all combinations of biophysical parameters against RS variables are shown in Table 25. The highest  $R$ -values of each biophysical parameter are indicated in bold. The percentage cover is best correlated with the NDVI variable derived from Landsat imagery acquired on 04/06/2010 ( $R = 0.81$ ). Both vegetation height and gross vegetation volume are most correlated with S-band FD odd bounce (surface scatter), with  $R$ -values of  $-0.57$  and  $-0.56$ , respectively. The scatterplots of these correlations are shown in Figure 41.

Table 25 – Pearson correlation coefficients (R-value) of biophysical parameters for all RS variables for entire sample location set (n=100).

Cell fill colour corresponds to a gliding scale from red (R= 0) to green (R>0.6). The highest R-values of the three respective biophysical parameters are indicated in bold.

Biophys. param.	DSM	RGB_R	RGB_G	RGB_B	NDVI_2010	NDVI_2011
Cover (dm <sup>2</sup> /m <sup>2</sup> )	0.63	-0.37	-0.35	-0.32	<b>0.81</b>	0.78
Height (cm)	0.38	-0.35	-0.42	-0.33	0.25	0.22
Volume (dm <sup>3</sup> )	0.45	-0.32	-0.38	-0.30	0.31	0.29
Biophys. param.	S_Int_HH	S_Int_HV	S_Int_VV	S_CP_H	S_CP_A	S_CP_alpha
Cover (dm <sup>2</sup> /m <sup>2</sup> )	0.21	0.40	-0.20	0.39	-0.51	0.29
Height (cm)	0.04	0.32	-0.29	0.38	-0.52	0.48
Volume (dm <sup>3</sup> )	0.03	0.33	-0.29	0.41	-0.52	0.48
Biophys. param.	S_FD_Odd	S_FD_Dbl	S_FD_Vol	S_VZ_Odd	S_VZ_Dbl	S_VZ_Vol
Cover (dm <sup>2</sup> /m <sup>2</sup> )	-0.21	-0.21	0.40	-0.02	0.20	0.40
Height (cm)	<b>-0.57</b>	-0.55	0.32	-0.20	0.13	0.32
Volume (dm <sup>3</sup> )	<b>-0.56</b>	-0.54	0.32	-0.21	0.11	0.33
Biophys. param.	X_Int_HH	X_Int_HV	X_Int_VV	X_CP_H	X_CP_A	X_CP_alpha
Cover (dm <sup>2</sup> /m <sup>2</sup> )	0.03	0.43	-0.01	0.46	-0.40	-0.32
Height (cm)	-0.25	-0.01	-0.36	0.22	-0.39	-0.35
Volume (dm <sup>3</sup> )	-0.23	0.02	-0.34	0.25	-0.36	-0.30
Biophys. param.	X_FD_Odd	X_FD_Dbl	X_FD_Vol	X_VZ_Odd	X_VZ_Dbl	X_VZ_Vol
Cover (dm <sup>2</sup> /m <sup>2</sup> )	-0.48	-0.45	0.39	0.16	-0.06	0.44
Height (cm)	-0.38	-0.50	-0.06	-0.20	-0.36	0.00
Volume (dm <sup>3</sup> )	-0.39	-0.50	-0.03	-0.18	-0.34	0.03

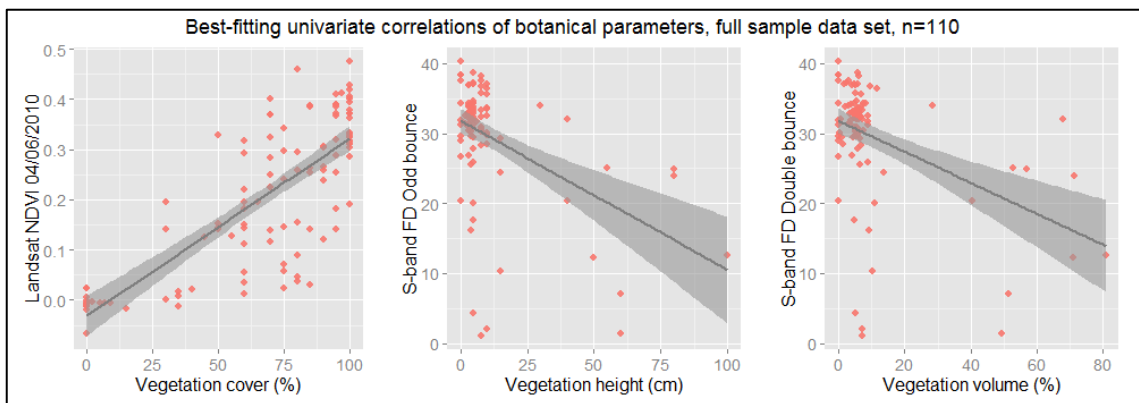


Figure 41 – Scatterplots of the best-fitting RS variables for biophysical parameters, based on the full sample data set (n=110).

In the scatterplots can be observed that there is a reasonably strong and positive linear correlation between percentage vegetation cover and NDVI. The other two biophysical parameters are less well correlated with any RS variable, especially sample locations

with higher GVV (mostly upper salt marsh *Juncus maritimus*). Therefore a subset of the sample locations was created of low vegetation volume (GVV < 20). The *R-values* of relationships between biophysical parameters and RS variables of this subset are presented in Table 26.

Table 26 – Pearson correlation coefficients (*R-value*) of biophysical parameters for all RS variables for subset of sample locations with GVV < 20%. (n=81).  
Cell fill colour corresponds to a gliding scale from red (*r*= 0) to green (*r*>0.6). The highest *R-values* of the three respective biophysical parameters are indicated in bold.

Biophys. param.	DSM	RGB_R	RGB_G	RGB_B	NDVI_2010	NDVI_2011
Cover (dm <sup>2</sup> /m <sup>2</sup> )	0.57	-0.31	-0.29	-0.27	<b>0.81</b>	0.78
Height (cm)	-0.12	-0.17	-0.21	-0.14	0.00	-0.01
Volume (dm <sup>3</sup> )	0.10	-0.29	-0.30	-0.22	0.40	0.39
Biophys. param.	S_Int_HH	S_Int_HV	S_Int_VV	S_CP_H	S_CP_A	S_CP_alpha
Cover (dm <sup>2</sup> /m <sup>2</sup> )	0.26	0.37	-0.10	0.31	-0.42	0.15
Height (cm)	0.35	0.51	0.12	0.39	-0.37	0.49
Volume (dm <sup>3</sup> )	0.50	0.68	0.10	0.49	-0.57	0.48
Biophys. param.	S_FD_Odd	S_FD_Dbl	S_FD_Vol	S_VZ_Odd	S_VZ_Dbl	S_VZ_Vol
Cover (dm <sup>2</sup> /m <sup>2</sup> )	-0.01	-0.03	0.37	0.10	0.23	0.37
Height (cm)	<b>-0.63</b>	-0.52	0.52	0.20	0.48	0.51
Volume (dm <sup>3</sup> )	-0.41	-0.40	0.69	0.28	0.58	0.69
Biophys. param.	X_Int_HH	X_Int_HV	X_Int_VV	X_CP_H	X_CP_A	X_CP_alpha
Cover (dm <sup>2</sup> /m <sup>2</sup> )	0.17	0.54	0.16	0.45	-0.32	-0.33
Height (cm)	0.38	0.47	0.13	0.24	-0.29	-0.26
Volume (dm <sup>3</sup> )	0.48	0.71	0.27	0.35	-0.30	-0.43
Biophys. param.	X_FD_Odd	X_FD_Dbl	X_FD_Vol	X_VZ_Odd	X_VZ_Dbl	X_VZ_Vol
Cover (dm <sup>2</sup> /m <sup>2</sup> )	-0.42	-0.35	0.52	0.31	0.10	0.54
Height (cm)	-0.29	-0.29	0.48	0.34	0.23	0.47
Volume (dm <sup>3</sup> )	-0.39	-0.40	0.70	0.53	0.31	<b>0.71</b>

Analysis of the *R-values* of the subset shows that the best correlation coefficient of vegetation cover remains the Landsat NDVI variable of 04<sup>th</sup> of June 2010, slightly higher at 0.81. The *R-values* of the relationships between the remaining two biophysical parameters and RS variables are improved considerably though, with maxima of -0.63 and 0.71 for vegetation height and GVV, respectively. Scatterplots of the strongest correlations are presented in Figure 42. Compared to the scatterplots of the complete sample set (Figure 41), it shows that the sample subset correlation of

GVV with X-band HV intensity is considerably stronger than strongest correlation of full data set for GVV, with S-band FD surface scatter. The highest *R-values* for GVV in Table 26 are either S-band or X-band HV intensity, FD volume scatter or VZ volume scatter, all with *R-values* between 0.68 and 0.71.

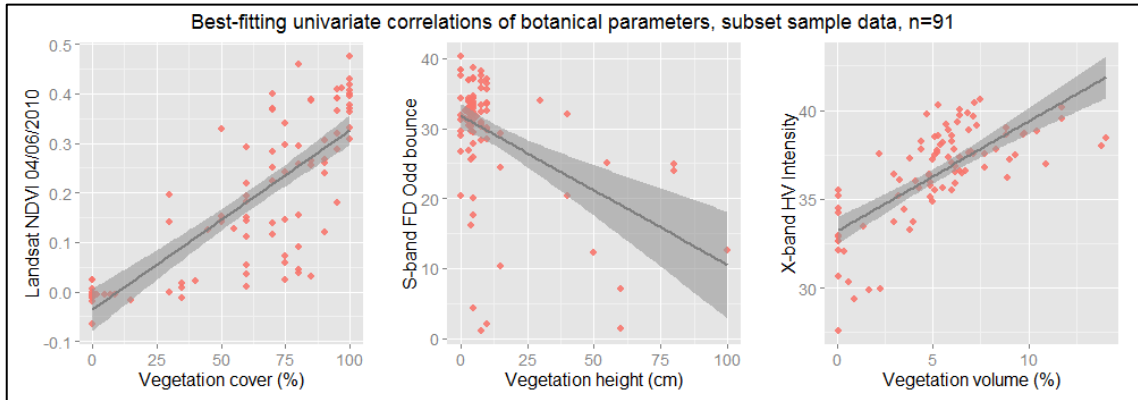


Figure 42 – Scatterplots of the best-fitting RS variables for biophysical parameters, based on a subset of the sample data set, GVV < 20% (n=91).

From the ULR regression the following observations were made:

- Vegetation height and volume correlated strongest with S-band FD surface scatter for the entire data set, with *R-values* of -0.57 and -0.56, respectively. For the subset data (volume < 20 dm<sup>3</sup>) the *R-values* were higher, with -0.63 for S-band FD surface scatter and 0.71 for both X-band HV backscatter and X-band VZ volume scatter, respectively. This indicated that the use of the data subset generated a slight improvement for correlation of vegetation height and a larger improvement for vegetation volume. It was worth noting that the data subset regressions X-band FD and VZ volume scatter variables correlated slightly better than S-band SAR variables.
- The exclusion of shrubby vegetation (volume > 20 dm<sup>3</sup>) improved the regression model based on X-band variables. This observation was similar to earlier analysis of the habitat classification results, which was that X-band was not capable to distinguish the shrubby *Juncus maritimus* vegetation from grassy vegetation habitats.

None of the RS variables used in this research for univariate linear regressions were sufficiently correlated to the biophysical parameters vegetation height and volume to allow consistent mapping of these parameters with a single RS variable. In Figure 41 the correlations for vegetation height and volume are



statistically significant, but they show a poor linear fit. The sample subset data correlations were better (Figure 42), but this data set was not representative of the vegetation in the entire research area.

### 7.3.1.2 Multivariate linear regression

Initial MLR analysis was carried out with the full sample collection with the four variable combinations models.  $R^2$ -values were calculated to assess which variable combination model fitted most accurately with the three different biophysical parameters (Table 27). The most accurate variable combination model for each of the three biophysical parameters is the model incorporating all variables, with adjusted  $R^2$ -values of 0.79, 0.64 and 0.60 for vegetation cover, vegetation height and GVV, respectively.

Table 27 – Adjusted coefficients of determination (adjusted  $R^2$ ) of MLR models of biophysical parameters, based on the full sample data set ( $n=110$ ).

Biophys. param.	DSM and optical	S-band SAR	X-band SAR	All RS variables
Cover ( $\text{dm}^2/\text{m}^2$ )	0.68	0.52	0.46	<b>0.79</b>
Height (cm)	0.43	0.49	0.40	<b>0.64</b>
Volume ( $\text{dm}^3$ )	0.40	0.46	0.39	<b>0.61</b>

Subsequently, the best-performing variable combination for each of the three biophysical parameters was calculated by using forward and backward stepwise variable selection. This was carried out to simplify the statistical models and reduce noise to the estimation. Besides, a number of variables in the full data set are broadly collinear. For example, S\_VZ\_Vol and S\_FD\_Vol are both measures of S-band volume scatter and therefore respond similarly to vegetation differences; it is advisable to leave variables out that are trying to do the same job. The adjusted  $R^2$ -values of the variable subsets for all four different combinations are shown in Table 28.

Table 28 – Adjusted coefficients of determination (adjusted  $R^2$ ) of MLR subset models of biophysical parameters, based on the full sample data set ( $n=110$ ).

Biophys. param.	Adjusted $R^2$	# of RS variables used
Cover ( $\text{dm}^2/\text{m}^2$ )	0.80	16
Height (cm)	0.67	12
Volume ( $\text{dm}^3$ )	0.65	11

Comparison of Table 27 and Table 28 shows a slight improvement of the adjusted  $R^2$ -values for the S-band SAR, X-band SAR and DSM/optical data combinations of 1% on average. A larger improvement is observed for the variable subset models based on the initial all available variable models. The adjusted  $R^2$ -values increase with 1%, 3% and 4% for the MLR models of vegetation cover, vegetation height and GVV, respectively.

Table 29 is an overview of variable coefficients and statistical significance of the subset MLR model for vegetation cover. In the subset MLR model of vegetation cover, 16 of the original 30 variables remain. The five most significant variables are DSM, S-band VV intensity, X-band VZ surface scatter, RGB red channel and S-band VZ surface scatter. This indicates that the biophysical parameter vegetation cover correlates best with a combination of SAR, optical and elevation variables.

Table 29 – Significance analysis of MLR coefficients of the subset model for vegetation cover.  
Significance codes: 0 < \*\*\* < 0.001, 0.001 < \*\* < 0.01 and 0.01 < \* < 0.05.

Variable	Estimate	Standard error	t value	Pr(> t )	Significance
(Intercept)	43.27	46.97	0.92	0.3593	
S_Int_VV	-10.81	2.342	-4.61	1.30E-05	***
S_CP_H	88.91	63.13	1.41	0.1623	
S_CP_alpha	-1.068	0.675	-1.58	0.1169	
S_FD_Odd	-0.462	0.184	-2.51	0.0137	*
S_FD_Dbl	0.438	0.185	2.36	0.0203	*
S_FD_Vol	-16.53	7.647	-2.16	0.0333	*
S_VZ_Odd	12.11	3.803	3.18	0.0020	**
S_VZ_Vol	16.63	6.581	2.53	0.0132	*
X_Int_HH	-3.902	2.411	-1.62	0.1090	
X_Int_VV	-5.998	2.347	-2.56	0.0122	*
X_CP_H	-52.79	32.38	-1.63	0.1064	
X_VZ_Odd	10.51	3.123	3.36	0.0011	**
DSM	18.17	3.783	4.80	6.00E-06	***
RGB_R	-1.038	0.318	-3.26	0.0015	**
RGB_G	0.922	0.353	2.61	0.0105	*
NDVI_2010	45.96	16.57	2.77	0.0067	**

Table 30 is the corresponding coefficient and significance table for the subset MLR model for vegetation height. This model is based on the 12 most significant remaining

variables, of whom the five most significant ones are, in descending order, DSM, S-band VZ surface scatter, X FD volume scatter, NDVI of 2011 and S-band HH intensity.

Table 30 – Significance analysis of MLR coefficients of the subset model for vegetation height.  
Significance codes: 0 < \*\*\* < 0.001, 0.001 < \*\* < 0.01 and 0.01 < \* < 0.05.

Variable	Estimate	Standard error	t value	Pr(> t )	Significance
S_Int_HH	6.057	1.564	3.87	0.0002	***
S_VZ_Odd	-6.551	1.505	-4.35	3.30E-05	***
S_VZ_Vol	2.226	0.834	2.67	0.0089	**
X_Int_HV	-24.24	8.207	-2.95	0.0040	**
X_Int_VV	3.943	1.578	2.50	0.0141	*
X_CP_A	-49.79	24.81	-2.01	0.0476	*
X_FD_Vol	-19.19	4.791	-4.01	0.0001	***
X_VZ_Vol	37.71	10.72	3.52	0.0007	***
DSM	15.39	2.788	5.52	2.80E-07	***
RGB_G	-0.978	0.273	-3.59	0.0005	***
RGB_B	0.721	0.284	2.54	0.0127	*
NDVI_2011	-55.86	13.99	-3.99	0.0001	***

The MLR coefficients and significance table for the subset model for vegetation volume is shown in Table 31. The subset MLR model is based on 11 variables of which the top five most significant are in descending order: DSM, X-band FD volume scatter, S-band CP entropy, RGB blue channel and X-band VZ volume scatter.

Table 31 – Significance analysis of MLR coefficients of the subset model for vegetation volume (GVV).  
Significance codes: 0 < \*\*\* < 0.001, 0.001 < \*\* < 0.01 and 0.01 < \* < 0.05.

Variable	Estimate	Standard error	t value	Pr(> t )	Significance
(Intercept)	91.78	35.08	2.62	0.0103	*
S_HH	5.066	1.603	3.16	0.0021	**
S_CP_H	113.7	25.16	4.52	1.70E-05	***
S_VZ_Dbl	-3.106	2.053	-1.51	0.1336	
X_HV	-22.30	8.287	-2.69	0.0084	**
X_VV	2.180	1.092	2.00	0.0486	*
X_FD_Vol	-23.02	4.769	-4.83	5.10E-06	***
X_VZ_Vol	40.57	10.80	3.76	0.0003	***
DSM	17.97	2.872	6.26	1.00E-08	***
RGB_G	-1.049	0.276	-3.80	0.0003	***
RGB_B	0.770	0.290	2.66	0.0092	**
NDVI_2011	-53.66	15.39	-3.49	0.0007	***

From the previous tables it appears that all three optimised subset MLR models comprise a mix of S-band and X-band SAR, optical and DSM variables. MLR analysis is a statistically sound regression method. However, it assumes normal distribution of the variable populations, which is not necessarily the optimal approximation for SAR data sets.

The following observations can be made:

- Analysis of the multivariate linear regression results based on all available RS variables (Table 27) and an optimised variable subset (Table 28) showed significant higher  $R^2$ -values for all three biophysical parameters, when compared to the  $R^2$ -values of the univariate linear regression results. Closer examination of the significance tables of the most accurate variable subsets (Table 29 for vegetation cover, Table 30 for vegetation height and Table 31 for vegetation volume) showed that each biophysical parameter was most accurately modelled with multivariate linear regressions by a combination of optical, LiDAR, S-band and X-band SAR variables.
- Analysis of relative performance of regression models based on S-band or X-band SAR variables alone shows that S-band variable models correlated better than the X-band variable models for all three biophysical parameters (Table 27). Analysis of the variable subset models showed that X-band variables are more significant for the regression models for vegetation height and volume, whereas the S-band variables are more significant for the vegetation cover model. This confirmed the findings of the univariate linear regression analysis, which also indicated that X-band SAR variables correlated better with vegetation height and volume than S-band SAR variables.

### **7.3.2 Biophysical parameter regression mapping**

In this section results of regression methods applied for mapping are presented, focussing on Multivariate Least-Squares (MLS), Support Vector Machine (SVM) and Random Forest (RF) regression methods. Four RS variable input models were used: All variables, S-band SAR variables, X-band SAR variables and elevation and optical

variables. In order to keep the size of this thesis manageable, only the three biophysical parameter maps of the best fitting regression models will be displayed.

### 7.3.2.1 *MLS regression*

Accuracy assessments of MLS regression mapping are shown in Table 32. Similar to the initial regression analysis, adjusted  $R^2$ -values are used to assess regression model performance. It can be observed that the models based on SAR variables perform considerably worse than the model based on DSM and optical variables; the X-band SAR regression model for vegetation height is less than 10% accurate.

*Table 32 – Accuracy assessment of MLS regression of biophysical parameters. Expressed in adjusted coefficients of determination (adjusted  $R^2$ ), based on selection of samples from a buffer zone around field survey sample locations (n=5797).*

<b>Biophys. param.</b>	<b>DSM and optical</b>	<b>S-band SAR</b>	<b>X-band SAR</b>	<b>All RS variables</b>
<b>Cover (<math>\text{dm}^2/\text{m}^2</math>)</b>	0.66	0.28	0.21	<b>0.72</b>
<b>Height (cm)</b>	0.32	0.26	0.09	<b>0.50</b>
<b>Volume (<math>\text{dm}^3</math>)</b>	0.33	0.26	0.12	<b>0.52</b>

### 7.3.2.2 *SVM regression*

Adjusted  $R^2$ -values from accuracy assessment of SVM regression results show that this regression method results in higher correlations than the MLS regression method. Vegetation cover is modelled with 90% accuracy when the DSM and optical variables are used. Vegetation height and volume (GVV) are both modelled 68% accurate, also based on DSM and optical variables.

*Table 33 – Accuracy assessment of SVM regression of biophysical parameters. Expressed in adjusted coefficients of determination (adjusted  $R^2$ ), based on selection of samples from a buffer zone around field survey sample locations (n=5797).*

<b>Biophys. param.</b>	<b>DSM and optical</b>	<b>S-band SAR</b>	<b>X-band SAR</b>	<b>All variables</b>
<b>Cover (<math>\text{dm}^2/\text{m}^2</math>)</b>	<b>0.90</b>	0.36	0.37	0.78
<b>Height (cm)</b>	<b>0.68</b>	0.26	0.07	0.59
<b>Volume (<math>\text{dm}^3</math>)</b>	<b>0.68</b>	0.18	0.10	0.57

SVM feature selection has been carried out on the three biophysical parameter regression models. The plots of SVM feature selection analysis of the regression models based on all variables are displayed in Figure 43. In these plots decrease of root mean squared error (RMSE) of the SVM models with increasing number of input variables are shown. For the vegetation cover regression model the optimal number of input variables is 18, before RMSE increases again. For the vegetation height and

volume models the optimal number of variables is 11 and 22, respectively. For the SVM modelling of vegetation cover the NDVI\_2011 variable is the most important, for vegetation height the S-band SAR CP alpha angle and for vegetation volume S-band SAR FD volume scatter are the most important initial variables.

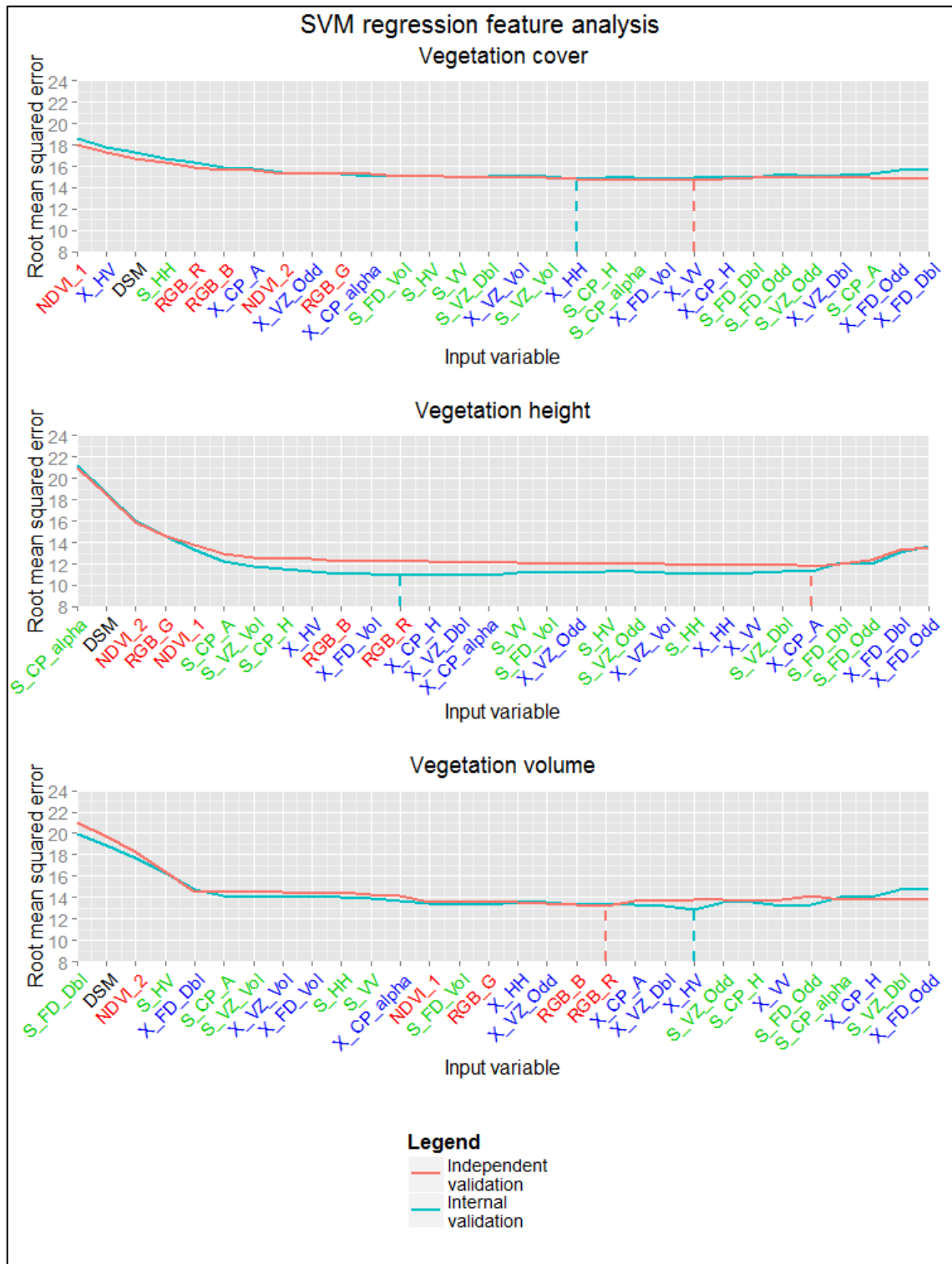


Figure 43 – SVM feature analysis of biophysical parameter regressions with all available RS variables. Colours on the labels on the X-axis according to variable type.

### 7.3.2.3 RF regression

In Table 34 the adjusted  $R^2$ -values of the RF regression models are shown. Similar to the SVM regression analysis results, DSM and optical variable input combinations generate the most accurate RF results, with adjusted  $R^2$ -values of 0.88, 0.65 and 0.66 for vegetation cover, height and volume, respectively. The models based on S-band and X-band SAR variables result in the lowest accuracies, particularly the X-band input model.

Table 34 – Accuracy assessment of RF regression of biophysical parameters. Expressed in adjusted coefficients of determination (adjusted  $R^2$ ), based on selection of samples from a buffer zone around field survey sample locations (n=5797).

Biophys. param.	DSM and optical	S-band SAR	X-band SAR	All variables
Cover (dm <sup>2</sup> /m <sup>2</sup> )	0.88	0.45	0.53	0.77
Height (cm)	0.65	0.35	0.22	0.56
Volume (dm <sup>3</sup> )	0.66	0.34	0.26	0.55

Analysis of variable importance is carried out for the RF models incorporating all available variables (Figure 44). Even though these models generate less accurate modelling results than the regression models based on optical and DSM variables, variable importance analysis of these models can tell more about relative importance of different RS sensors.

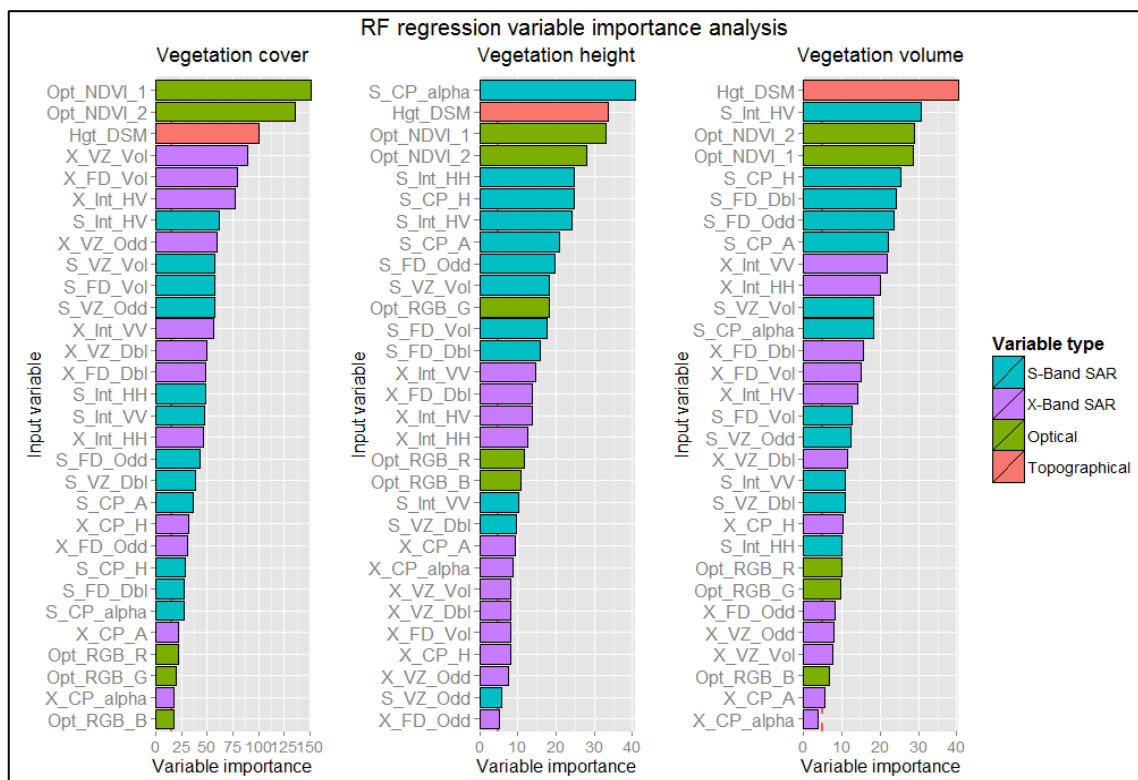


Figure 44 – RF variable importance analysis of biophysical parameter regressions with all available RS variables.

From the variable importance plot (Figure 44) a few observations can be made:

- On average, the most consistently important variables for modelling of all three biophysical parameters are elevation DSM and NDVI variables. These variables among the four most important variables for all three RF biophysical parameter regression models. This differs from the results of Chapter 6, in which was shown that SAR contributed to mapping of salt marshes. This difference will be further discussed in Chapter 7.3.3.
- For the modelling of vegetation cover DSM and NDVI are most important input variables. Following the three most important variables, three X-band SAR variables are most important variables. The rest of the top ten consists of S-band and X-band variables. Most of the SAR variables in the top ten, irrespective whether S-band or X-band, are variables that are responsive to vegetation, like FD and VZ Volume scatter or HV intensity. Optical R, G and B variables are at the bottom of the variable importance ranking.
- The most important variable for the modelling of vegetation height is S-band CP alpha angle. This is somewhat surprising, the RF regression model for vegetation height based on S-band SAR variables is 30% less accurate than the model based on optical and DSM variables. The DSM and NDVI variables are the subsequent most important variables. Rest of the top ten variables consists only of S-band SAR variables. X-band SAR variables are less important in the RF model, most of the bottom half of the variables consist of these variables.
- Analysis of variable importance of the RF regression model for vegetation volume shows that, besides DSM and NDVI variables, S-band SAR variables are most important. Most important SAR variable is S-band HV intensity, second most important after the DSM variable. The optical R, G and B channel are of little importance, similarly to the vegetation cover model.



### 7.3.2.4 Biophysical parameter maps

From the analysis of multivariate regression mapping results SVM regression has shown to be the most accurate. The biophysical parameter maps of vegetation cover (Figure 45), vegetation height (Figure 46) and vegetation volume (Figure 47) all provide a realistic image of vegetation type expressions in different parts of the salt marsh. Vegetation cover is highest in the dense salt marsh meadows and the *Juncus maritimus* habitats and decreases gradually towards the pioneer *Salicornia* and *Spartina anglica* habitats. Low vegetation height is mapped in the salt marsh meadows and pioneer *Salicornia*. Pioneer *Spartina anglica* is slightly taller and the shrubby *Juncus maritimus* reaches heights of approximately 1 meter. Vegetation volume is largely dependent upon vegetation height and therefore the pattern in the vegetation volume map is very similar to the vegetation height map, with highest volume modelled in the *Juncus maritimus* habitat and lowest volume in the salt marsh meadows habitat.

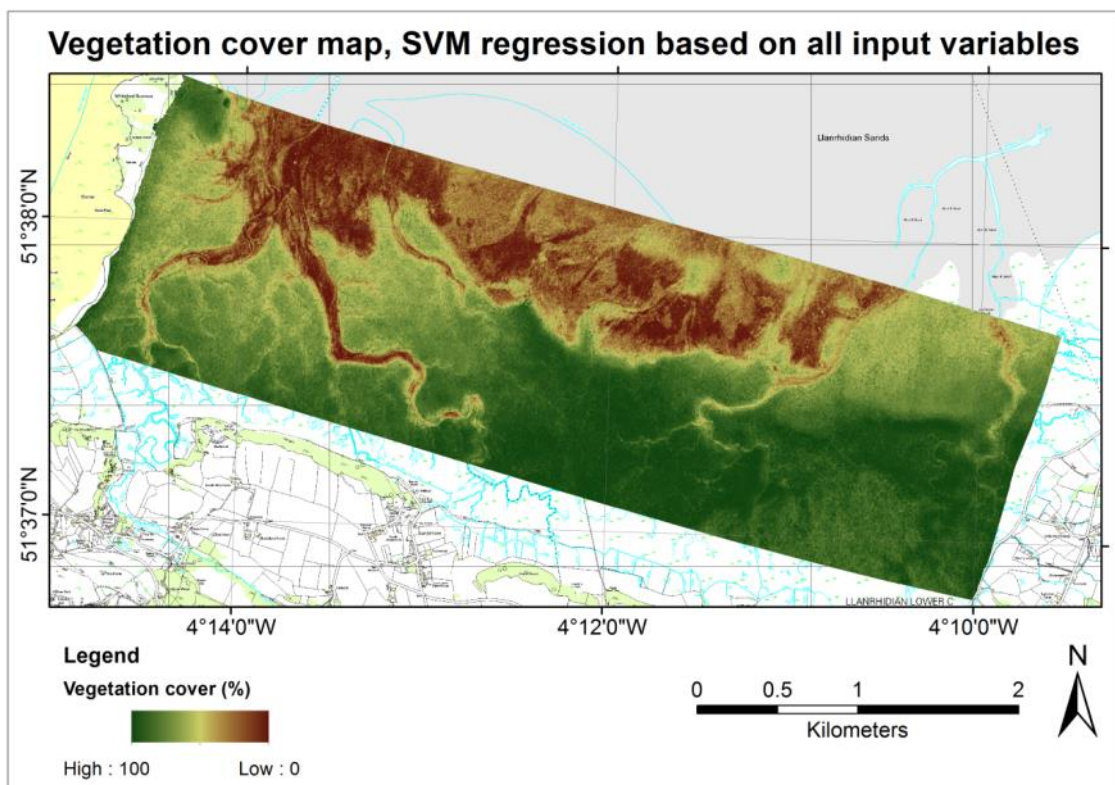


Figure 45 – Vegetation cover map, based on SVM regression with all available RS variables.

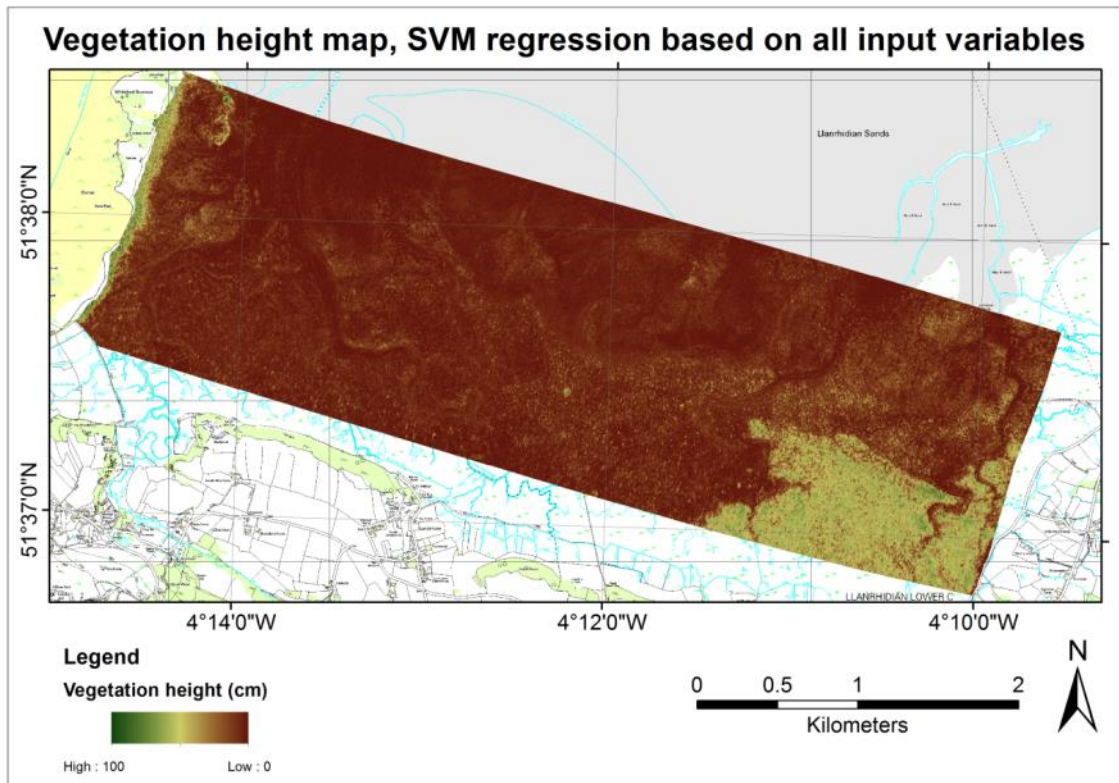


Figure 46 – Vegetation height map, based on SVM regression with all available RS variables.

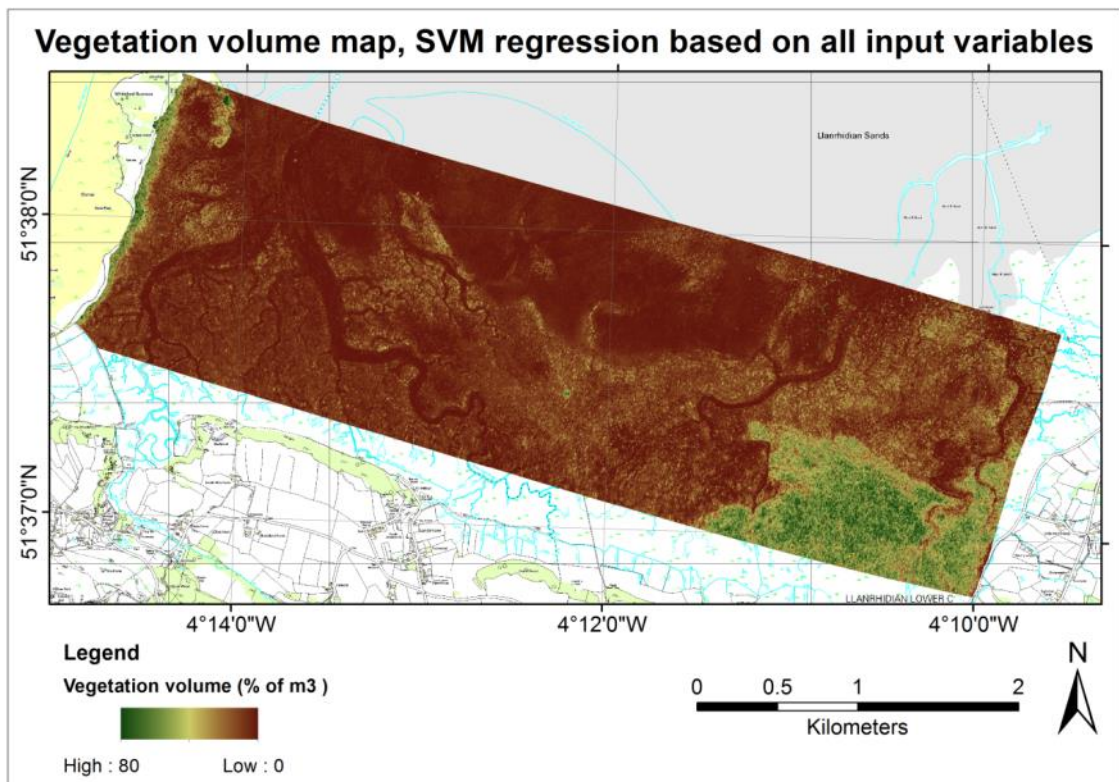


Figure 47 – Vegetation volume map, based on SVM regression with all available RS variables.

### 7.3.3 Integration of results

The RS variables were used to model structural biophysical parameters (percentage vegetation cover, vegetation height and gross vegetation volume) with regression modelling. Similar to the supervised image classification approach, different regression techniques were tested and only the most successful were used for mapping of biophysical parameters. Initial univariate regression modelling results showed that vegetation cover is correlated strongest with optical NDVI variables, whereas vegetation height and volume correlate best with S-band SAR variables.

Multivariate linear regression analysis indicated that the optimal combination of input variables to model any of the three biophysical parameters is a combination of SAR, optical and elevation variables. This is consistent with the outcomes of the supervised habitat classification (Chapter 6.3.2) and indicates that SAR, optical and elevation variables are complementary to each other. From multivariate SVM and RF regression variable importance analyses it emerged that the most accurate SVM and RF regression models were based on optical and elevation variables alone. This contrasted with the accuracies from the supervised habitat classifications based on the SVM and RF classifiers, which reported highest accuracy values for the models based on SAR, optical and elevation variables. It showed that inclusion of SAR for either regression or classification can lead to fundamentally different results. This might be ascribed to SAR data noise, which is not problematic for classification clustering, but suppresses accuracy in regression models. This observation will be further discussed in the next section. Nonetheless, RF variable importance analysis of the regression models based on all variables revealed that SAR variables dominated the importance analysis of vegetation height and volume.

The regression model results showed that optical variables were better suited to model two-dimensional vegetation cover. LiDAR and SAR variables were better suited to provide information about the third (height) dimension and were better for modelling vegetation height and volume. Furthermore, S-band SAR variables generally correlated stronger with vegetation height and volume than X-band SAR variables. X-band SAR variables are generally better correlated with vegetation cover than S-band SAR variables. This indicates that S-band SAR signal penetrates more into the canopy of the salt marsh vegetation, whereas X-band SAR does not penetrate significantly. X-

band SAR was, however, better capable of detecting subtle differences in surface roughness associated with bare sand and mudflats and pioneer salt marsh vegetation. This is a confirmation of the results of the SAR variable analysis (Chapter 5) and the salt marsh habitat mapping (Chapter 6).

## **7.4. Discussion**

In this section the results of the regression analyses of the biophysical parameters (vegetation cover, vegetation height and vegetation volume) are discussed. Initially, attention is given to results of the univariate linear regressions, followed by the multivariate regressions based on linear, SVM and RF models. In the last part of this section the presented biophysical parameter maps are discussed.

### **7.4.1 Regression variable analysis**

Analysis of ULR regression results showed that optical and LiDAR variables correlate more strongly to vegetation cover density than SAR variables. Contrastingly, S-band SAR variables show stronger correlations with vegetation height and volume. When the variables are combined in any multivariate regression model (MLR, MLS, SVM or RF) the optical NDVI and LiDAR variables are generally the most significant regression variables for vegetation cover. In the multivariate regression variable combinations for vegetation height and volume the importance of SAR is significant. This is especially clear from the SVM feature analysis (Figure 43) and the RF variable importance analysis (Figure 44) for vegetation height modelling, where S-band SAR CP alpha angle is the most important variable for both regressions.

The relationship of vegetation biomass with SAR backscatter has been researched extensively, starting with Le Toan et al. (1992). They found that L-band and P-band SAR correlated strongly with forest vegetation, especially for cross-polarised intensity channels. These findings were further confirmed by Patel et al. (2006), who focussed on shrub-tree vegetation, standing 3-4 meters high. They found that L-band SAR was preferable over C-band, although both frequency bands were deemed fit for use in these habitats. Instead of comparing qualitative performance of different microwave frequencies, Englhart et al. (2011) combined multi-frequency (X-, C- and L-band) and multi-temporal SAR data in a forest setting. They argued that combining various SAR

variables in a multivariate linear model could improve regression results considerably, even when only two multi-frequency SAR variables were used.

#### **7.4.2 Biophysical parameter mapping variable analysis**

The SVM regression accuracy assessment showed improved accuracy for all three biophysical parameters, with the highest  $R^2$ -values for the models based on optical and elevation variables alone. A variable subset analysis was carried out for all three biophysical parameters to determine optimal variable input for the SVM regressions based on all available variables (Figure 43). Even though these regression models were not the most accurate, they provided information about the relative contribution of all different RS variables. These plots showed the NDVI and DSM variables were generally most important for all biophysical parameter SVM regression models, accompanied by either a number of X-band SAR variables for vegetation cover, a number of S-band variables for vegetation height and a mix of S-band and X-band for vegetation volume. The Root Mean Square Error (RMSE) of all three SVM models decreased until an optimal number of variables was reached; the optimal number of variables for vegetation cover was 18, for vegetation height 11 and for vegetation volume 22. It showed that SVM regression can provide improved regression results when a selection of key variables was used. These findings correspond to related research, Mountrakis et al. (2011) concluded that SVM regression was well suited for ecological applications. Meanwhile, Zheng et al. (2008) showed that SVM regression could be used for data fusion and Moser and Serpico (2009) deemed it a powerful method for RS analysis.

The RF regression showed similar results, the highest accuracies were obtained with the variable model based on optical and elevation variables alone. The accuracies were 1 to 3% lower than the SVM regression results on average. Variable importance plots of the RF regressions for the three biophysical parameters of the RF regression models based on all variables were shown in Figure 44.

The most important variables for RF regression of vegetation cover were NDVI and elevation variables, followed by a number of X-band SAR variables. This was very similar to the variable importance analysis of the RF vegetation extent classification (Figure 37) and the SVM regression vegetation cover. The variable importance for vegetation height showed different variable importance ranking: the most important

variable was S-band CP alpha angle, followed by elevation and NDVI variables. To refresh the memory: CP alpha angle is a measure of the predominant scattering mechanism in an image pixel. With regard to this Tan et al. (2007) and Li et al. (2012) have shown in studies involving rice growth that vegetation height or phenological state has influence on the dominant scatter mechanism.

The importance of X-band SAR variables for vegetation height RF regression was low, all X-band variables were found in the lower half of the variable importance plot. This coincided with findings from the initial SAR variable analysis (Chapter 5), X-band SAR was not well suited to distinguish between different vegetation habitats, and especially the shrubby *Juncus maritimus* habitat was poorly identified from the other (grassy) habitats. The RF regression variable importance plot of the vegetation volume parameter showed that the LiDAR DSM elevation variable was most important, followed by S-band HV backscatter intensity and the NDVI variables. The variables after these top four most important ones were a combination of S-band and X-band SAR polarimetric decomposition and backscatter intensity variables. The variable importance plot of the vegetation volume is roughly comparable to the variable importance plot of the RF habitat classification (Figure 35).

### **7.4.3 Biophysical parameter mapping accuracy**

Even though the variable importance analysis of the RF regression and the variable subset analysis of the SVM regression indicated that a mix of SAR, optical and elevation variables improves regression results, it was noted that the regression accuracy of the variable models based on optical and elevation variables were higher than accuracy of the models that included SAR variables. This was valid for both SVM and RF regression results, although not for MLS regression. This contradicted the findings from the SVM and RF classification results, which showed highest accuracies for a combination of SAR, optical and elevation variables. Understanding why this difference occurred is crucial for future application of the classification and regression methods. The fundamental difference between regression and classification is that classifiers attempt to classify pixels on a discrete scale, whereas regression methods use a continuous scale. SAR data is inherently noisier than optical data due to the speckle effect (Lee and Ainsworth 2010). Whereas classification can deal with some noisy data

with outliers, for regression analysis outlying values can decrease the accuracy of the model (Breiman 1993). Optical and elevation data shows less variance than SAR data, which results in a smooth and consistent regression model, with fewer outliers that degrade the regression fit. For habitat mapping (Chapter 6) the best classification models are based upon a mix of variables providing consistently different information about each class. In the Considerations and recommendations chapter (Chapter 8) recommendations are provided for future applications of these classification and regression techniques.

### **7.5. Summary**

In this chapter it was shown that modelling and mapping of biophysical parameters with multivariate regression techniques provided new insight into the behaviour of the different RS variables used in this research. SVM and RF regressions were shown to be both capable of modelling biophysical parameters, and it is recommended to use these algorithms more commonly in ecological studies. However, the ideal variable input combinations depended on the modelled biophysical parameter. Analysis of the three biophysical parameters considered showed that for each of these parameters different regression methods and variable selections yielded the best results. It is therefore advised to use variable performance analysis to determine the most suitable variable combination for biophysical parameter analysis.



## **8. Considerations and recommendations**

In this chapter a comprehensive discussion of the followed research methodology is discussed in terms of made assumptions, validity and limitations. In the second section of this chapter the contributions of this research to science and recommendations for further research are described.

### **8.1. Methodological considerations**

In this section the used methodologies are discussed. Some of the major assumptions will be discussed, as well as the validity, limitations and repeatability of the research.

#### **8.1.1 Pre-processing**

The calibration routine for the Astrium Airborne SAR Demonstrator is described by Natale et al. (2011). They described that the SAR instrument was calibrated using the Van Zyl calibration technique (van Zyl 1990). This calibration routine correct for inter-channel imbalances by using returns from natural targets and trihedral corner reflectors. Even though this technique does not need an external calibration target, and it is capable of correcting for cross-talk effects between polarimetric channels, it does not provide coefficients to convert SAR backscatter to commonly used sigma-nought ( $\delta^0$ ) values (Attema 1991). Sigma-nought is a standardised measure of radar backscatter per square meter and is used to set one standard backscatter unit for backscatter intensity values of different SAR instruments. Unfortunately, these coefficients were not available for the airborne SAR data used in this research, so therefore no comparison with SAR imagery from other sources could be carried out on a quantitative basis. Nonetheless, the Van Zyl calibration allowed qualitative analysis of both S-band and X-band for the airborne SAR data.

The pre-processing of SAR data involved a correction for antenna pattern. This correction adjusts the amplitude of the SAR signal in the slant range according to an average across-swath curve for each polarimetric channel (Figure 12). The three polarimetric channels showed different attenuation curves along the slant range and were corrected with different amplification curves. Even though this can influence variables extracted from the three backscatter intensity channels, correction for antenna pattern was deemed necessary because it corrected for distortions caused by the SAR system layout (Freeman 1992). One side-effect is over-amplification of SAR



signal which causes noise in the far slant range. In the data set used for this research this is particularly visible in the far slant range part of the X-band SAR image (Figure 16).

### **8.1.2 Data analysis**

A number of arguments could be made regarding the methodology followed for the data analysis in this research.

#### **8.1.2.1 Vegetation classes**

Considering the habitat classification, a point of discussion could be whether the vegetation habitat classes used in this research were a good representation of the major habitats present in the research area. Table 7 indicated the relationships between the vegetation classes used in this research and classes defined by the NVC and Habitat Directive Annex 1 classifications. The Annex 1 classification scheme was closely followed. An exception was made for the *Juncus maritimus* class, which is grouped with salt marsh meadows under the Annex 1 class 'Atlantic salt meadow'. The *Juncus maritimus* class (which has a separate NVC class 'SM18') is botanically very different from the other upper salt marsh meadow habitats, characterised by a perennial shrubby appearance. As such, this vegetation habitat appeared clearly in S-band SAR imagery, although less so on X-band SAR data. It was decided to use this class as a different vegetation habitat in order to research to what extent it overlapped with other more shrubby habitats, like *Spartina anglica*. The confusion matrix of the most accurate RF habitat classification (Table 19) showed little confusion between the *Juncus maritimus* and *Spartina anglica* habitats, with only 27 *Juncus maritimus* reference pixels classified as *Spartina anglica* and no mis-classified pixels in the other direction. SAR backscatter intensity (Figure 21) and VZ polarimetric decomposition boxplots (Figure 27) showed that the *Spartina anglica* and *Juncus maritimus* habitats overlapped to some extent, but that for image classification there is enough distinction.

#### **8.1.2.2 Variable importance**

The dominance of both NDVI and elevation variables in both classification and regression analyses was another methodological point of discussion. It could be argued

that the inclusion of SAR in the research data set complicated the analyses unnecessarily. SAR data, especially quad-polarimetric SAR, is not readily available and processing tools are not as advanced as those for optical or LiDAR RS data. Nonetheless, in the discussion of the results it was shown that the use of multi-sensor RS data sets is preferential over data sets composed of a single RS data sensor. The complete data set used in this research has shown to be more capable of distinguishing different vegetation habitats. Other researchers have tested multi-sensor RS approaches and concluded that these data sets provide additional information, use of multi-sensor data sets is advised (Pohl and Van Genderen 1998; Hall and McMullen 2004). Further discussion on this topic is beyond the scope of this research. One of the main objectives of this research was to investigate whether SAR can provide benefits for habitat mapping and monitoring. This has been confirmed for all classification and most regression models. These models were improved by inclusion of SAR variables. However, higher accuracies were noted for the SVM and RF regression models based on variable combinations excluding SAR variables. Availability of quad-polarimetric SAR data is limited; acquisition of quad-polarimetric SAR data is infrequent and expensive. Nonetheless, for most common applications quad-polarimetric data offers unique additional information that is not provided by other data types or even single or dual-polarimetric SAR.

### **8.1.2.3 Data consistency**

Another point of methodological discussion was the large time gap between the SAR data acquisition (July 2010) and the recording of reference field data (July 2013). The reason for this time gap is pragmatic: it was decided in November 2012 that the airborne SAR data set would form the basis of the research. In late autumn most of the annual plants (*Salicornia*, *Spartina anglica*) are senescent. Therefore it was decided to plan the field work in a period in which the phenological state of the annual plants is comparable to the moment of SAR data acquisition, which was the following summer in July 2013. In the three years between image acquisition and field survey field work was carried out by CCW in summer 2012. They recorded an increase of pioneer salt marsh vegetation cover, compared to the CCW habitat survey of 1998 (personal communication with Lily Pauls (NRW)). It was less likely that significant vegetation

change occurred in the upper parts of the salt marsh in the three years between SAR data acquisition and field work. These areas are characterised by stable vegetation cover in the past decade. This was confirmed with a visual interpretation of Google Earth multi-date aerial photography (imagery ranging from 1999 until 2010). From the Google Earth imagery it can also be observed that the pioneer zone of the salt marsh is subject to significant vegetation cover dynamics, especially in the western part of the pioneer zone of the research area. This observation is confirmed by the vegetation extent dynamics map (Figure 39) and the habitat dynamics map (Figure 40). Time-gaps between RS image acquisition and recording of reference data often occur in temporal RS studies (Singh 1989), although no general consensus what time gap is still acceptable exists. This is dependent on the dynamics in the research area, which is unfortunately high in the lower parts of this research area. Therefore it has to be acknowledged that classification and regression errors occurred related to the time gap between RS image acquisition and the recording of field reference data, although it could not be quantified how large this error was.

### **8.1.3 Environmental and seasonal factors**

It is important to discuss the environmental setting in which this research has taken place. These factors influence the RS variables and henceforth the outcomes considerably.

#### ***8.1.3.1 Tidal level***

In a salt marsh setting the moment of data acquisition is crucial. During high tidal level the lower parts of the salt marsh are generally submerged, adding difficulty to the acquisition of good quality RS imagery. According to Lee et al. (2012), tidal variations results in large backscatter variations of different vegetation habitats. They argued that the best RS imagery is acquired at low tide. For distinction between un-vegetated tidal flats and pioneer salt marsh vegetation particularly, data acquired during low tide is preferential. According to the tidal recordings in our research area at the moment of SAR acquisition (NTSLF 2012), the tidal level was +0.20m OD (see paragraph 4.2), which was lower than the lowest point in the research area. The SAR image shows two distinctive types of tidal flats, some areas are covered with a remaining thin layer of water while other parts of the sand and mudflats are dry. The wetness of tidal flats

influences the backscatter signatures (Lee et al. 2011). They concluded that the surface wetness of tidal flats is dictated by a complex interaction of inundation, desiccation and drainage. In the SAR data used for this research it was observed that in the areas covered with a thin layer of water specular reflection occurs; the thin water layer acts as a mirror for microwaves, scattering much of the microwave signal away. The resulting backscatter signal in these areas have a low signal to noise ratio as there is little backscatter recorded. Processing of this weak signal leads to erroneous variables, especially polarimetric decomposition variables. On dry tidal flats the dominant scatter mechanism is surface scattering. None of the salt marsh vegetation habitats were covered with water during SAR acquisition; even the pioneer vegetation habitats remain largely dry. It has to be stressed that during neap tides the higher parts of salt marshes are not covered. These are covered only a few times per year during the spring tides. Timing of tidal level should be a consideration when the research focusses on tidal flats and pioneer salt marsh areas, for middle and upper parts of salt marshes it is of lesser importance.

#### ***8.1.3.2 Soil moisture***

Soil moisture has a significant effect on radar backscatter, thus research into the use of SAR to model soil moisture variations has commonly been carried out (Dubois et al. 1995; Dabrowska-Zielinska et al. 2009). Kasischke et al. (2003) argued that for monitoring of wetlands with SAR, soil moisture is one of the key parameters. It was mentioned that seasonal changes in soil moisture can be detected with SAR and can be used to monitor these habitats. In this research no particular attention was given to soil moisture variations, it was assumed this is constant over the entire research area. In case repeated SAR acquisitions are planned, consideration of soil moisture variations is advised.

#### ***8.1.3.3 Phenology***

Phenological stage of vegetation under consideration is a significant factor that determines the optimal moment of RS data acquisition (Reed et al. 2009). As was discussed in Chapter 8.1.2.3, the collection of reference field data was done in the same season as the SAR data acquisition. In the temporal analysis of salt marsh vegetation habitats carried out by Lee et al. (2012) it was observed that perennial

vegetation species have SAR backscatter signatures that are relatively constant throughout the year, whereas SAR backscatter signatures from annual plant species are more variable. Clint Slatton et al. (2008) argued that both water level and phenological stage are important environmental parameters in SAR RS monitoring studies in pioneer salt marshes, and to lesser extent in the upper parts of salt marshes. In their research they did not use a multi-temporal SAR data set; they assumed that environmental parameters are constant throughout the research area. However, if multi-polarimetric SAR data is used for vegetation monitoring and repeated SAR acquisitions take place, corrections for water level, soil moisture and phenology have to be made.

## **8.2. Research feasibility and recommendations**

In this section the meaning and validity of the research is discussed in a wider perspective. Attention is given to what this research indicated and its repeatability. Consequently, recommendations are given for follow-up research based on the results of this study.

### **8.2.1 Feasibility and repeatability of the research**

This research has shown that detailed salt marsh habitat mapping and modelling can be achieved with a combination of RS variables. This has been the first research that utilised the full capabilities of quad-polarimetric SAR to map individual salt marsh vegetation habitats. Therefore, it is necessary to question the feasibility and repeatability of this research to identify room for improvement and for possible follow-up research.

The availability of quad-polarimetric multi-frequency SAR data is currently limited. The acquisition of the airborne SAR imagery over the Llanrhidian Marshes was part of a survey campaign to test the performance of the AirSAR system over different land cover types. Currently, AirSAR is installed on the research airplane of the Natural Environment Research Council (NERC) and some further test flights have been carried out in the summer of 2014 (NERC 2014) for a UK-based consortium of investigators, supported by funding from the Satellite Applications Catapult in Harwell. S-band and X-band SAR thus have the prospect of being acquired on a more regular basis.

Ease of use of polarimetric SAR data can be improved if better pre-processing tools would be available. Geo-registration of the SAR data used in this research is done by selecting manual GCPs. This can be done very accurately in areas where stable GCPs are available, like built-up areas. In natural habitats stable GCPs are more difficult to find.

Considering the polarimetric decomposition variable calculations, the SAR processing software tool PolSARpro includes a number of processing templates for other airborne SAR systems, as E-SAR, F-SAR, AIRSAR and UAVSAR (ESA 2013). In order to facilitate the processing and analysis of AirSAR data it is advised to develop similar processing tools.

### **8.2.2 Research contributions**

So far the technical aspects of the use of airborne polarimetric SAR have been discussed. In this section the research results contribution in terms of improvement for mapping of coastal habitats.

As discussed in the literature review (Chapter 2.1), research and policy development of ecosystem-based habitat management is popular. The results from this research demonstrated that advanced RS technologies were able to provide useful synoptic tools to improve ecosystem management strategies. RS technologies have undergone considerable improvements since the dawn of this industry in the 1970s. The Sentinel missions are part of the European Copernicus earth observation programme. This will make RS data become more readily available (Attema et al. 2007). These missions will monitor the Earth's surface regularly with both optical and microwave sensors and the RS data will be publicly available. Directly related to S-band SAR data, this research has successfully shown that this microwave frequency band can be used to map and monitor shrubby and grassy vegetation habitats.

This research looked thoroughly into the use of polarimetric descriptor variables extracted from airborne SAR data. Acquisition of quad-polarimetric SAR data is relatively rare; most SAR data is acquired in either single or dual polarimetric mode. Nonetheless, outcomes of this research have shown that polarimetric decomposition variables provided additional capabilities for the discrimination of salt marsh habitats with high detail. As such, this is an important contribution indicating this data type is worth using for further land cover mapping studies.

This research did not focus on the intricate workings of the chosen classification algorithms, instead it has primarily been a study on the application of high-resolution polarimetric SAR for habitat mapping and the used classification algorithms were tested primarily for their suitability to deal with this data type. However, this research has shown that both the SVM and RF classifiers are robust classifiers that provide useful information about algorithm performance. It has to be stressed that SVM and RF models are based on a randomly selected bootstrapped set of input samples. Therefore, each time the classifiers are run the class partitions are slightly different. Furthermore, each SVM and RF classification is trained for the specific RS variable data set, for each different RS data set the SVM or RF classification model needs to be calculated. This limits the transferability of the methodology, the classification models are optimised for a specific data set. Other classification methods, like Object-Based Image Analysis (OBIA) rule-based classifiers, have shown to be better transferable between different RS data sets (Blaschke 2010).

Additionally, the use of multivariate regression models has shown that these techniques are capable of handling multi-source RS data to produce realistic approximations of biophysical parameters. Research into the use of SAR variables for mapping vegetation biomass (Englhart et al. 2011) has been mostly limited to the applications in forests. The results from this research show that these models can also be translated to a coastal salt marsh setting.

### **8.2.3 Future research**

The results of this research indicate that airborne SAR does provide valuable additional information about vegetation cover and structure. Nonetheless, acquisition of airborne SAR is limited and applied research into applications for ecological monitoring sparse. There has been research into application of airborne SAR in agriculture (Hajnsek et al. 2006), but there has been limited applied research for product development. Research into the application of airborne SAR for mapping and monitoring natural habitats could help develop tools for regular monitoring. Some research topics for follow-up research could be:

1. Research of further combination of optical, LiDAR and SAR data. As this research has shown, all three RS types offer specific different advantages.

Simultaneous acquisition is often not possible and most research focusses on the use of one of the data types (Thomson et al. 2003; Lee et al. 2012). The inclusion of the AirSAR system on the NERC airborne survey plane (NERC 2014) is one of the best opportunities for concurrent acquisition of high resolution optical and SAR data. Besides SAR variables alone, derivative variables from optical and topographical RS sensors can be used as input variables as well, as Hladik and Alber (2014) have shown. They used GIS variables extracted from a single LiDAR Digital Elevation Model (DEM) input layer in a salt marsh setting to classify salt marsh habitats. Their model based on RS derived variables was more accurate than the model based on non-RS GIS variables. Additionally, additional data products can be produced from optical RS sensors to support vegetation mapping. In this research it was shown that medium-resolution NDVI variables based on Landsat imagery are generally more important for distinction between vegetation habitats than very high resolution aerial photography R, G and B channels. Variables extracted from Landsat and other optical RS imagery by biophysical formulations like Tasseled Cap transformation or Leaf Area Index (LAI) are also found to provide more useable information than reflectance channels alone (Walton 2008). Summarising, further research is needed on the addition of additional topographical and optical variables in order to determine how these variables can improve aggregate classification.

2. Research of the ideal spatial resolution for the habitat under consideration. Airborne SAR systems can acquire data in sub-metre resolution, but this not always necessary and relatively costly (Robinson 2012). The type of habitat under consideration dictates the ideal spatial resolution needed for mapping. In heterogeneous salt marsh habitats high spatial resolution can provide information about subtle changes, but in more homogeneous habitats lower spatial resolution might be sufficient.
3. Investigation of the ideal SAR frequency for mapping natural habitats. Which microwave frequency is most suitable depends upon the habitat under consideration. Results from this and previous research indicate that each SAR frequency domain has its own specific field of application (Schmullius and Evans 1997). Forests are generally best mapped with longer SAR wavelengths,



whereas for grassy habitats shorter wavelengths are better. This research has been one of the first to research the use of S-band SAR. In order to support application development for the upcoming NovaSAR-S mission (launch planned in 2016), more research is needed to investigate S-band SAR capabilities. The results of this research showed that S-band SAR can be a useful frequency for mapping grassy and shrubby habitats. It is advised to research the behaviour of S-band SAR in land cover types.

4. Further research into the use of SAR polarimetric decomposition variables for habitat mapping. The calculation of polarimetric decomposition variables requires acquisition of coherent quad-polarimetric data, which is not commonly acquired. As this research has shown, the use of polarimetric decomposition variables provides extra discriminative tools for mapping habitats than the use of polarimetric backscatter channels alone. Therefore, if the data is available, it is advised to research further potential of SAR polarimetric decomposition variables for mapping habitats.
5. Investigation of the most suitable temporal resolution for habitat monitoring. For agricultural applications, it is essential to monitor monthly or even weekly during the growing season. This frequency can be lower for the monitoring of natural habitats, perhaps once or twice per year. Finding the right moment for image acquisition is dependent upon the land cover type under consideration; some habitats are best mapped in the growing season, some in more senescent state. Change analysis of salt marsh (or other) vegetation habitats with multi-temporal SAR data sets have shown to be able to improve classification results (Waske and Braun 2009), and it would be very interesting to apply multi-temporal SAR analysis in a salt marsh setting to investigate inter-annual variability of these specific habitats.
6. Research of transferability of high-resolution habitat mapping with SAR from airborne scale to satellite scale. With the launch of the first of the Sentinel-1 satellites, the availability of good-quality, freely available C-band SAR will increase sharply in the coming years. This provides many opportunities for regular monitoring of natural habitats. The Sentinel-1 missions are capable of acquiring SAR data in dual-polarimetric mode, which will allow the

discrimination of different land cover types (Attema et al. 2007). The Radarsat missions have shown that polarimetric C-band SAR data on a spaceborne platform can be applied for a number of coastal applications (Moon et al. 2010). These satellites are capable of acquiring SAR data in quad-polarimetric mode; research based on quad-polarimetric Radarsat data has shown that products derived from this satellite has good potential for mapping land cover. Additionally, the quad-polarimetric ALOS PALSAR mission has shown to be very useful for mapping coastal areas (Lucas et al. 2007; Wang and Allen 2008). With the planned ALOS-2 mission (JAXA 2012) quad-polarimetric spaceborne SAR will continue to be acquired. It is proposed to carry out research similar as this research on the use derived polarimetric decomposition from these satellites.

## 9. Conclusions

In this thesis a number of research experiment results were carried out to investigate the potential of RS data for the mapping and modelling of salt marsh habitats. A clear focus has been put on the exploitation of airborne quad-polarimetric SAR data. The results from the different analyses show that inclusion of quad-polarimetric SAR for mapping and modelling of vegetation habitats with RS technologies adds valuable information, although the different research experiments showed that this data type has practical and technical limitations.

A review of literature on coastal zone management policies and practices and the potential use of novel RS sensors (i.e. polarimetric SAR) for mapping and monitoring of natural coastal habitats (Chapter 2.1.1) showed that there is a move towards ecosystem-based management of coastal areas. Specifically, ecosystem-based and monitoring of low-lying coastal areas, like salt marshes, was deemed essential to mitigate for the expected effects of climate change. It has been acknowledged that RS technologies offer unique capabilities to monitor and map coastal areas with relative ease. A significant amount of research has been carried out to research the applicability of optical and LiDAR RS sensors for coastal management purposes, a limited amount of research focussed on the combined use of optical, LiDAR and polarimetric SAR.

At the end of the Literature Review chapter a number of research questions were stated. In the following section each research question will be re-stated and the key findings are discussed and conclusions drawn.

1. *How are polarimetric SAR backscatter signatures affected by salt marsh characteristics, like specific environmental parameters (sea level, soil moisture or soil salinity) or botanical structure?*

The S-band and X-band SAR data sets used in this research represent medium-long and shortest wavelength frequencies commonly used for SAR RS applications, respectively. S-band has rarely been used in SAR RS, but is proposed as the frequency band for an upcoming SAR satellite (NovaSAR-S). Analyses of SAR backscatter signatures showed variations in the responses of the S-band and X-band SAR data, depending on botanical

structure and environmental parameters. In each of the five habitats considered for this analysis, the sand and mudflat habitat showed the highest variability in backscatter intensity for both frequencies for the HH and VV polarimetric channels. This has been ascribed to variations in soil moisture, expressed as a thin film of surface water in certain areas, contrasting with dry sand and mudflats in others. In the areas where a thin film of water is present, some SAR signal was reflected specular, resulting in low returned backscatter. For the four salt marsh vegetation habitats considered, the most discriminative polarimetric SAR backscatter channel was the HV polarisation. The *Spartina anglica* and *Juncus maritimus* habitats showed higher backscatter in this polarisation than the *Salicornia spp.* and salt marsh meadows. This difference was ascribed to the higher volume of above-ground vegetation in the former habitats. It was found out that X-band was more sensitive in detecting subtle differences in surface roughness in the pioneer zone, with lower standard deviation of in HV polarisation than S-band for the *Salicornia spp.* habitat. This indicated that X-band SAR was better at identifying subtle changes in surface roughness associated with pioneer vegetation than S-band. Therefore X-band has been regarded as the most suitable frequency to map and discriminate sparsely vegetated pioneer salt marsh areas.

Analysis of the differences between S-band and X-band SAR variables showed that the average variance of backscatter intensity variables for the salt marsh habitats in S-band was 3.68 and 2.27 for X-band. This indicated that S-band shows more variability between the salt marsh habitats and was better suited for discrimination between them.

Polarimetric decomposition variables offered additional discriminative information for the considered salt marsh habitats. It was shown that the average standard deviation for the different habitats for all backscatter intensity variables (both S-band and X-band) was 3.59 and the mean standard deviation from VZ polarimetric decomposition variables was 3.26. This showed that polarimetric decomposition variables provided slightly additional discrimination between salt marsh habitats compared to backscatter intensity channels. However, the limited availability of quad-polarimetric SAR data hampers a more generic uptake of polarimetric decomposition variables. Dual-polarimetric SAR data, with at least one cross-polarimetric channel has shown to be almost as useful and is recommended to be used for similar future research.

2. *Does the inclusion of SAR in a RS data set based on optical and LiDAR data improve mapping of both salt marsh extent and individual salt marsh habitats?*

Mapping of salt marsh habitats was carried out with unsupervised and supervised classifiers. Unsupervised classification with the K-means Wishart classifier, utilising CP polarimetric decomposition variables showed that habitat classification based on SAR variables alone resulted in marginal results. Especially the habitat map based on X-band variables showed extensive mis-classifications of the salt marsh habitats. Two major factors influencing the low accuracy of the habitat classification with the K-means Wishart classifier were the presence of speckle in the SAR images and the low data quality in the far slant range of the SAR image.

The supervised classifications, carried out with the SVM and RF classifiers showed that the combined use of optical, LiDAR and SAR variables resulted in significantly better habitat maps than any of the maps based on any of these variables alone. The highest RF classification accuracy achieved with optical and LiDAR or SAR variables alone were 60.41 % and 62.86%. Combining the optical, LiDAR and SAR variables improved the RF habitat classification accuracy to 78.20%. The SVM classification accuracies were 58.25%, 59.24% and 72.09% for optical and LiDAR, SAR or all variables combined, respectively. This showed that combined use of multi-source RS variables increased accuracy significantly for the two classifiers.

Analysis of the importance of different variables for SVM and RF classification indicated that particularly NDVI optical and LiDAR variables were most important variables for habitat mapping, followed by a combination of S-band and X-band SAR variables. This indicated that the NDVI and LiDAR variables provided the least ambiguous information about salt marsh habitats. NDVI provides information about photosynthetic activity of vegetation, which appeared to differ between salt marsh habitats, while the high importance of LiDAR showed that salt marsh zonation are largely dictated by elevation and related inundation frequency. However, SAR did provide strong additional information, primarily related to the botanical structure of salt marsh habitats that complements the previously mentioned data types well.

Of the two supervised classifiers used in this study (SVM and RF), the RF classifier showed to be generating the best results. The overall accuracies of both SVM and RF classifications were very comparable, with slightly higher accuracies for the RF

classification results. The resulting habitat maps showed that the RF classifier provided very detailed habitat discrimination. Simultaneously it suppressed SAR speckle to a large extent, visually more than the SVM classifier.

Analysis of temporal change of salt marsh habitats and extent in the research area was carried with the salt marsh habitat and a general salt marsh vegetation extent map generated with the RF classifier. These were compared with two older vegetation extent maps from different sources, one habitat map based on data from 1998 and a salt marsh extent map from 2007. Even though the data types used and methodologies of the three extent maps were different, changed analysis based on these maps has revealed consistent trends in vegetation cover dynamics. In specific areas vegetation cover retreat has been observed throughout the entire time span, whereas in other areas it has been expanding. Habitat extents have changed considerably in the pioneer zone of the research area, whereas it remained less changed in the upper parts of the salt marsh.

- 3. Is a combined RS data set from optical, LiDAR and SAR sensors better suited for regression modelling of biophysical parameters (vegetation cover, height and volume) than regression models based on a data set based on a single RS sensor?*

Several regression methods have been used to analyse correlations between the three biophysical parameters considered in this research and the SAR, optical and elevation variables. Univariate linear regression results indicated that NDVI variables correlate strongest with vegetation cover, whereas S-band SAR variables showed the strongest correlation with vegetation height and cover. This pattern was also observed with multivariate regressions (MLS, SVM and RF). Vegetation cover was best modelled with NDVI and elevation variables, with a maximum  $R^2$ -value of 0.90 for the SVM regression based on optical and elevation variables alone. The highest  $R^2$ -values for both vegetation height and volume are lower; the highest are both 0.68, based on the optical and elevation variables alone with SVM regression. It can be concluded that biophysical parameters can be modelled with SAR, optical and elevation data in multivariate regression models to great extent. Vegetation cover correlates strongly

with optical and elevation variables, for vegetation height and volume SAR variables provide a complementary information to optical and elevation parameters.

The research results indicate that SAR provides excellent additional tools for ecological mapping. Even though repeatability of this research is questioned, the acquisition of quad-polarimetric SAR data is sparse; the research results indicate that the methodologies in this research are well translatable to other SAR platforms. Dual-polarimetric and quad-polarimetric satellite SAR data could be used in conjunction with optical and elevation data sets to improve mapping of natural habitats.

From the conclusions stated above a single key message from this research can be distilled:

**Salt marsh habitats, or indeed any natural (coastal) habitat need to be mapped for purposes of monitoring or management. Some of the most promising technologies to do so are provided by Remote Sensing technologies. Synthetic Aperture Radar provides novel ways to map natural habitats with different frequency and polarimetric capabilities. This research has shown that SAR is an excellent tool to provide additional data besides more established optical and LiDAR RS systems. As such, it is advised to use SAR complementary with other RS data sources for ecological mapping.**

## **Appendices**

Appendix A – Ecological field survey (July 2013) data sheets

Appendix B – Pictures for selected sample locations

Appendix C – Flowchart of analysis steps

Appendix D – Flowchart of SAR data pre-processing steps

Appendix E – Publications



Appendices

Appendix A – Ecological field survey (July 2013) data sheets

Location	Photo ID 1	Photo ID 2	Latitude (WGS84)	Longitude (WGS84)	X coordinate (OS)	Y coordinate (OS)	Grazing activity(1=no grazing, 5=overgrazed)	Species (% of total plant cover)												Vegetation cover (dm <sup>2</sup> /m <sup>2</sup> )	Average vegetation height (cm)	Gross vegetation volume(dm <sup>3</sup> /m <sup>2</sup> )	NVC vegetation class (SM_)			
								<i>Salicornia spp.</i>	<i>Spartina anglica</i>	<i>Puccinellia maritima</i>	<i>Festuca rubra</i>	<i>Juncus gerardii</i>	<i>Juncus maritimus</i>	<i>Glaux maritima</i>	<i>Limonium binervosum</i>	<i>Suaeda vera</i>	<i>Plantago maritima</i>	<i>Armeria maritima</i>	<i>Halimione portulacoides</i>					<i>Athrocneumum perenne</i>	<i>Althea officinalis</i>	
1	5940	802	51.620187	-4.203378	244419	194539	4	5		60				1	30	4						90	8	6.51	10	
2	5941	804	51.620386	-4.202948	244456	194527	4			40					40			5					80	10	6.02	10
3	5942	807	51.621400	-4.202720	244499	194518	5	10	40	40													60	5	7.67	6
4	5944	810	51.622405	-4.202099	244564	194532	4	5	10	60					10		5						90	10	7.00	10
5	5945	817	51.622798	-4.201514	244533	194566	4	20	10	60													70	5	6.22	10
6	5947	828	51.623620	-4.201689	244539	194617	4	3		70					15	5							95	5	5.98	10
7	5948		51.624257	-4.201485	244526	194682	4	3	30	60				5	15	2							80	5	8.29	10
8	5949		51.624630	-4.201200	244556	194717	3		40	5			40										60	30	28.41	18
9	5950		51.625147	-4.200433	244550	194746	2		3			80		10									70	50	37.78	18
10	5951		51.626120	-4.200863	244539	194798	1				5	70		15									100	100	80.67	16
11	5952		51.626450	-4.200969	244571	194878	1					80											95	80	57.00	16
12	5953	846	51.626711	-4.201112	244617	194868	5		10	80								5					70	10	4.72	13
13	5954	848	51.627135	-4.200917	244672	194862	4		10	70					10	5							30	5	2.18	10
14	5955	849	51.627540	-4.201123	244719	194854	4	10	10	70													75	5	5.83	10
15	5956		51.627868	-4.201414	244777	194842	2	10	10							40	30						70	10	6.38	9
16	5957		51.628460	-4.201052	244829	194907	3	30	5	40									20				80	5	8.84	13
17	5958		51.628820	-4.201236	244911	194956	3	5	60		30												60	10	8.81	6

Appendices

Location	Photo ID 1	Photo ID 2	Latitude (WGS84)	Longitude (WGS84)	X coordinate (OS)	Y coordinate (OS)	Grazing activity(1=no grazing, 5=overgrazed)	Species (% of total plant cover)													Vegetation cover (dm <sup>2</sup> /m <sup>2</sup> )	Average vegetation height (cm)	Gross vegetation volume(dm <sup>3</sup> /m <sup>2</sup> )	NVC vegetation class (SM__)
								<i>Salicornia</i> spp.	<i>Spartina anglica</i>	<i>Puccinellia maritima</i>	<i>Festuca rubra</i>	<i>Juncus gerardii</i>	<i>Juncus maritimus</i>	<i>Glaux maritima</i>	<i>Limonium binervosum</i>	<i>Suaeda vera</i>	<i>Plantago maritima</i>	<i>Armeria maritima</i>	<i>Halimione portulacaoides</i>	<i>Athrocnemum perenne</i>				
18	5959		51.629193	-4.201070	244967	194987	3	25			70					10					85	5	5.95	10
19	5960		51.629684	-4.200629	245056	195014	3	35	5	50						5					75	10	7.22	10
20	5961		51.630251	-4.199974	244985	195018	3	15	75		5										75	15	13.78	6
21	5962	862	51.631927	-4.198860	244966	195035	4	10	80												60	10	11.67	6
22	5963		51.632680	-4.198121	244957	195069	2		90												70	15	14.00	6
23	5964		51.633211	-4.198400	244925	195091	3	40			20							15			80	8	9.65	7
24	5965		51.633025	-4.200841	244907	195129	3	15			70				5						90	5	5.55	10
25	5966		51.629879	-4.208100	244882	195155	3	10	10	50					5						60	8	5.12	10
26	5967		51.630297	-4.209041	244877	195186	4	10	10	70					5						80	4	6.32	10
27	5968		51.629788	-4.209785	244881	195223	4	10	65	20											60	8	9.79	6
28	5969		51.629348	-4.209535	244859	195288	3	50	20	20											50	8	6.94	10
29	5970		51.629058	-4.210020	244805	195321	5	10	25	30					20						60	8	7.06	10
30	5971		51.628783	-4.210564	244773	195341	2								80						85	50	64.50	18
31	5972		51.628062	-4.210039	244783	195298	3	5	20						60						65	40	40.34	18
32	5973	872	51.626947	-4.209027	244772	195277	3	10	90												60	30	11.70	6
33	5974		51.625710	-4.208421	244746	195261	1								90						95	80	57.00	18
34	5980	884	51.624146	-4.206667	247483	193614	5				75			5		5	5				100	3	4.94	16
35	5981	886	51.615184	-4.169825	247514	193636	3							70	5	5					95	40	67.93	18
36	5982		51.615724	-4.170034	247533	193748	5				75			5		5		5			100	4	5.11	16

Appendices

Location	Photo ID 1	Photo ID 2	Latitude (WGS84)	Longitude (WGS84)	X coordinate (OS)	Y coordinate (OS)	Grazing activity(1=no grazing, 5=overgrazed)	Species (% of total plant cover)													Vegetation cover (dm <sup>2</sup> /m <sup>2</sup> )	Average vegetation height (cm)	Gross vegetation volume(dm <sup>3</sup> /m <sup>2</sup> )	NVC vegetation class (SM__)	
								<i>Salicornia</i> spp.	<i>Spartina anglica</i>	<i>Puccinellia maritima</i>	<i>Festuca rubra</i>	<i>Juncus gerardii</i>	<i>Juncus maritimus</i>	<i>Glaux maritima</i>	<i>Limonium binervosum</i>	<i>Suaeda vera</i>	<i>Plantago maritima</i>	<i>Armeria maritima</i>	<i>Halimione portulacoides</i>	<i>Athrocneum perenne</i>					<i>Althea officinalis</i>
37	5983	895	51.615817	-4.170668	247579	193858	4				65			20			10	5				95	4	6.37	16
38	5984	896	51.616395	-4.171111	247621	193901	4				65											95	4	3.80	16
39	5985	898	51.616963	-4.170824	247612	193992	4				70			5	5		5					100	5	5.18	16
40	5986	900	51.617754	-4.171292	247628	194063	4		10		70			10								85	5	6.04	16
41	5987		51.618630	-4.170521	247649	194104	4				70			20			5	5				100	2	6.65	16
42	5989	910	51.618209	-4.169460	247704	194160	4				70			10				10				95	3	5.49	16
43	5990		51.619267	-4.171579	247677	194269	5				70				10	10						97	5	4.42	16
44	5991		51.619823	-4.172328	247671	194306	3	10		40				10				10		20		70	8	6.14	10
45	5992		51.620228	-4.172975	247662	194335	4			30	1				10		30		15			75	5	5.44	10
46	5995		51.620463	-4.173843	247677	194382	2			10	15				5		10		50			50	3	4.06	7
47	5996	916	51.621531	-4.173645	247664	194427	1	5		80								10				35	5	2.30	10
48	5997		51.622905	-4.173748	247645	194464	1	5		80					5							30	5	1.72	10
49	5998	921	51.623523	-4.173925	247672	194529	1	50							50							5	5	0.58	8
50	5999		51.624131	-4.173971	247661	194570	1	70		10					10							7	5	0.92	8
51	6000		51.625039	-4.174113	247673	194611	2	10	20	60												35	5	3.31	10
52	6001		51.625984	-4.174011	247705	194665	1	15	5	70								3				75	5	5.81	10
53	6003		51.627446	-4.173834	247753	194726	1	40	60													2	10	0.36	8
54	6004		51.628411	-4.173842	247835	194910	1	85	15													9	10	1.42	8
55	6005	930	51.629377	-4.173720	247889	194992	1	90		5												35	8	5.07	8

Appendices

Location	Photo ID 1	Photo ID 2	Latitude (WGS84)	Longitude (WGS84)	X coordinate (OS)	Y coordinate (OS)	Grazing activity(1=no grazing, 5=overgrazed)	Species (% of total plant cover)													Vegetation cover (dm <sup>2</sup> /m <sup>2</sup> )	Average vegetation height (cm)	Gross vegetation volume(dm <sup>3</sup> /m <sup>2</sup> )	NVC vegetation class (SM__)
								<i>Salicornia</i> spp.	<i>Spartina anglica</i>	<i>Puccinellia maritima</i>	<i>Festuca rubra</i>	<i>Juncus gerardii</i>	<i>Juncus maritimus</i>	<i>Glaux maritima</i>	<i>Limonium binervosum</i>	<i>Suaeda vera</i>	<i>Plantago maritima</i>	<i>Armeria maritima</i>	<i>Halimione portulacoides</i>	<i>Athrocnum perenne</i>				
56	6006	932	51.629888	-4.173580	247871	195052	1	60	30	5											40	15	6.42	8
57	6007		51.628216	-4.172852	247702	195036	1		90												15	8	3.00	4
58	6008		51.626602	-4.171852	247189	194702	3			70				10							60	4	3.83	16
59	6009	945	51.625624	-4.171477	247125	194750	2			50	30							5			60	3	2.96	10
60	6010		51.624746	-4.171244	247072	194695	3				40						30				80	2	3.54	16
61	6011		51.624029	-4.171119	247088	194646	3		15		40				5	30	5				85	3	6.17	16
62	6012		51.623058	-4.170999	247053	194615	4	10			70			10	5						75	4	4.97	16
63	6013		51.622323	-4.172411	247015	194585	4	10			70										60	3	3.23	16
64	6014	9563	51.620122	-4.171918	247049	194504	4	10			70				15						85	3	4.92	16
65	6015		51.618930	-4.170551	247115	194378	5	5			70					5	10				95	4	4.86	16
66	6016		51.618457	-4.169620	247153	194239	5	5			70			5		5	10				75	3	4.26	16
67	6017		51.617317	-4.169042	247269	194061	5				70			5		10	5				100	3	5.00	16
68	6022		51.615184	-4.169825	249789	192989	2						80						20		100	60	74.00	18
69	6023	970	51.615724	-4.170034	249776	193049	3				40		30								90	40	32.91	18
70	6024		51.615817	-4.170668	249733	193061	2				30		40						20		100	30	48.00	18
71	6026		51.616395	-4.171111	249704	193126	2						80						10		100	60	76.67	18
72	6030		51.616963	-4.170824	249726	193188	2				5		70						15		100	50	70.78	18
73	6031	977	51.617754	-4.171292	249696	193277	2				70			5		20					100	8	4.84	16
74	6032		51.618630	-4.170521	249752	193373	3				70			5		20					100	5	4.84	16

Appendices

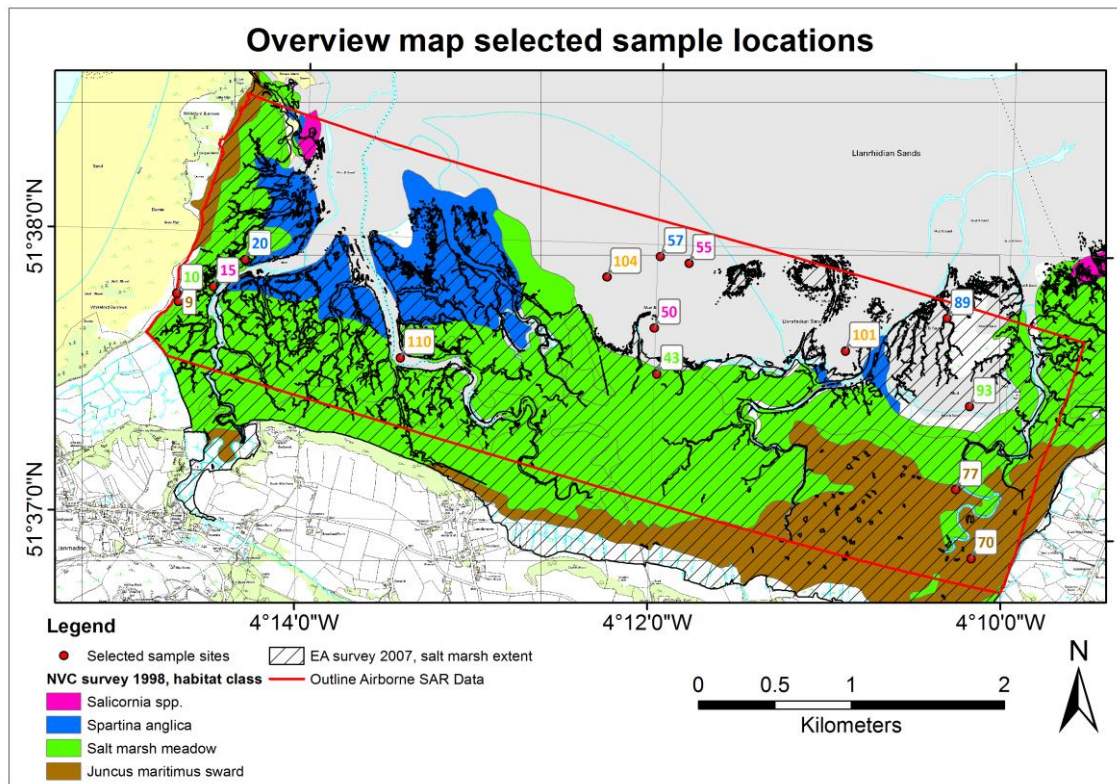
Location	Photo ID 1	Photo ID 2	Latitude (WGS84)	Longitude (WGS84)	X coordinate (OS)	Y coordinate (OS)	Grazing activity(1=no grazing, 5=overgrazed)	Species (% of total plant cover)												Vegetation cover (dm <sup>2</sup> /m <sup>2</sup> )	Average vegetation height (cm)	Gross vegetation volume(dm <sup>3</sup> /m <sup>2</sup> )	NVC vegetation class (SM__)	
								<i>Salicornia</i> spp.	<i>Spartina anglica</i>	<i>Puccinellia maritima</i>	<i>Festuca rubra</i>	<i>Juncus gerardii</i>	<i>Juncus maritimus</i>	<i>Glaux maritima</i>	<i>Limonium binervosum</i>	<i>Suaeda vera</i>	<i>Plantago maritima</i>	<i>Armeria maritima</i>	<i>Halimione portulacoides</i>					<i>Athrocnemum perenne</i>
75	6033		51.618209	-4.169460	249824	193324	3				20		40							40	100	55	52.80	18
76	6034		51.619267	-4.171579	249681	193446	2						90							10	100	70	77.00	18
77	6035		51.619823	-4.172328	249631	193509	2						80							5	100	70	78.24	18
78	6036	982	51.620228	-4.172975	249588	193556	3			30			40								100	5	10.86	16
79	6037		51.620463	-4.173843	249528	193584	2					70	5							15	100	80	71.44	18
80	6038	985	51.621531	-4.173645	249546	193702	4			50			10		5	5	20	10			70	5	5.15	16
81	6039		51.622905	-4.173748	249543	193855	4			50			5		20						95	5	4.43	16
82	6040		51.623523	-4.173925	249533	193924	5			30											100	3	4.00	16
83	6041	988	51.624131	-4.173971	249532	193992	4	10	20	50					5						70	3	6.92	10
84	6042		51.625039	-4.174113	249525	194093	3	30	10	50											90	5	9.00	10
85	6043	994	51.625984	-4.174011	249535	194198	3	20	10	50					20						70	4	6.37	10
86	6044		51.627446	-4.173834	249552	194360	4	30	30	20					10						50	8	6.83	10
87	6045	998	51.628411	-4.173842	249555	194467	4	5	75	20											45	10	7.54	6
88	6046		51.629377	-4.173720	249566	194575	3	5	80	15											30	10	5.25	6
89	6047	1000	51.629888	-4.173580	249578	194631	2	10	85						5						55	15	10.40	6
90	6049	1005	51.628216	-4.172852	249623	194444	3	20		40					40						90	5	7.38	10
91	6050	1006	51.626602	-4.171852	249687	194262	3	30	10	40					5						70	8	7.33	10
92	6051	1007	51.625624	-4.171477	249709	194153	3	20		50					10						90	5	7.09	10
93	6052		51.624746	-4.171244	249722	194055	4	10	30	40					10						50	10	5.72	10

Appendices

Location	Photo ID 1	Photo ID 2	Latitude (WGS84)	Longitude (WGS84)	X coordinate (OS)	Y coordinate (OS)	Grazing activity(1=no grazing, 5=overgrazed)	Species (% of total plant cover)												Vegetation cover (dm <sup>2</sup> /m <sup>2</sup> )	Average vegetation height (cm)	Gross vegetation volume(dm <sup>3</sup> /m <sup>2</sup> )	NVC vegetation class (SM__)	
								<i>Salicornia spp.</i>	<i>Spartina anglica</i>	<i>Puccinellia maritima</i>	<i>Festuca rubra</i>	<i>Juncus gerardii</i>	<i>Juncus maritimus</i>	<i>Glaux maritima</i>	<i>Limonium binervosum</i>	<i>Suaeda vera</i>	<i>Plantago maritima</i>	<i>Armeria maritima</i>	<i>Halimione portulacaoides</i>					<i>Athrocnemum perenne</i>
94	6053		51.624029	-4.171119	249729	193975	4	5		50			5			10	10				80	4	5.35	10
95	6054	1009	51.623058	-4.170999	249734	193866	4			30			40			20	5				95	4	9.30	13
96	6055		51.622323	-4.172411	249634	193788	3	5		30			30			30					85	3	7.65	13
97	6056		51.620122	-4.171918	249661	193542	4				30		10			40	10				100	3	6.22	16
98	6060	1013	51.618930	-4.170551	249751	193407	2				30		60						10		95	60	51.49	18
99	6061		51.618457	-4.169620	249814	193352	3				50		40			10					100	6	8.90	16
100	6062		51.617317	-4.169042	249850	193224	2				20		40	10					30		100	60	49.40	18




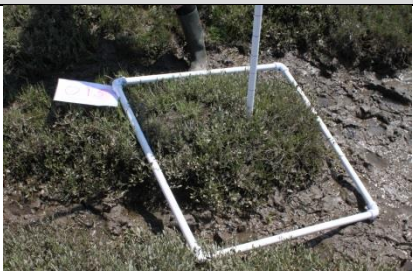




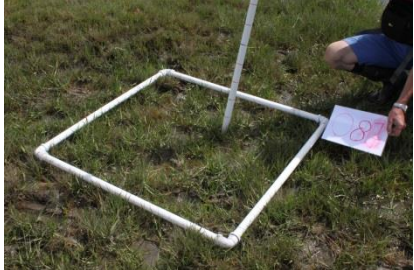


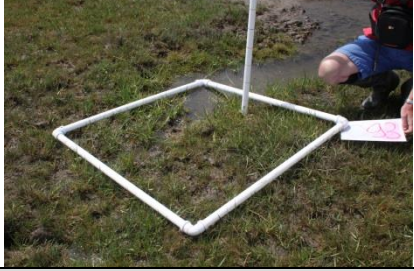



## Appendix B – Pictures from selected sample locations

### Location map



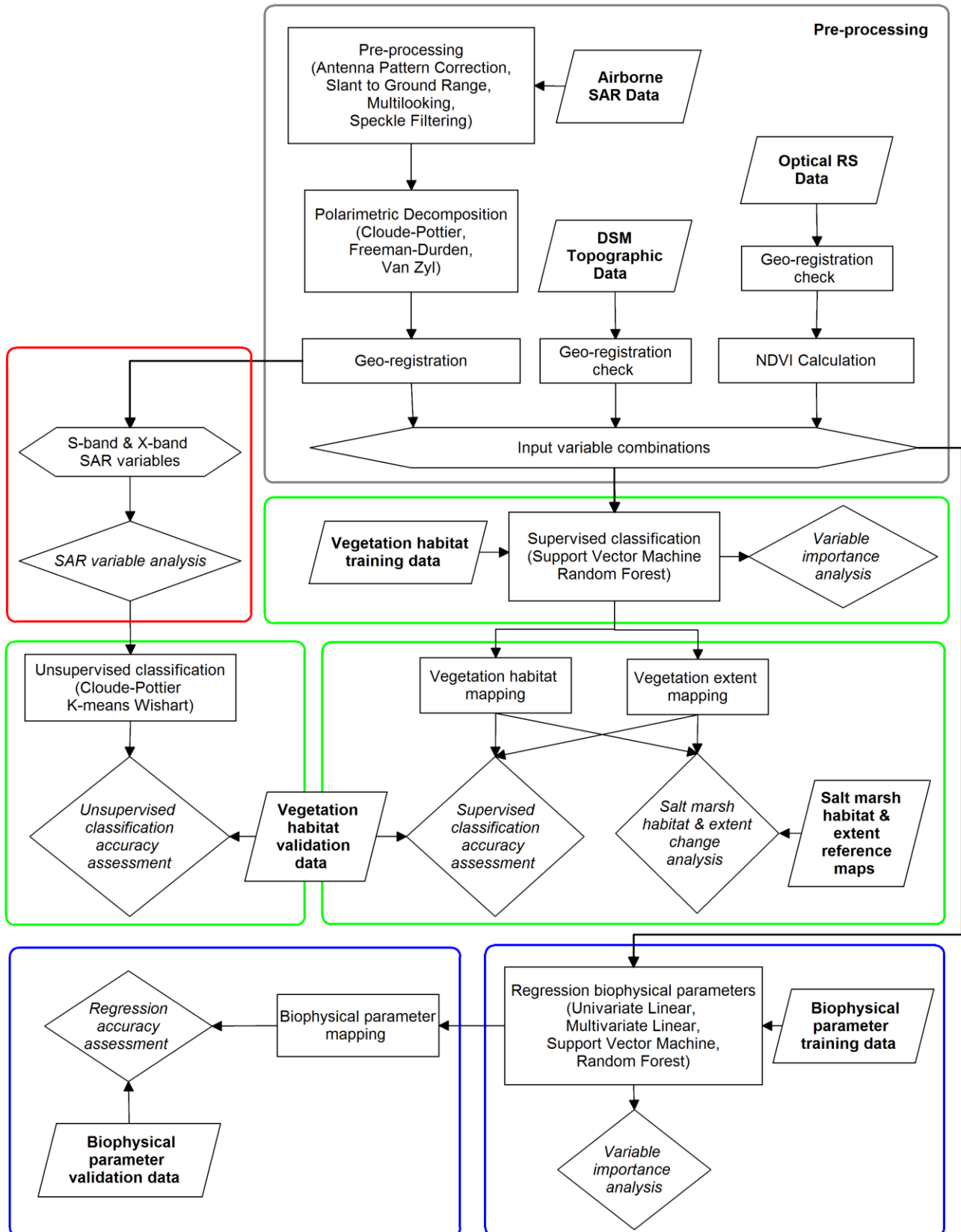


Sample location pictures

Bare sand and mudflats		
Location 110	Location 104	Location 101
		
<i>Salicornia spp.</i>		
Location 15	Location 50	Location 55
		
<i>Spartina anglica</i>		
Location 20	Location 57	Location 89
		
Salt marsh meadow		
Location 10	Location 43	Location 93
		
<i>Juncus maritimus</i>		
Location 9	Location 70	Location 77
		



Appendix C – Flowchart of analysis steps

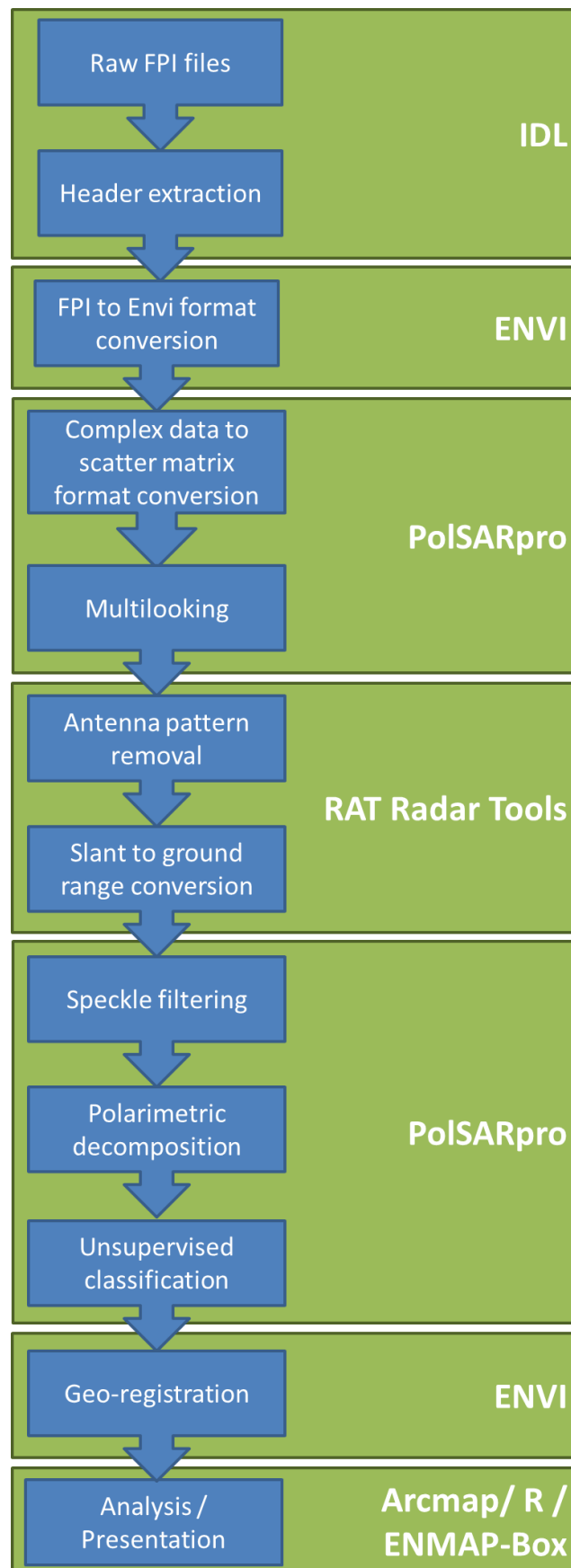


Chapter 5

Chapter 6

Chapter 7

Appendix D – **Flowchart of SAR data pre-processing steps**



## Appendix E – Publications

- van Beijma, S.J., Comber, A., & Lamb, A.** (*in press*). SAR-Based EO of Salt Marsh Habitats in Support of Integrated Coastal Zone Management. In H. Balzter (Ed.), *Earth Observation for Land and Emergency Monitoring; Innovative concepts for*
- van Beijma, S.J., Comber, A., & Lamb, A.** (2014). Random forest classification of salt marsh vegetation habitats using quad-polarimetric airborne SAR, elevation and optical RS data. *Remote Sensing of Environment*, 149, 118-129
- van Beijma, S.J., Comber, A., & Lamb, A.** (2013). Classification and monitoring of salt marsh habitats with multi - polarimetric airborne SAR. In ESA (Ed.), *Living Planet Symposium 2013*. Edinburgh
- van Beijma, S.J., Comber, A., & Lamb, A.** (2013). Classification of Salt Marsh Habitats with Multi-Polarimetric and Multi-Frequency Airborne SAR. In, *6th EARSeL Workshop on Remote Sensing of the Coastal Zone* (p. 7). Matera, Italy
- van Beijma, S.J., Comber, A., Lamb, A., & Brown, S.** (2013). Classification and monitoring of salt marsh habitats with multi-polarimetric and multi-frequency SAR. In, *POLinSAR 2013* (p. 6). ESRIN, ESA, Frascati, Italy
- van Beijma, S.J., Comber, A., & Lamb, A.** (2012). Temporal analysis of optical and SAR remote sensing for monitoring of intertidal salt marshes. In, *1st EARSeL Workshop on Temporal Analysis of Satellite Images*. Mykonos, Greece

## Bibliography

- Adam, E., O. Mutanga and D. Rugege. 2010: Multispectral and hyperspectral remote sensing for identification and mapping of wetland vegetation: a review. *Wetlands Ecology and Management* 18(3), pp. 281-296.
- Adam, P. 1990: *Saltmarsh ecology*. Cambridge: Cambridge University Press.
- Adam, P. 2002: Saltmarshes in a time of change. *Environmental Conservation* 29(1), pp. 39-61.
- Airbus DS. 2015: GeoStore. Date Available from: <http://www.geo-airbusds.com/geostore/>.
- Alber, M., E. M. Swenson, S. C. Adamowicz and I. A. Mendelsohn. 2008: Salt Marsh Dieback: An overview of recent events in the US. *Estuarine, Coastal and Shelf Science* 80(1), pp. 1-11.
- Allen, J. R. L. 1989: Evolution of salt-marsh cliffs in muddy and sandy systems: A qualitative comparison of British West-Coast estuaries. *Earth Surface Processes and Landforms* 14(1), pp. 85-92.
- Attema, E., P. Bargellini, P. Edwards, G. Levrini, S. Lokas, L. Moeller, B. Rosich-Tell, P. Secchi, R. Torres, M. Davidson and P. Snoeij. 2007: Sentinel-1, The Radar Mission for GMES Operational Land and Sea Services. *ESA Bulletin* 131(pp. 11-17).
- Attema, E. P. 1991: The active microwave instrument on-board the ERS-1 satellite. *Proceedings of the IEEE* 79(6), pp. 791-799.
- Axelsson, P. 1999: Processing of laser scanner data—algorithms and applications. *ISPRS Journal of Photogrammetry and Remote Sensing* 54(2), pp. 138-147.
- Axmanová, I., L. Tichý, Z. Fajmonová, P. Hájková, E. Hettenbergerová, C.-F. Li, K. Merunková, M. Nejezchlebová, Z. Otýpková, M. Vymazalová and D. Zelený. 2012: Estimation of herbaceous biomass from species composition and cover. *Applied Vegetation Science* 15(4), pp. 580-589.
- Bakker, J. P. 1985: The impact of grazing on plant communities, plant populations and soil conditions on salt marshes. *Vegetatio* 62(1-3), pp. 391-398.
- Bakker, J. P. 1989: *Nature management by grazing and cutting*. Berlin: Springer.

## Bibliography

- Ballester-Berman, J. D. and J. M. Lopez-Sanchez. 2010: Applying the Freeman–Durden decomposition concept to polarimetric SAR interferometry. *Geoscience and Remote Sensing, IEEE Transactions on* 48(1), pp. 466-479.
- Barrett, E. C. 2013: *Introduction to environmental remote sensing*. Abingdon: Routledge.
- Beaudoin, A., T. Le Toan, S. Goze, E. Nezry, A. Lopes, E. Mougin, C. Hsu, H. Han, J. Kong and R. Shin. 1994: Retrieval of forest biomass from SAR data. *International Journal of Remote Sensing* 15(14), pp. 2777-2796.
- Belluco, E., M. Camuffo, S. Ferrari, L. Modenese, S. Silvestri, A. Marani and M. Marani. 2006: Mapping salt-marsh vegetation by multispectral and hyperspectral remote sensing. *Remote Sensing of Environment* 105(1), pp. 54-67.
- Bird, E. 2008: *Coastal Geomorphology: An Introduction*. Chichester: John Wiley & Sons.
- Blaschke, T. 2010: Object based image analysis for remote sensing. *ISPRS Journal of Photogrammetry and Remote Sensing* 65(1), pp. 2-16.
- Boorman, L. A. 2003: *Saltmarsh Review. An overview of coastal saltmarshes, their dynamic and sensitivity characteristics for conservation and management*. JNCC. p. 114.
- Bos, D., J. P. Bakker, Y. Vries and S. Lieshout. 2002: Long-term vegetation changes in experimentally grazed and ungrazed back-barrier marshes in the Wadden Sea. *Applied Vegetation Science* 5(1), pp. 45-54.
- Breiman, L. 1993: Hinging hyperplanes for regression, classification, and function approximation. *Information Theory, IEEE Transactions on* 39(3), pp. 999-1013.
- Breiman, L. 2001: Random Forests. *Machine Learning* 45(1), pp. 5-32.
- Brisco, B., M. Kapfer, T. Hirose, B. Tedford and J. Liu. 2011: Evaluation of C-band polarization diversity and polarimetry for wetland mapping. *Canadian Journal of Remote Sensing* 37(1), pp. 82-92.
- Carling, P. A. 1981: *Sediment transport by tidal currents and waves: observations from a sandy intertidal zone (Burry Inlet, South Wales)*. Oxford: Blackwell Scientific Publications.
- CCRS. 2008: *Advanced Radar Polarimetry Tutorial*. Canada Centre for Remote Sensing. p. 97.

## Bibliography

- Chi, M., R. Feng and L. Bruzzone. 2008: Classification of hyperspectral remote-sensing data with primal SVM for small-sized training dataset problem. *Advances in space research* 41(11), pp. 1793-1799.
- Choe, B.-H., D.-j. Kim, J.-H. Hwang, Y. Oh and W. M. Moon. 2011: Detection of oyster habitat in tidal flats using multi-frequency polarimetric SAR data. *Estuarine, Coastal and Shelf Science* 0),
- Choe, B.-H., D.-j. Kim, J.-H. Hwang, Y. Oh and W. M. Moon. 2012: Detection of oyster habitat in tidal flats using multi-frequency polarimetric SAR data. *Estuarine, Coastal and Shelf Science* 97(0), pp. 28-37.
- Clint Slatton, K., M. M. Crawford and L.-D. Chang. 2008: Modeling temporal variations in multipolarized radar scattering from intertidal coastal wetlands. *ISPRS Journal of Photogrammetry and Remote Sensing* 63(5), pp. 559-577.
- Cloude, S. R. and E. Pottier. 1997: An entropy based classification scheme for land applications of polarimetric SAR. *Geoscience and Remote Sensing, IEEE Transactions on* 35(1), pp. 68-78.
- Coastwatch. 2010: Coastwatch Water Quality Monitoring Service - GMES Service. Date accessed: 17/11/2011. Available from: <http://www.enviport.org/GMES/services/coastal/index.htm>.
- Collins, S. 2012. EU Policy Developments in Integrated Coastal Zone Management (ICZM) and Maritime Spatial Planning (MSP). Presented at: Coastal Futures 2012, London.
- Congalton, R. G. 1991: A review of assessing the accuracy of classifications of remotely sensed data. *Remote Sensing of Environment* 37(1), pp. 35-46.
- Congalton, R. G. and K. Green. 2008: *Assessing the accuracy of remotely sensed data: principles and practices*. CRC press.
- Corbane, C., S. Lang, K. Pipkins, S. Alleaume, M. Deshayes, V. E. G. Millán, T. Strasser, J. V. Borre, S. Toon and F. Michael. 2015: Remote sensing for mapping natural habitats and their conservation status—New opportunities and challenges. *International Journal of Applied Earth Observation and Geoinformation* 37), pp. 7-16.

## Bibliography

- Costanza, R., R. d'Arge, R. De Groot, S. Farber, M. Grasso, B. Hannon, K. Limburg, S. Naeem, R. V. O'Neill and J. Paruelo. 1997: The value of the world's ecosystem services and natural capital. *Nature* 387(6630), pp. 253-260.
- Countryside Council for Wales. 2005: Carmarthen Bay and Estuaries / Bae Caerfyrddin ac Aberoedd - European Marine Site. Countryside Council for Wales. p. 114.
- Countryside Council for Wales. 2011: Burry Inlet SPA. Date accessed: 04/09/2013. Available from: <http://www.ccg.gov.uk/landscape--wildlife/protecting-our-landscape/special-sites-project/burry-inlet-spa.aspx>.
- Countryside Council for Wales. 2015: Burry Inlet SPA. Date accessed: 02/04/2015. Available from: <http://www.ccg.gov.uk/landscape--wildlife/protecting-our-landscape/special-sites-project/burry-inlet-spa.aspx>.
- Cutler, D. R., T. C. Edwards Jr, K. H. Beard, A. Cutler, K. T. Hess, J. Gibson and J. J. Lawler. 2007: Random forests for classification in ecology. *Ecology* 88(11), pp. 2783-2792.
- Dabrowska-Zielinska, K., M. Gruszczynska, S. Lewinski, A. Hoscilo and J. Bojanowski. 2009: Application of remote and in situ information to the management of wetlands in Poland. *Journal of Environmental Management* 90(7), pp. 2261-2269.
- Davranche, A., G. Lefebvre and B. Poulin. 2010: Wetland monitoring using classification trees and SPOT-5 seasonal time series. *Remote Sensing of Environment* 114(3), pp. 552-562.
- DEFRA. 2006: Shoreline management plan guidance. Volume 1: Aims and requirements. Department for Environment, Food and Rural Affairs. p. 48.
- Dehouck, A., V. Lafon, N. Baghdadi and V. Marieu. 2012. Use of optical and radar data in synergy for mapping intertidal flats and coastal salt-marshes (Arcachon Lagoon, France). Presented at: Geoscience and Remote Sensing Symposium (IGARSS), 2012 IEEE International, IEEE.
- Dehouck, A., V. Lafon, N. Baghdadi, A. Roubache and T. Rabaute. 2011. Potential of TerraSAR-X imagery for mapping intertidal coastal wetlands. Presented at: 4. TSX Science Team Meeting, Wessling. DLR.

## Bibliography

- Dickinson, C., P. Siqueira, D. Clewley and R. Lucas. 2013: Classification of forest composition using polarimetric decomposition in multiple landscapes. *Remote Sensing of Environment* 131(0), pp. 206-214.
- Doody, P., M. Ferreira, S. Lombardo, I. Lucius, R. Misdorp, H. Niesing, A. Salman and M. Smallegange. 2004: Living with coastal erosion in Europe; Sediment and space for sustainability. Results from the EUROSION study. European Communities. p. 38.
- Dubois, P. C., J. Van Zyl and T. Engman. 1995: Measuring soil moisture with imaging radars. *Geoscience and Remote Sensing, IEEE Transactions on* 33(4), pp. 915-926.
- Earth Observation Center (EOC) DLR. 2014: EnMAP-Box. Date accessed: 14/01/2014. Available from: <http://www.enmap.org/?q=enmapbox>.
- EC. 2011: Integrated Coastal Zone Management, Information and Technology in ICZM, practices around Europe. European Commission. p. 35.
- Ecoshape. 2011: Building with Nature. Date accessed: 21/12/2011. Available from: <http://www.ecoshape.nl/>.
- EEA. 2006: The changing faces of Europe's coastal areas. European Environmental Agency. p. 107.
- Englhart, S., J. Franke, V. Keuck and F. Siegert. 2012. Aboveground biomass estimation of tropical peat swamp forests using SAR and optical data. Presented at: Geoscience and Remote Sensing Symposium (IGARSS), 2012 IEEE International, IEEE.
- Englhart, S., J. Jubanski and F. Siegert. 2013: Quantifying Dynamics in Tropical Peat Swamp Forest Biomass with Multi-Temporal LiDAR Datasets. *Remote Sensing* 5(5), pp. 2368-2388.
- Englhart, S., V. Keuck and F. Siegert. 2011: Aboveground biomass retrieval in tropical forests — The potential of combined X- and L-band SAR data use. *Remote Sensing of Environment* 115(5), pp. 1260-1271.
- Environment Agency. 2011: The extent of saltmarsh in England and Wales: 2006-2009. Environment Agency. p. 57.



## Bibliography

- Environment Agency. 2011: Shoreline Management Plans (SMPs). Date accessed: 22/12/2011. Available from: <http://www.environment-agency.gov.uk/research/planning/104939.aspx>.
- Environment Agency and Natural England. 2011: Operational Use of Remote Sensing for Environmental Monitoring. p. 88.
- ESA. 2013: PolSARpro - The Polarimetric SAR Data Processing and Educational Tool. Date accessed: 12/02/2013. Available from: <http://earth.eo.esa.int/polsarpro/>.
- European Commission. 1992: Council Directive 92/43/EEC of 21 May 1992 on the conservation of natural habitats and of wild fauna and flora. Date accessed: 09/07/2012. Available from: <http://eur-lex.europa.eu/LexUriServ/LexUriServ.do?uri=CELEX:31992L0043:EN:HTML>.
- FAO. 2003: Status and trends in mangrove area extent worldwide. Food and Agricultural Organisation. p.
- FAO. 2007: The World's mangroves, 1980-2005. Food and Agricultural Organisation. p. 77.
- Farleigh, M. R. 2010: Morphographical Analysis of the Burry Inlet Salt Marshes. BSc thesis. University of Glamorgan.
- Fatoyinbo, T. E. and M. Simard. 2012: Height and biomass of mangroves in Africa from ICESat/GLAS and SRTM. International Journal of Remote Sensing 34(2), pp. 668-681.
- Ferro-Famil, L., E. Pottier and J.-S. Lee. 2001: Unsupervised classification of multifrequency and fully polarimetric SAR images based on the H/A/Alpha-Wishart classifier. Geoscience and Remote Sensing, IEEE Transactions on 39(11), pp. 2332-2342.
- Foresight. 2011: Migration and Global Environmental Change. The Government Office for Science. p. 237.
- Freeman, A. 1992: SAR calibration: An overview. Geoscience and Remote Sensing, IEEE Transactions on 30(6), pp. 1107-1121.
- Freeman, A. and S. L. Durden. 1998: A three-component scattering model for polarimetric SAR data. Geoscience and Remote Sensing, IEEE Transactions on 36(3), pp. 963-973.

## Bibliography

- Frost, V. S., J. A. Stiles, K. S. Shanmugan and J. Holtzman. 1982: A model for radar images and its application to adaptive digital filtering of multiplicative noise. *Pattern Analysis and Machine Intelligence, IEEE Transactions on 2*), pp. 157-166.
- Gade, M., W. Alpers, C. Melsheimer and G. Tanck. 2008: Classification of sediments on exposed tidal flats in the German Bight using multi-frequency radar data. *Remote Sensing of Environment 112*(4), pp. 1603-1613.
- Gade, M., S. Melchionna, K. Stelzer and J. Kohlus. 2014: Multi-frequency SAR data help improving the monitoring of intertidal flats on the German North Sea coast. *Estuarine, Coastal and Shelf Science 140*(0), pp. 32-42.
- Gade, M., K. Stelzer and J. Kohlus. 2011. On the Use of Multi-Frequency SAR Imagery for a Surveillance of the Wadden Sea Ecosystem on the German North Sea Coast. Presented at: 4. TSX Science Team Meeting, Wessling. DLR.
- Garbutt, A. and M. Wolters. 2008: The natural regeneration of salt marsh on formerly reclaimed land. *Applied Vegetation Science 11*(3), pp. 335-344.
- Garbutt, R. A., C. J. Reading, M. Wolters, A. J. Gray and P. Rothery. 2006: Monitoring the development of intertidal habitats on former agricultural land after the managed realignment of coastal defences at Tollesbury, Essex, UK. *Marine Pollution Bulletin 53*(1-4), pp. 155-164.
- Gens, R. 2010: Remote sensing of coastlines: detection, extraction and monitoring. *International Journal of Remote Sensing 31*(7), pp. 1819-1836.
- Genuer, R., J.-M. Poggi and C. Tuleau-Malot. 2010: Variable selection using random forests. *Pattern Recognition Letters 31*(14), pp. 2225-2236.
- Gilmore, M. S., E. H. Wilson, N. Barrett, D. L. Civco, S. Prisloe, J. D. Hurd and C. Chadwick. 2008: Integrating multi-temporal spectral and structural information to map wetland vegetation in a lower Connecticut River tidal marsh. *Remote Sensing of Environment 112*(11), pp. 4048-4060.
- Giri, C., E. Ochieng, L. L. Tieszen, Z. Zhu, A. Singh, T. Loveland, J. Masek and N. Duke. 2011: Status and distribution of mangrove forests of the world using earth observation satellite data. *Global Ecology and Biogeography 20*(1), pp. 154-159.
- Gislason, P. O., J. A. Benediktsson and J. R. Sveinsson. 2006: Random Forests for land cover classification. *Pattern Recognition Letters 27*(4), pp. 294-300.

## Bibliography

- GMES. 2011: Global Monitoring for Environment and Security. Date accessed: 07/10/2011. Available from: <http://www.gmes.info/>.
- Guida, R., A. Iodice and D. Riccio. 2010: Height retrieval of isolated buildings from single high-resolution SAR images. *Geoscience and Remote Sensing, IEEE Transactions on* 48(7), pp. 2967-2979.
- Guida, R., A. Natale, R. Bird, P. Whittaker, M. Cohen and D. Hall. 2012. Canopy classification with S-band polarimetric SAR data. Presented at: Geoscience and Remote Sensing Symposium (IGARSS), 2012 IEEE International,
- Habitats Directive. 1992: Council Directive 92/43/EEC of 21 May 1992 on the conservation of natural habitats and of wild fauna and flora. Brussels, Belgium
- Hahmann, T., S. Martinis, A. Twele, A. Roth and M. Buchroithner. 2008. Extraction of water and flood areas from SAR data. Presented at: 7th European Conference on Synthetic Aperture Radar (EUSAR), 2008
- Hajnsek, I., R. Bianchi, M. Davidson, G. D'Urso, J. Gomez-Sanchez, A. Hausold, R. Horn, J. Howse, A. Loew and J. Lopez-Sanchez. 2006. AgriSAR 2006 - Airborne SAR and optics campaigns for an improved monitoring of agricultural processes and practices. Presented at: EGU, Vienna. Geophysical Research Abstracts.
- Hall, D. L. and S. A. McMullen. 2004: *Mathematical techniques in multisensor data fusion*. Boston: Artech House.
- Haslett, S. K. 2003: *Coastal Systems*. Abingdon: Routledge.
- Henderson, F. M. and A. J. Lewis. 2008: Radar detection of wetland ecosystems: a review. *International Journal of Remote Sensing* 29(20), pp. 5809-5835.
- Hensley, S., C. Jones and Y. Lou. 2012. Prospects for operational use of airborne polarimetric SAR for disaster response and management. Presented at: Geoscience and Remote Sensing Symposium (IGARSS), 2012 IEEE International, IEEE.
- Heumann, B. W. 2011: Satellite remote sensing of mangrove forests: Recent advances and future opportunities. *Progress in Physical Geography* 35(1), pp. 87-108.
- Hladik, C. and M. Alber. 2014: Classification of salt marsh vegetation using edaphic and remote sensing-derived variables. *Estuarine, Coastal and Shelf Science* 141(0), pp. 47-57.

## Bibliography

- Hong, S.-H., S. Wdowinski and S.-W. Kim. 2010: Evaluation of TerraSAR-X Observations for Wetland InSAR Application. *Geoscience and Remote Sensing, IEEE Transactions on* 48(2), pp. 864-873.
- Huang, C., L. Davis and J. Townshend. 2002: An assessment of support vector machines for land cover classification. *International Journal of Remote Sensing* 23(4), pp. 725-749.
- Huang, C. and J. Townshend. 2003: A stepwise regression tree for nonlinear approximation: applications to estimating subpixel land cover. *International Journal of Remote Sensing* 24(1), pp. 75-90.
- Huang, L., Z. Li, B.-S. Tian, Q. Chen, J.-L. Liu and R. Zhang. 2011: Classification and snow line detection for glacial areas using the polarimetric SAR image. *Remote Sensing of Environment* 115(7), pp. 1721-1732.
- Hubbard, J. C. E. and R. E. Stebbings. 1967. Distribution, dates of origin, and acreage of *Spartina townsendii* (s.l.) marshes in Great Britain. Presented at: Proceedings of the Botanical Society of the British Isles, London.
- Iervolino, P., R. Guida and P. Whittaker. 2013. NovaSAR-S and Maritime Surveillance. Presented at: IGARSS Proceedings,
- JAXA. 2012: Advanced Land Observing Satellite-2 'Daichi-2' (ALOS-2). Date Available from: [http://www.jaxa.jp/projects/sat/alos2/index\\_e.html](http://www.jaxa.jp/projects/sat/alos2/index_e.html).
- JNCC. 2004: Common Standards Monitoring Guidance for Saltmarsh Habitats. Joint Nature Conservation Committee,. p. 22.
- JNCC. 2006: Annex 1 Classification schemes. Joint Nature Conservation Committee,. p.
- JNCC 2011: Making Earth Observation work for UK biodiversity. Date accessed: 22/12/2011. Available from: <http://jncc.defra.gov.uk/page-5563>.
- JNCC. 2015: UK Habitat Classifications. Date accessed: 06/04/2015. Available from: <http://jncc.defra.gov.uk/page-1425>.
- Kamthonkiat, D., C. Rodfai, A. Saiwanrungskul, S. Koshimura and M. Matsuoka. 2011: Geoinformatics in mangrove monitoring: damage and recovery after the 2004 Indian Ocean tsunami in Phang Nga, Thailand. *Nat. Hazards Earth Syst. Sci.* 11(7), pp. 1851-1862.

## Bibliography

- Kasischke, E. S. and L. L. Bourgeau-Chavez. 1997: Monitoring South Florida Wetlands Using ERS-1 SAR Imagery. *Photogrammetric Engineering & Remote Sensing* 63(3), pp. 281-291.
- Kasischke, E. S., K. B. Smith, L. L. Bourgeau-Chavez, E. A. Romanowicz, S. Brunzell and C. J. Richardson. 2003: Effects of seasonal hydrologic patterns in south Florida wetlands on radar backscatter measured from ERS-2 SAR imagery. *Remote Sensing of Environment* 88(4), pp. 423-441.
- Katsanevakis, S., V. Stelzenmüller, A. South, T. K. Sørensen, P. J. S. Jones, S. Kerr, F. Badalamenti, C. Anagnostou, P. Breen, G. Chust, G. D'Anna, M. Duijn, T. Filatova, F. Fiorentino, H. Hulsman, K. Johnson, A. P. Karageorgis, I. Kröncke, S. Mirto, C. Pipitone, S. Portelli, W. Qiu, H. Reiss, D. Sakellariou, M. Salomidi, L. van Hoof, V. Vassilopoulou, T. Vega Fernández, S. Vöge, A. Weber, A. Zenetos and R. t. Hofstede. 2011: Ecosystem-based marine spatial management: Review of concepts, policies, tools, and critical issues. *Ocean & Coastal Management* 54(11), pp. 807-820.
- Klemas, V. 2011: Remote sensing of wetlands: case studies comparing practical techniques. *Journal of Coastal Research* 27(3), pp. 418+.
- Koch, B. 2010: Status and future of laser scanning, synthetic aperture radar and hyperspectral remote sensing data for forest biomass assessment. *ISPRS Journal of Photogrammetry and Remote Sensing* 65(6), pp. 581-590.
- Kuenzer, C., S. van Beijma, U. Gessner and S. Dech. 2014: Land surface dynamics and environmental challenges of the Niger Delta, Africa: Remote sensing-based analyses spanning three decades (1986–2013). *Applied Geography* 53(0), pp. 354-368.
- Lardeux, C., P.-L. Frison, C. Tison, J.-C. Souyris, B. Stoll, B. Fruneau and J.-P. Rudant. 2009: Support vector machine for multifrequency SAR polarimetric data classification. *Geoscience and Remote Sensing, IEEE Transactions on* 47(12), pp. 4143-4152.
- Le Toan, T., A. Beaudoin, J. Riom and D. Guyon. 1992: Relating forest biomass to SAR data. *Geoscience and Remote Sensing, IEEE Transactions on* 30(2), pp. 403-411.
- Lee, H., H. Chae and S.-J. Cho. 2011: Radar Backscattering of Intertidal Mudflats Observed by Radarsat-1 SAR Images and Ground-Based Scatterometer

## Bibliography

- Experiments. *Geoscience and Remote Sensing, IEEE Transactions on* 49(5), pp. 1701-1711.
- Lee, J.-S. and T. L. Ainsworth. 2010. An overview of recent advances in Polarimetric SAR information extraction: Algorithms and applications. Presented at: IEEE International Geoscience and Remote Sensing Symposium (IGARSS), Honolulu.
- Lee, J.-S., W.-M. Boerner, D. L. Schuler, T. L. Ainsworth, I. Hajnsek, K. P. Papathanassiou and E. Lüneburg. 2004: A review of polarimetric SAR algorithms and their applications. *Journal of Photogrammetry and Remote Sensing* 9(3), pp. 31-80.
- Lee, J.-S., M. R. Grunes, T. L. Ainsworth, D. Li-jen, D. L. Schuler and S. R. Cloude. 1999: Unsupervised classification using polarimetric decomposition and the complex Wishart classifier. *Geoscience and Remote Sensing, IEEE Transactions on* 37(5), pp. 2249-2258.
- Lee, J.-S. and E. Pottier. 2009: *Polarimetric radar imaging: from basics to applications*. CRC press.
- Lee, J.-S., J.-H. Wen, T. L. Ainsworth, K.-S. Chen and A. J. Chen. 2009: Improved sigma filter for speckle filtering of SAR imagery. *Geoscience and Remote Sensing, IEEE Transactions on* 47(1), pp. 202-213.
- Lee, M. 2001: Coastal defence and the Habitats Directive: predictions of habitat change in England and Wales. *The Geographical Journal* 167(1), pp. 39-56.
- Lee, Y.-K., J.-W. Park, J.-K. Choi, Y. Oh and J.-S. Won. 2012: Potential uses of TerraSAR-X for mapping herbaceous halophytes over salt marsh and tidal flats. *Estuarine, Coastal and Shelf Science* 115(0), pp. 366-376.
- Li, K., B. Brisco, S. Yun and R. Touzi. 2012: Polarimetric decomposition with RADARSAT-2 for rice mapping and monitoring. *Canadian Journal of Remote Sensing* 38(02), pp. 169-179.
- Lillesand, T. M., R. W. Kiefer and J. W. Chipman. 2004: *Remote sensing and image interpretation*. John Wiley & Sons Ltd.
- Lönnqvist, A., Y. Rauste, M. Molinier and T. Hame. 2010: Polarimetric SAR Data in Land Cover Mapping in Boreal Zone. *Geoscience and Remote Sensing, IEEE Transactions on* 48(10), pp. 3652-3662.
- Lu, D., P. Mausel, E. Brondízio and E. Moran. 2004: Change detection techniques. *International Journal of Remote Sensing* 25(12), pp. 2365-2401.

## Bibliography

- Lucas, R., K. Medcalf, A. Brown, P. Bunting, J. Breyer, D. Clewley, S. Keyworth and P. Blackmore. 2011: Updating the Phase 1 habitat map of Wales, UK, using satellite sensor data. *ISPRS Journal of Photogrammetry and Remote Sensing* 66(1), pp. 81-102.
- Lucas, R. M., Carreiras, J., Proisy, C., Bunting, P. 2008. ALOS PALSAR applications in the tropics and subtropics: characterisation, mapping and detecting change in forests and coastal wetlands. Presented at: JAXA ALOS PI Conference, Tokyo.
- Lucas, R. M., A. L. Mitchell, A. Rosenqvist, C. Proisy, A. Melius and C. Ticehurst. 2007: The potential of L-band SAR for quantifying mangrove characteristics and change: case studies from the tropics. *Aquatic Conservation: Marine and Freshwater Ecosystems* 17(3), pp. 245-264.
- Maghsoudi, Y., M. J. Collins and D. G. Leckie. 2013: Radarsat-2 Polarimetric SAR Data for Boreal Forest Classification Using SVM and a Wrapper Feature Selector. *Selected Topics in Applied Earth Observations and Remote Sensing, IEEE Journal of* 6(3), pp. 1531-1538.
- Mason, D. C., T. R. Scott and S. L. Dance. 2010: Remote sensing of intertidal morphological change in Morecambe Bay, U.K., between 1991 and 2007. *Estuarine, Coastal and Shelf Science* 87(3), pp. 487-496.
- Mason, D. C., T. R. Scott and H.-J. Wang. 2006: Extraction of tidal channel networks from airborne scanning laser altimetry. *ISPRS Journal of Photogrammetry and Remote Sensing* 61(2), pp. 67-83.
- May, V. J. 2007: Carmarthen Bay. In (ed.), *Geological Conservation Review*. Peterborough: JNCC. pp. 15.
- McGranahan, G., D. Balk and B. Anderson. 2007: The rising tide: assessing the risks of climate change and human settlements in low elevation coastal zones. *Environment and Urbanization* 19(1), pp. 17-37.
- Medcalf, K. A., J. A. Parker, N. Turton and C. Finch. 2011: Making Earth Observation Work for UK. Biodiversity Conservation – Phase 1. Report to the JNCC and Defra. Environment Systems. p. 83.
- Melgani, F. and L. Bruzzone. 2004: Classification of hyperspectral remote sensing images with support vector machines. *Geoscience and Remote Sensing, IEEE Transactions on* 42(8), pp. 1778-1790.

## Bibliography

- Millin-Chalabi, G., J. Schumm, B. Gupta, Y. Tun, J. Kandeh and K. Kitmitto. 2011. The landmap service: reaching new horizons in data management and e-learning. Presented at: RSPSoc Annual Conference,
- Moffett, K. B., D. A. Robinson and S. M. Gorelick. 2010: Relationship of salt marsh vegetation zonation to spatial patterns in soil moisture, salinity, and topography. *Ecosystems* 13(8), pp. 1287-1302.
- Möller, I. 2006: Quantifying saltmarsh vegetation and its effect on wave height dissipation: Results from a UK East coast saltmarsh. *Estuarine, Coastal and Shelf Science* 69(3-4), pp. 337-351.
- Moon, W. M., G. Staples, K. Duk-jin, P. Sang-Eun and P. Kyung-Ae. 2010: RADARSAT-2 and Coastal Applications: Surface Wind, Waterline, and Intertidal Flat Roughness. *Proceedings of the IEEE* 98(5), pp. 800-815.
- Moser, G. and S. B. Serpico. 2009: Automatic parameter optimization for support vector regression for land and sea surface temperature estimation from remote sensing data. *Geoscience and Remote Sensing, IEEE Transactions on* 47(3), pp. 909-921.
- Mountrakis, G., J. Im and C. Ogole. 2011: Support vector machines in remote sensing: A review. *ISPRS Journal of Photogrammetry and Remote Sensing* 66(3), pp. 247-259.
- Mumby, P., E. Green, A. Edwards and C. Clark. 1999: The cost-effectiveness of remote sensing for tropical coastal resources assessment and management. *Journal of Environmental Management* 55(3), pp. 157-166.
- myOcean. 2011: Ocean Monitoring and Forecasting. Date accessed: 07/10/2011. Available from: <http://www.myocean.eu.org/>.
- Nagendra, H. 2011: Report on criteria for selection of suitable EO datasets and identification of EO datasets with adequate range of spectral, spatial and temporal resolutions for each site. *BIO\_SOS*. p. 52.
- Nagendra, H., R. Lucas, J. P. Honrado, R. H. G. Jongman, C. Tarantino, M. Adamo and P. Mairota. 2013: Remote sensing for conservation monitoring: Assessing protected areas, habitat extent, habitat condition, species diversity, and threats. *Ecological Indicators* 33(0), pp. 45-59.



## Bibliography

- Natale, A., R. Bird, P. Whittaker, R. Guida, M. Cohen and D. Hall. 2011. Demonstration and analysis of the applications of S-band SAR. Presented at: 3rd International Asia-Pacific Conference on Synthetic Aperture Radar (APSAR), Seoul. IEEE.
- NERC. 2014: Airborne Research & Survey Facility. Date accessed: 07/05/2014. Available from: <http://arsf.nerc.ac.uk/>.
- Nicholls, R. J., P. P. Wong, V. R. Burkett, J. O. Codignotto, J. E. Hay, R. F. McLean, S. Ragoonaden and C. D. Woodroffe. 2007: Coastal systems and low-lying areas. In M.L. Parry, O. F. Canziani, J. P. Palutikof, P. J. van der Linden and C. E. Hanson (ed.), *Climate Change 2007: Impacts, Adaptation and Vulnerability. Contribution of Working Group II to the Fourth Assessment Report of the Intergovernmental Panel on Climate Change*. Cambridge, UK: Cambridge University Press. pp. 315-356.
- NTSLF. 2012: National Tidal and Sea Level Facility. Date accessed: 05/05/2014. Available from: <http://www.ntsfl.org/>.
- Oliver, C. and S. Quegan. 2004: *Understanding synthetic aperture radar images*. Raleigh, NC: SciTech Publishing.
- OURCOAST. 2011: OURCOAST, ICZM in Europe. Date accessed: 17/11/2011. Available from: <http://ec.europa.eu/ourcoast/index.cfm>.
- Pal, M. 2003. Random forests for land cover classification. Presented at: IEEE International Geoscience and Remote Sensing Symposium (IGARSS '03), IEEE.
- Pal, M. and G. M. Foody. 2010: Feature Selection for Classification of Hyperspectral Data by SVM. *Geoscience and Remote Sensing, IEEE Transactions on* 48(5), pp. 2297-2307.
- Patel, P., H. S. Srivastava, S. Panigrahy and J. S. Parihar. 2006: Comparative evaluation of the sensitivity of multi-polarized multi-frequency SAR backscatter to plant density. *International Journal of Remote Sensing* 27(2), pp. 293-305.
- Pembrokeshire Council. 2011: MANAGEMENT UNIT No. 6/7 Llanrhidian Marsh to Whitford Point. Shoreline Management Partnership. p. 7.
- Pendleton, L., D. C. Donato, B. C. Murray, S. Crooks, W. A. Jenkins, S. Sifleet, C. Craft, J. W. Fourqurean, J. B. Kauffman and N. Marbà. 2012: Estimating global “blue carbon” emissions from conversion and degradation of vegetated coastal ecosystems. *PloS one* 7(9), pp. 1-7.

## Bibliography

- Pohl, C. and J. Van Genderen. 1998: Review article multisensor image fusion in remote sensing: concepts, methods and applications. *International Journal of Remote Sensing* 19(5), pp. 823-854.
- Pradhan, C. 2007: Development of 'Marine' Earth Observation Requirements as Input to the Defra Earth Observation Strategy". LogicaCMG. p. 110.
- Prosser, M. V. and H. L. Wallace. 1999: Burry Inlet and Loughor Estuary SSSI, NVC Survey 1998. Countryside Council for Wales. p. 83.
- Pye, K. and P. W. French. 1993: Erosion and Accretion Processes on British Saltmarshes: Volume IV: Modelling of Saltmarsh and Mudflat Processes. Cambridge Environmental Research Consultants. p.
- Reed, B. C., M. D. Schwartz and X. Xiao. 2009: Remote sensing phenology. In A. Noormets (ed.), *Phenology of ecosystem processes*. New York: Springer. pp. 231-246.
- Reigber, A. and O. Hellwich. 2010: RAT (Radar Tools): A free SAR image analysis software package. Date Available from: [https://www.cv.tu-berlin.de/fileadmin/fg140/RAT\\_Radar\\_Tools .pdf](https://www.cv.tu-berlin.de/fileadmin/fg140/RAT_Radar_Tools.pdf).
- Reigber, A., M. Jäger, M. Neumann and L. Ferro-Famil. 2010: Classifying polarimetric SAR data by combining expectation methods with spatial context. *International Journal of Remote Sensing* 31(3), pp. 727-744.
- Reigber, A., R. Scheiber, M. Jager, P. Prats-Iraola, I. Hajnsek, T. Jagdhuber, K. P. Papathanassiou, M. Nannini, E. Aguilera, S. Baumgartner, R. Horn, A. Nottensteiner and A. Moreira. 2013: Very-High-Resolution Airborne Synthetic Aperture Radar Imaging: Signal Processing and Applications. *Proceedings of the IEEE* 101(3), pp. 759-783.
- Rencher, A. C. and F. C. Pun. 1980: Inflation of R<sup>2</sup> in best subset regression. *Technometrics* 22(1), pp. 49-53.
- Richards, J. A. 2009: *Remote Sensing with Imaging Radar*. Heidelberg: Springer-Verlag.
- Robinson, P. (2012). RS applications for ICZM, personal communication. JNCC.
- Rodriguez-Galiano, V. F., B. Ghimire, J. Rogan, M. Chica-Olmo and J. P. Rigol-Sanchez. 2012: An assessment of the effectiveness of a random forest classifier for land-cover classification. *ISPRS Journal of Photogrammetry and Remote Sensing* 67(0), pp. 93-104.

## Bibliography

- Rodwell, J. S. 2000: Salt-marsh communities. In J. S. Rodwell (ed.), British plant communities. Volume 5: Maritime communities and vegetation of open habitats. Cambridge: Cambridge University Press. pp. 15-112.
- Schmitt, A., B. Brisco, S. Kaya and K. Murnaghan. 2010: Polarimetric Change Detection for Wetlands.
- Schmullius, C. C. and D. L. Evans. 1997: Review article Synthetic aperture radar (SAR) frequency and polarization requirements for applications in ecology, geology, hydrology, and oceanography: A tabular status quo after SIR-C/X-SAR. *International Journal of Remote Sensing* 18(13), pp. 2713-2722.
- Shu, Y., J. Li and G. Gomes. 2010: Shoreline Extraction from RADARSAT-2 Intensity Imagery Using a Narrow Band Level Set Segmentation Approach. *Marine Geodesy* 33(2-3), pp. 187-203.
- Silvestri, S. and M. Marani. 2004: Salt-marsh vegetation and morphology: Basic physiology, modelling and remote sensing observations. In S. Fagherazzi, M. Marani and L. K. Blum (ed.), *The Ecogeomorphology of Tidal Marshes*. Washington, DC: American Geophysical Union. pp. 5-25.
- Singh, A. 1989: Review article digital change detection techniques using remotely-sensed data. *International Journal of Remote Sensing* 10(6), pp. 989-1003.
- Souza-Filho, P. W. M. and W. R. Paradella. 2003: Use of synthetic aperture radar for recognition of Coastal Geomorphological Features, land-use assessment and shoreline changes in Bragança coast, Pará, Northern Brazil. *Anais da Academia Brasileira de Ciências* 75(pp. 341-356.
- Stevens, S. 2009: Monitoring of Intertidal Vegetation by Remote Sensing. Date accessed: 16/12/2011. Available from: [http://www.ceh.ac.uk/sci\\_programmes/water/documents/5 Stevens Satellite imagery saltmarsh.pdf](http://www.ceh.ac.uk/sci_programmes/water/documents/5_Stevens_Satellite_imagery_saltmarsh.pdf).
- subCoast. 2011: subCoast - Assesing and Monitoring Subsidence Hazards in Coastal Lowland around Europe. Date accessed: 29/11/2011. Available from: <http://www.subcoast.eu/>.
- Suchar, V. A. and N. L. Crookston. 2010: Understory cover and biomass indices predictions for forest ecosystems of the Northwestern United States. *Ecological Indicators* 10(3), pp. 602-609.

## Bibliography

- Taghvakish, S. 2012: Refined Freeman-Durden for Harvest Detection using PolSAR data. PhD thesis. University of Calgary.
- Tan, C.-P., J.-Y. Koay, K.-S. Lim, H.-T. Ewe and H.-T. Chuah. 2007: Classification of multi-temporal SAR images for rice crops using combined entropy decomposition and support vector machine technique. *Progress In Electromagnetics Research* 71(pp. 19-39.
- Thomson, A. G., R. M. Fuller, M. G. Yates, S. L. Brown, R. Cox and R. A. Wadsworth. 2003: The use of airborne remote sensing for extensive mapping of intertidal sediments and saltmarshes in eastern England. *International Journal of Remote Sensing* 24(13), pp. 2717-2737.
- Touzi, R., W. M. Boerner, J. S. Lee and E. Lueneburg. 2004: A review of polarimetry in the context of Synthetic Aperture Radar: concepts and information extraction. *Canadian Journal of Remote Sensing* 30(3), pp. 380-407.
- Tuxen, K., L. Schile, D. Stralberg, S. Siegel, T. Parker, M. Vasey, J. Callaway and M. Kelly. 2011: Mapping changes in tidal wetland vegetation composition and pattern across a salinity gradient using high spatial resolution imagery. *Wetlands Ecology and Management* 19(2), pp. 141-157.
- Ungar, I. A. and S. R. J. Woodell. 1996: Similarity of Seed Banks to Aboveground Vegetation in Grazed and Ungrazed Salt Marsh Communities on the Gower Peninsula, South Wales. *International Journal of Plant Sciences* 157(6), pp. 746-749.
- van der Wal, D., P. M. J. Herman and A. Wielemaker-van den Dool. 2005: Characterisation of surface roughness and sediment texture of intertidal flats using ERS SAR imagery. *Remote Sensing of Environment* 98(1), pp. 96-109.
- van Zyl, J. J. 1990: Calibration of polarimetric radar images using only image parameters and trihedral corner reflector responses. *Geoscience and Remote Sensing, IEEE Transactions on* 28(3), pp. 337-348.
- Van Zyl, J. J., M. Arii and K. Yunjin. 2011: Model-Based Decomposition of Polarimetric SAR Covariance Matrices Constrained for Nonnegative Eigenvalues. *Geoscience and Remote Sensing, IEEE Transactions on* 49(9), pp. 3452-3459.
- Vincent, R. K. 1997: *Fundamentals of geological and environmental remote sensing*. Prentice Hall Upper Saddle River, NJ.

## Bibliography

- Walton, J. T. 2008: Subpixel urban land cover estimation: comparing cubist, random forests, and support vector regression. *Photogrammetric Engineering and Remote Sensing* 74(10), pp. 1213-1222.
- Wang, C., M. Menenti, M.-P. Stoll, A. Feola, E. Belluco and M. Marani. 2009: Separation of ground and low vegetation signatures in LiDAR measurements of salt-marsh environments. *Geoscience and Remote Sensing, IEEE Transactions on* 47(7), pp. 2014-2023.
- Wang, Y. and T. R. Allen. 2008: Estuarine shoreline change detection using Japanese ALOS PALSAR HH and JERS-1 L-HH SAR data in the Albemarle-Pamlico Sounds, North Carolina, USA. *International Journal of Remote Sensing* 29(15), pp. 4429-4442.
- Waske, B. and M. Braun. 2009: Classifier ensembles for land cover mapping using multitemporal SAR imagery. *ISPRS Journal of Photogrammetry and Remote Sensing* 64(5), pp. 450-457.
- Woodhouse, I. H. 2006: *Introduction to microwave remote sensing*. Boca Raton, FL: CRC Press, Taylor & Francis Group.
- Woodhouse, I. H. 2006: Predicting backscatter-biomass and height-biomass trends using a macroecology model. *Geoscience and Remote Sensing, IEEE Transactions on* 44(4), pp. 871-877.
- Wooster, M. 2007: *Remote sensing: sensors and systems*. *Progress in Physical Geography* 31(1), pp. 95-100.
- Yu, Y. and S. T. Acton. 2004: Automated delineation of coastline from polarimetric SAR imagery. *International Journal of Remote Sensing* 25(17), pp. 3423-3438.
- Zedler, J. B. and S. Kercher. 2005: Wetland resources: status, trends, ecosystem services, and restorability. *Annu. Rev. Environ. Resour.* 30(pp. 39-74.
- Zhang, L., J. Zhang, B. Zou and Y. Zhang. 2008. Comparison of Methods for Target Detection and Applications Using Polarimetric SAR Image. Presented at: PIERS, Hangzhou, China.
- Zheng, S., W.-z. Shi, J. Liu and J. Tian. 2008: Remote sensing image fusion using multiscale mapped LS-SVM. *Geoscience and Remote Sensing, IEEE Transactions on* 46(5), pp. 1313-1322.

## Bibliography

Zisenis, M. 2010: 10 messages for 2010; Coastal ecosystems. European Environmental Agency. p. 17.